Universitat Politècnica de València
Departamento de Máquinas y Motores Térmicos

Online Control of Automotive systems for improved Real-World Performance

PhD Dissertation

Presented by

Varun Pandey

Advised by

Dr. Benjamín Pla Moreno

Valencia, July 2021

Dedication

This thesis is dedicated to all my respected teachers and my darling young `Züri`.

Acknowledgments

This thesis is possible due to many people to whom I would eternally remain grateful. Foremost, it is difficult to overstate my gratitude to my thesis supervisor, Dr.Benjamin Pla Moreno. His continuous enthusiasm, optimism and encouragement kept me on my toes during the development of this thesis and is really appreciated. I owe him for introducing me to the research world and guiding me all the way to work on the critical scientific problems. Apart from helping me to solve the complex control problems, he also instilled in me a culture of detail-orientation. On a personal front, his unfailing kindness, advises and support helped me sail through many turbulent moments and for which I am grateful.

My work at CMT would have been far less enjoyable, without the friendship and moral support of my lab colleagues. While I remain indebted to Pau Bares, Alvin Barbier, Andre Aronis, Irina Jimenez, Alexandra, Chaitanya and Aditya. I remain ever-grateful for making my life in Valencia feel like home. I will always cherish those never-ending conversations that we have had over cerveza and bravas.

I remain eternally grateful to the Spanish Ministry of Economy and Competitiveness and the direction of CMT motores for fully financing my research. A special note of thanks is due to Amparo Cutillas, and the other administrative officials, for hand-holding during all the bureaucratic tasks.

I would like to show my sincere gratitude to Professors Christopher Onder for giving me an opportunity to be part of his research team at Zurich for an internship. I thoroughly enjoyed the research stay, all thanks to, Raffae Hedingerl, Stijn van Dooren, Ritzmann Johannes and David Machacek. With the incredible team it was possible to perform required simulations and experiments in an incredibly short span of time.

None of this would have been possible without the love, support and inspiration of my parents Sulekha and Ravindra. I remain grateful to them for being a source of reliable calm and developing in me a basic trust in my own capacities and chances of fulfillment. To my brother Rahul too, I remain grateful for helping me recognize the importance of being persistent and resilient. Finally, this thesis would never have converged in the way it did without the mature love and unwavering support of my friend and wife, Ananya. Her unreserved intellectual and emotional support has been the fuel for this journey.

Contents

List of Acronyms

Part I

Introduction

Chapter 1

Thesis Overview

Contents

1.1 Background

The new sustainable growth strategy proposed by European Commission in 2019 [EGD 2019], essentially requires the development of sustainable transportation that is climate neutral, cost and energy efficient and non-polluting. According to the authors in [Sims *et al.* 2014], the on-road vehicles contribute to 22% of the Green House Gases (GHG) emission which is responsible for global warming. As per the report by European Energy Agency [EEA 2019], from 2010 to 2016, CO_2 per kilometre (g CO_2/km) declined steadily by 22 g. The average emissions from new passenger cars increased in 2018 by 2.8 g CO_2/km. According to the data in 2019, CO_2/km increased further resulting in 122.4 g of CO_2 per kilometre. This is well above the European Union (EU) target of 95 g CO_2/km in 2020 as shown in Figure 1.1.

The nitrogen oxides (NO_x) are identified as another prominent pollutant coming from the road transportation. It not only has adversarial impact on ozone concentration but also effects the human health [Sims *et al.* 2014]. However, according to the data in [AQR 2019] the NO_x emissions due to road transportation in the EU-28 countries have been reduced by 40% since the year 2000. This reduction in NO_x is majorly due to the stricter emission standards

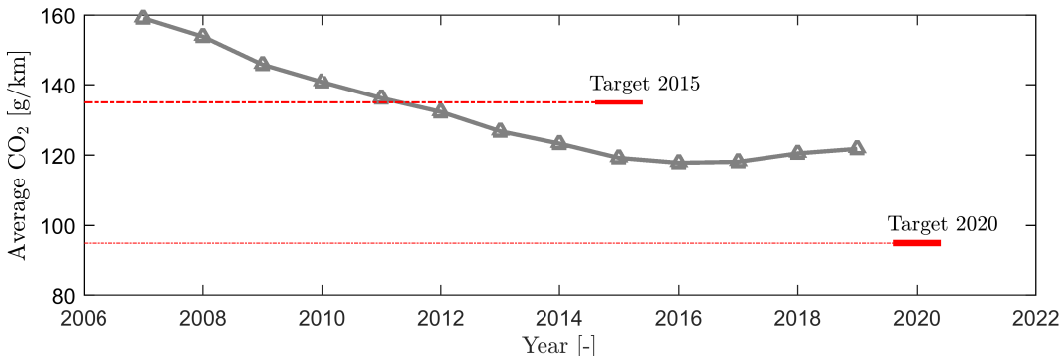

Figure 1.1: European Environment Agency for newly registered motor vehicles, In red are the CO_2 target in 2015 and 2020, the gray line is the average CO_2 emissions from the new vehicles since 2006 to 2019

imposed by government and advancement in the vehicle technology specially with the introduction of after-treatment devices in the vehicles. During last decades the EU has progressively tried to limit the pollutant emissions (the NO_x limits in Figure 1.2) and the target is to tighten these figures in the near future with more stringent emission standards.

The limits imposed on the pollutant emissions for a vehicle is a big challenge for the automotive industry. Vehicle Type Approval (TA) procedure for the Euro standards was criticized for it being non-representative of the real-driving conditions [Demuynck *et al.* 2012]. Before 2018, the TA procedure consisted of testing a vehicle on the NEDC on a rolling test bench under several operating conditions. This was addressed by calibrating the engine control and vehicles to pass the test on this cycle. During the actual driving missions which are far from the NEDC, vehicle under-performs in efficiency and emits more pollutants as presented in Figure 1.3, than what was declared during the TA testing. The uncertainities in the real-world lead to inefficient vehicles on the road with higher fuel and emission levels as shown by the authors in [Mock *et al.* 2012] and [Mock *et al.* 2013]. According to Chen Yuche and Jens [Yuche & Jens 2014], NO_x emissions by European diesel cars are shown to have not decreased, despite the continuous tightening of the NO_x TA limits from EU1 to EU6. As compared to the current TA limit value of 0.080 g/km, real-world NO_x emissions are found to be even more than 0.32 g/km, these differences have been shown by many authors like in Samuel et. al in [Samuel *et al.* 2005], Veerle et. al [Veerle *et al.* 2016] and by Zacharof et. al in [Zacharof *et al.* 2016]. Significant efforts have been made over the past 5 years to reduce emissions of air pollutants, particularly in the wake of Dieselgate [Die 2019].

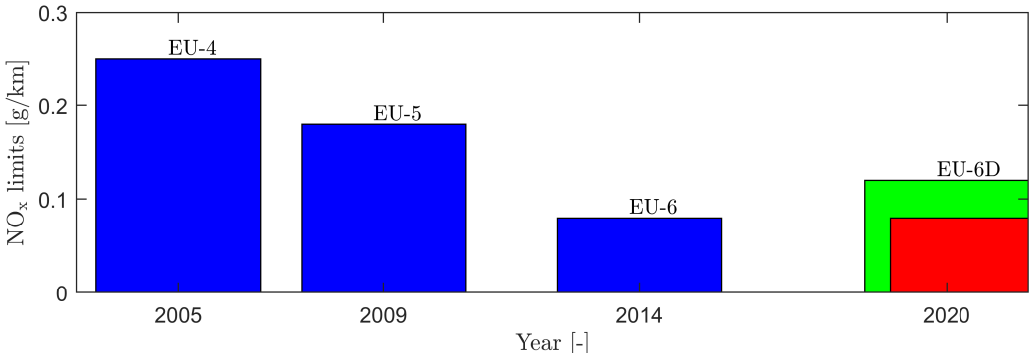

Figure 1.2: European Diesel emission regulatory limits for NO_x from 2005 to 2020. The blue bars represent the NO_x limits for NEDC, the red bar is for the limits on NO_x during WLTC and the green bar is for the Real Driving Emission (RDE) limits for NO_x

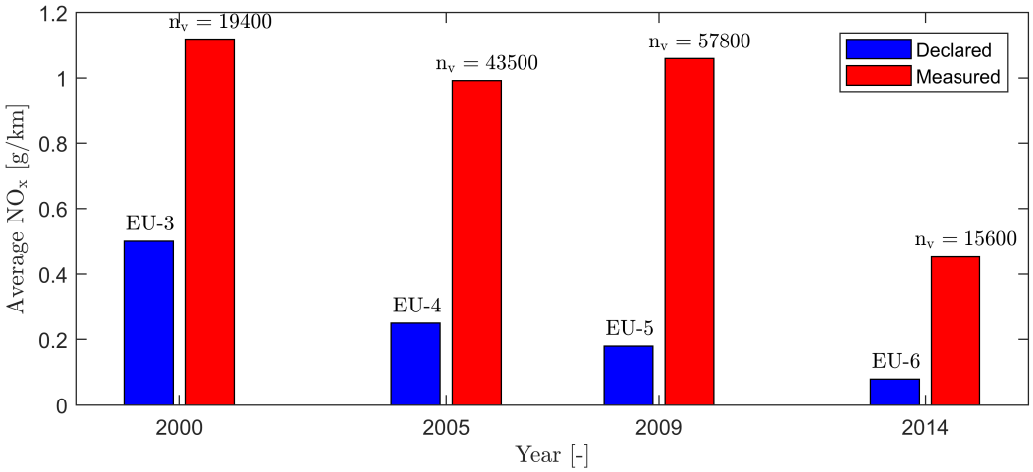

Figure 1.3: Comparison of the average NO_x emissions measured for n_v number of vehicle by European standards (EU-3,4,5,6) to their respective limits from the year 2000 to 2014

In 2018, the EU adopted a more realistic driving cycle, the WLTC [Tutuianu *et al.* 2013] to eliminate the difference between declared and actual emissions. In the EU6D regulations for light duty vehicles, the dynamo-meter based TA procedure is complimented with on-road emission testing by means of the portable emission measurement device [Weiss *et al.* 2012]. These tests pose several new challenges for automotive manufacturers as vehicle design and control strategies become more complex. Among the research domains that can contribute to address the aforementioned challenges, one can identify the following ones:

- Development of low emission alternative powertrains that run on a fuel other than traditional petroleum fuels (petrol or diesel):

  Popular alternative powertrain systems are Electric Vehicles (EV) [Frieske *et al.* 2013], Hybrid Electric Vehicles (HEV), solar powered vehicle [Singh *et al.* 2019], bio-fuel among other. Such technologies are usually compared for energy efficiency and pollutant emissions with the conventional vehicles using the life cycle analysis approach. The authors in [Tagliaferri *et al.* 2016], use cradle-to-grave approach to identify the energy extensive processes during manufacturing, usage and disposal phases of the conventional and EV vehicles. During the assessment of the GHG emissions of a battery electric vehicle in comparison with a conventional Internal Combustion Engine (ICE) vehicle, the well to wheel analysis by Moro et. al [Moro & Helmers 2015] found that an EV can save up to 50–60% of GHG .

- Development of high efficiency powertrain components:

  The authors in [Payri *et al.* 2015] present a comprehensive review of different technologies that are developed for meeting regulations. In the conventional vehicles, the continuous improvement in the design of Diesel and gasoline engines (such as advanced Exhaust Gas Recirculation (EGR) technology [Thangaraja & Kannan 2016, Galindo *et al.* 2020], Variable Geometry Turbocharger (VGT) [Feneley *et al.* 2017], combustion improvement through Homogeneous Charge Compression Ignition (HCCI), Reactivity Controlled Compression Ignition (RCCI) [Guardiola *et al.* 2018],.. etc. The after-treatment devices such as Selective Catalytic Reduction (SCR) [Pla *et al.* 2020]) have also facilitated the emission reduction. In the EVs, the research areas include development of high capacity batteries while addressing the issues of autonomy, durability and cost [Zakaria *et al.* 2019]. The transition from the conventional vehicle to full electric vehicles is slow and has served as a nucleus in the development of HEV. The research in HEVs is largely focused

on the topological, optimal component sizing and Energy Management Strategy (EMS).

- Development of advanced vehicular control system:

  The optimal engine control, EMS in HEVs, development of autonomous vehicles and connected vehicle have gained huge momentum in the last decades. Broadly speaking, the objective of the automotive controls is to operate the vehicle or any of its subsystems in the most efficient way while fulfilling several constraints at the system and surrounding levels. As the complexity of engine and vehicle kept growing with the new technological developments, the demand for more complex control system also grew. The opportunities arising due to the improved computational capabilities, connected vehicles and more sophisticated modelling and control techniques are paving the way for adoption of optimal control theory in the automotive industry. For instance, the typical approach in conventional engines was based on the calibrated maps that contain control set-points as a function of several variables. These set-points are interpolated according to the current sensor readings, estimations and then corrected for dynamic transients. It requires a lot of experimental and heuristic knowledge for obtaining a single calibration. Automated frameworks are proposed by the authors in [Stuhler *et al.* 2002, Jiang *et al.* 2012, Hellström *et al.* 2013] to address this costly and time demanding solution. The optimal control theory is found relevant in not just engine controls but also in transmission control, EMS for HEV among others. The efficient driving is also shown to have significant impact on fuel saving and emission by Sciarretta et.al [Sciarretta & Vahidi 2020a]. Autonomous driving eliminates any human intervention in vehicle speed control and drives the vehicle in the most energy efficient way for a given powertrain system. An optimal control perspective for efficient driving is presented in [Han *et al.* 2019].

This thesis is focused on the third topic, i.e. the optimisation of control for modern powertrain systems. The control is important in itself, but also serves as a technology enabler for the first two topics of the above list. Following section describes the problem that has been addressed in this work.

1.2 Problem description

The problem addressed in the current thesis is to optimise the vehicle control such that the fuel consumption and constraints regarding the powertrain behaviour, for instance pollutant emissions or battery state of the charge for

HEVs is respected in actual driving missions. The thesis proposes model-based control that approximates the minimum energy consumption of the vehicle subject to constraints (emissions, electric range, ...) in real driving conditions by applying optimal control techniques. To do that, three main topics are covered:

- Models that are capable of estimating (in real-time) the general behaviour and performance of the powertrain based on its requirements (vehicle speed, acceleration, torque demand, environmental conditions) and control settings (engine management , power-split).
- Statistical models capable of estimating future operating conditions from the vehicle's history, in addition to other information provided by the infrastructure (Infrastructure to Vehicle (I2V)) or other vehicles (Vehicle to Vehicle (V2V)) that is available.
- Optimization algorithms that combined with the above elements can provide optimal powertrain controls that minimize energy while satisfying emissions or other forms of constraints.

1.3 Objective

The main objective of this thesis is to extend the application of optimal control of powertrain in real driving conditions. To this end, there are two design verticals explored during the development of this thesis – powertrain and vehicle speed optimisation as presented in Table 1.1:

Powertrain Optimisation	**Vehicle speed optimisation**
- Adaptive Control of diesel engine - Variable smoothening of diesel engine calibration - Adaptive EMS in a HEV	- Optimal vehicle speed in urban scenario - Speed Advisory in Real Driving

Table 1.1: The verticals explored in the thesis for improvement in real-world performance of a vehicle and the applications developed under each vertical

The first two topics in the powertrain optimisation are related to the classical engine control for the conventional vehicles. In particular, the first application is a standard problem of adaptive control of fuel injection in a diesel engine for improving efficiency and constraining the NO_x emissions for the entire trip. This can be easily modified to cover other systems such as EGR, VGT, urea injection and also to aspects such as soot and response time. To

do that two main problems are required to be addressed: At first the curse of dimensionality arising due to the number of extra variables and then development of models to estimate outputs such as soot and dynamics. The second problem arises from the optimisation procedure itself. The second application is regarding the auto-smoothening of the calibration maps of a diesel engine in real driving conditions. For which a single tuning parameter is used to obtain a trade-off between fuel consumption, NO_x emissions and the engine torque reference following capability.

The modern powertrain systems are rapidly progressing towards hybridisation and electrification. Therefore, the scope of powertrain optimisation is not limited to the engine control but also covers the control of HEVs. The third problem is regarding the online EMS of a HEV. The State-of-the-Art (SOA) offline EMS is extended with a cycle prediction strategy for making it an online application. In particular, the performance of developed method is compared with SOA EMSs in terms of fuel efficiency and capability to track the reference State-of-Charge (SoC).

Even though the controllability of the powertrain system is high, the complexity of the control problem increases multi-fold with the increasing number of control parameters. During its implementation in powertrain systems with several control inputs and constraints, the optimal powertrain control problem becomes extremely complex and eventually over-weighs the performance related benefits. For this reason, another research vertical is also investigated in this thesis: Control of vehicle speed in real-driving conditions. Such control problems have less number of actuators (acceleration pedal, braking pedal etc..) but the number of states and disturbances is much higher since it includes all the powertrain related states plus the ones related to the driver and the environment. Therefore, the observability (in passive or active control) is very limited in real-time. The observabilty is related to the ability of the set of sensors and sources of information to estimate the state of the system. The limitation is due to the amount of information (I2V or V2V) that is required to be processed to obtain an optimal control solution. On the other side, even if the optimal actuations provided with a good estimation of the system state could be calculated, those actuations arrive to the powertrain through the driver whose controllability is questionable (at least in the case of being a human being). In any case, due to the high impact of the vehicle speed profile on its performance in terms of fuel consumption and emissions, this second veritcal is related to Advanced Driving Assistance System (ADAS) which has three major sub-domains: the vehicle safety, the efficiency and the driving comfort. As this thesis is focused on the development of methods for improving the vehicle efficiency in real driving conditions, only the efficiency sub-domain is investigated. Specially, two applications are developed — the

first application is regarding the speed optimisation of a vehicle in the urban scenario with the information of the traffic light phasing. The objective is to assess the impact of optimisation on the fuel consumption and NO_x emissions with the traffic light information. The second application is a speed advisory in real driving mission for improved fuel economy and travel time.

Other than designing the above control applications for real driving scenario, the thesis also present the findings of an assessment regarding the NO_x emission dispersion due to the driving dynamics within the Real Driving Emission (RDE) regulation (EU6D) limits. The following section describes the thesis organisation with briefing about the contents.

1.4 Thesis Organisation

This thesis has ten chapters (divided into sections and subsections) which are organised in five parts. The first part is about the introduction and contains two chapters: The chapter 1 introduced the background of the sustainable transportation strategy adopted by the government in recent time with an emphasis on the real driving emissions. The control role for automotive powertrain management was presented with focus on the requirement of new control methods to deal with the latest emission regulation. Finally, a general outline of the problem is described with a clear definition of the thesis objective. The chapter 2 is focused on analysing the current SOA advances in the control of automotive systems with emphases on SOA of the applications developed in this work. The first section is about the advancement of the diesel engine control methods in real driving emission perspective. The second section is about the energy management of the hybrid electric vehicles in recent years. Finally, the work available in literature related to the vehicle speed optimisation with the objective of efficiency improvement are presented within a framework of advanced driving assistance system.

The following part is about the theoretical tools developed in the thesis and it contains 3 chapters: The chapter 3 is regarding the vehicle model used in this work. These models were used at several instances in the development of this thesis. The vehicle dynamics are addressed with a longitudinal model. Gear-box, ICE, electric motor, power-coupling device and battery models are described in different sections. The chapter 4 introduces optimisation tools with their mathematical formulations and supported by suitable examples. The first section elaborates the dynamic programming as a tool for finding a global optimal solution. The second section is regarding the Pontryagins Minimum Principle and its extension to the Equivalent Consumption Minimisation Strategy. The chapter 5 introduces a tool developed for driving cycle

prediction in real world conditions. The tool is first described in its mathematical form and then, the method of prediction is described with the help of a simple example.

Then, there is a part describing the experimental setups being used in the development of the applications. This part has chapter 6 which present descriptive layout of the relevant engine/vehicle components and instrumentations. The specification of the engine/vehicle are also tabulated. The four test setups are marked in alphabetical order from A to D and are refered during the description of the application in the following parts.

The fourth part is about the applications developed during this work and has three chapters: The chapter 7 present the three design applications under the vertical of powertrain optimisation as discussed previously in Table 1.1. Each application is described using a standard format that covers five topics: Beginning with the application specific introduction and followed by the method description, case studies used for their validation, results and summary/conclusions. The chapter 8 present two design applications under the vertical of vehicle speed optimisation (refer Table 1.1). A similar structure as in chapter 7 is used to describe the developed methods and important findings. Finally, chapter 9 present an assessment of the impact of driving dynamics on real driving NO_x emissions. Presenting the summary of experimental results and the conclusions that can be derived from the study.

Finally, the last part is about the overall conclusions and the outlook of this thesis described in chapter 10. In this chapter the summary of the research and future scope of the work is presented.

Chapter 2

State-of-the-Art

Contents

In conventional vehicles, five layers of intelligent vehicle control can be identified as presented in Figure 2.1:

- Component Control: This includes electronic hardware components such as sensors, actuators and Electronic Control Unit (ECU)s.
- Drivetrain Unit Control (DUC): They are the controllable vehicle drivetrain units, for example the engine, motor, transmission, suspension, brake and the steering system.
- Powertrain Control: This is a overall control of the drivetrain units on a vehicle level influencing the whole vehicle motion.
- Vehicle Control: At this level, direct V2V communications and direct V2I communications are controlled such that driving is safe and economical.

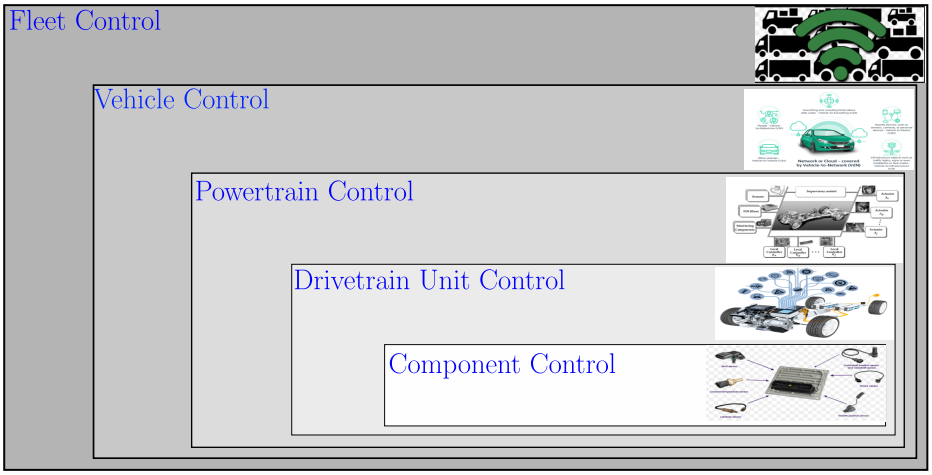

Figure 2.1: The five layers of vehicle control

- Fleet Control: This layer controls the entire vehicle flow. Based on the current location, the vehicle fleets are controlled for safe and efficient transportation.

This thesis addresses three levels of the vehicle control: DUC, Powertrain Control and the Vehicle Control. The first section in this chapter present the SOA in the DUC focusing on the engine controls, the second section is regarding the SOA in Powertrain control of the HEV. Powertrain control is usually referred to as the combined control unit for the engine and the transmission system where, the power demanded by the driver at the wheel is generally provided by one to two power sources (ICE, battery, fuel cell). The last chapter is regarding the SOA in vehicle control.

2.1 Drivetrain Unit Control - Internal Combustion Engine

The automatic control of the engine, may be dated back to 1924 with the invention of carburettors [Ritter & Tillotson 1924] for mixing air with the fuel to supply for combustion. In the early 80's the rising-rate fuel pressure regulators were introduced by [Sugaya 1978] which exponentially increased fuel pressure depending on the boost pressure. During the same period the turbocharging system also introduced the control complexity in the air management system. After the introduction of the after-treatment devices [Stanglmaier *et al.* 2002], the stand-alone ECUs were required to control the ICE in a more powerful and a complex manner. The latest engine control systems allow an optimal

coordination of fuel-injection, turbocharging, EGR, Exhaust After-Treatment (EAT) in stationary and transient conditions. Generally, the main objectives of the engine control can be summarized as:

- The torque demanded by the driver through acceleration pedal must be met resulting in good drivability.
- The engine must operate at high thermal efficiencies resulting in low fuel consumption while emissions must be within the regulatory limits.
- The system must function in a safe operating region derived from the individual limits (such as mechanical) of all the elements.

With many mutually dependent subsystems, the engine control is a very complex problem and the control theory plays an important role in enabling its optimisation. SOA engine optimisation method is usually based on feedback and feed-forward controllers. Fixed look-up tables generate the set-points for feed-forward controller. The look-up tables also referred in the literature as the maps are obtained using the calibration process as shown by the authors in [Isermann 2014] with a goal of minimising fuel consumption while fulfilling the regulatory and customer constraints regarding the emissions and driving comfort. The SOA engine calibration process is described in the following subsection.

2.1.1 Engine Calibration

The engine calibration is a process of feeding the engine ECU with a set of information that define the actions of the actuators during its operation. The goal of engine calibration process is to obtain optimal and drivable actuation maps. The SOA engine calibration begins with identifying the set of operating points (engine speed and engine torque) which are representative of the engine operation zone (largely dependent on the vehicle application). During the engine calibration process the actuator settings are identified which, optimise the engine efficiency at the identified operating points while, simultaneously limiting the emission and other requirements on a pre-defined driving cycle. The control structure of the modern diesel engines consists of feed-forward and feedback controllers. The article by Castagne et al. [Castagné *et al.* 2008] gives an overview of several calibration methods. The authors explain traditional local approaches, characterised by a phase of smoothing after local optimal settings are found, as well as global approaches, which directly include engine speed and load parameters in the model.

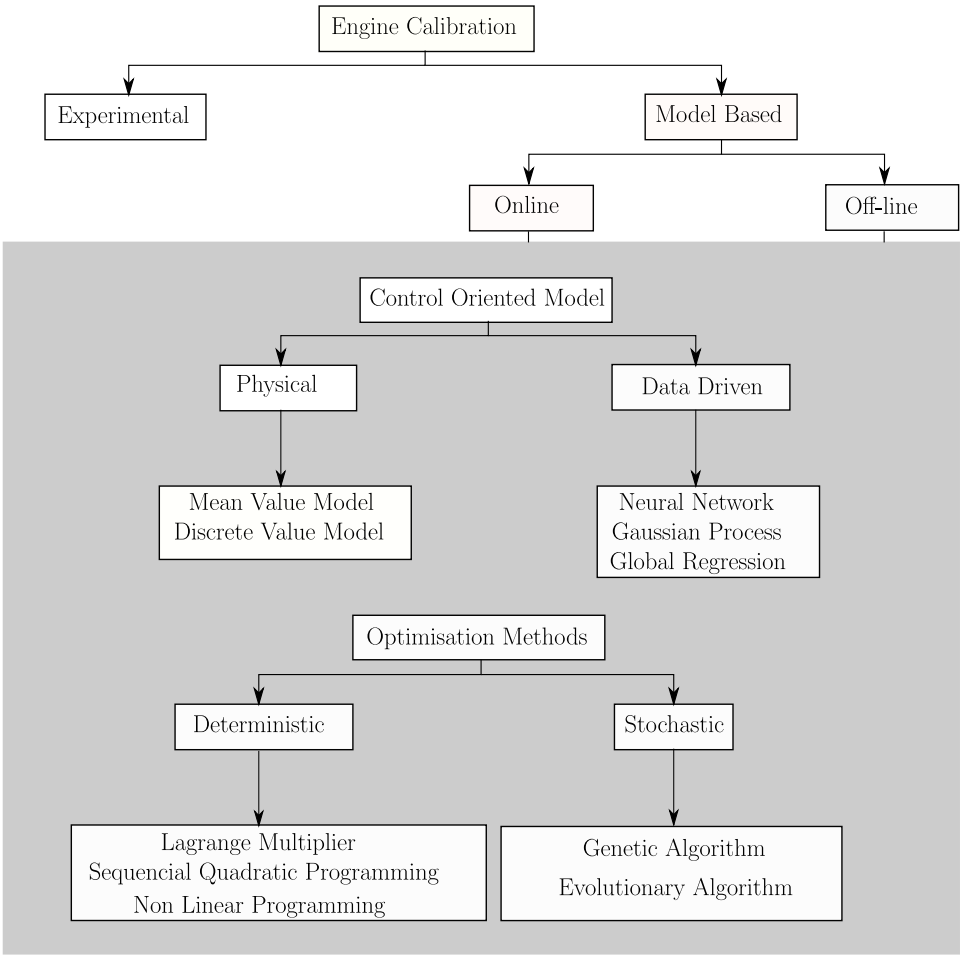

Figure 2.2: State-of-the-art Engine Calibration Methods.

As presented in Figure 2.2, the calibration is either based on the experimental or the model-based approach. References to various literature is presented by the authors in [Kampelmühler *et al.* 1993], [Rao *et al.* 1979],[Schöggl *et al.* 2002].

Experiment-based calibration: In the experiment based approach, the optimisation problem may be solved using the Lagrange multipliers where, the cost of the optimisation is the fuel consumption over a predefined driving cycle and each constraint is attached with a Lagrange multiplier. Thereafter, following procedure is required:

- All the Lagrange multipliers are set to zero to obtain the fuel optimal solution.

- If all the constraints are fulfilled, the actuators settings recorded as a function of the operating point and used as feed-forward maps in the calibration
- If any of the constraint is not fulfilled, the corresponding multiplier is tuned until the solution is reached.

The experiment based calibration method require calibration experts and even then does not guarantee an optimal solution. With the advent of powerful computational tools such as MBC tool by MATLAB, the modern calibration process includes model-based phases in addition to the experiment-based phases.

Model-based calibration: To reduce the complexity arising due to the high number of control inputs and mutually contradicting objectives several researchers have explored model-based calibration approach (a combination of Control Oriented Model (COM)s and optimisation techniques). In recent time, the model based approach is gaining ever more popularity due to the availability of high computational power. These methods are capable of calibrating the engine in an online [Tan *et al.* 2017, Bachler *et al.* 2003, Asprion *et al.* 2014] or an offline [Hiroyasu *et al.* 2002, Luján *et al.* 2018, Alonso *et al.* 2007] setting. Many of the commercially available calibration tools [Sampson 2009] are purely designed for model-based offline optimisation and do not have a connection to the engine test bench. The AVL CAMEO 4 consists of a test bed and office version with an additional toolbox called as iPROCEDURE ADAPTIVE DOE and is capable of performing online optimisation. The BMW also has its own tool MBMINIMIZE tool to perform online calibration [Sung *et al.* 2007] among others.

The process of model-based engine calibration has been broadly divided into three steps by the authors in [Langouët *et al.* 2011, Park *et al.* 2017]. The first step is to select steady-state operating points which are representative of the engine operation. Then, a global engine model is developed and validated using measurement data from steady-state experiments. Finally, optimisation and smoothing are carried out for a representative driving cycle, with the goal of minimizing fuel consumption, while meeting constraints on pollutant emission and ensuring good drivability. The constraint over pollutant emissions such as NO_x, Particulate Matter (PM), CO and HC are well defined by the government agencies as presented in the Figure 2.3. The EU has enforced the type-approval process based on the representative cycles like NEDC and more recently WLTC. The other constraint is regarding the drivability and is often defined only qualitatively. Assis et al. [Assis *et al.* 2003] define drivability as the capability of the engine to deliver the torque requested by the

driver in a way which is pleasant to the driver. From a vehicle perspective, the driver subjectively provides feedback regarding drivability during the vehicle development phase. Pedal tip-in and tip-out are the typical drivability testing scenarios. The authors show that, even though the torque produced by the engine is desired to be equal to that demanded by the driver, it may result in undesirable behaviour due to powertrain excitation's during large torque steps. The authors propose a rail pressure control strategy to dampen the impact of sudden jumps in the engine torque. Nessler et al. [Nessler *et al.* 2006] define drivability as the transition felt by the driver between engine speed and load points during real vehicle driving, which means that a constant power supply is necessary during acceleration phases while avoiding sudden reduction of torque in order to have a good drivability. The authors propose to reduce the Gaussian curvature of the optimal calibration maps in order to obtain smoother maps. In the articles by Nishio et al. [Nishio *et al.* 2018] and Niedernolte et al. [Niedernolte *et al.* 2006], a constraint in the step size for each parameter is applied to generate drivable calibration maps. However, some loss of optimality has been shown by the authors in terms of engine performance due to the manual elimination of the peaks in the map. This method requires all other parameters to be adjusted consistently in order to achieve the target torque. However, no relationship has been shown between map smoothing on the torque reference following capability and the engine performance. From an engine perspective, other than calibration map smoothing, some transient compensation strategies are also applied in order to obtain smooth transients, which in fact is another method of improving drivability. Adaptation of exhaust-gas recirculation (EGR) and fuel injection has an impact on transient emissions and drivability, as shown in the article by Zentner et al.[Zentner *et al.* 2013]. The authors propose an EGR and injection limiter to reduce NO_x emissions and to improve drivability and the drivability was characterised by the transient response of the engine during load steps.

The model based technique is fundamentally based on a control oriented model and an optimisation method (as described in the following paragraphs) for performing the engine calibration (online or offline).

Control Oriented Model: The control-oriented models with reasonable precision but low computational cost are ideal for testing the complex control strategies on the engine system. These models are either based on the physical equations and experiments necessary to identify some key parameters, or they are based on the experimental data. The control oriented physical modelling in the ICE is classified by the authors in [Guzzella & Onder 2010] as Mean Value Modelling (MVM) and Discrete Event Modelling (DEM). The MVM approach neglects the discrete cycles of the engine and assume that all pro-

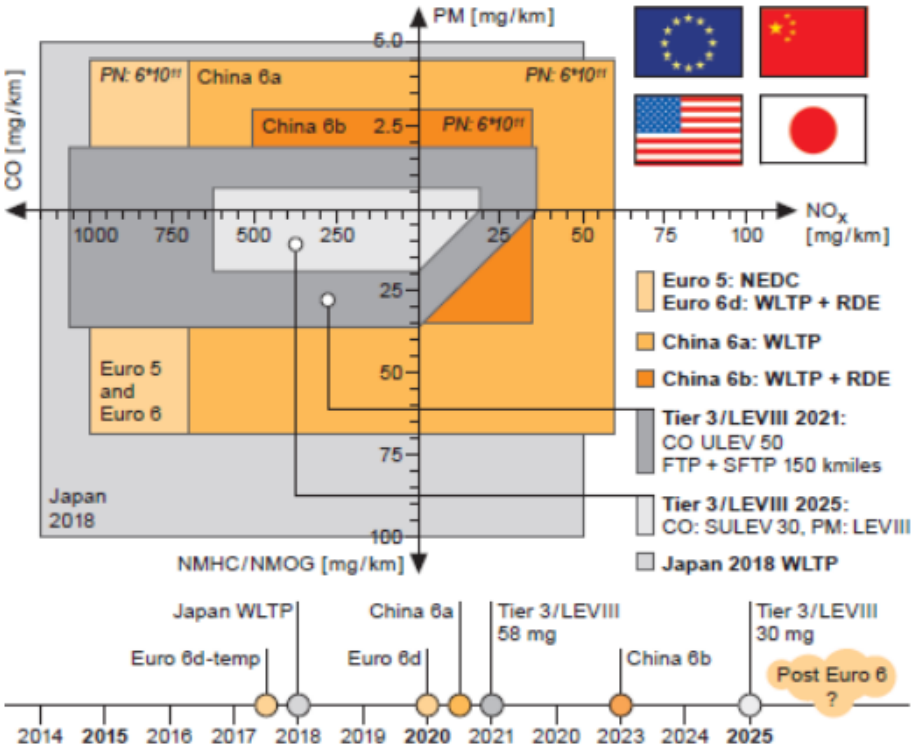

Figure 2.3: Emission constraints in different world region, The figure is extracted from the report of Continental automotive [con 2019]

cesses and effects are spread out over the engine cycle. Whereas, in the DEM approach the reciprocating behaviour of the engine is also modelled. There is a lot of literature available which describe the methods and their implementation in the control perspective [Jung 2003, Baldi *et al.* 2015, Pinamonti *et al.* 2017, Guardiola *et al.* 2012, Guardiola *et al.* 2014, Jiang *et al.* 2009, Martin *et al.* 2018, Torregrosa *et al.* 2011, Payri *et al.* 2005].

The empirical models use the experimental data from an engine of certain specification where the interesting control actuators are varied as much as possible within their boundary conditions. The desired model output variables are stored as a function of the control actions. Such models are data driven since the predicted outputs are based on simple functions of the measured data. There are several data driven models described in the literature, where very popular are based on the Neural network [Atkinson *et al.* 2008], Gaussian process [Berger *et al.* 2011], global regression [Grahn *et al.* 2012], etc.

Optimisation Methods: The multi-objective optimisation for online or offline calibration is classified in two categories by the authors in [Cavazzuti 2013]: The deterministic and stochastic optimisation. The deterministic algorithms are commonly based on the computation of the gradient and in some cases also on the hessian of the objective function. The deterministic optimisation approach is further subdivided into constrained and unconstrained optimisation methods. The constrained optimisation methods have been widely used in the literature for Diesel engine calibration where, the very popular are Lagrangian method [Hochschwarzer *et al.* 1992], Sequential quadratic programming [Hafner & Isermann 2003], Non-linear programming [Rao *et al.* 1979]. On the other hand the Stochastic optimisation methods are based on randomness with slower convergence as compared to the deterministic algorithms. In the literature, stochastic methods are found in the diesel engine calibration as particle swarm optimisation algorithm [Zhang *et al.* 2018], genetic algorithm [Millo *et al.* 2018], evolutionary alogrithms [Ma *et al.* 2015] etc. In the thesis [Schmied 2004], the author proposed a new method called Multistoch which is based on designing dynamic experiments using constrained functional quantification.

As discussed, the existing engine control is based on the fixed calibration maps which are optimal for a driving cycle known in advance. With new regulations the vehicle emissions should be constrained in the real driving conditions. The following section is regarding the SOA of engine control in real-driving perspective.

2.1.2 Engine Control in real driving perspective

Despite a substantial effort during the last decades in order to reduce the fuel consumption and emissions in light duty vehicles by means of improved powertrain design and controls [Payri *et al.* 2015], noticeable discrepancies are still observed between declared and real driving consumption and pollutant figures [Pelkmans & Debal 2006, Weiss *et al.* 2011]. One of the main reasons for such a deviation is that the driving cycles considered by regulations only represent to some extent the set of conditions that a vehicle may face during their entire life. To make-up for such a limitation, the current regulations have introduced RDE testing procedures as a method to reduce the gap between declared performance and that perceived by users. In any case, those facts point out the impact that driving conditions, including traffic but also driving style, have on fuel-consumption and emissions. To this aim, the traditional control scheme based on fixed calibration can be upgraded by including some degree adaptation introducing the following three features to address the issue of real-driving uncertainty:

- Vehicle speed prediction model: The prediction model can be based on the available information about vehicle speed on a given route by including information from a database of real-world driving and to generate the driving cycle using a stochastic process. SOA for construction of synthetic driving cycles is to randomly append driving segments, where a segment is a driving sequence between two stops as demonstrated by Michel in [Michel 1996]. An issue with such a method as mentioned by Jie and Debbie in [Jie & Debbie N 2002], is that it gives no consideration for differentiation in modal events (e.g. cruise, idle, acceleration and deceleration) and also there is no way to set the length of the cycle. In [Jie & Debbie N 2002], Jie and Debbie proposes to use a stochastic process for binning of data until certain statistical criteria are met. The bins are based on which modal event they belong to and are extracted from the measured driving cycles. However, due to the size of these snippets, it is still difficult to achieve the desired driving distance and at the same time obtain driving cycles that are representative of real world. Another way would be to generate single velocity and acceleration states at any instant, instead of the entire bin. One option is to generate driving cycles by using Markov chains, as described in [TK & ZS 2011]. This includes extracting information from a database of real-world traffic and then analysing the data to generate driving cycles using a stochastic process. In the article by Gong et. al [Gong *et al.* 2011], the Markov chain approach is shown to be the most popular method for generating representative driving cycles.

In the article by Francois et. al [François 2017], a considerable dispersion has been reported in the driving dynamics of average drivers and vehicles. In the article [Josh & Vicente 2016] by Josh et. al it has been shown that the driving conditions (including freezing or hot ambient temperatures, driving dynamics, driving at high speeds, driving at higher altitude and diesel particulate filter regeneration events) not covered by the RDE test are to have a relatively high contribution to overall NO_x emissions. As a matter of fact, driver monitoring and driver style correction can improve fuel economy. According to Rajan et. al in [Rajan *et al.* 2012], driver style and driving events like city and highway driving both affects vehicle energy demand. Hence, both have to be considered in developing a vehicle. A lot of work is focused towards improving driver style by providing driver assist both in conventional vehicles as shown by the Guenter et. al in [Günter Reichart *et al.* 1998] and for HEVs as shown by the authors in [Fazal *et al.* 2010].

- Vehicle model: For estimating the engine performance in real-time a simplified vehicle model is required. Although, some works have applied Optimal Control to vehicle powertrains without the so called quasi-static engine simplifications [Asprion *et al.* 2014, Luján *et al.* 2018, Maroteaux & Saad 2015], very simplistic 0D models as followed by the authors in [Ozatay *et al.* 2014b, Ozatay *et al.* 2014c, Sciarretta *et al.* 2015a]. In the article by Yang et al. [Zhijia *et al.* 2013] should be applied for online purpose.

- A supervisory controller is also required to control the engine for minimised fuel consumption with constrained emissions. Optimal control theory has been widely used in literature as consolidated by the authors in [Jonas *et al.* 2014] to address complex control problem. However, application of these methods in engine management system is still a big challenge due to their computational cost. Some other methods have been focused on lower level engine control for Spark-Ignition engine. Extremum seeking method has been widely used in [Hellström *et al.* 2013, Corti *et al.* 2013, Popovic *et al.* 2006], most of the work is related to online optimal calibration but does not include real driving emission constraint. The authors in [Andreas *et al.* 2010], present a theoretical basis and algorithmic implementation for allowing the engine to learn the optimal actuator settings in real-time. Even though short transients have been presented for online optimisation, the applicability of this method in real driving condition still remains an unsolved issue. Other methods, like Equivalent Consumption Minimisation Strategy (ECMS) and Model Predictive Control (MPC) as in [Petri

et al. 2018, Nishio & Shen 2019], seem to be more promising in real-time engine control. Stephan et. al [Stephan *et al.* 2014] proposed an ECMS method to provide a solution for online optimal control of Diesel engine with constraint in NO_x emission. The authors assume a constant emission reference target which leads unrealistic emission in real-world driving. In the article by Gokul et.al [Gokul *et al.* 2019], MPC is formulated to maximise the fuel efficiency while tracking boost pressure and exhaust gas recirculation rate references, in the face of uncertainties, adhering to the input, safety constraints and limits on emissions averaged over some finite time period. Authors in [Guardiola *et al.* 2016], present a model based approach to adapt the engine calibration depending on the driver behaviour and the target pollutant emissions: they consider a fixed probability matrix for expected engine operating points, which does not represent a real world scenario.

2.2 Powertrain Control - Hybrid Electric Vehicle (HEV)

With two energy sources the HEVs present a system with higher degree of freedom with improved possibilities of reducing the fuel consumption and the emissions than traditional powertrains exclusively based on ICEs. This potential can be realised through optimisation in any of the three HEV system levels : the powertrain topology (series HEV, Parallel Hybrid Electric Vehicle (pHEV), series-parallel HEV), the technology and sizing of the components and the EMS. Extensive literature is explored by the authors in [Tran *et al.* 2020] and [Bradley & Frank 2009] regarding the topology of HEVs. However, this section is focused on describing the various types of EMS in the literature for HEVs. In contrast to the conventional vehicle, in HEVs, the power demand by the driver can be fulfilled by combining the powers from an ICE and EM. The number of possible combinations depends on the powertrain topology. For instance, in pHEV configuration the power can be delivered by the ICE and EM exclusively or in a combination, the battery can be also recharged using the regenerative braking system. The main objective of the EMS in a HEV is to minimise the fuel consumption of the vehicle while fulfilling the energy demand of the driver and restraining the battery SoC within a certain range. The EMS must also ensure to operate the system to fulfil the constraints regarding ICE, EM and battery.

In general, the pHEVs operating modes are classified by the author in [Markel 2006] as Charge Depleting (CD), Charge Sustaining (CS). In CD, the SoC may fluctuate but on-average decreases while driving. However, in

CS mode the SoC is maintained at a certain level. The EMS for pHEVs are designed to fulfil the conditions of desired operating mode and are broadly classified by the authors in [Tran *et al.* 2020] as : Heuristic, Optimisation-based and learning-based.

2.2.1 Heuristic Supervisory Controller

The early control strategy for the HEVs was based on heuristic considerations which results in Boolean rules [Guzzella & Sciarretta 2005, Moura *et al.* 2011, Gong *et al.* 2008, Peng *et al.* 2015]. These methods require exhaustive experiments and experience to set up a rule based control system. According to the authors in [Guzzella & Sciarretta 2005], there are two guiding principles of the heuristic supervisory controller in hybrid vehicles: The first principle is to use the engine only if it can run at high efficiency, while in the conditions where the engine efficiency can not be high the electric mode should be preferred. The engine is used during the warm-ups to activate the catalyst. In [Peng *et al.* 2017], the authors propose a method to calibrate the heuristic control strategy with the global optimisation result. The dynamic programming is applied to obtain the optimal powertrain energy management strategy for a series-parallel HEV over a driving cycle and the calibration is built based on the optimisation results. The second principle is that the battery SoC must be observed and regulated in such a way that the SoC must remain within a certain predefined limit. The main advantage of these methods is that they are robust, intuitive and made to directly translate control specifications. The rule-based controllers require experimental database and the behaviour of heuristic controller strongly depends upon the driving conditions. If the vehicle operates far from the conditions for which the controller was calibrated, the performance deteriorates [Hofman *et al.* 2006]. The optimal supervisory controllers aim at eliminating the disadvantages of the rule based controls by introducing a well-defined mathematical approach for optimisation.

2.2.2 Optimal Supervisory controller

In the optimisation based methods, the performance index J is either simply the mass of fuel or a combination of other performance indexes based over a mission of duration t_f. The other performance indexes may include the emission rates of a regulated pollutant, drivability of the vehicle in terms of acceleration and jerk-free vehicle operation, frequency of mode switches, battery life, etc... depending on the vehicle application. In Equation 2.1, a

simplified cost J is defined for a performance index L.

$$J = \int_0^{t_f} L(\omega(t), u(t), x(t))\ dt \tag{2.1}$$

$\omega(t)$ is the disturbance, in the case at hand the main disturbance is the driving cycle that has to be followed, $u(t)$ are the control signals and $x(t)$ are the state variables related to the system dynamics. For studying the energy management strategy of the HEVs, the models are usually designed using quasi-static approach where most of the mechanical, electrical and thermal dynamics of the subsystems are eliminated. However, there are some states which are included such as the battery SoC dynamics, temperature dynamics of the after-treatment devices ([Kum *et al.* 2013]), battery ageing etc. The most common is the battery SoC which is not only required to be constrained instantaneously but also the terminal SoC(t_f) must be close to a pre-determined value. This value is dependent on the type of HEV considered and its operating mode such as charge depleting, charge sustaining etc. The constraints on these state variables are handled using the soft (penalising the deviation from the desired level) or a hard integral constraint (must reach the desired SoC level). The hard constraint is feasible only if the driving cycle is perfectly known in advance. However, the soft constraint can be applied in the online optimisation. Other than the integral constraints on the battery energy consumption there are local constraints that are supposed to be handled by the optimal controller. Such as, the mechanical limits of the ICE, EM, charging and discharging rates, torque response, etc. The Optimal Control (OC) methods are either solved offline or online. In the offline method optimisation problem is solved on a desktop without any link to the experimental setup and therefore real time calculations are not required. However, in the online methods optimisation problem is solved on a real time control platform with a link to the experimental setup. The classical methods used in the offline approach are Dynamic Programming (DP) [Gong *et al.* 2007], Pontryagin's Minimisation Principle [Kim *et al.* 2014], and meta-heuristic search methods i.e. the Genetic Algorithm, Particle Swarm Optimisation and Simulated Annealing. The online methods are Equivalent Consumption Minimisation Strategy (ECMS originally developed by [Paganelli *et al.* 2000]) and Deterministic or Stochastic Model Predictive Control [Johannesson *et al.* 2007].

Offline Methods An offline Optimal Control (OC) strategy is a non-causal since it relies on future information. It requires a priori knowledge of the driving cycle and therefore they are often used to obtain a standard optimal solution for comparing the results obtained with the online methods. One of the very popular method to solve the non-causal optimisation is the DP

[Bryson & Ho 2018]. In the DP, computation burden is directly dependent on the number of states and therefore simplified models can be used to solve the optimsation problem. The DP requires to grid the states and time variables. It uses the performance index in Equation 2.1 with an extension to any point in the time-state space by defining it as a cost-to-go function of time and the state. In [Vinot *et al.* 2007, Scordia *et al.* 2005, Debert *et al.* 2012], authors have shown the application of the DP in optimisation of EMS of HEV. As mentioned, the computation burden of the DP has a drawback in the implementation of complex problems, several improved algorithms [Yang *et al.* 2019, Lee *et al.* 2020, Li & Gorges 2019] have been developed.

Other optimisation method that permits a reduction of the computation effort is the PMP which, minimises the following Hamiltonian (H) function at each time step.

$$u^*(t) = \underset{v}{\operatorname{argmin}}\{H(t, x(t), v, \mu(t))\} \tag{2.2}$$

$$H(t, x, v, \mu) = L(\omega(t), u) + \mu.f(\omega(t), u, x) \tag{2.3}$$

where t is a continuous variable, $\mu(t)$ is the co-state which is described by the Euler-Lagrange equation as:

$$\dot{\mu}(t) = -\frac{\partial}{\partial x}H \tag{2.4}$$

the function $f(.)$ depends on the SoC, which is dependent on the open-circuit voltage and internal resistance of the battery. However, this dependency can be neglected in the case of electric hybrid systems where only large deviation of the SoC can cause substantial variations of the internal battery parameters. Consequently, the co-state is assumed to be constant along an optimal trajectory. Therefore, the problem reduces to finding a constant value of the co-state (μ_o) for a given vehicle mission. The relationship between the μ_o and $SoC(t_f)$ is monotonous and μ_o is usually determined using iterations by correcting the previous estimation and the difference between the target SoC and actual SoC in each iteration. In the case with constant μ, a new meaning is acquired by the Hamiltonian function. Since the battery open-circuit voltage is constant under this assumption, both terms on the right-hand side of Equation 2.4 can be reduced to power terms:

$$P_H(t, u(t)) = P_f(\omega(t), u(t)) + \mu_s.P_e(\omega(t), u(t)) \tag{2.5}$$

In this equation, $P_f(\omega(t), u(t))$ is the power of the fuel and $P_e(\omega(t), u(t))$ is the battery electro-chemical power. The dimensionless scaling of the co-state is termed as equivalence factor μ_s and is defined as:

$$\mu_s = -\mu_o . \frac{H_{LHV}}{U_{OC} . Q_o} \tag{2.6}$$

The formulation in Equation 2.4 is called the Pontryagin's Minimum Principle and has been explored in the literature [Hou *et al.* 2014, Buie *et al.* 2004]. This method requires a priori knowledge of the driving cycle which is not the case in real driving missions. The workaround to this drawback are the causal methods represented by the equation in and are called the ECMS which are described in the following section.

Causal Methods In contrast to the offline methods, the online methods must be causal as they should not require a priori knowlegde of the driving cycle and resulting in suboptimal (hopefully near optimal) solutions. The online methods are real-time implementable with a limited computation time and memory. Three categories were identified by the authors in [Zhang *et al.* 2020] namely, instantaneous optimization-based EMSs (ioEMS), predictive EMSs (pEMS) and learning based EMSs (lEMS).

In the ioEMSs the power split is optimised by minimizing the instantaneous cost (fuel consumption and other performances) at each instant. In recent times ECMS and Adaptive Equivalent Consumption Minimisation Strategy (A-ECMS) are explored by many researchers. The ECMS shows promising but slightly sub-optimal results with a challenge of properly determining the equivalent factor (μ_s) [Tulpule *et al.* 2011]. The ECMS combined with the cycle prediction methods is the realisation of the Pontryagins Minimum Principle (PMP) in real time. The co-state in the PMP was estimated offline and was constant for a known driving mission. In contrast, the co-state in the ECMS is estimated online usually leading to a variable co-state. The uncertainty in the future driving conditions is curbed by correcting the value of the co-state in real time. The real-time control performance of an ECMS is heavily related to the equivalent factor. Therefore, a well tuned equivalent factor is essential to improve the performance of ECMS. The future power requirement and the current SoC are used to determine the equivalent factor. To determine a proper value of equivalent factor, A-ECMS is proposed which refreshes the control parameters according to the current and future power demand. There are several methods available in the literature regarding the online estimation of the co-state. The non-causality is addressed in the literature by taking advantage of the driving information [Payri *et al.* 2014]. To

recognise and predict future driving conditions, researchers propose different prdictive techniques, the authors in [Guardiola *et al.* 2013, Payri *et al.* 2012] use statistic and clustering techniques to classify the driving characteristics and Markov chain-based method are used to develop driving cycles based on previously recorded velocity profiles on a given route. Out of several methods available in literature Neural Network (NN)and Markov Chain (MC) based methods are most popular. In the article by the authors in [Xie *et al.* 2018], a comparison of the two approaches is shown in terms of prediction accuracy and computation speed.

The MPC is another option in predictive EMSs for an unknown driving mission. Compared with other EMSs, MPC is based on the system prediction information to obtain a rolling horizon optimization. The MPC is a receding horizon control strategy with a predictive scheme using three main steps. Firstly, over a prediction horizon the optimal inputs are calculated which minimise the objective function subject to the constraints. Then, from the calculated optimal inputs, the first element is implemented to the physical plant and finally, the entire prediction horizon is moved forward. This process is iterated from the first step. The MPCs are formalised in the literature in several ways to optimize the power split, such as hybrid MPC [Li & Goerges 2017], distributed MPC [Josevski & Abel 2016], variable horizon MPC [Cao *et al.* 2017]. In [Marx & Soffker 2012], the authors propose nonlinear MPC for energy management with an adaptive prediction time horizon. Another form of MPC is Stochastic Model Predictive Control (SMPC) and is proposed in [Li *et al.* 2016]. In this method, the distribution of driver's future power demand can be obtained and the MPC is adopted to obtain the optimal power split for a HEV bus commuting on a particular route.

2.3 Advanced Driving Assistance System (ADAS)

The research community has been traditionally more focused on the engine design including realistic driving conditions [Ortiz-Soto *et al.* 2012] or even close loop emissions control [Tschanz *et al.* 2013] than on the optimisation of vehicle operating conditions due to the intrinsically complex nature of this optimisation problem. The important research efforts have been focused on the development and integration of engine technologies aimed to improve fuel efficiency and emissions of light duty vehicles. Those efforts have materialised in important reductions in emissions and fuel consumption according to regulation cycles, however, their impact on real driving is limited [Pelkmans & Debal 2006, Weiss *et al.* 2011]. Amongst other reasons, the vehicle operating conditions play a major role in global efficiency and emissions, therefore,

differences between real driving and regulation cycles give rise to the usual fact that the actual consumption exceeds that from the vehicle specifications. Note the lack of controllability of the system since the driver manipulability is, at least, arguable, and it is evident that there are other factors affecting driving that are completely out of control (reactions of other drivers, weather,...). According to the US Environmental Protection Agency (EPA) and Natural Resources Canada (NRCan), there is up to 35% fuel economy difference between drivers in the same fleet of vehicles. Similar results are reported from a field experiment by Eaton Corporation, which reported 30% fuel economy difference amongst pick-up drivers. The difference in fuel consumption, pollutant emissions and trip duration of the vehicles commuting on the same route is majorly due to two reasons:

- Difference in the driver behaviour: On a given road condition (i.e. two hypothetical vehicles on a route at the same time and position but with different drivers), the two drivers are likely to act differently. The related line of research is focused on how the driver should behave to minimise fuel consumption and emissions. In [Ulleberg & Rundmo 2003], the authors conclude that the driver personality primarily influences the driving behaviour. The assessment of the impact of different driving styles on safety is based on the statistical analysis of the behaviour of several drivers while driving. The literature about the impact of driving behaviours on safety is available from past four decades [Cramton 1969], [Canale & Malan 2002], [BLOCKEY & HARTLEY 1995]. However, the impact of driving style on fuel consumption and emissions is a more recent topic and is addressed by the authors in [Ross 1994], [Tong *et al.* 2000], [Ping *et al.* 2019]. An aggressive driver is more likely to accelerate/decelerate the vehicle faster than an average driver. Such behaviour when cumulated for a driving mission results in difference in fuel consumption and emissions in the order of 30-35% [Verma *et al.* 2013]. Several publications address how to monitor the driver behaviour and promote Eco-Driving. An example of such a tool is presented by [Vagg *et al.* 2013] where, they propose to encourage economical driving behaviour by giving feedback to the driver with a light code showing his driving aggressiveness (product of velocity and acceleration), since an aggressive driving style will naturally lead to higher fuel consumption. A similar approach is presented and evaluated in [Larsson & Ericsson 2009].

- Difference in the speed profiles due to randomness in traffic situation: A vehicle on the same route at different times consume different amount of fuel, emits different amount of pollutant emissions and covers the same

distance in different time. A vehicle commuting on the same route will have different velocity profiles due on the traffic situation. The traffic situation is largely dependent on two factors: Static environmental factors and dynamics conditions of the traffic. In static environment there are lanes, intersection, position and timings of the traffic light signals. The dynamic traffic conditions are largely due to the intensity of the traffic and randomness arising due to the real time traffic situation.

The improvement of computation capabilities, the introduction of Optimal Control in powertrain management and the increase of cost-effective sensors and information sources (Global Positioning System (GPS), V2V, V2I, ...) have lead to an intensive research activity in the assisted driving techniques. The rapid progress in intelligent transportation systems has significantly increased availability of traffic information that can be integrated to the vehicle control system for reducing the impact of randomness in driving on fuel consumption, pollutant emissions and travel time.

Traditionally, an Advanced Driving Assistance System (ADAS) tracks and utilizes information (such as vehicle location, distance of the objects to the driver, lane detection, etc.) so as to allow a vehicle to drive more safely. The research on ADAS can be broadly classified into two categories: The passive assistance systems that act as a feedback advisory to the driver. The active assistance systems where, driving is automated to some extent such as adaptive cruise control and vehicle collision avoidance where the driver is operating exclusively without any dependence to these systems. The new developments are into using ADAS as a tool for promoting Eco-Driving (ED) either passively or actively. ED is a way to optimise the velocity profile, with the aim of reducing the fuel consumption [Ozatay *et al.* 2014b, Ozatay *et al.* 2014c, Sciarretta *et al.* 2015a] in actual driving. The driving advisory systems provide velocity and acceleration recommendations that take travel time, fuel consumption and emissions into account using the route and the traffic light schedule information. The integration of the route and traffic information such as the position of nearby vehicles, timing and positioning of the traffic signal at the intersections [Rakha & Kamalanathsharma 2011, Yang *et al.* 2020], road grade[Bakibillah *et al.* 2018], route maps [Minett *et al.* 2011], etc. into the cruise control systems to reduce the overall energy consumption are the popular research topics. A study on freeway-based eco-driving systems showed fuel savings of the order of 10-20 % when real-time signals were used [Barth & Boriboonsomsin 2009]. For this reason ED is a hot topic in the automotive control sector that has been approached during the last decades with different methods, e.g. in [Li *et al.* 2011] with MPC, in [Stanger & del Re 2013] by using look-ahead information or [Naranjo *et al.* 2003] with

fuzzy-logic controllers.

Other than ED, Vehicle Platooning is another application of cruise control which allows vehicle platoons with optimal inter vehicle distances. This highly increases the roadway capacity, while the energy consumption is reduced due to the reduction of aerodynamic drags and unnecessary speed fluctuations. On several occasions, research work has proven the approach in simulations [Milanes *et al.* 2014, van Arem *et al.* 2006, Fernandes & Nunes 2012], relatively few of them have conducted experiments to prove their strategy [Kianfar *et al.* 2012, Ploeg *et al.* 2014, Englund *et al.* 2016]. In [Tsugawa *et al.* 2011], the authors show that Platooning of 10m gap at 80km/h can reduce energy by about 15% (measurement) by the aerodynamic drag reduction, and CO_2 by 2.1% along an expressway (simulation) when the 40 % penetration in heavy trucks by the roadway capacity increase. In the present thesis, the applications developed were related to the ED and the following subsection describes the SOA of cruise control and ED.

2.3.1 Cruise Control and Eco-Driving

The automatic speed control for vehicles was introduced by Wolfe et al. in [George F Wolfe 1938]. The objective of the invention was to indicate the driver through a resistance to the movement of the acceleration pedal that a pre-determined speed of the vehicle has been reached. In 1950, Teetor [Teetor 1950] invented the modern speed control device for resisting the operation of the accelerator. The first car Imperial, that implemented Teetor's system was in 1958. In 1965, American Motors corporation introduced a an automatic speed control system. Soon in 1968, Radio Corporation of America introduced the automotive cruise control system. Since then, the automotive car industry has been developing advanced Cruise Control Systems in order to improve the performance measured in terms of driving comfort, driving safety and fuel efficiency. Modern cruise control is not limited to maintaining a desired vehicle driving speed, but it also incorporates the communication of the vehicle with the infrastructure and the other vehicles in order to improve the degree-of-freedom. All the information is used to improve the performance and such systems are termed as cooperative adaptive cruise control systems in the literature. [Li *et al.* 2011, Bu *et al.* 2010, Ploeg *et al.* 2011]. This line of study is aimed to obtain a vehicle speed profile to minimise fuel consumption on a given route. This is a problem that matches the field of OC. In fact, OC has been applied to the speed profile optimization since 1977 in the work of [Schwarzkopf & Leipnik 1977], who calculated the optimal speed profile on a hill. From then on, and specially during the last decade, several OC techniques have been applied to the vehicle speed trajectory optimization at different

scenarios. Some of these approaches are PMP in [Fröberg *et al.* 2006, Petit *et al.* 2011, Sciarretta *et al.* 2015b], DP in [Hellström *et al.* 2009, Hellström *et al.* 2010b, Ozatay *et al.* 2014a] and Direct Methods (DM) in [Saboohi & Farzaneh 2009, Reig 2017]. Due to the complexity of reproducing real driving conditions, most of them focus on particular driving conditions (highway, traffic lights, ...) and address this topic from a modelling perspective. A comprehensive review of them can be found in [Sciarretta & Vahidi 2020b]. In addition, few of the previous studies include the report of the optimal vehicle speed profile to the driver and the assessment of their impact on the fuel consumption. An example of such study is [Ozatay *et al.* 2014a] where, authors propose a cloud-based optimization of the vehicle speed profile by DP that is downloaded in the vehicle for a given route.

In this work the ED techniques are explored in line with the research in [Hooker 1988]. Hooker et. al show, how the vehicle speed profile can be responsible for up to 30% of the fuel consumption. Other studies [Passenberg *et al.* 2009] point out that ED can reduce fuel consumption by about 5% compared to standard driving . OC theory is explored in the literature to address the problem of finding the optimal velocity profile on several occasions. The cost involved in such a problem formulation is generally in the form of minimising a function from intial to final time:

$$Q_f = \int_{t_i}^{t_f} q_f(v(t), a(t))\ dt \tag{2.7}$$

where, q_f is the fuelling rate, $v(t)$ is the vehicle velocity, $a(t)$ is the vehicle acceleration. The goal of the optimisation is to find the speed trajectory $v(t)$ that minimises the cost index in Equation 2.7. In the literature, there are several advanced methods like Model Predictive Control [Li *et al.* 2011, Stanger & del Re 2013, Bageshwar *et al.* 2004], Stochastic Dynamic Programming [Weißmann *et al.* 2018, Johannesson *et al.* 2007], etc to solve the above problem. Apart from the main objective there are other constraints that are required to be taken into account while solving the OCP:

- The ego vehicle must not crash with any vehicle and therefore a minimum inter vehicle distance is required to be maintained.
- The ego vehicle must also adhere the traffic rules i.e. stoping at red traffic lights, safe lane change, maximum permissible speed etc.
- The powertrain related limitations must also be taken into account.
- The driving comfort which is acceptable by a human driver must also be ensured at all time.

Combining all these essential requirements turns the OCP into a non-linear optimisation problem within prediction horizon subject to the dynamic and non-linear constraints.

Part II

Theoretical Tools

Chapter 3

Vehicle Model

Contents

The vehicle velocity and acceleration of vehicle motion in the plane can be calculated by applying Newton's equations by balancing forces and momentum. The main external forces on the vehicle are balanced with the vehicle inertial forces in the longitudinal, lateral and the vertical axis. However, including the lateral vehicle dynamics largely increase the model complexity with limited effect on the vehicle performance in terms of fuel economy and emissions. As the scope of this thesis is limited to the evaluation of the fuel consumption and emissions, the lateral forces are not included in the developed vehicle dynamic model. A straight road was considered and regarded as a smooth surface with no vibrations from the road generating vertical displacement in the cabin. Usually, there are two main philosophies used to model the vehicle powertrain: the backward modelling approach (or vehicle driven or non-causal) and the forward modelling approach (or driver driven or causal) as shown in Figure 3.1.

In a forward-looking model, in order to follow the desired vehicle speed trace, the accelerator or brake pedal signals are sent from the driver model

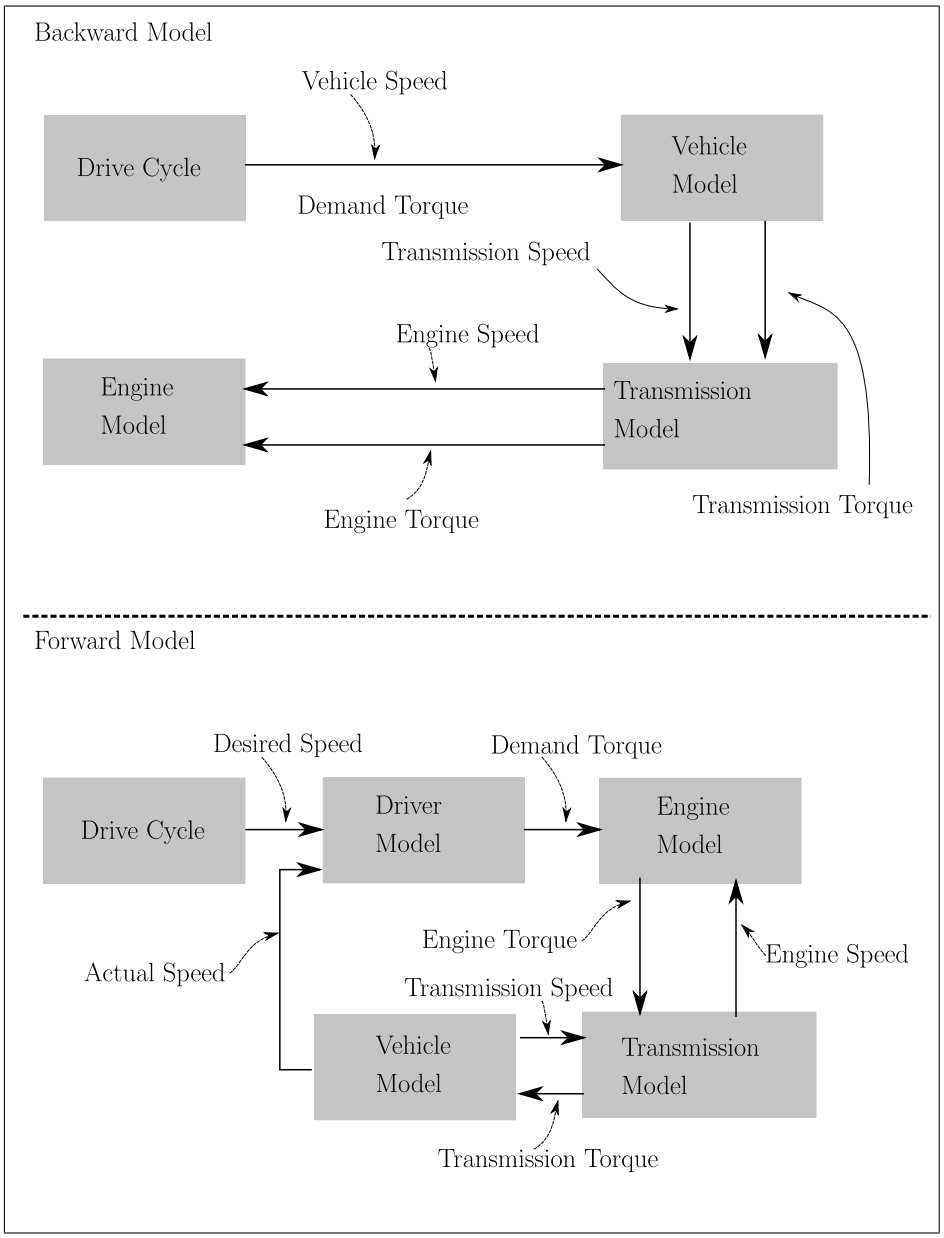

Figure 3.1: Scheme of longitudinal forces acting on a vehicle.

to the different powertrain component controllers (throttle for engine, displacement for clutch, gear number for transmission, or mechanical braking for wheels). The driver model controls the acceleration signal (usually a PI type controllers) depending upon the error between the desired and the actual speed profile. As components are reactive to the commands as in real world, advanced component models are implemented, taking into account transient effects (such as engine starting, clutch engagement/disengagement, etc.). Hence, the developer can design realistic control strategies. By contrast, in a backward-looking model, the desired vehicle speed is imposed to calculate the engine speed and finally, find out the operating conditions of each component in order to follow the desired cycle speed. Due to this model organization, only quasi-static models can be used without being able to realise the control dynamics and therefore transient effects can not be taken into account. The backward modelling approach is useful to define trends while forward looking approach is used for selection of powertrain configurations and control development. Due to inherent time delay in forward approach, backward approaches are more suitable for solving the optimisation problem. During the development of this thesis, both the philosophies were used depending on the requirement of the application. This chapter describes the modelling techniques of the components that were used during the work. It contains six section- The first section describes the longitudinal model of the vehicle and the following sections are regarding the modelling technique of the relevant components.

3.1 Longitudinal Vehicle Dynamics

The longitudinal vehicle dynamics model is based on the dynamics of the vehicle that generate forward motion. Figure 3.2, shows the set of forces acting on a typical vehicle longitudinal motion on an inclined road.
The non-conservative forces related with friction are represented by aerodynamic drag (F_a) and rolling resistance (F_r). The aerodynamic forces depend on the vehicle shape and influence the vehicle motion in six degrees of freedom. However, for a standard passenger vehicle, aerodynamic resistance has the major influence on the vehicle dynamics. This is in line with the simplification required for studying the longitudinal dynamics. The aerodynamic drag depends on the vehicle's frontal area A, the drag coefficient C_d and the vehicle speed (v). There are two causes of the aerodynamic resistance acting on the vehicle in motion: the first is the viscous friction by the surrounding air on the vehicle surface. On the other hand, the pressure difference between the front and the rear of the vehicle resulting in the separation of the air flow.

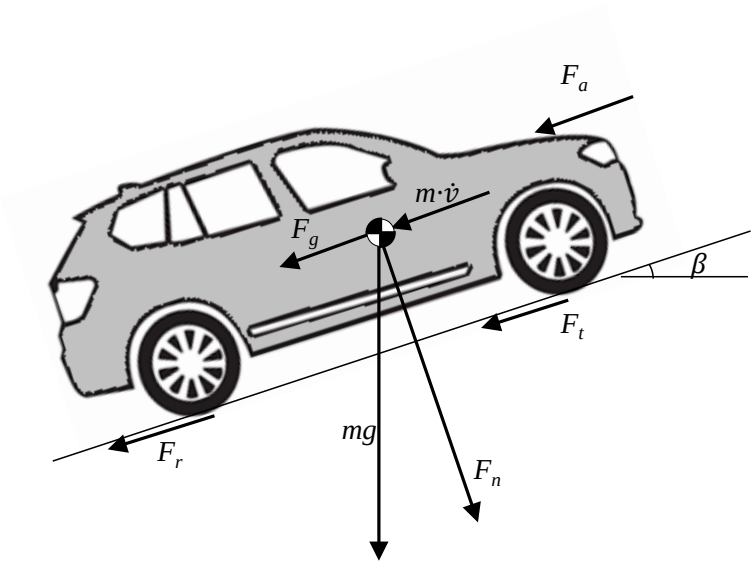

Figure 3.2: Scheme of longitudinal forces acting on a vehicle.

A detailed analysis of particular effects is only possible with specific measurements in a wind tunnel. Usually, the vehicle is simplified to be prismatic body to model the aerodynamic resistance force and Equation 3.1 is used to calculate the force.

$$F_a = \frac{1}{2} A C_d \rho v^2 \tag{3.1}$$

The force, that resists the motion of the tire on the road also called the rolling resistance is calculated by Equation 3.2:

$$F_r = \mu m_v g cos\beta \tag{3.2}$$

where μ is a friction coefficient, dependent on the tyre-tarmac contact, and therefore difficult to evaluate accurately. The most important influencing quantities are vehicle speed , tire pressure and road surface conditions while the rolling friction coefficient may be assumed to be constant. Generally, the coefficient is assumed to be in the range of 0.01 to 0.015 for light duty vehicles. Regarding the rest of parameters, m_v is an equivalent vehicle mass accounting for the vehicle mass but also for the inertia of the powertrain rotating parts. The inertia of the rotating masses (wheel and transmissions) of the powertrain can be taken into account in the respective sub-models. g is the gravity constant and β represents the road grade, that also leads to a force against the vehicle advance when it climbs (F_g) which expression is:

$$F_g = m_v g sin\beta \tag{3.3}$$

Note that the energy required to overcome F_g when the vehicle is climbing can be theoretically recovered when going downhill to the initial position. Finally,

the traction force comes ultimately from the engine torque or from the brakes, then:

$$F_t = \begin{cases} \frac{\eta_t(u_{gb}) M_{eng}(n_{eng}, u_{pedal})}{r_w R_t(u_{gb})} & \text{if } u_{pedal} > 0 \\ u_{pedal} \hat{F}_b & \text{otherwise} \end{cases} \tag{3.4}$$

where M_{eng} is a non-linear function depending on the engine speed (n_{eng}) and pedal (u_{pedal}) representing engine torque, in the case at hand a map based on experimental data. This torque is transferred to the wheels by means of the transmission, which efficiency (η_t) and ratio (R_t) depend on the selected gear (u_{gb}). Particularly, in the current model, both η_t and R_t are affine functions of u_{gb}. The wheel radius necessary to pass from torque to force is represented by r_w. Finally, a simple force balance leads to the following ordinary differential equation:

$$\dot{v} = \frac{1}{m_v}.(F_t(t) - (F_a(t) + F_r(t) + F_g(t))) \tag{3.5}$$

which is the main equation of the vehicle longitudinal dynamics. The integration provides the instanteneous vehicle speed making it a forward modelling approach. While the parameters in Equation 3.1 to Equation 3.4 can be obtained experimentally or estimated from literature, Equation 3.5 allows tracking the velocity evolution as a function of an initial state, the driver actuation (u_{pedal}, u_{gb}) and problem perturbations such as the road grade. It must also be noticed that all the forces do not act at the centre of mass of the vehicle which, produce moment and a variation on the pitch. However,these moments are assumed to be cancelled by the reaction to the normal force on the point of contact between the tires and the road.

When braking, the force applied to the wheels is proportional to a maximum braking force ($\hat{F}_b$) through variable u_{pedal}. For the sake of model simplicity, both throttle and braking pedals (u_{pedal} and u_b) are modelled with a single variable (u_{pedal}) ranging from -1 to 1. This assumption involves that situations where both pedals are actuated at the same time cannot be modelled. The clutch is not modelled, so the potential losses in this element during normal operation should be included in η_t while slipping during gear change is neglected. In order to reduce the number of actuators of the model, the braking and throttle actions (u_b and u_{pedal}) have been lumped in a single actuator (u) such that:

$$u_{pedal} = \begin{cases} u & \text{if } u_{pedal} \geq 0 \\ 0 & \text{if } u_{pedal} < 0 \end{cases} \tag{3.6}$$

$$u_b = \begin{cases} 0 & \text{if } u_{pedal} \geq 0 \\ u & \text{if } u_{pedal} < 0 \end{cases} \tag{3.7}$$

In this sense, analysing Equation 3.6 to Equation 3.7 one can observe that the model has single state (v) and actuator (u) since the gear shift follows a predefined policy depending on the engine speed, and accordingly on the vehicle speed. In the following section the powertrain models developed during this thesis are presented.

3.2 Gear Box

In a conventional vehicle, the internal combustion engine is used to meet the power demanded by the driver. The transmission of power from the engine to the wheels passes through gearbox and clutch. Assuming zero losses at the clutch, gearbox is modelled as a discrete set of gear ratios with a fixed efficiency. The torque and the angular speed required at the gearbox output are calculated based on the following equations:

$$\omega_W = \frac{v}{r_W} \tag{3.8}$$

$$\dot{\omega}_W = \frac{\dot{v}}{r_W} \tag{3.9}$$

$$\tag{3.10}$$

$$T_W = \begin{cases} r_W.F_t, & \text{if } v > 0 \\ 0, & \text{if } v = 0 \end{cases}$$

The parameter r_W is the wheel radius, T_W the torque at the wheel. The wheel inertia and constant torque loss is neglected. The gearbox is modelled as the transmission ratios with constant efficiencies. The speed and torque required at the gearbox input to satisfy the demanded speed and torque at the wheel are calculated by

$$\omega_g = \nu_g(g_b).\omega_W \tag{3.11}$$

$$\dot{\omega}_g = \nu_g(g_b).\dot{\omega}_W \tag{3.12}$$

$$\tag{3.13}$$

$$T_g = \begin{cases} \frac{T_W}{\eta_g.\nu_g(g_b)}, & \text{if } T_W \geq 0 \\ \frac{T_W.\eta_g}{\nu_g(g_b)}, & \text{if } T_W < 0 \end{cases}$$

Where ω_g is the angular speed input to the gear box, ω_W is the angular speed of the wheels, $\dot{\omega}_g$ is the angular acceleration input to the gearbox, $\dot{\omega}_W$ is the angular acceleration of the wheels, g_b is the selected gear number and

$\nu_g(g_b)$ the corresponding transmission ratio. T_g is the torque input to the gearbox. The ICE torque include inertial terms which is a product of the angular acceleration and the required torque.

3.3 Internal Combustion Engine

The design of an ICE model is usually driven from the application requirements. In the present work, there are two type of applications that are being studied: the first type of applications are regarding the control of an internal combustion engine for maximum fuel efficiency and emission reduction in real driving missions. These applications require an engine model that is capable of predicting the trends in fuel consumption and emissions responding to the variations in engine operating points (ω_e, $\mathrm{T_e}$) and a few engine actuators (such as $u_{vgt}, u_{egr}, u_{soi}$ etc..). The second kind of applications, obtain an optimal speed trajectory of a vehicle on a real driving mission. Wherein the engine calibration is fixed and does not require access. The only actuator, controller has an access to is the throttle position u_{pedal} and therefore an even more simplistic engine model is applicable. The two aforementioned engine model types are described in the following paragraphs:

Type 1 In this type of engine models, the fuel consumption and engine out emissions are modelled at each operating point using static response models. The following three steps are carried out to obtain the engine response models.

- At first, the steady-state measurements are carried out at the engine test-bench. The desired control inputs are varied at each operating point and the desired torque is obtained by controlling the fuel injection quantity. The feasible range of control inputs is explored at each operating point. Usually Design-of-Experiment (DOE) technique is used to reduce the number of tests required for the purpose of building the engine response models. In this thesis a full factorial DOE technique was used. One of such measurement campaign was conducted for the operating points shown in Figure 3.3, the black dot represent the points tested during the campaign and black line is the limiting torque.

- After completing the measurement, point-by-point models (which is also referred to as steady-state model) are created, and they are interpolated using appropriate method. These models are capable of predicting the effect of the input variables on the output variables.

- The prediction capability of the model is validated experimentally at the operating points which were not included during the model creation.

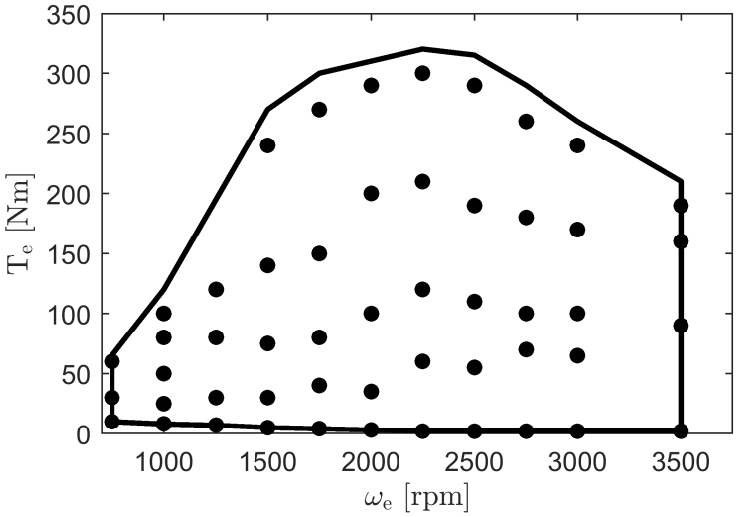

Figure 3.3: Engine operating points measured during the testing campaign, the black line is the limiting torque for the engine

The comparison of the predicted values with measured data provides an insight on the model quality. In Figure 3.4 and Figure 3.5 the black dots represent the measurement points used for model creation. The point represented by the cross are the validation point and the surface is approximated model for fuel consumption and NO_x emission as a function of start-of-injection and burned gas ratio. The model validation is carried out by simulating the engine model at several steady-state operating points. The results Root Mean Square Error(RMSE) is presented in Figure 3.6, which shows 5% and 10% RMSE in fuel consumption and NO_x emission respectively.

Type 2 In the vehicle speed optimisation problems when the engine calibration is fixed, the fuel and the NO_x emissions are modelled as maps depending on the throttle position. In this sense, in the vehicle model, the engine torque, the fuel consumption and NO_x emissions are calculated by simple interpolation of experimental data as a function of engine speed (n_{eng}) and load (u_{pedal}). The corresponding maps shown in Figure 3.7 have been obtained experimentally in the chassis dynamometer. Note that, in line with other works in the literature [Guzzella & Sciarretta 2005], the engine dynamics are completely neglected, the main reasons for such a simplification are:

- A detailed engine model including dynamics substantially increases the

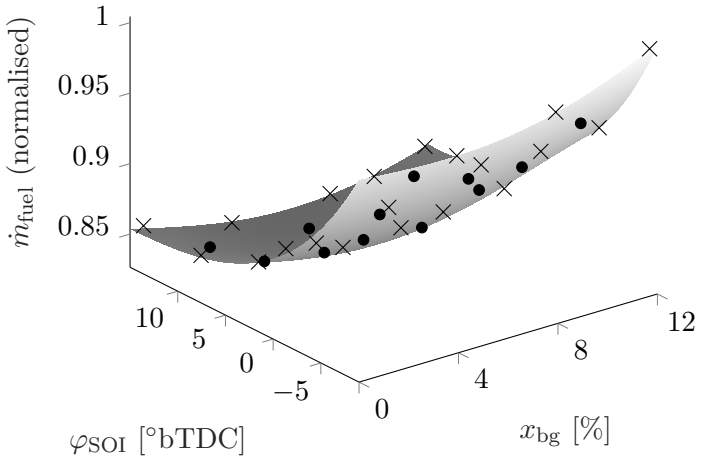

Figure 3.4: Local model of Fuel consumption at 1800 rpm and 200Nm. The x-axis represents timing of start of injection before the top dead centre in degrees. On the y axis there is burnt gas ratio, in the z axis there is normalised rate of fuel injected

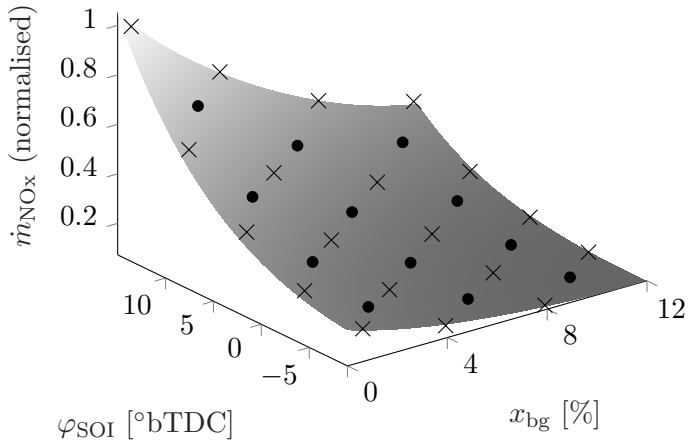

Figure 3.5: Local model of NO_x at 1800 rpm and 200Nm.The x-axis represents timing of start of injection before the top dead centre in degrees. On the y axis there is burnt gas ratio, in the z axis there is normalised rate of fuel injected

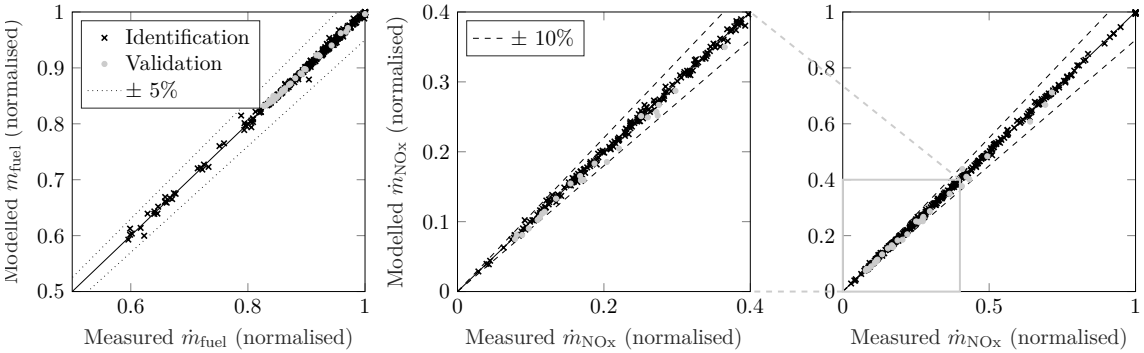

Figure 3.6: Validation results of the engine steady state model

complexity of optimisation problem with its corresponding increase in computational time.

- Vehicle dynamics are much slower than the main engine dynamics specially when efficient driving is foreseen and transients are minimised.

The model simplification should not impact much the ability to capture the plant behaviour. The Figure 3.8 shows the correlation between the fuel consumed in the tested driving cycles, circles represent driving cycles with arbitrary driving to identify the model and black bullets show the model validation. Despite the simplicity of the model, the results show a correlation of $R^2 = 87\%$ and differences in the fuel consumption at the end of the cycle are below 0.16l/100km for 80% of the driving cycles considered. In particular, for the validation set (black dots), the maximum error is below 0.15l/100km.

3.4 HEV architecture

A pHEV has been chosen to show the potential of the control strategy while the method can be adapted to deal with other powertrain types (series, series-parallel, charge sustaining,...). In this architecture, i.e parallel arrangement ,the vehicle can be driven by the ICE, the Electric Motor (EM), or both simultaneously. Thus, there are different solutions to provide the power required by the driver with different costs and impacts in future operation, which poses an interesting optimization problem. The battery is charged either by an external power source, by the ICE or by regenerative braking through the EM. The main characteristics of the vehicle considered in the present thesis are shown in Table 3.1, while the layout and main energy flows in the powertrain are shown in Figure 3.9.

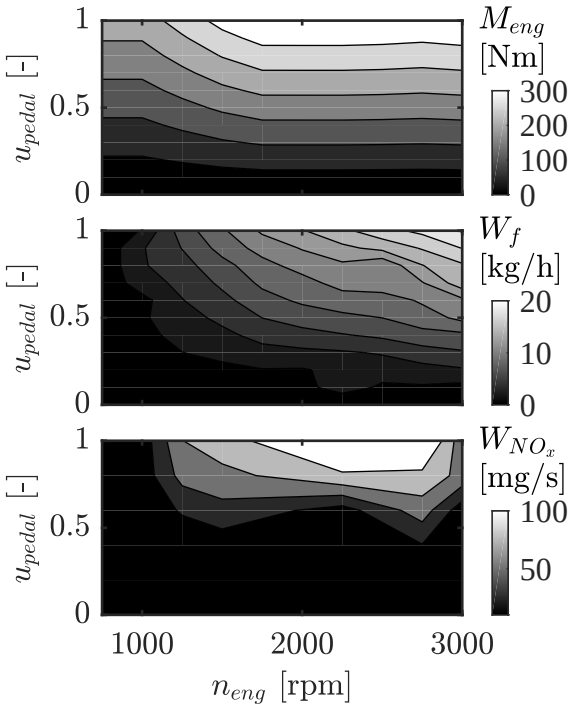

Figure 3.7: Experimental engine maps for torque (M_{eng} in upper plot), fuel consumption (W_f in medium plot) and NO_x emissions (NO_x in lower plot) used as quasi-steady engine model.

Table 3.1: Description of the main vehicle features

Vehicle mass	2120 kg
Engine power	98 kW
Motor power	24.5 kW
Battery power	59 kW
Battery energy capacity	0.0432 MJ
Number of gears	6

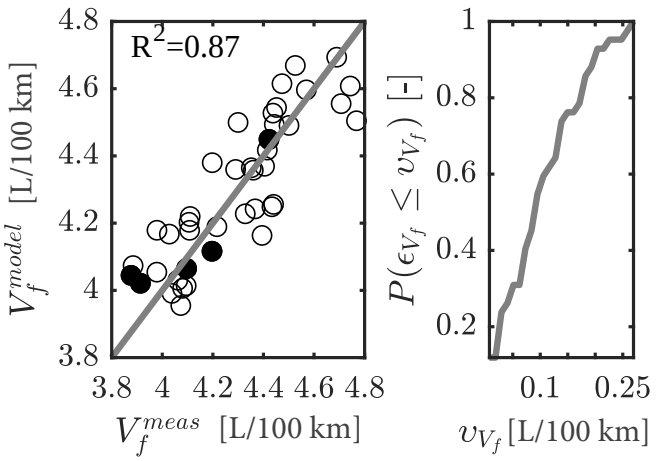

Figure 3.8: Vehicle model performance. Left: comparison between measured and modelled fuel consumption during the set of driving cycles tested. Right: Percentage of cycles with modelling error (ε_{V_f}) below certain limit ν_{V_f}.

The aim of developing HEV model in this thesis is to support the development of control algorithm which manages its power flow. The engine is modelled as a quasi-static subsystem whose inputs are the desired torque and engine speed with fuel flow as the output. The torque generation dynamics are fast and hence negligible. The energy management is performed at a much slower rate than the torque control. Accordingly, the engine is also modelled as quasi-steady maps with limits over the torque. The maps are presented in Figure 3.10. The first plot represents the engine efficiency map with respect to the engine speed and the torque and the second plot presents the ICE operating region with minimum and maximum power with respect to the engine speed.

3.5 Electric Motor

In Figure 3.9, the parallel architecture of the HEV is presented. The power sources are the battery and the internal combustion engine. They can together or individually propel the vehicle through the driveline that constitutes a torque coupler and a gearbox(GB). The energy can be recuperated in the battery during vehicle deceleration.

The power split device manage the supply of energy to the wheels by splitting the power demand between the electric motor and the internal combustion engine. The design of power splitter is not in the scope of this thesis however, the study is focused on how the power is been split. In particular, the

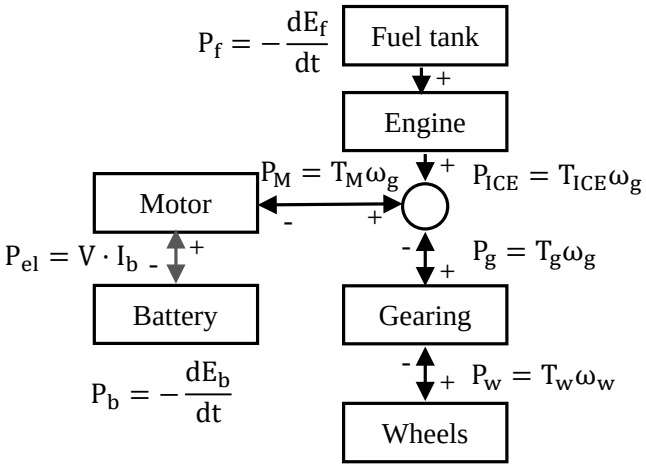

Figure 3.9: Layout of a parallel HEV

thesis proposes a novel energy management strategy for a pHEV architecture. The electric motors are assumed to have fast dynamics and it generates the requested torque while respecting the maximum torque limtis. The implementation of the electric motor require efficiency maps along with the limit maps based on the angular speed. The maps are presented in Figure 3.12. The first plot shows the variation in motor efficiency with respect to the motor speed and the torque. The second plot represent the operating zone of the motor with limits over the motor power with respect to the motor speed.

3.6 Power- coupling device in pHEV

The most critical system design for hybrid vehicle performance is its transmission system. The objective of the vehicle transmission system is to maintain power units to provide suitable traction power under various working conditions while operating under high efficiency. The torque coupling mechanism as shown in Figure 3.9, is crucial component in the hybrid propulsion system. This mechanism integrates the input mechanical power from two independent sources into output mechanical power within its physical constraints. In this thesis, the system is considered 100% efficient assuming the same power flows in and out of the system. In the particular parallel architecture used in this thesis and shown in Figure 3.9, the torque demanded can be satisfied by the linear superimposition of two input torques as shown below.

$$T_g = T_{ICE} + T_{EM} \tag{3.14}$$

The angular velocity of each port cannot be independently controlled be-

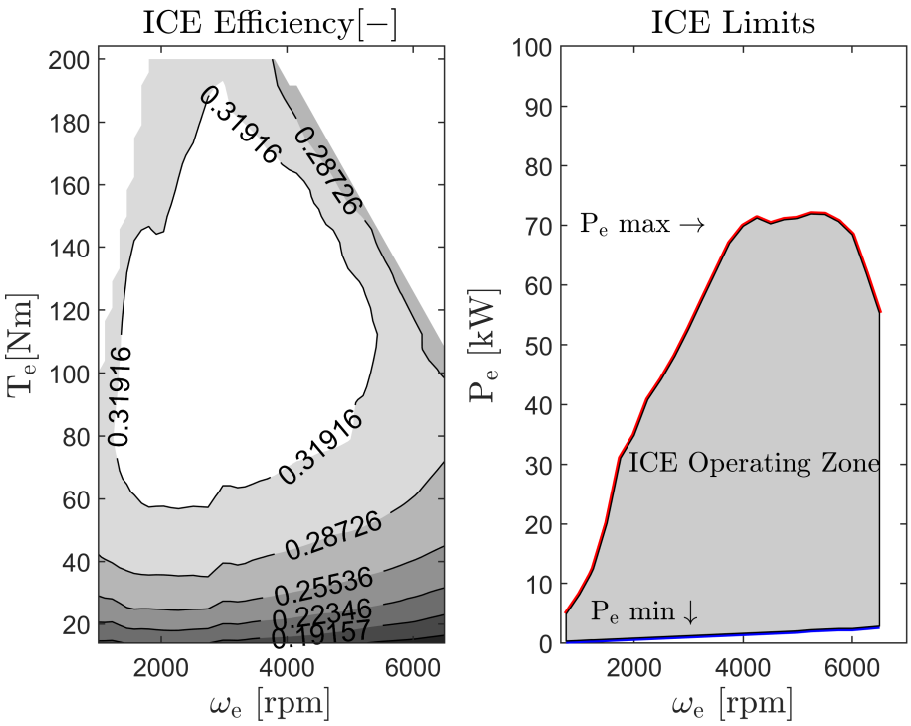

Figure 3.10: ICE Model

cause both motor and ICE are coupled to the same axis. Therefore, the angular velocity constraint can be expressed as:

$$\omega_g = \omega_{ICE} = \omega_{EM} \tag{3.15}$$

3.7 Battery

To simulate the behavior of an HEV, a battery model is required to evaluate the output voltage considerations to the battery SoC. A battery pack is usually obtained by connecting several cells in series and therefore a numerical model is developed considering one single cell. On the similar line, in this thesis, the battery pack is modelled as single cell following the Thevenin equivalent circuit of the battery pack presented in Figure 3.12. A simple model is used to obtain terminal voltage of the battery as follows

$$V_b = V_{OC} + R.I_b \tag{3.16}$$

$$P_b = V_b.I_b \tag{3.17}$$

Where V_b is the battery voltage, V_{OC} is the battery open circuit voltage. R is the internal resistance of the battery depending on the SoC and I_b is

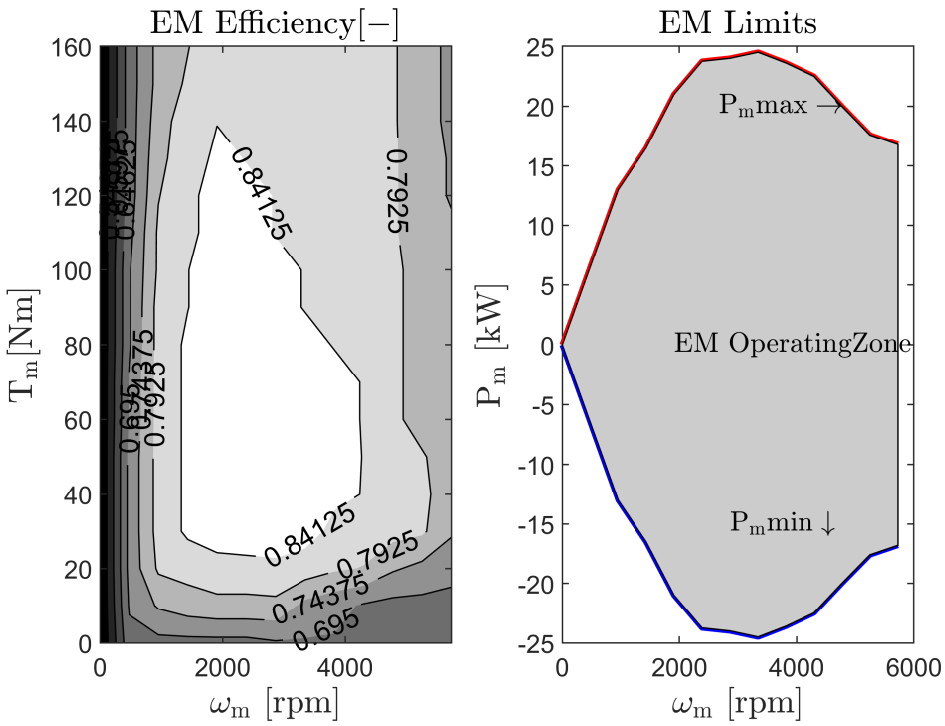

Figure 3.11: Electric motor model. The maximum efficiency is 0.92 at 2300 rpm and 60Nm.

the battery current. The backward model is solved for battery current as a function of power used to charge or discharge the battery. This lead to the following equation:

$$I_b = \frac{V_{OC} - \sqrt{V_{OC}^2 - 4.R.P_b}}{2.R} \tag{3.18}$$

$$\dot{SoC} = -\frac{I_b}{C_b} \tag{3.19}$$

with C_b the battery capacity. Using the manufacturer charge and discharge charts, it is possible to reconstruct the map of V_{OC} and of internal resistance R depending on the state of charge and temperature. However, this thesis simplifies the model further to consider the temperature constant and consequently to calculate and to represent on a map the as a function of the battery SoC and the battery current.

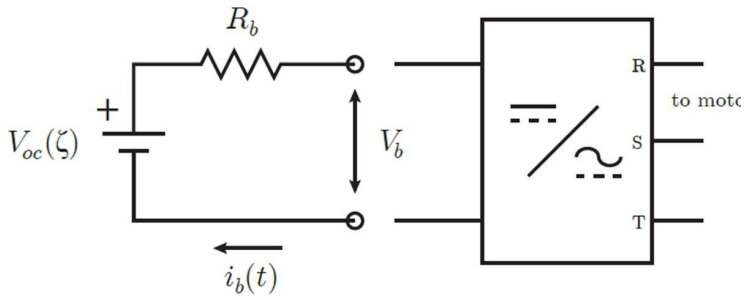

Figure 3.12: Simplified battery Model

Chapter 4

Optimisation tool

Contents

In an optimal control problem, the trajectories of the control variables u of a dynamic system f are calculated for minising a cost index. The cost index is quantifiable, such as energy consumption, time, etc. The state of the dynamic system is driven by the differential equation given by:

$$\dot{x} = f(x, u, t) \tag{4.1}$$

where, x represent the state and t is the time dependence.

There are two optimisation techniques that were the basis of the online control methods explored during the development of this thesis: Dynamic programming and Pontryagins Minimum Principle. The intention of this section is not to describe them in detail, but to provide insight in some ideas that are used in the thesis.

4.1 Dynamic Programming and its Application

The DP was originally developed by Richard Bellman [Bellman 1970], who stated that an optimal policy has the property that, whatever the initial state and initial decision are, the remaining decisions must constitute an optimal policy with regard to the state resulting from the first decision. This means that the problem can be broken into sub-problems of lower size which are to

be optimised separately. Given that a start and final state is defined combining the optimal solutions of each sub-problem the solution of the overall problem can be constructed. By using the dynamic programming an optimal control input is found such that a pre-defined cost function is minimised while handling multiple constraints on the system states and the control inputs. In DP problems the following discrete-time dynamic system is considered by the authors in [Guzzella & Sciarretta 2005]:

$$x_{k+1} = f(x_k, u_k, w_k), \ k = 0, 1, ...N - 1. \tag{4.2}$$

where, x_k are the dynamic states, u_k are the control inputs and w_k are the disturbances which are discretised in time and value. The control inputs u_k is a function of state x_k and w_k is known for all k. A control sequence is denoted by $u = \{u_0, u_1, ..., u_{N-1}\}$, and the cost associated with it on the problem 4.2 is defined by the following equation. Note that the initial condition is assumed to be x_0.

$$J_u(x_0) = g_N(x_N) + \sum_{k=0}^{N-1} g_k(x_k, u_k(x_k)) \tag{4.3}$$

The optimal trajectory $u^* = \{u_0^*, u_1^*, ..., u_{N-1}\}$ is the trajectory that minimizes J_u. Let us assume that when using u^* a given state x_t is reached at time t. Now consider the optimization problem with the initial condition x_t at time t and the cost-to-go E from time t to N is defined by

$$E\{g_N(x_0) + \sum_{k=t}^{N-1} g_k(x_k, u_k(x_k), w_k)\} \tag{4.4}$$

Then the truncated policy $u^*(x_t) = u_t^*, u_{t+1}^*, u_{t+2}^*, u_{t+3}^*..., u_{N-1}^*$ is optimal for this new problem.

$$J_k(x_k) = \min_{u_k}\{g_k(x_k, u_k) + J_{k+1}(f_k(x_k, u_k))\} \tag{4.5}$$

then, if $u_k^* = u_k^*(x_k)$ minimised the right side of the above equation for each x_k and k, the policy u^* is optimal.

The above formulation results in an optimal solution however, the complexity of the programming algorithm is exponentially realted to the number of states and the control inputs. This limits the usage of the algorithm for lower order problems. During the implementation of DP algorithm the higher discretization of state and input spaces in a continuous application yield more accurate solution requiring high computational time. The computational requirement is substantially reduced by using the set implementation of the DP

Algorithm 1 Calculate Optimal u_s^*

for k =N-1 to 1 **do**
  $[x_{k+1}G] \leftarrow F(X_{grid}, U_{grid}, k, ...)$
  $J_k \leftarrow G + V(x_{k+1}, k+1)$
  $J(t_x, k) \leftarrow min\ J_k$
  $u(t_x, k) \leftarrow argmin\ J_k$

algorithm. Where, instead of using the standard for-loops for every state, every input variable and time the following algorithms are used as follows.

The formulation of DP is presented below using a simple application. A frictionless ball starts from rest to cover a short distance of 3 meters in a maximum time of 4 seconds. The objective is to find the best speed profile minimising acceleration which is inherently related to the energy needed to move the ball from the starting to the ending point. The constraints are regarding the maximum speed v_{max} and minimum v_{min} and acceleration limits u_{min} and u_{max}. Considering speed (v) and distance (l) as system states, their dynamics are governed by the equation of motion as follows:

$$\begin{aligned} \dot{l} &= v \\ \dot{v} &= u \end{aligned} \tag{4.6}$$

The cost to go is modeled as J:

$$J(u) = \sum_{t=0}^{T} (1 + |u|) \tag{4.7}$$

while the control inputs are limited to discrete valeus of u:

$$u \in [-1, 0, 1]\ m/s^2 \tag{4.8}$$

with some constraints on distance and velocity:

$$\begin{aligned} l_0 &= 0 \\ l_{end} &= 3 \\ v_0 &= 0 \\ v_{end} &= 0 \\ l_{min} \leq l &\leq l_{max} \\ v_{min} \leq v &\leq v_{max} \end{aligned} \tag{4.9}$$

Where l_{min} and l_{max} are 0 and 3 m respectively. v_{min} and v_{max} are 0 and 3 m/s respectively.

To solve this problem using dynamic programming we move systematically from one side to the other as described in algorithm 1. Suppose that we move backward from right to left. At the last intersection at 4 s there is no decision to make. The first decision is made at 3 s. At this time the ball should have covered 2m and must be at 1m/s as shown in figure 4.1. The optimal cost-to-go with respect to two states at each time step is presented in the first column plots of figure 4.2. Clearly, the corresponding optimal control input at 4s is u = -1 m/s as shown in the second columns plots. Which implies that the optimal strategy is to decelerate the vehicle to rest. As we move leftwards at 2 s in 4.1, the optimal acceleration presented moving upwards in figure 4.2 is 0 m/s^2 while maintaining constant velocity of 1 m/s. Further left at 1 s, the optimal acceleration is still 0 while maintaining the speed at 1 m/s. Finally at 0 s, the vehicle should acclerate at 1 m/s^2 to go from 0 to 1 m/s.

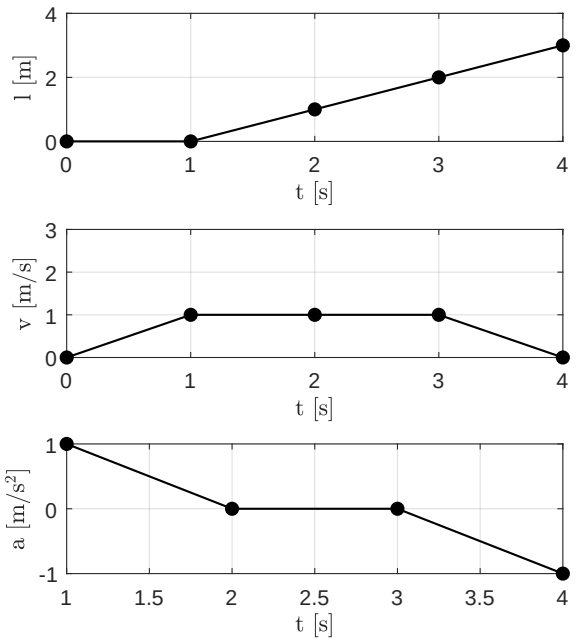

Figure 4.1: Realisation of the DP algorithm, on x-axis is the time and on y-axis are the distance, velocity and acceeration.

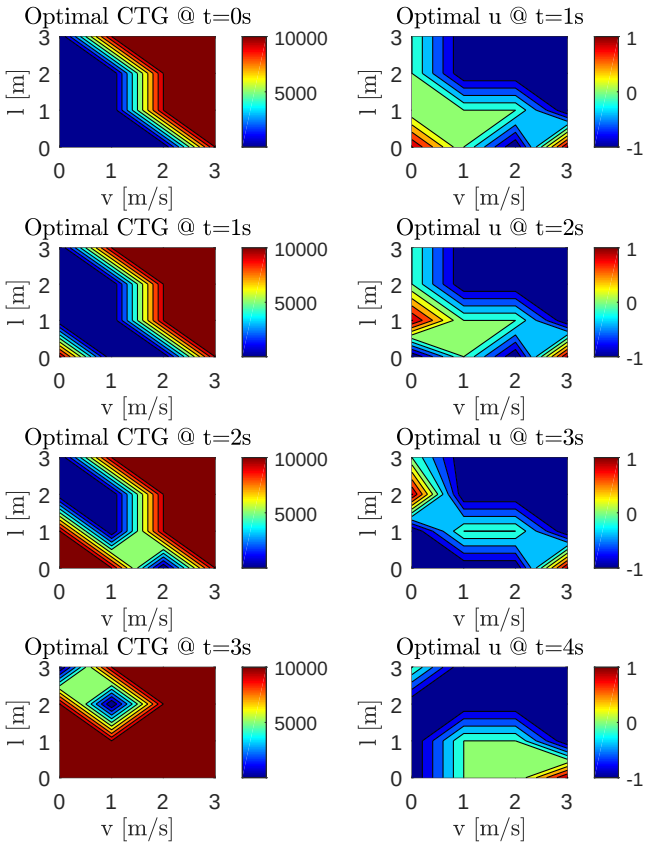

Figure 4.2: Realisation of the DP algorithm. The contour represent cost-to-go. in the first column and optimal strategy in the second column

4.2 Pontryagin's minimum Principle, application and extension to ECMS

In the previous section the DP is presented as an optimisation tool for solving the control problems with multiple states and control inputs. DP provides the optimal global solution while the curse of dimensionality makes it computationally challenging. For this reason, the PMP is one of the popular method which is applied to solve the optimal control problem. The PMP is a generalization of the Euler-Lagrange equations that also include problems with

constraints on the control inputs. The problem considered for minimisation is given by

$$\begin{aligned} J &= \phi(x(t_f)) + \int_{t_0}^{t_f} F(x(t), u(t))dt \\ subject\ to: &\ \dot{x} = f(x,u),\ x(t_0) = x_0,\ and\ x(t_f) = x_f \end{aligned} \tag{4.10}$$

The Hamiltonian function is defined as $H(x, u, p)$, where p is costate that depends on time.

$$H = F + p^T f \tag{4.11}$$

For a fixed t_f, the J is modified by adding a term that adds up to zero as $\dot{x} = f(x, u)$.

$$J = \phi(x(t_f)) + \int_{t_0}^{t_f} f(x(t), u(t))dt + \int_{t_0}^{t_f} p(t)^T (f(x,u) - \dot{x})dt \tag{4.12}$$

$$J = \phi(x(t_f)) + \int_{t_0}^{t_f} (H(x,u,p) - p^T \dot{x})dt \tag{4.13}$$

The optimal control strategy $u(t)$ is associated with state trajectory $x(t)$. A different control strategy $v(t)$ which is not very far from the optimal, if applied, results in the state trajectory which is close to $x(t)$ and can be represented as

$$x(t) + \delta x(t) \tag{4.14}$$

The change in the state trajectory yields a corresponding change in the modified performance index. We represent this change as δJ:

$$\begin{aligned} \delta J = \phi(x(t_f) + \delta x(t_f)) - \phi(x(t_f)) + \\ \int_{t_0}^{t_f} (H(x + \delta x, v, p) - H(x, u, p) - p^T \delta \dot{x})dt \end{aligned} \tag{4.15}$$

The integral above is calculated by parts resulting in

$$\int_{t_0}^{t_f} (p^T \delta \dot{x})dt = p(t_f)^T \delta x(t_f) - p(t_0)^T \delta x(t_0) - \int_{t_0}^{t_f} \dot{p}^T \delta x dt \tag{4.16}$$

note that $\delta x(t_0) = 0$ because, a change in the control strategy does not change the initial state. Taking into account the above, the cost function can be rewritten as

$$\begin{aligned} \delta J = \phi(x(t_f) + \delta x(t_f)) - \phi(x(t_f)) - p(t_f)^T \delta x(t_f) + \\ \int_{t_0}^{t_f} (H(x + \delta x, v, p) - H(x, u, p) + \dot{p}^T \delta x)dt \end{aligned} \tag{4.17}$$

the term $\phi(x(t_f) + \delta x(t_f)) - \phi(x(t_f))$ is replaced with its first order approximation while $H(x, v, p)$ is added and subtracted under the integral to obtain.

$$\begin{aligned} \delta J = (\nabla_x \phi_{t=t_f} - p(t_f))^T \delta x(t_f) + \\ \int_{t_0}^{t_f} (H(x + \delta x, v, p) - H(x, v, p) + H(x, v, p) - H(x, u, p) + \dot{p}^T \delta x) dt \end{aligned} \tag{4.18}$$

The $(H(x + \delta x, v, p)^{-} H(x, v, p)$ is replaced with its first order approximation,

$$\begin{aligned} \delta J = (\nabla_x \phi_{t=t_f} - p(t_f))^T \delta x(t_f) + \\ \int_{t_0}^{t_f} (\frac{\partial H}{\partial x} \delta x + H(x, v, p) - H(x, u, p) + \dot{p}^T \delta x) dt \end{aligned} \tag{4.19}$$

If p is the solution to the differential equation

$$\frac{\partial H}{\partial x} + \dot{p}^T \delta x = 0 \tag{4.20}$$

with the final condition

$$p(t_f) = \nabla_x \phi_{t=t_f} \tag{4.21}$$

reduces the deviation in the cost to

$$\delta J = \int_{t_0}^{t_f} (H(x, v, p) - H(x, u, p)) dt \tag{4.22}$$

If the u is optimal then $(H(x, v, p) - H(x, u, p))$ must be greater than zero. The necessary conditions for u to minimise J subject to the constraints in the Equation 4.11 are:

$$\dot{p} = -(\frac{\partial H}{\partial x})^T \tag{4.23}$$

where $H = H(x, u, p) = F(x, u) + p^T f(x, u)$

$$H(x^*, u^*, p^*) = \min_u \{H(x, u, p)\} \tag{4.24}$$

The PMP can be used to solve the minimum fuel problem described in 4.7-4.9. The goal was to derive the state to the origin with minimum cost. The states in the problem are distance(x_1) and velocity(x_2) while the dynamics are governed by:

$$\begin{aligned} \dot{x_1} = x_2 \\ \dot{x_2} = u \end{aligned} \tag{4.25}$$

If we apply u=±1, the system response can be represented by the following equations:

$$\begin{aligned} if\ u = 1, \\ x_2(t) = t + c_1 \\ x_1(t) = \frac{1}{2}t^2 + c_1 t + c_2 \\ x_1(t) = \frac{1}{2}(t + c_1)^2 + c_3 x_1(t) = \frac{1}{2}x_2(t)^2 + c_3 \end{aligned} \tag{4.26}$$

the hamiltonian for the system can be formulated as:

$$\begin{aligned} H = 1 + |u| + [p_1\ p_2][0\ 1; 0\ 0][x_1; x_2] + [0; 1]u \\ H = 1 + |u| + p_1.x_2 + p_2.u \end{aligned} \tag{4.27}$$

the equation of the co-state can be derived as:

$$\begin{aligned} \dot{p} = -{H_x}^T \\ \dot{p_1} = -H_{x_1} \\ \dot{p_1} = 0 \\ p_1 = c\dot{p_2} = -H_{x_2} \\ \dot{p_2} = -p_1 \\ p_2 = -c_1 t + c_2 \end{aligned} \tag{4.28}$$

the above equation shows that p_2 is linear in time.

To find the optimal control, the value of u making 0 the derivative of the Hamiltonian respect to u should be found:

$$H_u = \frac{u}{|u|} + p_2 \tag{4.29}$$

then :

$$H_u = \begin{cases} p_2 + 1, & \text{if } u \geq 0 \\ p_2 - 1, & \text{if } u < 0 \end{cases}$$

Note that provided the value of p_2, H_u is constant, leading to a linear dependence of H with u.

Therefore the control law can be described using the three conditions based on the sign of H which depends size of p_2 .

$$u(t) = \begin{cases} -u_m, & \text{if } 1 < p_2(t) \\ 0, & \text{if } -1 < p_2(t) < 1 \\ u_m, & \text{if } p_2(t) < -1 \end{cases}$$

Therefore the control depends on p_2(t) - but since it is a linear function of time, it is only possible to get at most 2 switches. Also, since $\dot{x}_2(t) = u$, and since we must stop at t_f, then must have that u $= \pm u_m$ at t_f. The problem then reduced to finding two switches occuring at t_1 and t_2 while from t_1 to t_2 there will be coasting phase with u =0.The possible optimal solutions based on the control law u(t) are represented in Figure 4.3. Application of the constraints result in the black line which is consistent with the results from dynamic programming explained in the previous section.

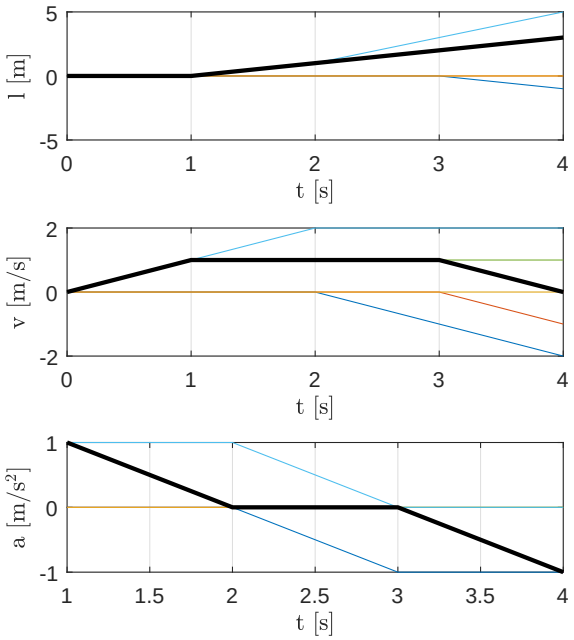

Figure 4.3: Realisation of the PMP algorithm, on x-axis is the time and on y-axis are the possible distance, velocity and acceleration for minimised cost. The dark black line is the optimal solution meeting the constraints.

Chapter 5

Driving cycle prediction

Contents

An online energy management strategy that is optimal and can be implemented in real time has been a topic of interest by researchers and the industry. Optimal control methods guarantee an optimal solution if the driving cycle is perfectly known in advance. However, perfect knowledge of the driving cycle is not possible and ECMS allows to find a suboptimal solution with some estimation of the driving conditions. To this end, online calculation of the co-state is required to deal with the changing driving scenarios. Thus, any estimation of future information to feed the ECMS control module with appropriate values of the equivalence factor is required. Usually, driving cycle prediction techniques are used to forecast the distribution of various future driving conditions like velocity, acceleration, driver behaviour etc. The forecast is primarily used in the predictive energy management strategies of the vehicle. On one hand, in the conventional vehicles, the forecast can be used to optimise the engine control while on the other hand, the energy management strategy is optimised for the hybrid electric vehicles. In this chapter a popular method based on MC is described for the purpose of driving cycle prediction. The first section describes the MC principle followed by a section regarding its application in the cycle prediction.

5.1 Markov Chain Principle

A collection of random variable $(X(r))$ is referred to as stochastic process. The index r is often considered to be time (t) and depending on the application it is either continuous-time or discrete-time process. The Markov Chain (MC) is a stochastic process $X_t, t = 0, 1, 2, 3, 4...$ having the property that given the present state, the future is conditionally independent of the past. The stochastic process takes on a finite number of possible values or states. The representation $X_n = i$ means that the process is in state i at time n. If the process is in state i, there is a fixed probability P_{ij} that it will be in the state j at the next time step. The defining property of the MCs is

$$P\{X_{n+1} = j | X_n = i, X_{n-1} = i_{n-1}, ..., X_1 = i_1, X_0 = i_0\} = P_{ij} \tag{5.1}$$

for all states i_0, i_1, i_{n-1}, i, j and all $n \geq 0$. Since probabilities are non-negative and the process must make a transition into some state, we have

$$\begin{gathered} P_{ij} \geq 0 \; for \; i, j \geq 0 \; and \\ \sum_{j=0}^{\infty} P_{ij} = 1, \; for \; i = 0, 1, ... \end{gathered} \tag{5.2}$$

A simple example with a velocity prediction can be used to explain the MCP better, suppose that a vehicle is driven during some time interval and the minimum and the maximum speed of the vehicle during this period is 0 and 40 km/h respectively. The vehicle velocity is a state that can be assumed to be any integer between 0 and 40. In order for this process to be a MC, the probability that the velocity of vehicle in the next time step is a given value, lets say 30 km/h depends only on the velocity at current time step. In that case, the model is MC and the different probabilities are transformed into a transition matrix. For a MC, P represent the matrix of one-step transition probabilities P_{ij}, so that

$$P = \begin{bmatrix} P_{00} & P_{01} & P_{0j} & ... \\ P_{10} & P_{11} & P_{1j} & ... \\ ... & ... & ... & ... \\ P_{i0} & P_{i1} & P_{ij} & ... \end{bmatrix}$$

In the below transition matrix, the probability of process in state i to transcend to state j in the next time step is 0.4.In P, we the rows of the matrix are representing the state the process is currently in, and the columns represent the state that they are going to. The process either stays in the same state or moves to other one and therefore the sum of the probabilities along any row

of P must be equal to 1.

$$P = \begin{bmatrix} 0.2 & 0.22 & 0.37 & ... \\ 0 & 0.2 & 0.35 & ... \\ ... & ... & ... & ... \\ 0.1 & 0.25 & 0.4 & ... \end{bmatrix}$$

The above probability is a one-step transition probability and it can be further extended to n-step transition probability P_{ij}^n. P_{ij}^n is the probability that a process proceeds from the state i to the state j over n additional steps. In a MC, state j is said to be accessible from state i if $P_{ij}^n \geq 0$ for some $n \geq 0$. If two states in a MC can communicate, they are said to be in the same class. If there are more than one class in a process if is not possible to travel freely from one class to another as there exist no communication between two classes. The driving cycle prediction using MC also assumes that the vehicle speed in the next time step is dependent only upon the velocity at the current time step. The following section describes the process of synthesizing the driving cycle and the assumptions required for them to be a MC.

5.2 Implementation of MC principle in Driving cycle prediction

In the present work, the MCP based driving cycle prediction tool was developed for its application in building RDE-regulated driving cycles, engine control in real-driving scenario and in energy management of HEVs on real driving mission. These applications are described in chapter 7,chapter 8 and chapter 9 however, the tool is described in this section. The synthesis process of the driving cycle has three major steps- data collection and post-processing, defining state and obtaining the TPM and finally decoding the future states. The description of the synthesis process is presented as a flow chart in Figure 5.1.

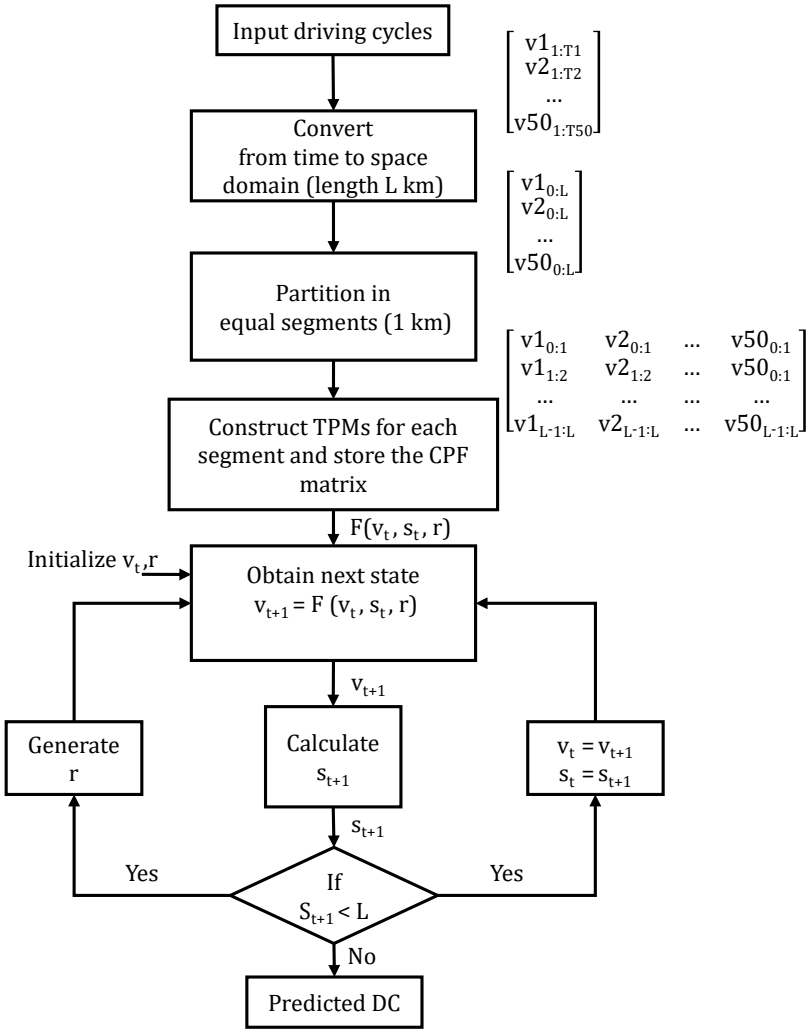

Figure 5.1: Illustration of velocity generator in urban phase

- Data Collection and Postprocessing:

  The first step in the development of driving cycle prediction tool is to choose a driving mission and a driver to conduct the experimental task. In this thesis, a route between Valencia and Canals is chosen which comprises urban and motorway phases. The experimental data is obtained by driving the vehicle on the route for several trips while recording the time, speed and the position of the vehicle. The randomness in the recorded driving cycles is due to the traffic conditions and driver behaviour on a particular day. However, since all the experiments are conducted by the same driver, on an average its impact is assumed to be considerably low. During the tests, a GPS was used and ECU read-

ings were accessed by means of a Vag-Com communication system to measure vehicle velocity and engine parameters, mainly speed and estimated torque. The driving cycles obtained from the above experimental campaign are the input driving cycles in Figure 5.1. The obtained driving cycles are converted from the time domain to the space domain to obtain distance dependent TPMs. In order to take into account the particularities of driving conditions depending on the vehicle position, e.g. differences between urban and highway driving, the obtained velocity profiles are divided into several segments, in the case at hand with 1 km length. Following the post processing of the data the TPMs are constructed.

- Construction of the TPMs:

  The short driving cycles obtained for each segment are used to model the vehicle speed as a Markov process, where the vehicle speed is considered a random process (V) satisfying:

$$\begin{aligned} P(V_{n+1} = v_{n+1} | V_1 = v_1, V_2 = v_2, \ldots, V_n = v_n) \\ = P(V_{n+1} = v_{n+1} | V_n = v_n) \end{aligned} \tag{5.3}$$

  where v_j represent possible values of V, subindex n is the present time, $n+1$ represents some point in the future and subindex $1, 2, ..., n-1$ points in the past. Equation 5.3 states that given the present state ($V_n = v_n$) the probability for this random process for the next future ($V_{n+1} = v_{n+1}$) is independent of the past. In this sense, estimating the transmission matrix can be done by observing the sequences of states and the frequency in the transitions between them. For practical reasons, the data has been discretized in steps of 1 km/h in velocity. Let $N_{i,j}$ the number of times the vehicle speed is i in a given time ($V_{n+1} = i$) provided that was j in the previous instant ($V_n = j$). The probability of being in state i given that it was in state j in the previous time can be estimated as: All the transition probabilities are stored as a TPM for each segment and are represented as (TPM_k), where k represents the segment have been extracted from the experiemental data. After the TPMs are constructed, the Cumulative Probabilty Function (CPF) ($\mathrm{F}(\mathrm{v_t}, \mathrm{s_t}, \mathrm{r})$) is built by integrating the TPM rows. In particular, the probabilities are assumed to be equal to the event frequency in each segment. The figure below shows the TPM for one segment.

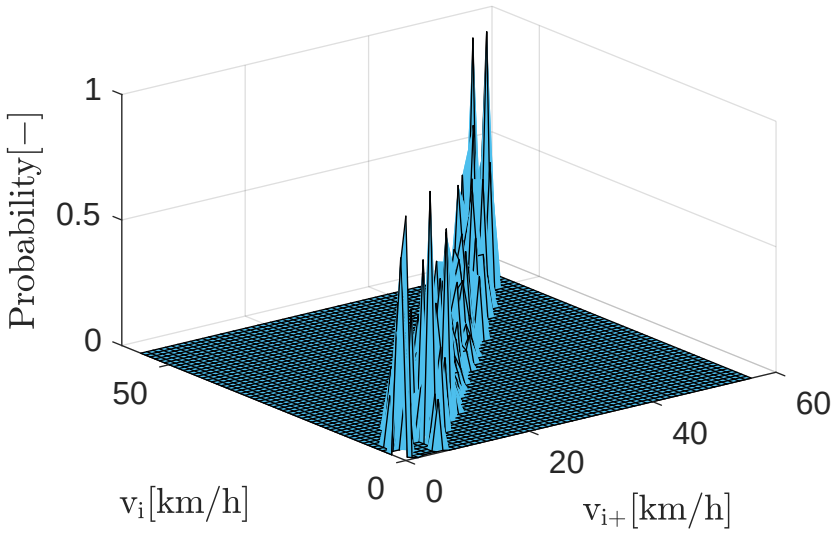

Figure 5.2: Speed transition probabilities from current speed v_i to v_{i+} in a representative segment

- Decode the future state:

  Once the function F have been built, the vehicle position within the route is used to choose the corresponding TPM. The current vehicle position (s_t) and speed (v_t) are used to estimate the driving cycle main parameters, consisting on the duration $\hat{T} - t$, vehicle speed and acceleration sequences ($\hat{v}_{t:\hat{T}}$ and $\hat{\dot{v}}_{t:\hat{T}}$) and estimated road slope evolution during the cycle ($\hat{\gamma}_{t:\hat{T}}$). Then at every time-step, the next vehicle speed is selected generating a random number between 0 and 1 ($r \in [0, 1]$) choosing the vehicle speed whose CPF is equal to this random number r. The integration of the vehicle speed allows to compute the next vehicle position in the route, which is used to estimate the road slope and identify the next TPM to be used. The process is repeated in time until the vehicle destiny is reached.

  Note that the availability of the current vehicle position requires a tracking device, e.g. GPS. On the other hand, the estimation of the road profile needs cartographic information and the specification of the route in order to compute the road slope by interpolating the estimated position obtained from integration of $\hat{v}_{t:\hat{T}}$.

  This step is illustrated with an example in Figure 5.3. For instance the initial velocity v_0 is 17 km/h. The generator randomly generates a

probability i.e. 0.98 and uses the cumulative probability function $CPF_{i,k}$ for i=17 km/h and selects accordingly the velocity for next time step i.e. 19.7 km/h (20 km/h, nearest integer). Then, in the next iteration, a CPF value is randomly generated (0.85) and similarly it predicts 22 km/h for the next time step. This process continues for t_k steps, and the then switches to a new TPM_k which is based on the different segment.

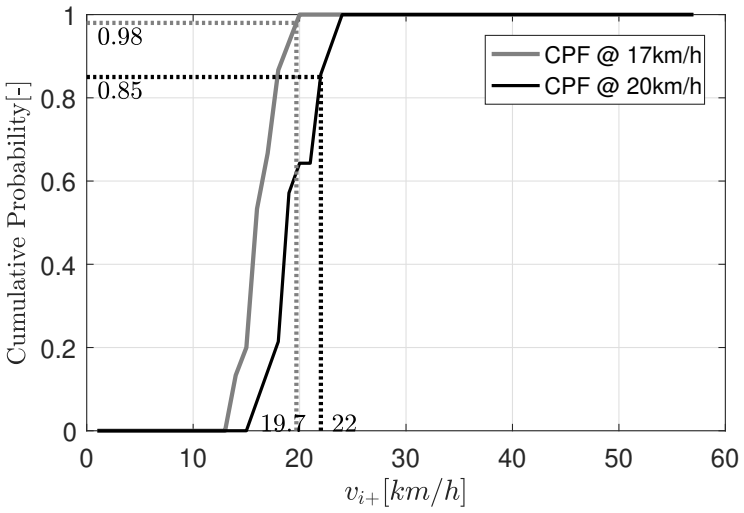

Figure 5.3: Illustration of velocity generator in urban phase

Part III

Experimental Setup

Chapter 6

Experimental Test Setup

Contents

During the development of a control application for a vehicle or an engine there are several instances when a real system is required to be tested either during the design process itself or in the verification and validation stage. The testing is performed in a controlled environment, which allow experimental reproducibility and validation over a wide range of conditions by designing the application specific case studies. There are several experimental campaigns run during this work, each campaign is detailed in the third part of the thesis. This chapter is focused on describing the testing setups with a brief introduction about the objective of each application. In specific, there are 6 different applications tested on four experimental setups. The first three applications (A.1, A.2, A.3) were tested on the same diesel engine test setup (Setup — A), with only slight differences. The fourth application (B.1) is tested on a four-cylinder diesel engine test bench (Setup — B). The experiments related to the fifth application (C.1) were conducted on a chassis dynamometer (Setup — C) and the last application (D.1) was tested on a real vehicle (Setup — D) which was driven between two locations in Spain.

Stroke x Bore[mm]	84.8 x 75
Displacement[cc]	1498
Compression ratio	16:1
Number of Cyl.	Inline 6
Valves per Cyl.	4
Rated Torque	300Nm @ 1750rpm
Emission std.	Euro 6

Table 6.1: Engine specification.

6.1 Experimental Setup - A

Application Objective A.1 To develop a control method that adapt the diesel engine calibration in a real driving mission for minimising the fuel consumption while restricting the NO_x emission under a predefined limit.

Test setup A.1 The diesel engine with specifications tabulated in (Table 6.1) was tested at CMT-Motores Termicos facilities whose schematic is presented in Figure 6.1. The engine is coupled to an asynchronous Horiba DYNAS 3 dynos which is controlled through the personal computer interface Horiba STARS. The dyno is able to perform steady-state, dynamic tests and in particular it is able to emulate the vehicle behaviour to carry out tests simulating the real driving speed profiles.

An open engine ECU was sourced from the manufacturer to study various engine control strategies. The base ECU is used to obtain the feed-forward calibration maps of the desired output parameters. The ETK port allows streaming and bypassing the important signals from an eternal ETAS setup. In the original ECU, the fuel path is controlled through the look-up tables depending on the engine speed, pedal position and corrections related to the temperatures, ambient conditions etc.. On the other hand, the air-path is more complex with the EGR valve and the VGT actuators acting together to achieve the desired air flow and the intake manifold pressure. Due to the coupling of two actuators, only one actuator is usually controlled in the close-loop. Depending on the engine operating condition, the controller is able to choose the actuator to be controlled. For instance, at low engine load and low engine speed condition, the EGR is very crucial for NO_x emissions and therefore the EGR valve is controlled in a close loop. While the VGT is controlled through feed-forward maps in open loop. On the other hand at high engine speed and high engine load the VGT is controlled in a close loop while EGR valve is controlled through a feed-forward map. It should be noted that all the close-loop control in the base ECU rely upon pre-calibrated PIDs.

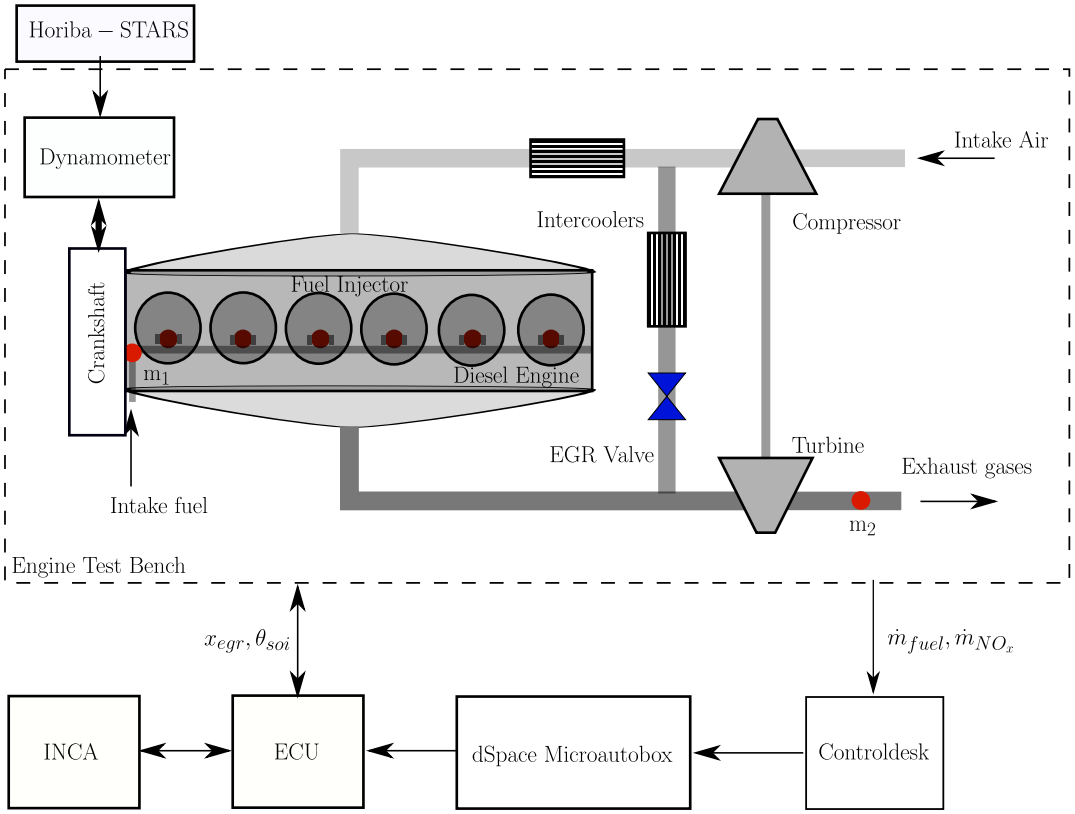

Figure 6.1: Experimental setup-A.1. At the node m_1, the start of injection was bypassed and controlled through dSpace. At m_2, the NO_x emission and the exhaust gas concentration is measured.

The design of experiment approach was used to model the engine torque and $\dot{m}_{NO_x}$ emissions as a function of the input parameters. To do that, the engine torque and $\dot{m}_{NO_x}$ emissions were measured while varying the parameters such as vgt position x_{vgt}, egr valve position x_{egr}, start of injection θ_{soi} and fuelling rate $\dot{m}_{fuel}$. For which, a rapid prototyping system (RPS) was connected via ECU ETK port allowing for sending and receiving the engine signals. This by-pass configuration is created using INTERCRIO and generated in the dSpace system.
The important measurement nodes for this application are represented by the red dots in the Figure 6.1. For the concentration's measurement in the test bench, the Horiba MEXA 7100 DEGR GA is used to measure the concentration of NO_x at one point of the exhaust line. This apparatus employs techniques like the non-dispersive infrared (NDIR) for the NO_x measurement. Regarding the data recording, the use of different systems to record data implies that three files are obtained for each experiment in this setup i.e. from dSpace, STARS and ETAS. In order to be able to phase the different files

afterwards, the RPS dSpace triggers a square signal, which allows phasing them in post-processing.

The real-time simulation of the developed controller interfaces with the engine test bench using actuators and sensors; these actuators and sensors have their own characteristics which detract from the realism of complete system response. The vehicle is emulated by a numerical model interacting with a physical engine system. A similar approach is also applied to validate the hybrid electric vehicle model in the following application A.2.

Application Objective A.2 To develop an online energy management strategy for a parallel hybrid electric vehicle on a real driving mission.

Test setup A.2 The application was tested in the same experimental setup described in A.1 except for the parameters that were bypassed and an additional input to the dSpace Microautobox. The need for real-time communication is satisfied by means of a Controller Area Network (CAN) bus. The experimental test platform uses CANopen protocol to integrate all the elements and assure synchronous distribution of reference speed and torque commands, as well as to read back the actual speed and torque. The torque required from the diesel engine is calculated using the vehicle backward model in the Simulink and is translated into the throttle position through a calibration map. To test a realistic hybrid electric vehicle on this engine testing setup, the torque sensor system provides the torque feedback signals from the test-bench back into the dSpace. Inside the dSpace, the reference and feedback torque signals generate error signals and the excess energy is absorbed by the electric motor in the vehicle dynamic model where the instantaneous battery state-of-charge is calculated. The HiL system allows the online assessment of the developed EMS controller. The total energy consumed in different measurements on a same driving cycle of length 20km produced a standard deviation of 43.5 kJ . This energy was later used for correcting the total fuel consumption during different experiments on the same driving cycle. The engine speed and the throttle position are calculated in advance using a vehicle backward model and are imposed in the Horiba - STARS. The engine speed which is an output of the real-time simulation on the dSpace must be synchronised with the engine speed that is an input from the Horiba STAR dyno control. This synchronisation was achieved manually in the present case by triggerng the bypassed signal and the driving cycle in STARs at the same moment. The fuel consumption is not a direct measurement, but rather a calibrated value within the ECU. The ECU usually contain signals giving an indication of the amount of fuel being injected into the cylinder. The remaining connection measurements are similar to the first application.

Application Objective A.3 To study the impact of driving dynamics in real driving emission test on NO_x emissions dispersion.

Test setup A.3 The diesel engine described in applications A.1 and A.2 with specifications as in Table 6.1 was used for the experiments. In addition, the engine was also equiped with a state-of-the art after-treatment system comprising Diesel oxidation Catalyst, Diesel Particulate Filter and Selective catalytic reduction system. No parameters were required to be bypassed for this application and therefore the dSpace and ControlDesk were redundant. Several driving cycles were imposed through Horiba-Stars while measuring the fuel consumption and NO_x emissions before and after the after-treatment system. The nodes m_1,m_2 and m_3 represent the approximation of the fuel intake, NO_x emissions before and after the after-treatment system respectively. The NO_x concentration was measured using the Horiba MEXA 7100 DEGR GA as in previous applications.

6.2 Experimental Setup - B

Application Objective - B.1 To develop a control method that varies the diesel engine calibration smoothing for minimising the fuel consumption while restricting the torque error and NO_x emissions under a predefined limit.

Test setup - B.1 The measurements presented in this study were obtained from a dynamic engine test-bench at ETH Zurich. The engine under consideration is a commercial heavy-duty Diesel engine.

The schematic of the application is presented in Figure 6.2. The work was carried out in a test bench mainly composed by an engine coupled to a dynamometric brake. The engine was a four-stroke, heavy-duty Diesel engine with four cylinders, turbocharged, intercooled EGR and with a common-rail injection system. This engine (see main specifications in Table 6.2) is representative of those typical used in Diesel construction equipment in Europe. The engine was instrumented to measure several key temperatures and pressures (intake air, fuel, exhaust gases, lube oil, etc.). A piezoelectric pressure transducer coupled to a charge amplifier was used for recording instantaneous in-cylinder pressure. Crankshaft rotational speed and instantaneous piston position were determined by means of an angle encoder. For the rapid prototyping of the software developed and tested in this study, a dSpace MicroAutoBox system was applied in combination with MATLAB/Simulink from MathWorks, Inc. This device is also used for the data acquisition of the various sensor signals. The engine speed is controlled by a highly dynamic dynamometer.

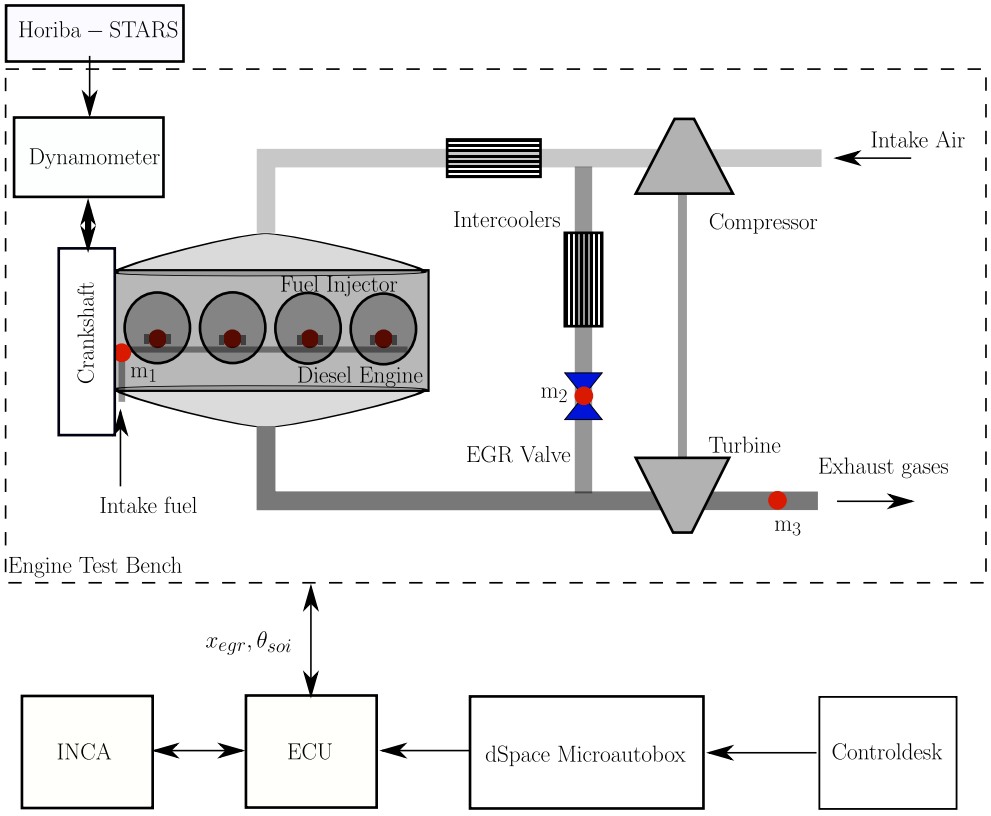

Figure 6.2: Experimental setup-B.1

Type	Heavy-duty Diesel engine
Engine displacement	7 litres
Number of cylinders	4
Rated power	200 kW @ 1900 rpm
Features	Common rail fuel injection, turbocharged, cooled EGR

Table 6.2: Engine characterstics

Therefore, the engine speed can be considered an exogenous input rather than an output of the system. The engine speed and torque are measured using rotary encoder and a torque transducer, respectively. The NO_x emissions are measured using a production type sensor mounted immediately downstream of the turbine. The fuel consumption is not directly measured but retrieved from the previously calibration maps on the ECU. The fresh air mass-flow entering the compressor is measured using a hot-film air mass flow sensor. In order to measure the amount of EGR, two CO_2 sensors (Cambustion NDIR500)are employed.

6.3 Experimental Setup - C

Application Objective - C To assess the impact of traffic light information availability in terms of fuel consumption and NO_x emissions.

Test setup - C A 2014 diesel vehicle meeting EURO 5 emissions standards was used in this work. The vehicle specifications are given in Table 6.3. The vehicle was installed on a twin axle chassis dynamometer as shown in Figure 6.3. Even though the vehicle in this study was 2-wheel drive, the rear wheels were motored to avoid vehicle controller errors during testing. The dynamometer is situated within a climatic chamber that controls temperature and humidity. The vehicle was driven by a Strahle Autopilot SAP2000 robot. Vehicle cooling was provided by an WLTC specification frontal fan where fan speed was controlled as a function of vehicle speed.

Data logging was undertaken from four separate computer systems:

1. An Influx Technologies Rebel data logger was connected to the vehicle ECU through the On-board diagnostics (OBD) port and measured approximately 70 different data channels relating to the engine control system.

2. The robot host computer which logged all information relating to the robot pedal positions, pedal actuation forces and internal controllers.

Table 6.3: Test vehicle specifications

	Vehicle
Engine displacement	2.0L
Max. power	100 kW
Max. Torque	320 Nm
Emissions level	EURO 5
After-treatment	DOC + DPF
Unladen mass	1800 kg
Gearbox Manual	6 Spd

3. An AVL RoadSim dynamometer host computer which logged speeds and forces on the individual axles of the system.

4. A Sierra CP Cadet test cell control computer which logged all information from emissions analysers.

In total around 150 data channels were recorded across all the data systems and all data was logged at 2 Hz (which was limited by the OBD logger).

In this work, the two key metrics from the experimental investigation are the fuel consumption and the NO_x emissions. For fuel consumption, it was decided to use the estimated fuel injection quantities from the engine controller. ECUs will usually contain signals giving an indication of the amount of fuel being injected into the cylinder. It is important to note that this is not a measurement, but rather a calibrated value within the ECU. Nevertheless, this fast signal can be a reasonable estimate of fuel consumption that offers a high resolution during transient events. In a modern engine, the numbers are usually available as a mass of fuel injected for each individual injection, and therefore the total fuel consumption is obtained by summation of the n individual injections as shown in Equation 6.1. For the test vehicle in this work, up to 4 individual injections were observed during normal running.

$$\dot{m}_f = \frac{2N_{eng}}{60} \sum_{i=1}^{n} m_{f,i} \tag{6.1}$$

Where N_{eng} is the engine rotational speed (rev/min) and $m_{f,i}$ is the fuel injected in grams during an engine cycle for injection number i of a total number of injections n.

NO_x emissions concentrations were sampled using a Horiba MEXA ONE system with the sampling point located downstream of the Diesel particulate filter (DPF) and Diesel Oxidation Catalyst (DOC). The mass flow of NO_x is them obtained using equation Equation 6.2 where the exhaust mass flow

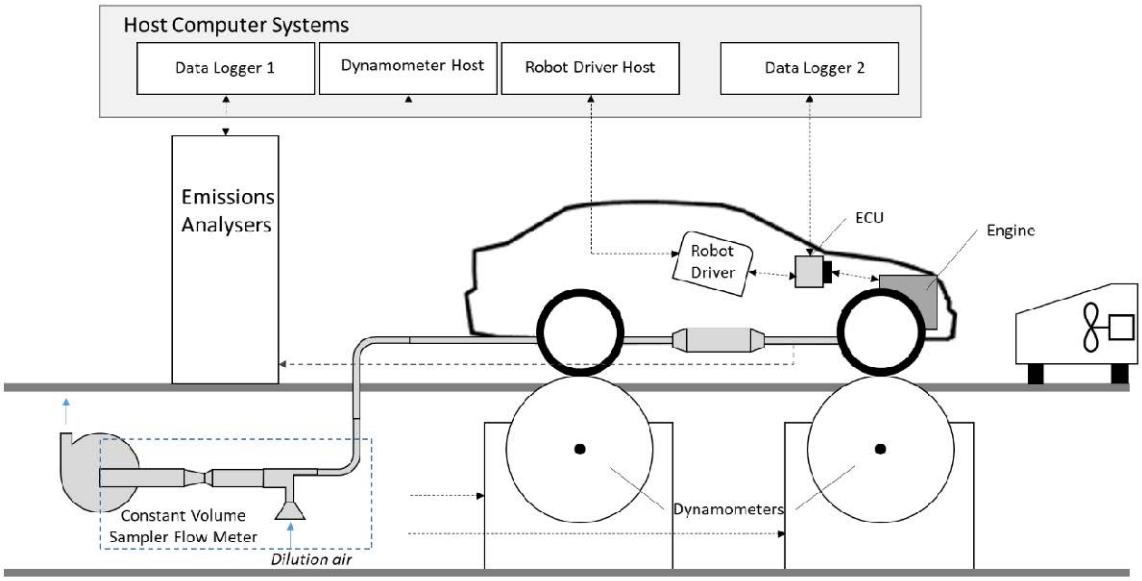

Figure 6.3: Chassis dynamometer layout illustrating key measurement and data acquisition devices. Experimental setup - C

($\dot{m}_{exh}$) is calculated from the air mass flow and fuel mass flow obtained from the engine management system.

$$\dot{m}_{NO_x} = \dot{m}_{exh} c_{NO_x} u_{NO_x} \tag{6.2}$$

where c_{NO_x} is the NO_x concentration in the exhaust gas and u_{NO_x} is a constant value obtained from emissions measurement standards.

6.4 Experimental Setup - D

Application Objective - D To optimise the speed profile in real time and recommend the driver, the optimal speed sequence that minimises the fuel consumption on a particular route.

Test setup - D A 2015 diesel vehicle meeting EURO 5 emissions specifications was used in this work. The main vehicle characteristics are shown in Table 6.4.

The vehicle was instrumented with the following sensors m_1,m_2 and m_3 shown in the schematic Figure 6.4:

- a GPS antenna,
- a NOx and λ sensor,

Table 6.4: Test vehicle specifications

	Vehicle
Engine displacement	1.4 L
Max. power	50 kW
Max. Torque	160 Nm
Emissions level	EURO 5
After-treatment	DOC + DPF
Unladen mass	1125 kg
Manual Gearbox	6 Spd

- a pressure transducer and an inductive sensor to measure in-cylinder pressure and phase it with the crank angle.

Also, OBD-II SAE J1979 mode 01 information is read by means of a Controller Area Network (CAN) interface. This information is captured and processed with a National Instruments PXI system equipped with analog inputs (board model), high speed CAN interface (board model) and a USB serial interface. A scheme of the instrumentation system is shown in Figure 6.4. This system allows to capture in-cylinder pressure with an angular resolution of one sample per degree at 5100 rpm, $\dot{m}_{NO_x}$ values ten times per second and On-board Diagnostics (OBD)-II relevant values five times per second. Geographical position of the vehicle is acquired with a temporal resolution of one sample per second, which is the GPRMC message period. Optimal speed references are also managed by the PXI system. This information is presented to the user in a screen and updated every two seconds. In Figure 6.4, the nodes m_1 is to acquire the crank angle θ_{cyl}, the node m_2 is for cylinder pressure P_{cyl} and m_3 is for exhaust emissions $\dot{m}_{exh}$ and $\dot{m}_{NO_x}$ emission.

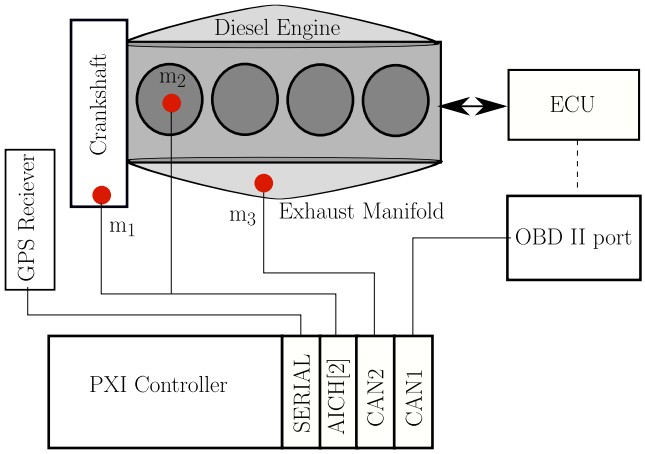

Figure 6.4: Scheme of the acquisition system. Experimental setup-D

Part IV

Applications to powertrain control, Design and Assessment

Chapter 7

Powertrain Control in Real Driving Mission

Contents

The objective of this chapter is to describe the applications developed for this thesis. The applications are either developed for control of diesel engine or hybrid electric vehicle. There are three sections in this chapter; each section is dedicated for an application in a structured way. The section 7.1 describes the modelling and validation of an adaptive diesel engine controller for a vehicle on real driving mission. The section 7.2 is regarding a new calibration method that enables variable-smoothing of a diesel engine for improved performance of a vehicle on real driving missions. Finally, section 7.3 is regarding an online controller for optimal energy management of a parallel hybrid electric vehicle for minimised fuel consumption and constrained state-of-charge on an unknown driving mission.

7.1 Adaptive control of Diesel Engine

7.1.1 Introduction

Motivated by the requirement of improvement in fuel-efficiency with minimal emissions, the control of diesel-engine is being investigated in this section. Despite the continuous tightening of the NO_x emission type approval limits, the difference between the type approval NO_x and the real world NO_x emissions has grown over the years ([Chen & Borken-Kleefeld 2014]). The reason for this discrepancy is the uncertainty due to driving dynamics, ambient temperature and road slope during real driving conditions which are not considered in the engine calibration process. SOA engine calibration method is based on feedback and feed-forward controllers. Fixed look-up tables are employed as the set-point generator and the feed-forward controller. The standard engine calibration approach consists on taking a limited set of driving cycle to make an optimisation and then use the obtained results to fill the calibration maps. However, in this case, the optimality of the calibration for a given driver will depend on the similarity between the considered driving set for calibration and his driving patterns. Moreover, this approach neglects other boundaries such as the traffic, pollution levels in the area or other environmental conditions. The presented approach poses the calibration problem as an optimal control problem by finding a set of optimal calibration maps in real time. The calibration maps contain the set points that minimise the instantaneous fuel consumption ($\dot{m}_f$) over a sequence of engine speed (ω_e) and torque (T_e), while fulfilling the integral constraint on (NO_x) emission on an unknown driving cycle. To solve the problem, a look-ahead strategy is proposed to periodically adapt the engine calibration such that the cumulative fuel consumption is

minimised while fulfilling the integral NO_x emission constraint. The strategy is to estimate the driving cycle and then calculate the vehicle performance (fuel consumption and the NO_x emission) on the estimated cycle using a 0-D vehicle model. The performance is calculated in parallel with different start-of-injection (SOI) calibration maps resulting in a set of SOI maps associated with different levels of cumulative fuel consumption and emissions. A supervisory controller updates the calibration from the available set of maps such that, the cost function is minimised while integral constraint is also fulfilled. The constraint on NO_x emission is time dependent and is calculated as the difference between the actual NO_x emission (measured by the sensor) and the NO_x limit for entire trip.

Specifically, this method involve three developments: The first is a driving cycle prediction tool (elaborated in chapter 5) which is based on the space-variant transition probability matrix obtained from an actual vehicle speed dataset. Then, a vehicle and an engine model described in chapter 3, to predict the fuel consumption and NO_x emissions on a driving cycle. Finally, an adaptive controller is proposed which calibrates the engine online, to fulfil the NO_x emission constraint at the end of the driving mission while minimising the fuel consumption. The developed control strategy was implemented and assessed on an engine test bench described in section 6.1. The engine performance using the proposed method is compared with the SOA static calibration technique for different NO_x emission limits on real world cycles.

7.1.2 Method description

As mentioned before, the online engine control require the following:

- A vehicle speed prediction model.
- A simple but accurate vehicle model to estimate the engine performance online.
- A controller to calculate and implement the optimal actuations in the real-time.

In this sense, the proposed control algorithm has three layers: The first layer is to predict the power demand of the vehicle, the second layer computes the expected fuel consumption and NO_x emissions depending on the SOI calibration map(from a limited set of possible calibrations). The last layer applies and holds the optimal calibration with minimum expected fuel consumption from those whose expected NO_x emissions are below a predefined limit.

In Figure 7.1, schematic of the high level control system of the developed method is presented. Where v_{estim} and v_{real} are the estimated and real vehicle

speeds respectively.Prediction Horizon Window (PHW) is the moving time window for which the fuel consumption and engine out NO_x emissions are cumulated. The length of the PHW is a design choice (calibration parameter) which affects the closeness of the cumulative NO_x emissions at the end of the cycle from target emissions/limits. Larger the window, farther will be the NO_x emissions from the target. On the contrary, short windows will avoid fuel reduction potential since the problem will be transformed on tracking a constant NO_x emission, and will have an excessive computation cost for the real-time implementation. The route is discretised in space, where each section is referred as a window and based on the predicted emissions for an upcoming window, the control actions that minimise fuel consumption keeping emissions under a limit, is calculated and stored as a calibration map, that is applied during the next time window. For the purpose of explanation, the schematic has three time frames represented by the three columns as past, present and upcoming time windows. During each PHW there are three processes happening in parallel, represented by the three rows. The top row represents the first process, which is regarding the estimation of driving cycle and calculation of engine speed and torque using a backward vehicle model. The vehicle model calculates the engine torque, fuel consumption and the NO_x emissions by interpolating the experimental data. The detailed description of the vehicle and engine model was presented in chapter 3. The second process as in central row is regarding the calculation of the optimal actuator settings and their conversion into the calibration maps. The calculation of the optimal calibration map is based on the predicted NO_x emissions for the upcoming PHW, the measured NO_x emission in the current window and the NO_x emission limit. At the end of each window, the calibration is updated based on the optimal control problem formulated in the following paragraph. Finally, the bottom row represents the third process which is regarding application of the updated calibration maps. In this study, the size of PHW (in red boxes) is chosen to be 100 sec. It must be noted that during the first time window, standard calibration map is applied.

Fuel consumption optimisation with constrained NO_x emissions The inputs to the low level controller shown in Figure 7.2 are the estimated vehicle velocity v(s), estimated engine speed ω_e, engine torque T_e and dynamic NO_x emission limit ($\widehat{NO_x}^{dyn}$) which is updated after every PHW based on Equation 7.1.

$$\widehat{NO_x}^{dyn} = \widehat{NO_x} - \frac{\int_0^s \dot{m}_{NO_x meas}}{\int_0^s v_{meas}(s)} ds \tag{7.1}$$

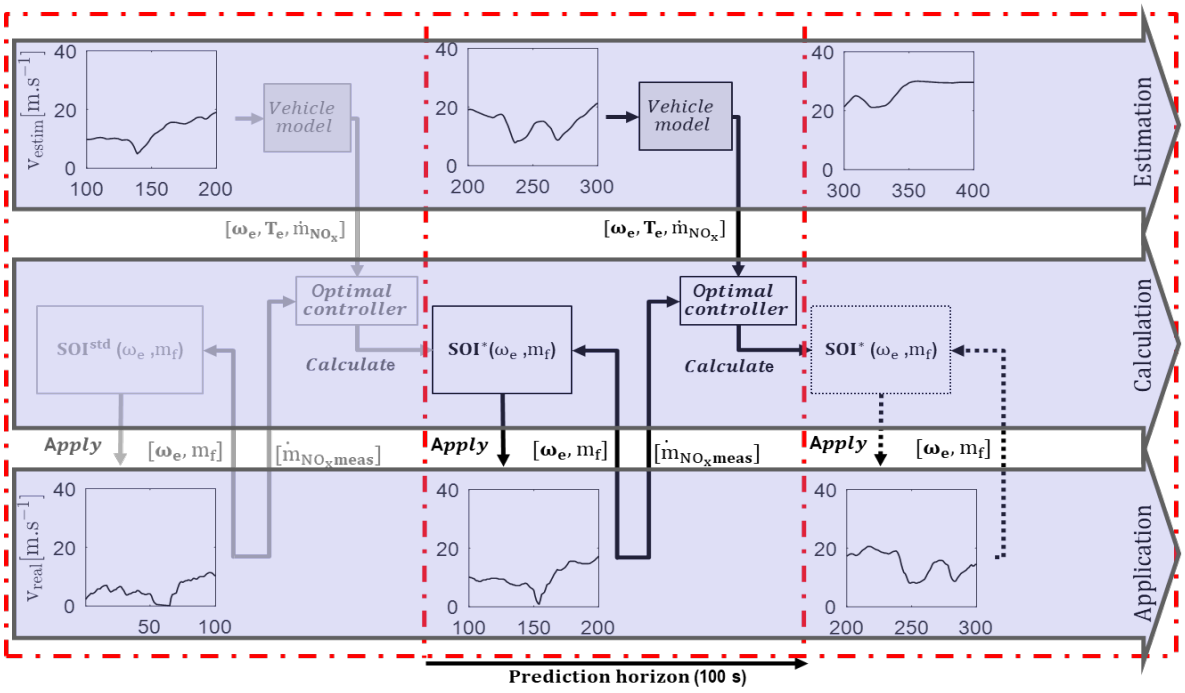

Figure 7.1: High level control schematic: Top row is vehicle speed prediction, middle row the calculation of optimal control and storing it as calibration maps and bottom row is the application of control to the real engine. Three columns represent time windows, where middle column represent the present time, left and right columns represent past and future time windows.

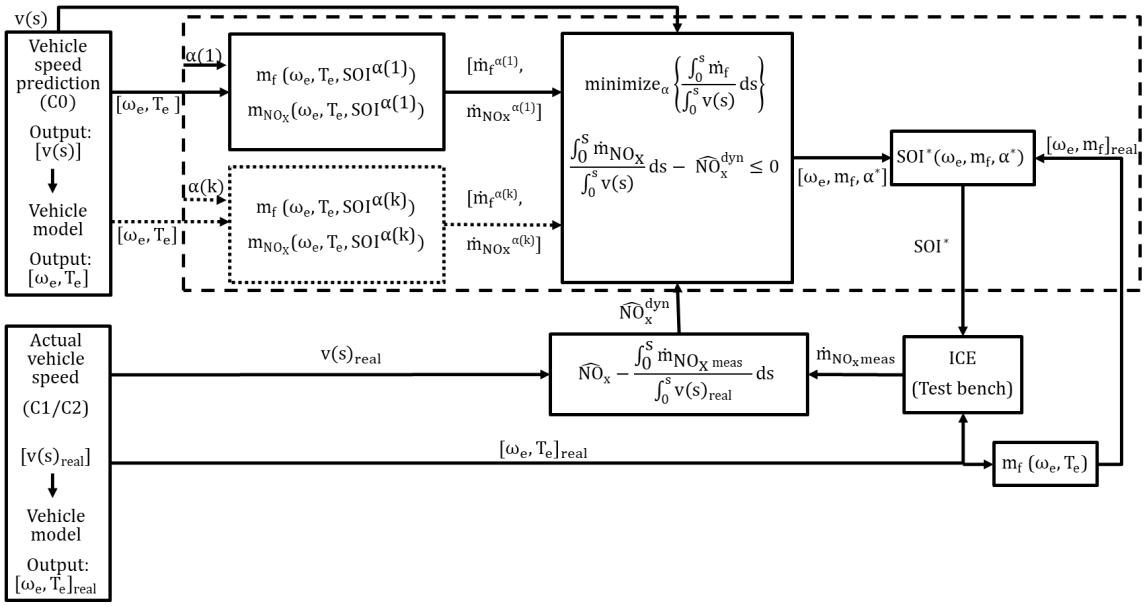

Figure 7.2: Low level controller schematic: Inside the dotted box are the fuel and NO_x models, a calculator and an adaptive calibration map for SOI actuation. Block in the top left has the vehicle velocity prediction model to obtain the v(s) and a vehicle backward model to obtain engine speed and torque traces for the corresponding v(s). Block in the bottom left is the actual engine speed and torque traces corresponding to the actual vehicle speed ($v(s)_{real}$) imposed on the engine test-bench. The ICE block represents engine test-bench.

Where, $\widehat{NO_x}$ is the predefined emission limit for the entire trip, $\dot{m}_{NO_x meas}$ is the rate of NO_x emissions measured by the sensor, $v_{meas}(s)$ is the measured vehicle velocity and s is the distance travelled by the vehicle.

Within the controller there are quasi-steady engine model and an optimiser. The engine model performs online calculation of fuel consumption and NO_x emissions during the transient operations with different calibration maps in parallel. This is achieved by modelling engine as a set of maps as in Equation 7.2

$$\begin{aligned} m_f(\omega_e, T_e, SOI^{\alpha(k)}) \\ NO_x(\omega_e, T_e, SOI^{\alpha(k)}) \end{aligned} \tag{7.2}$$

The two outputs of the engine model are the fuelling rate $\dot{m}_f$ and the NO_x emissions depending on the calibration index k. The three input parameters for the engine model are ω_e, T_e and $\alpha(k)$. The baseline calibration SOI^{std} is

perturbed using $\alpha(k)$ as shown in Equation 7.3.

$$\begin{aligned} \mathrm{SOI}^{\alpha(\mathrm{k})} = \mathrm{SOI}^{\mathrm{std}} + \alpha_0(\mathrm{k}) + \alpha_1(\mathrm{k}) * \omega_{\mathrm{e}}^{\mathrm{norm}} \\ + \alpha_2(k) * \mathrm{T}_{\mathrm{e}}^{\mathrm{norm}} \end{aligned} \tag{7.3}$$

where, α_0, α_1, $\alpha_2 \in [-1, 1]$, $\omega_{\mathrm{e}}^{\mathrm{norm}}$, $\mathrm{T}_{\mathrm{e}}^{\mathrm{norm}}$ are normalised engine speed and torque in euclidean space. Then, obtained calibrations are stored as vectors into a matrix A as in Equation 7.4, where α(k) is a vector of the three coefficients of the k_{th} calibration.

The lookup set must fulfil the following conditions:

- They must lie within the feasible actuator boundary. In the current study, SOI was explored within [$\mathrm{SOI}^{\mathrm{std}}$-3,$\mathrm{SOI}^{\mathrm{std}}$+3] CAD, which is in the feasible boundary shown in Figure 7.3 for the engine under study. The engine must have sensitivity to the changing calibrations within the look-up set.
- Calibration maps must be smooth enough in order to fulfil conditions of drivability. For ensuring map smoothness following strategy is used.

$$A = \begin{bmatrix} \alpha(1) \\ \alpha(2) \\ \alpha(3) \\ . \\ . \\ \alpha(k) \end{bmatrix}; \alpha = \begin{bmatrix} \alpha_0 & \alpha_1 & \alpha_2 \end{bmatrix} \tag{7.4}$$

Finally, the controller selects an optimal calibration α(k) by solving the problem in Equation 7.5, where fuel consumption is minimised for a given distance s while being within the dynamic $\mathrm{NO_x}$ limits .

$$\begin{aligned} \min_{\alpha(k) \in A} \int_0^s \frac{\dot{mf}}{v(s)} ds \\ subject\ to: \int_0^s \frac{\dot{m}_{NO_x}}{v(s)} ds - \widehat{\mathrm{NO}}_{\mathrm{x}}^{\mathrm{dyn}} \leq 0 \end{aligned} \tag{7.5}$$

The components of α are discretised in 3 elements leading to 27 combinations which is the size of the lookup set. Figure 7.4, presents sequence of optimal calibration map adapting with time for the first 600 s of a real driving cycle.

7.1.3 Designed use cases for method validation

In the current study three driving cycles are considered: The first cycle C0 is an estimated cycle, synthesized using the tool described previously. The

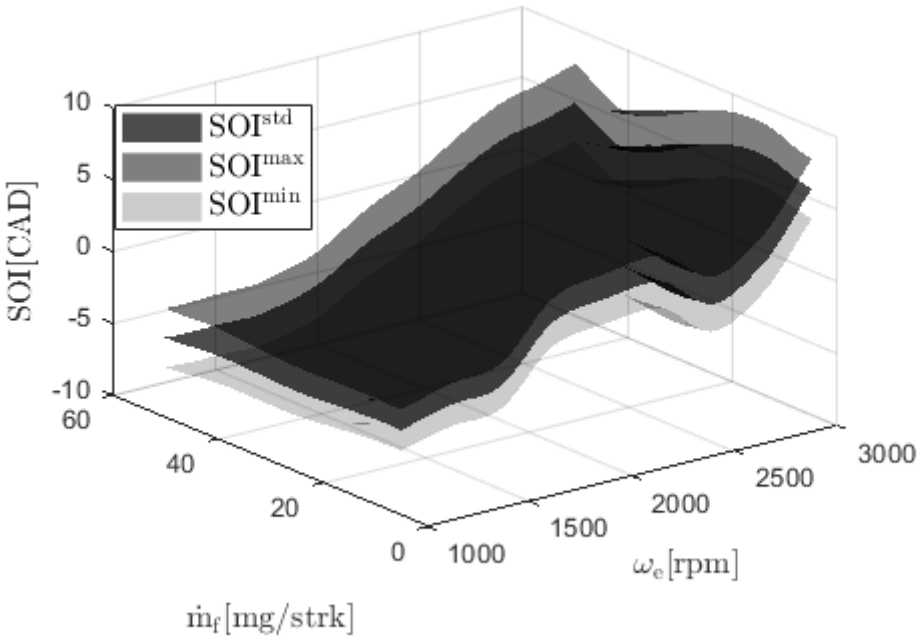

Figure 7.3: Standard SOI calibration map with the upper and lower boundary, within which the optimal maps have been explored

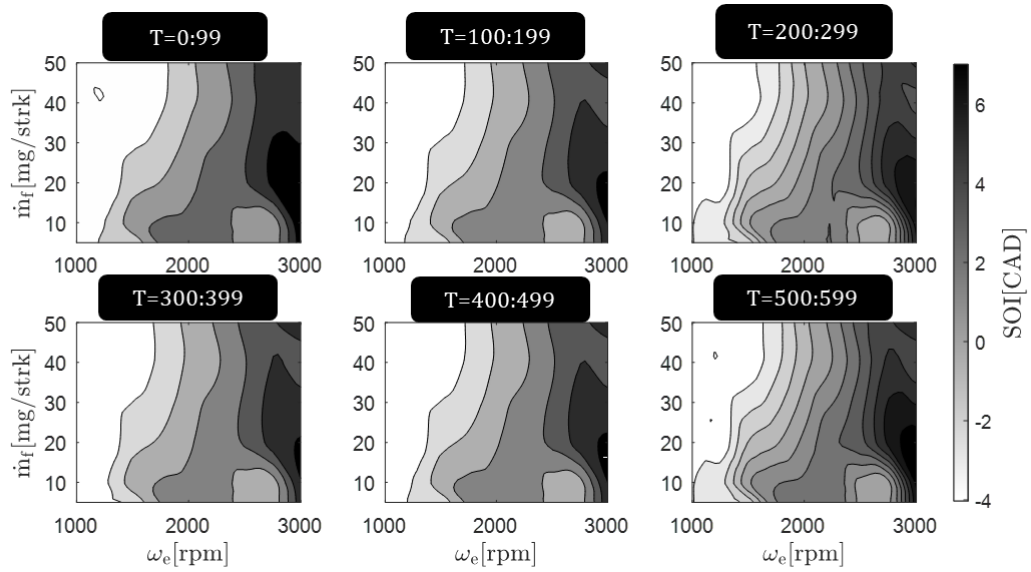

Figure 7.4: Representation of the adaptation of SOI calibration with time. Maps update at the end of the moving prediction horizon window of 100 s.

second and third cycles — C1 and C2 respectively are the real world cycle (recorded in past). In Figure 7.5, the evolution of the vehicle speed is presented. The plots at the bottom present the frequency of engine operations for the three cycles, it can be noticed that the aggressiveness of C0 is higher than C1 and less than C2. Using these three cycles, a case study was designed for the method validation. Three relevant scenarios are considered based on the driving dynamics of the predicted vehicle speed, driving dynamics of actual vehicle speed and limits over NO_x emissions.

- The first scenario Scen1 is when the actual driving cycle coincides with the estimated driving cycle.
- The second scenario Scen2 is when the aggressiveness of actual driving cycle is less than the estimated cycle.
- The third scenario Scen3 is when the aggressiveness of actual cycle is higher than the estimated cycle.

For each scenario, two cases case1 and case2 which are regarding the constraint on NO_x emission are presented, where case1 and case2 are with $\widehat{NO_x}$ less than 0.2 g/km and 0.3 g/km respectively for the trip.

7.1.4 Results

In Figure 7.6, Figure 7.9 and Figure 7.11, the results of the engine performance for the three scenarios are presented. The comparison is made with the engine performance using standard calibration std_{cal} (which in the present study is SOI^{std}). It should be recalled that during the first 100 sec the controller applies standard calibration regardless of the scenario or the case.

Scen1 : In Figure 7.6 the estimation of driving cycle is perfect; therefore the estimation of emissions for PHW would be different from the actual emissions only due to the error in engine modelling, the difference due to driving uncertainty would be zero. In Figure 7.8, an enlarged view of 0-360 sec is presented. The emissions in g/km are very high at the beginning of the cycle and therefore SOI is largely retarded for both the cases in order to reduce NO_x emissions. The difference in performance can be noticed with δm_f and δNO_x (defined in (Equation 7.6), as the percentage of cumulative deviation of fuel consumption or NO_x emissions for a *case* and standard calibration). At the beginning of this phase of the cycle NO_x emissions are largely reduced; while at the end of this phase as the emissions are less than the limits, the controller emphasises on saving the fuel.

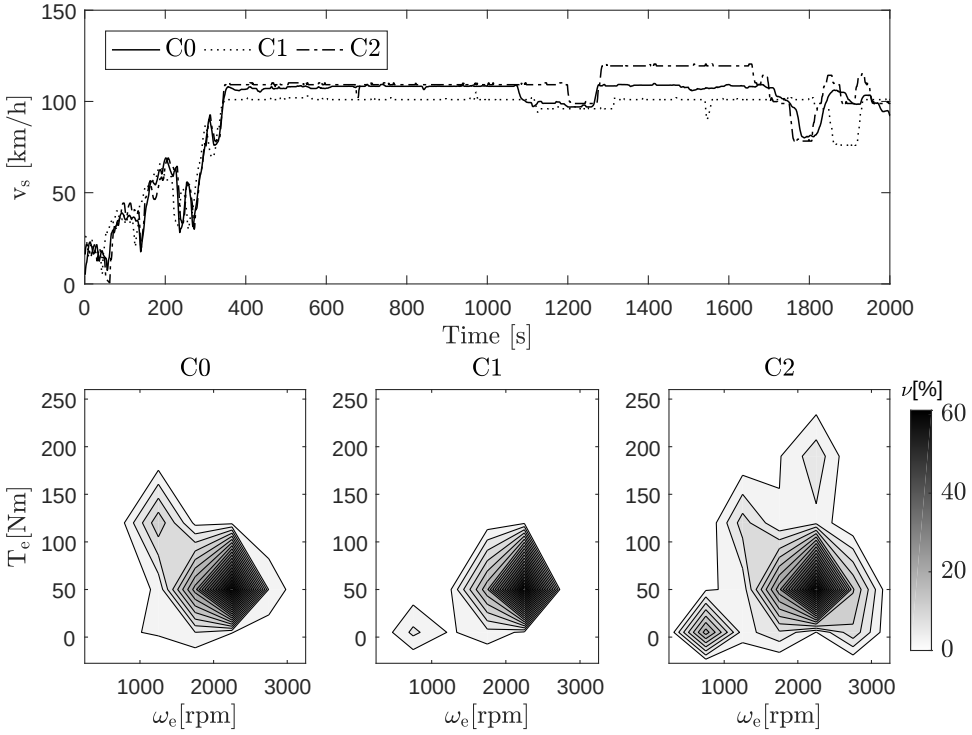

Figure 7.5: Predicted and measured vehicle speed on the route under consideration; frequency of engine operating points for the three cases velocity profiles

$$\begin{aligned}\delta m_f &= \frac{\int_0^s m_{f_{case1,2}} - \int_0^s m_{f_{std_{cal}}}}{\int_0^s m_{f_{std_{cal}}}} \times 100 \\ \delta \mathrm{NO_x} &= \frac{\int_0^s \mathrm{NO_{x_{case1,2}}} - \int_0^s \mathrm{NO_{x_{std_{cal}}}}}{\int_0^s \mathrm{NO_{x_{std_{cal}}}}} \times 100\end{aligned} \tag{7.6}$$

From 360-1800 sec vehicle speed is mostly constant (representative of the highway driving) and only few transients appear due to the road slope effect, for *case*1 the SOI is retarded more than *case*2 to have lower $\mathrm{NO_x}$ emissions at the end of the cycle. For case2 the emissions are within the $\widehat{\mathrm{NO_x}}$ while for case1 emissions are 0.21g/km. For a lower emission constraint, adapting the calibration to the actual driving scenario allows to have 14 % reduction in emissions with a penalty of 1.3 % in fuel consumption. If the $\mathrm{NO_x}$ constraint is relaxed to 0.3 g/km and the calibration is adapted to the actual driving cycle, as in Figure 7.7, fuel consumption can be reduced by 0.9 % while limiting the $\mathrm{NO_x}$ emissions below 0.3g/km. It can be observed that lower emission limit can be achieved with the calibration look-up set.

Scen2 : In Figure 7.9, the actual driving cycle is less aggressive than the estimated driving cycle, therefore the estimation of emissions for PHW would be higher than the actual emissions. From 100-360 s, even though the vehicle is running at lower velocity, the estimated emissions are more than actual and hence the SOI is retarded. For instance, during the second PHW, the estimation of emission is higher and therefore the control strategy is to minimise the emission as much as possible. At the beginning of third PHW the $\mathrm{NO_x}$ limit is corrected due to lower emission produced in second PHW. The higher $\widehat{\mathrm{NO_x}}^{\mathrm{dyn}}$ limit, makes a calibration, favouring better fuel efficiency. Thereby, for case1, 5% reduction in emissions is possible while insignificant increase in fuel consumption as shown in Figure 7.10. In case 2, the fuel consumption can be improved upto 3.9 % while staying within the emission limits. Moreover, in both the cases the limits on $\mathrm{NO_x}$ emissions are fulfilled at the end of the cycle.

Scen3 : In Figure 7.11, the actual driving cycle has higher aggressiveness than the estimated driving cycle. Accordingly, the estimation of emissions for PHW would be lower than the actual emissions, resulting in a strategy favouring $\mathrm{NO_x}$ reduction in the second PHW. Under-estimating the cycle aggressiveness leads to unfulfilled constraint in *case*1. In order to fulfil the $\mathrm{NO_x}$ limit, the SOI is largely retarded during the cycle. As presented in Figure 7.12, emissions are reduced by 14% with a 1.1% penalty in fuel consumption for

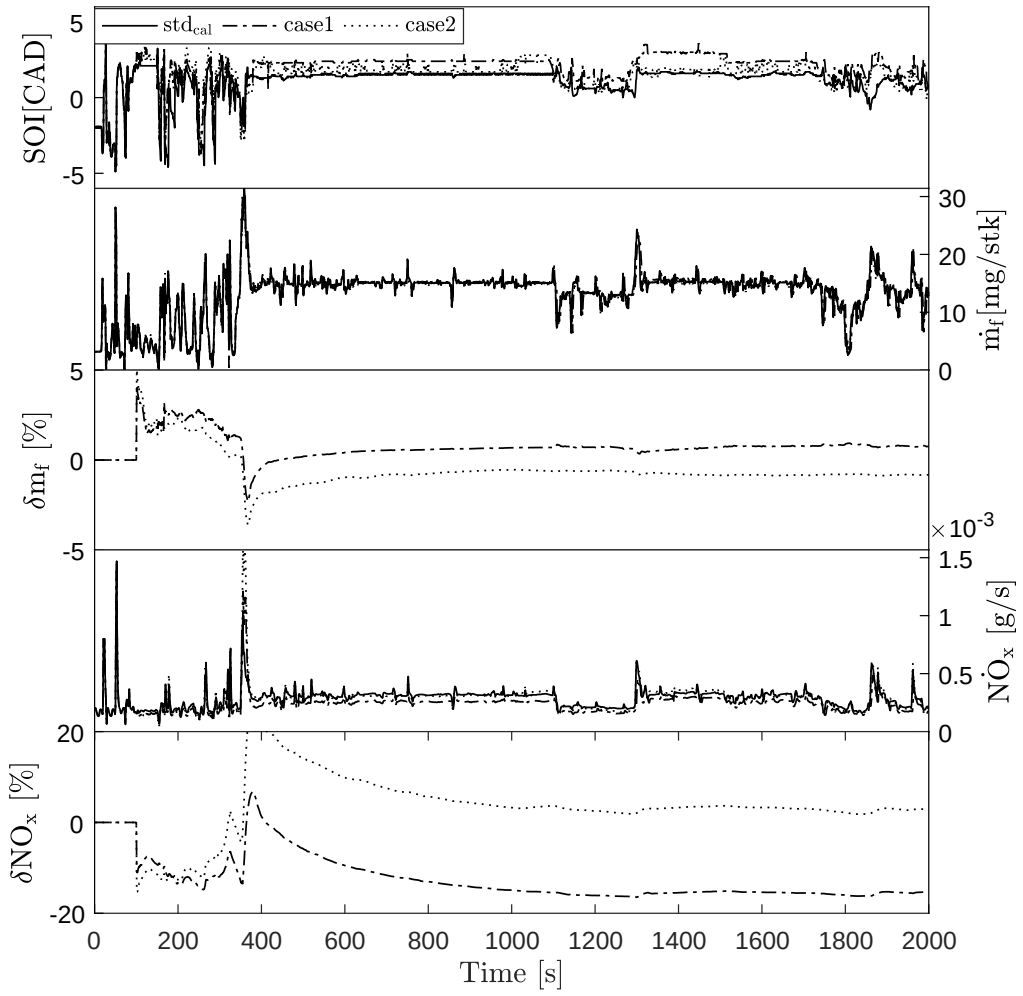

Figure 7.6: Scen1; Start-of-Injection; fuelling rate, difference of cumulative fuel mass, instantaneous NO_x emissions, difference of cumulative NO_x emissions

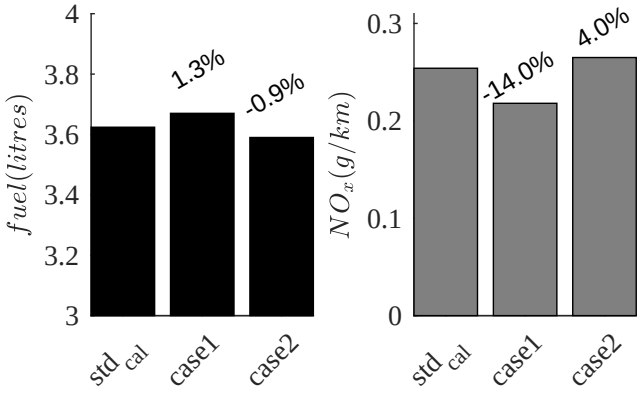

Figure 7.7: Scen1; Cumulative fuel consumption and NO_x emissions and their relative difference with standard calibration

case1. In case2, it is possible to reach the emission target of 0.3 g/km, while further reducing fuel consumption by 0.8 %.

The result can be summarised as:

- In scenarios 2, the constraints in both the cases are satisfied. Therefore, considering a driving cycle with higher aggressiveness for calculating calibration is a preferred approach to fulfilling the NO_x constraint.
- In the first and third scenario, the constraint in *case*1 can not be fulfilled, this is because the range of the look-up set for SOI is limited to 6 Crank Angle Degree (CAD). Including more actuators and increasing their range will directly influence the range of achievable NO_x emissions at the expense of control complexity. In addition to the control actions taken, there is an impact of the driving condition itself on the fuel consumption and emissions. However, with the developed methodology the emissions could be brought as close to the limit as possible by adaptation of the engine controls.

7.1.5 Summary and conclusions

The discrepancy in actual and declared Diesel engine emissions has raised a trend in applications which can optimise the engine performance during actual driving conditions. This section was aimed to present a pre-lookup based online adaptive calibration method to minimise fuel consumption with constrained NO_x emissions. The methodology followed during the development of application was also presented. Following the development of necessary tools, a case study was designed and tested on an engine testing set-up. The main findings of the study are as follows:

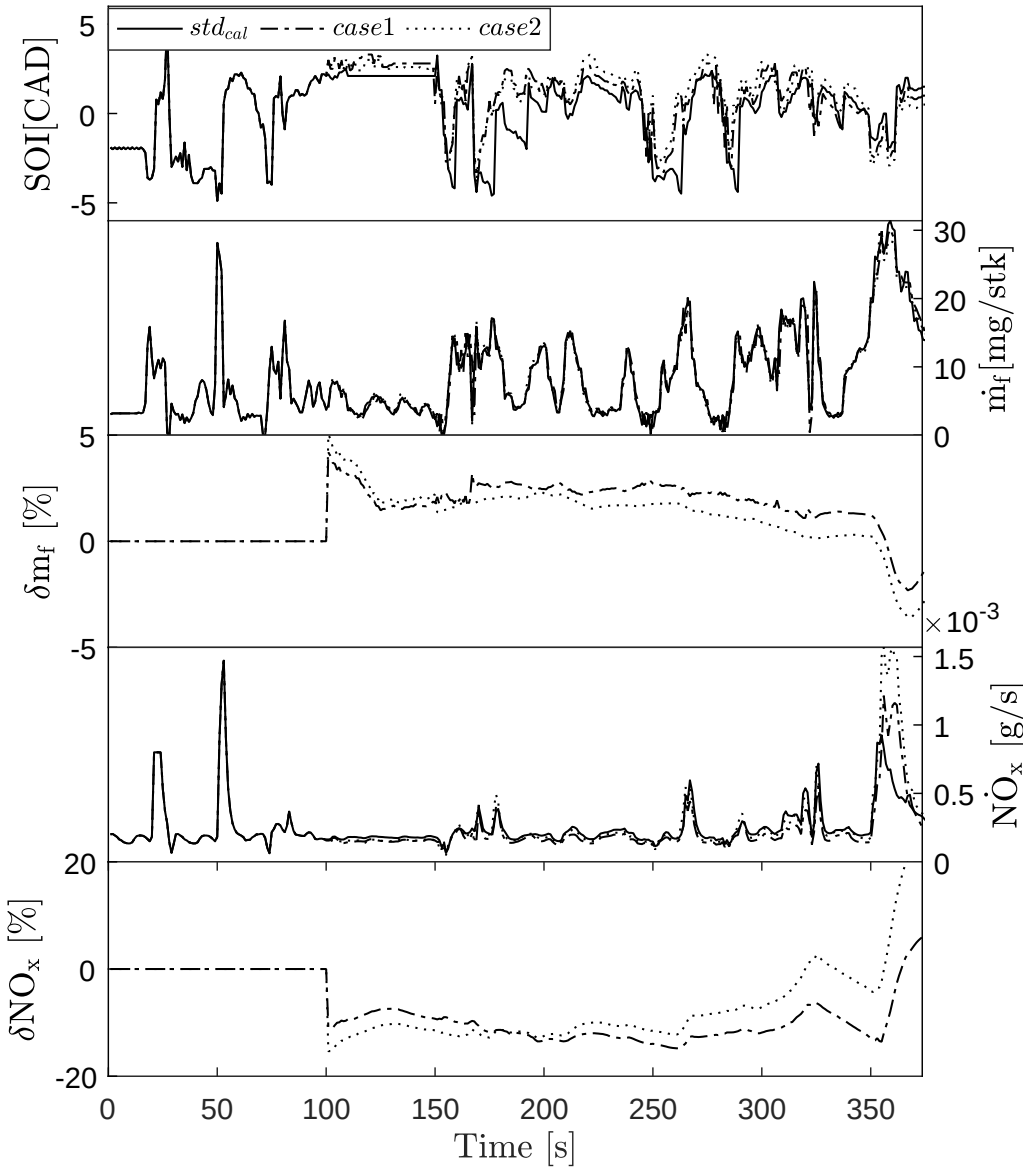

Figure 7.8: Scen1, Zoom : 0 − 360sec; Start-of-Injection; fuelling rate, difference of cumulative fuel mass, instantaneous NO_x emissions, difference of cumulative NO_x emissions

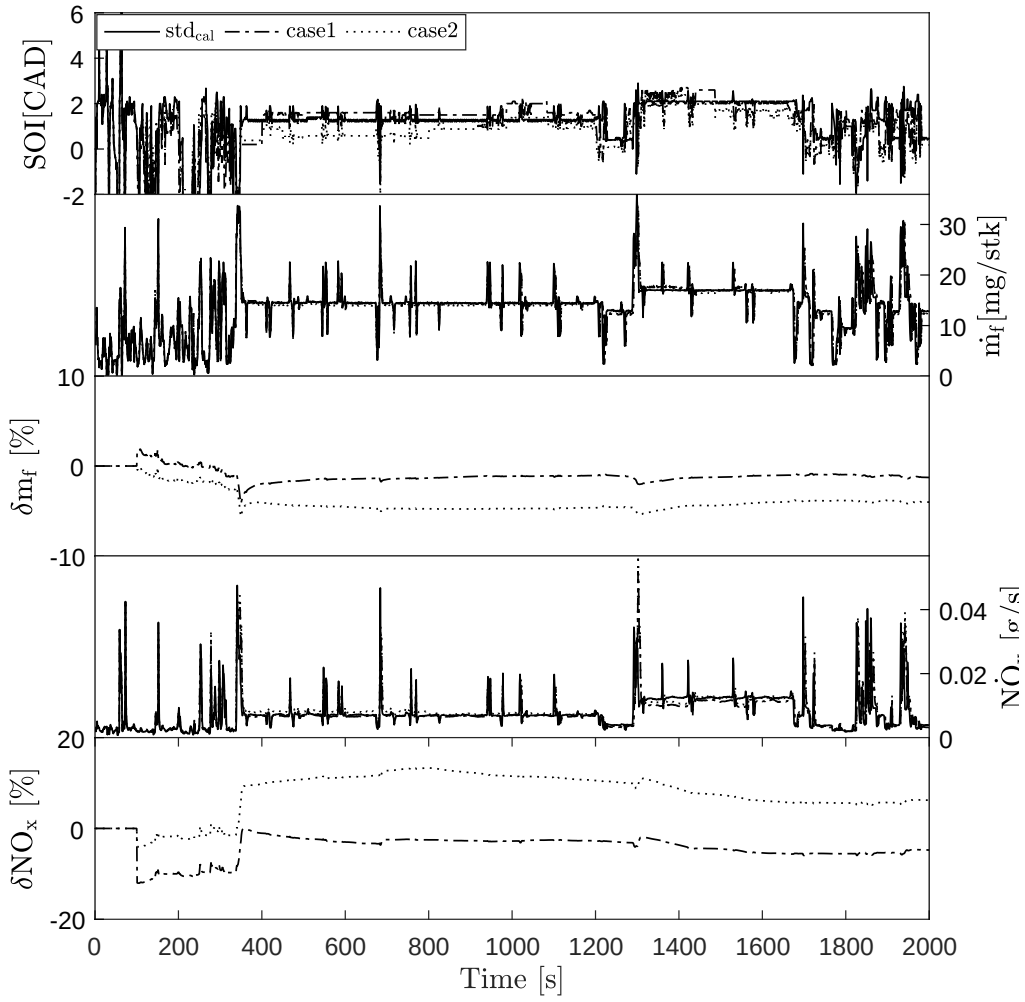

Figure 7.9: Scen2; Start-of-Injection; fuelling rate, difference of cumulative fuel mass, instantaneous NO_x emissions, difference of cumulative NO_x emissions

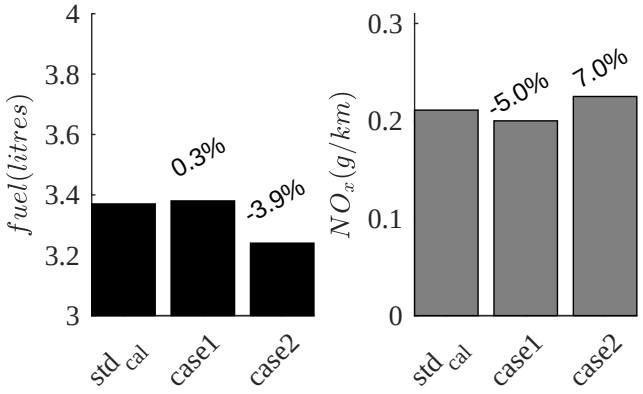

Figure 7.10: Scen2; Cumulative fuel consumption and NO_x emissions and their relative difference with standard calibration

- The implementation of the proposed methodology shows that the NO_x emissions can be constrained in real driving condition. The developed method is a mid-way to optimal control methods, which are computationally expensive for real-time application and state-of-the-art method based on fixed calibration which do not take into account most of the real driving uncertainties.

- The study demonstrates a real-time capable application of the Markov based cycle prediction tool also shown by Lujan et al. in [Luján *et al.* 2019]. The proposed method takes the advantage of available information about the velocity profile on a given route. This method is detailed in chapter 5.

- The study shows that aggressiveness is a critical parameter for evaluating real-time calibration of a Diesel engine. As the cycle prediction tool is efficiently able to capture the driving aggressiveness, with the proposed tool fuel consumption can be minimised up to 3 % while staying well within a predefined emission limit. Otherwise, the controller can not reduce the emissions below a certain level and then a driver advisory can be used to advise the driver about aggressiveness in order to fulfil emission targets.

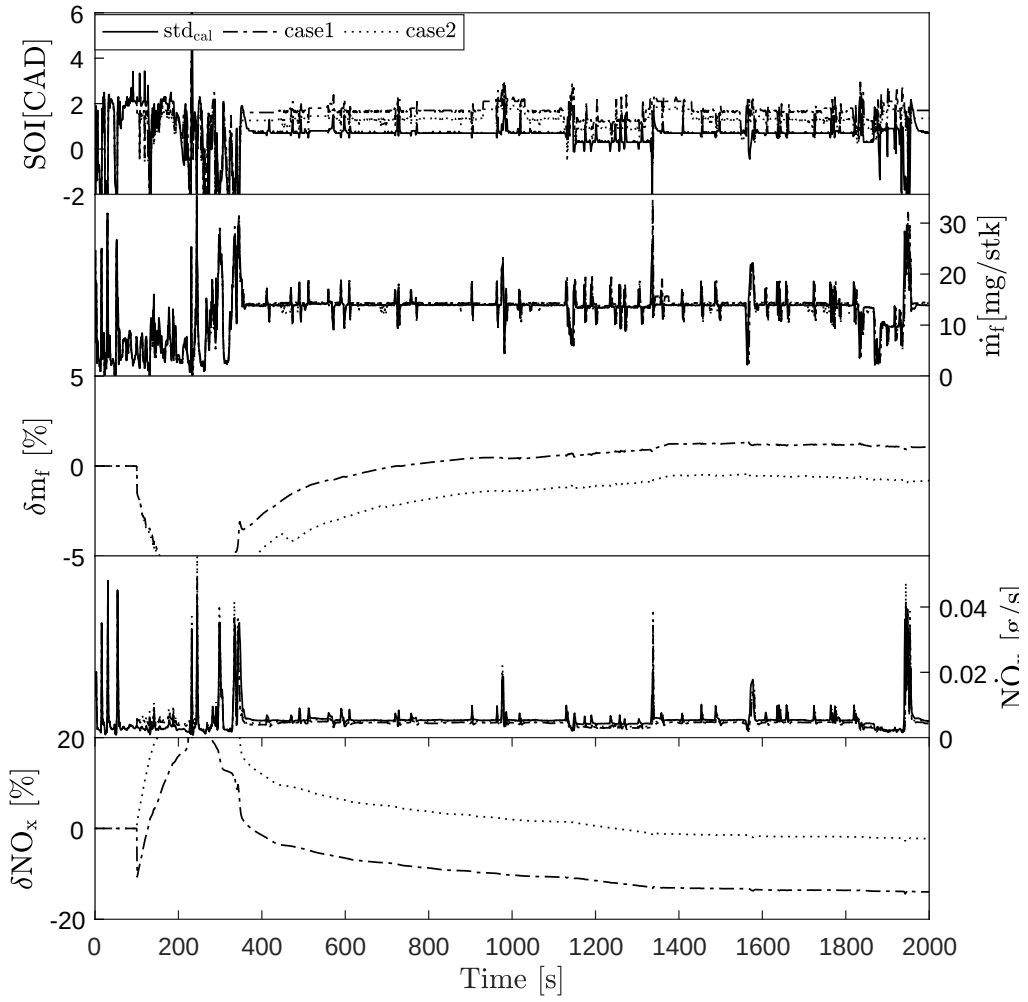

Figure 7.11: Scen3; Start-of-Injection; fuelling rate, difference of cumulative fuel mass, instantaneous NOx_x emissions, difference of cumulative NO_x emissions

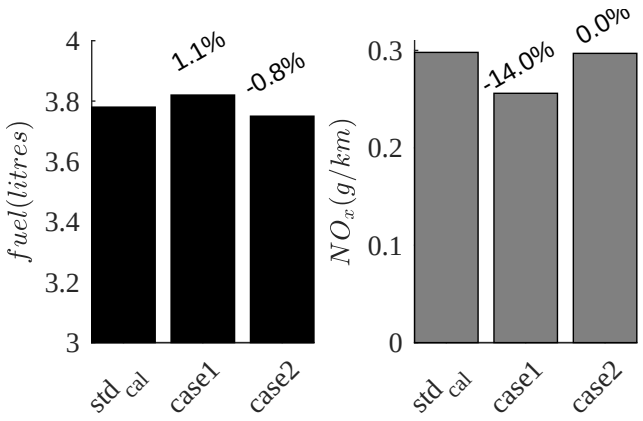

Figure 7.12: Scen3; Cumulative fuel consumption and NO_x emissions and their relative difference with standard calibration

7.2 Variable Smoothing of Diesel Engine Calibration

7.2.1 Introduction

The calibration process for Diesel engines involves three major steps. First, the engine speed and load domain—in which the engine is operated—is identified. Then, a global engine model is created, which can be used for offline simulations to estimate engine performance. Finally, optimal calibration maps are obtained by formulating and solving an optimisation problem, with the goal of minimizing fuel consumption while meeting constraints on pollutant emissions. This last step in the calibration process usually involves smoothing of the maps in order to improve drivability. The proposed method in this section presents a single tuning parameter for the trade-off between fuel consumption, NO_x emissions and drivability during transient engine operation. Drivability is addressed as the capability of the engine to follow a reference torque profile. A model-based optimal calibration approach is used to obtain maps which meet a specified NO_x emissions limit while minimizing the fuel consumption. Then, the tuning parameter is introduced to obtain different levels of map smoothness, which is based on the classical total variation method originally proposed by Rudin et al. [Rudin *et al.* 1992] and has been extensively used in the literature [Zhi *et al.* 2016, Aubert & Kornprobst 2006]. Finally, a time-varying smoothness strategy is generated and tested, with the goal to further improve engine performance and drivability, as compared to calibration maps with a fixed level of smoothness. The method was experimentally validated on a heavy-duty Diesel engine, and the non-road transient

cycle (NRTC) was used as a case study. The error between the reference and actual engine torque was used as a metric for drivability, and the error was found to decrease with increasing map smoothness.

7.2.2 Method Description

For the calibration of Diesel engines, it is common practice to model the input-output relationships statically [Berger 2012, Schüler 2001]. Various software tools are available to support the calibration engineer with the steady-state measurements and subsequent modelling [Gschweitl *et al.* 2001, Gutjahr *et al.* 2017, Mat 2017]. After that, model-based optimisation techniques are often used to find an engine calibration that yields the lowest possible fuel consumption while adhering to the limits on pollutant emissions [Hafner & Isermann 2003, Sequenz 2013].

For the engine in this study, the static engine model and model-based calibration were obtained as described in [van Dooren *et al.* 2019]. The control inputs u consist of the amount of fuel injected per cylinder and per cycle m_{inj}, the start-of-injection u_{soi} in degrees before top dead centre, and the desired burned gas ratio x_{bg} in the intake manifold. Whilst the amount of injected fuel is controlled to reach the requested torque T_e^{ref}, the two remaining control inputs u_{soi} and x_{bg} are the degrees of freedom to trade off fuel consumption $\dot{m}_f$ against engine-out NO_x emissions $\dot{m}_{NO_x}$. This is done as in [Elbert *et al.* 2017] by formulating and solving the following optimisation problem:

$$u^*(\omega_e, T_e, \mu_{NO_x}) = \arg\min_u \{(1-\mu_{NO_x})\cdot \dot{m}_f + \mu_{NO_x}\cdot \dot{m}_{NO_x}\} \tag{7.7}$$

The optimal control inputs u^* for each engine operating point depend on the weighting or "strategy parameter" $\mu_{NO_x} \in [0,1]$. Choosing a higher value for μ_{NO_x} results in lower engine-out NO_x emissions, but at the cost of a higher fuel consumption. While the engine strategy can—and usually is—fixed during the calibration process, the authors of [Elbert *et al.* 2017, Guardiola *et al.* 2016] have shown that an adaptive operating strategy can be used to adapt the raw emissions in a situation-specific manner.

The optimal values from (Equation 7.7) are stored on the engine control unit (ECU) as static maps that serve as a feed-forward controller. An EGR controller controls the intake valve and EGR valve position to reach the desired burned gas ratio.

Variable Map Smoothing The optimal calibration maps obtained from the previous section are usually non-smooth. The calibration engineer may

chose to smooth them manually or using available tools as in [Gschweitl *et al.* 2001, Gutjahr *et al.* 2017, Mat 2017]. The methods are usually based on filtering techniques, where the value of filtered data point is the average of original data point and its adjacent points. A group of adjacent points in the original data are multiplied point-by-point by a set of coefficients that defines the smooth shape, the products are added up and divided by the sum of the coefficients, which becomes one point of smoothed data. Subsequently, the set of coefficients is shifted one point down the original data and the process is repeated. Mean filtering methods are not well suited for specifically eliminating peaks from the maps. Another method used for smoothing is based on computing the second derivative (local curvature) at each point and then calculating the average of the squared values of the local curvature for the entire map.

The methods described above do not explicitly take into account the cost of smoothing in terms of closeness to the original map or the loss of optimality. In this work, a variational method is applied to obtain the smooth maps. The method is based on a classical variation model for image de-noising, originally proposed by Rudin et al. in [Rudin *et al.* 1992]. The problem is formulated as the following convex optimisation problem and solved by the primal-dual method as demonstrated by Zhi et al. in [Zhi *et al.* 2016]:

$$\min_{u} \int \{ (1-\mu_{sm}) \cdot (u-u^*)^2 + \mu_{sm} \cdot \nabla u_{x,y} \} \, dx \, dy \tag{7.8}$$

where u are the control inputs of the smoothed two-dimensional (x,y) calibration map and u^* denotes the optimal but non-smooth map, obtained from the model-based calibration method described in the previous section. For all the investigations presented in this application, a fixed engine strategy $\mu_{\mathrm{NO_x}} = 0.11$ was used.

The first term in Equation 7.8 accounts for the closeness of the obtained smoothed map to the original optimal but generally non-smooth map, and the second term contributes to the total variation of the obtained map. The closeness to the original map has been considered rather than the cost in terms of fuel consumption and $\mathrm{NO_x}$ emissions in (Equation 9.1). This is done to separate the optimisation and smoothing phases in the calibration process. The normalised total variation in the direction of engine speed and torque is $\nabla u_{x,y}$. The regularisation weight $\mu_{sm} \in [0,1]$ is used to tune the smoothness level of the maps. When $\mu_{sm} = 1$, only the second term in Equation 9.1 is minimised, producing the smoothest possible map. For $\mu_{sm} = 0$, no smoothing is applied, and the resulting map is the original non-smooth map.

The continuous problem in Equation 7.8 can be discretised and solved numerically as in Equation 7.9, where $n = 5$ is the grid size of the map under

consideration:

$$\min_{u} \sum_{i=1}^{n} \sum_{j=1}^{n} \{ (1 - \mu_{sm}) \cdot (u_{i,j} - u^*_{i,j})^2 + \mu_{sm} \cdot \nabla u_{i,j} \} \tag{7.9}$$

in which $\nabla u_{i,j}$ denotes the first order forward difference operation, defined as:

$$\nabla u_{i,j} = \begin{bmatrix} u_{i+1,j} - u_{i,j} \\ u_{i,j+1} - u_{i,j} \end{bmatrix} \tag{7.10}$$

Five calibration maps with different values of $\mu_{sm} \in \{0, 0.2, 0.4, 0.6, 0.9\}$ were calculated. Figure 7.13 and Figure 7.14 show the impact of varying μ_{sm} on the calibration maps for start-of-injection (u_{soi}) and burned gas ratio x_{bg}, respectively. The original maps u^* are shown in grey, and they are non-smooth. With increasing value of μ_{sm}, the smoothness of the maps visibly increases. As μ_{sm} is increased from zero, the maps initially get smoother where a maximum reduction of the total variation can be achieved. When μ_{sm} is further increased, also the remaining regions of the map become smoother.

In Figure 7.15, the impact of μ_{sm} on the primary and secondary terms of Equation 9.2 is shown. As expected, with increasing μ_{sm}, the normalised total variation of the map decreases at the cost of its distance from the original map.

7.2.3 Results

In this study the following two sets of experiment were conducted:

- The five calibration maps obtained from the method described in subsection 7.2.2 were tested on the engine test bench described in section 6.2. The Non-Road Transient Cycle (NRTC) cycle was run to obtain the trade-off between fuel consumption, NO_x emission and torque error.
- The optimal problem was solved to obtain a μ_{sm} profile for minimising the NO_x emission while constraining the fuel consumption and torque error within predefined limits. The obtained variable μ_{sm} strategy was tested on the engine.

Trade-off between Performance and Drivability The calibration maps in Figure 7.13 and Figure 7.14 show that with an increasing μ_{sm}, the SOI is advanced at lower engine speeds and torque, whereas SOI is retarded at higher engine speed and torque. On the other hand, the burned gas ratio is reduced at high engine torque and increased for $\mu_{sm} = 0.6$ and 0.8, regardless of the

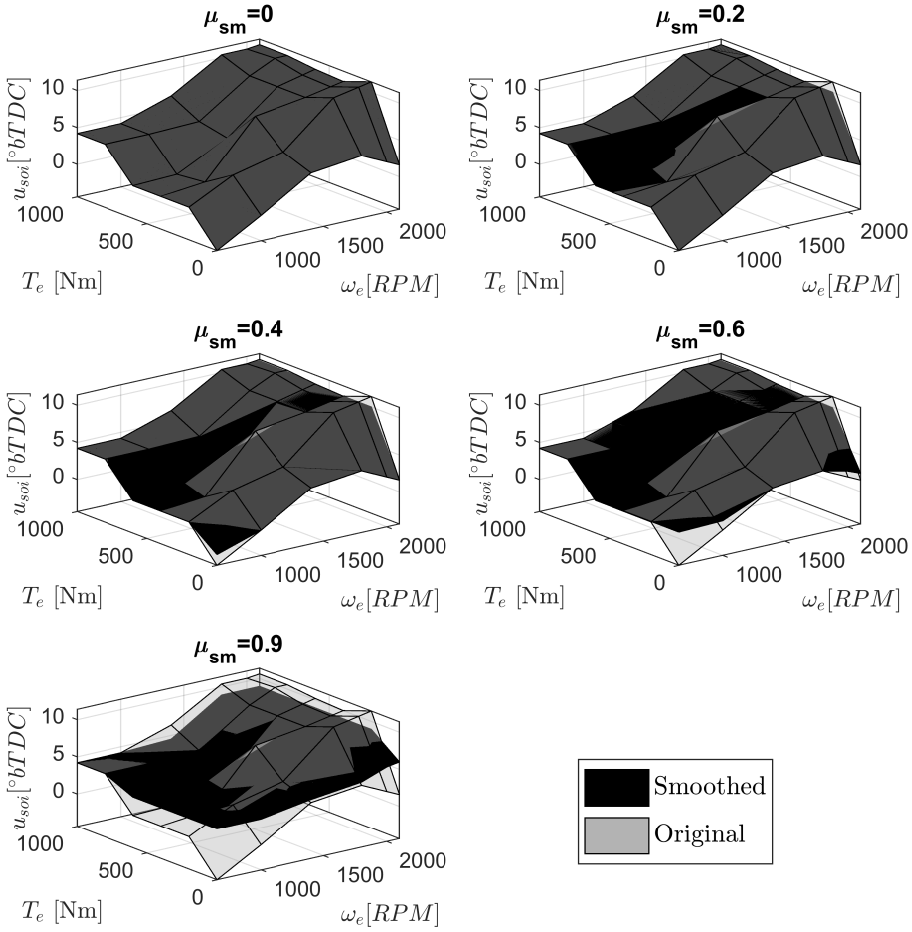

Figure 7.13: Impact of smoothing on *soi* calibration maps

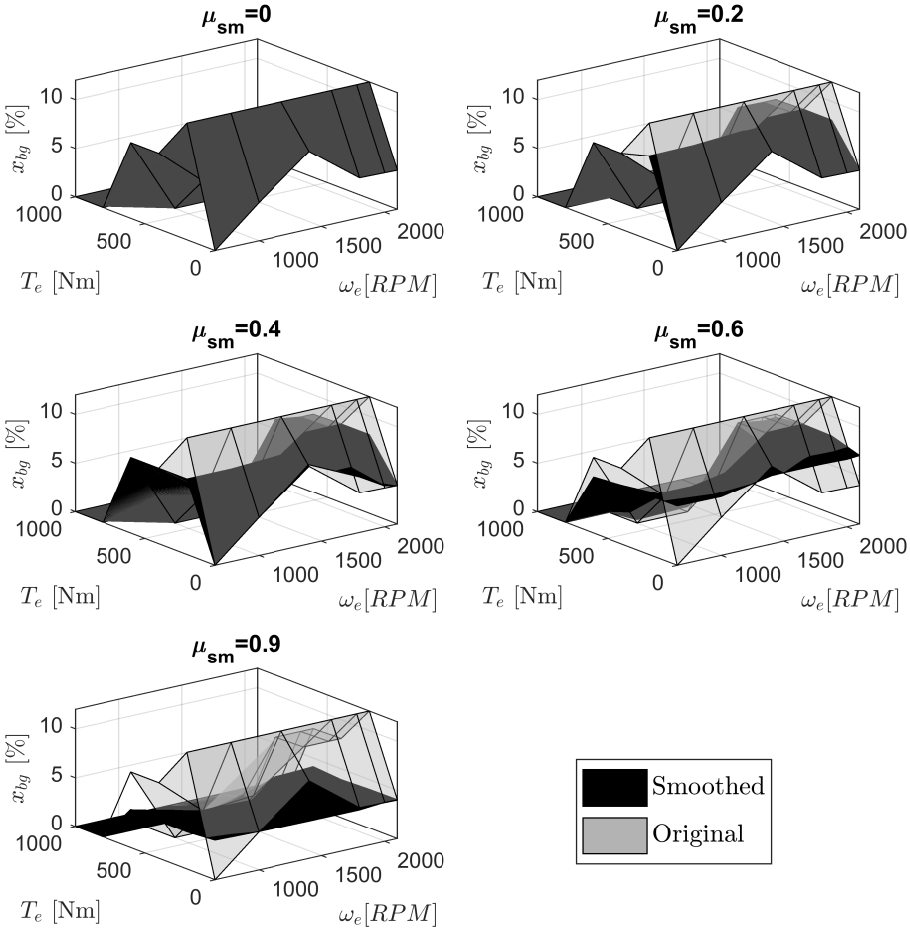

Figure 7.14: Impact of smoothing on *egr* calibration maps.

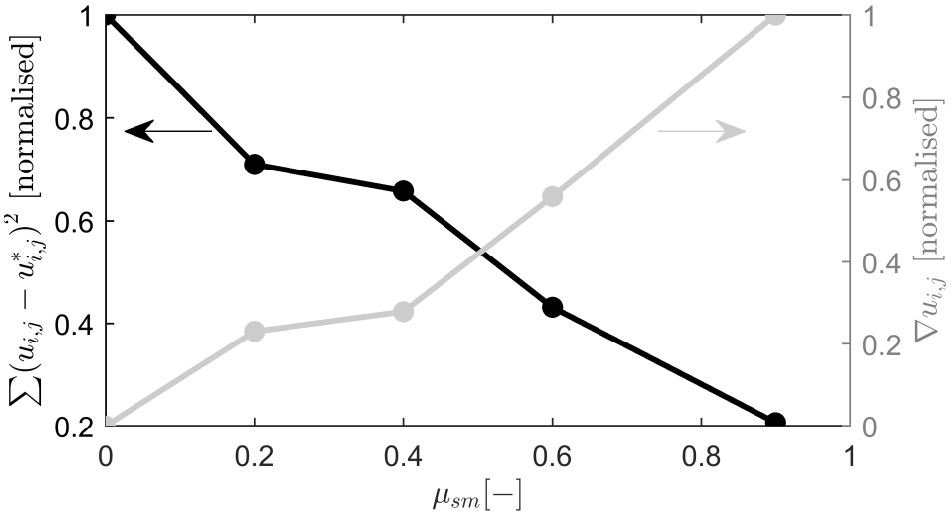

Figure 7.15: Impact of weighting factor on the total variation $\nabla u_{i,j}$ and distance from the original map $\sum(u_{i,j} - u^*_{i,j})^2$

engine speed. The obtained calibration maps are stored in the engine ECU as static maps to serve as a feed-forward controller. Taking the NRTC as a case study, the various maps are implemented and tested on the engine test-bench. The results are presented and discussed in this section.

Figure 7.16 shows the instantaneous engine torque, start-of-injection, burned gas ratio, fuel consumption, and NO_x emissions during the NRTC. The cumulative impact of the control actions can be clearly seen in the instantaneous NO_x emissions in the bottom plot.

In order to compare the torque response of each calibration map, the error between reference and actual engine torque is calculated for the cycle as:

$$T_e^{\text{error}} = \sum_{\text{NRTC}} (T_e^{\text{ref}} - T_e) \tag{7.11}$$

The top plot in Figure 7.17 shows the reference torque profile T_e^{ref}. In the bottom plot, normalised T_e^{error} is shown for the cycle. It is normalised by dividing T_e^{error} obtained with a specific calibration by the error obtained with $\mu_{sm} = 0$. As expected, with increasing smoothness of the calibration maps, the torque error is reduced consistently.

In Figure 7.18, the trade-off between fuel consumption, NO_x emissions, and torque error is shown. For $\mu_{sm} = 0.9$, the NO_x emissions increase by 9%, fuel consumption increases by 1%, and an improvement in torque response is observed. Table 7.1 consolidates the parameters related to the engine performance with different values of μ_{sm}. Based on this data, the calibration

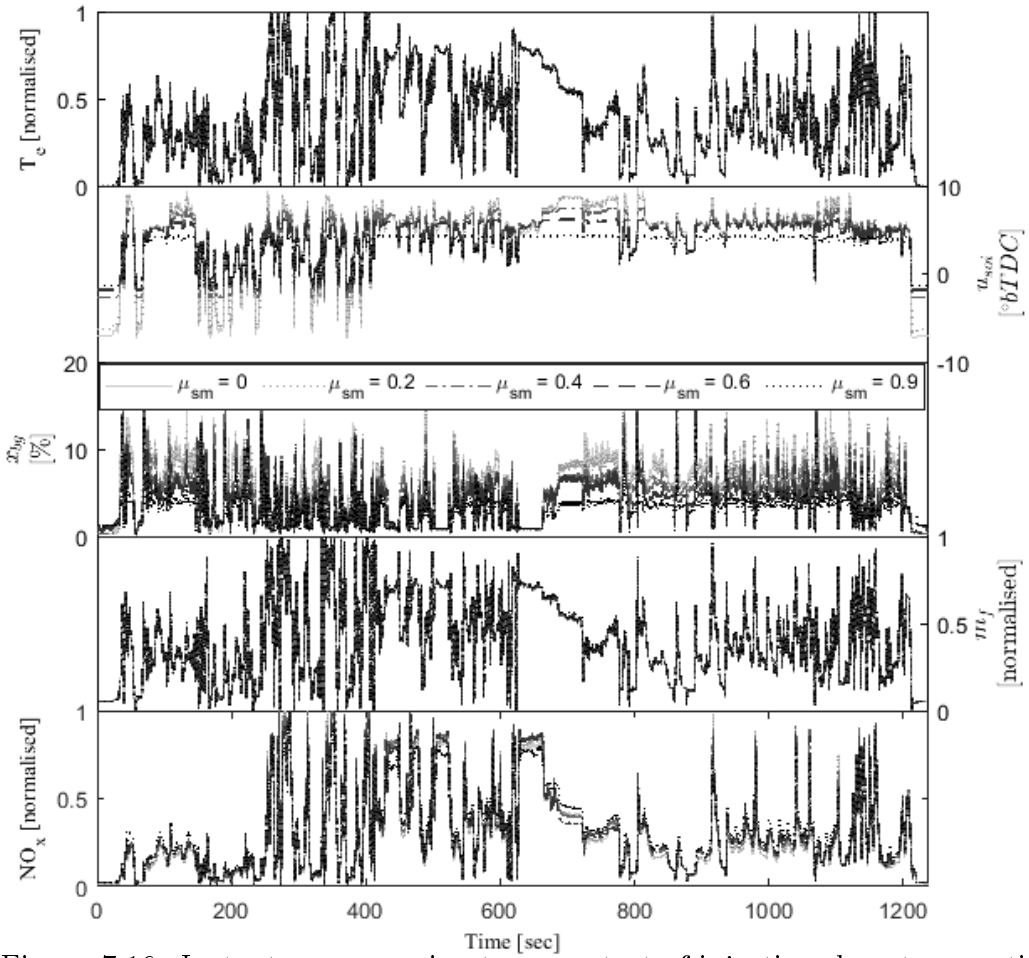

Figure 7.16: Instantaneous engine torque, start-of-injection, burnt gas ratio, fuelling rate, NO_x emissions measured at the test bench with different smoothness levels

μ_{sm}	0	0.2	0.4	0.6	0.9
BSFC	0.991	0.99	0.989	0.992	1
NO_x	0.916	0.938	0.977	0.979	1
T_{error}	1	0.977	0.955	0.943	0.917

Table 7.1: Impact of μ_{sm} on BSFC (normalised), NO_x emissions (normalised) and T_e^{error} for NRTC

engineer may chose the value of μ_{sm} that fulfils the performance requirements.

Time-varying Smoothness Calibration A map smoothing method was developed and used to obtain a trade-off between fuel consumption, NO_x emissions and T_e^{error} in the previous section. Based on the resulting trade-off, a time-varying smoothness strategy is proposed to minimise the NO_x emissions while constraining fuel consumption and T_e^{error}. A case study is designed to assess the impact of time-varying smoothness on the engine performance. From the set of five calibrations of the previous section, $\mu_{sm} = 0.2$ is assumed to be the favourable choice of a calibration engineer based on the emission and the drivability constraints. The objective of the case study is to obtain a sequence of μ_{sm} for the NRTC to minimise NO_x emissions while obtaining the same or less fuel consumption and torque error as compared to the fixed smoothness

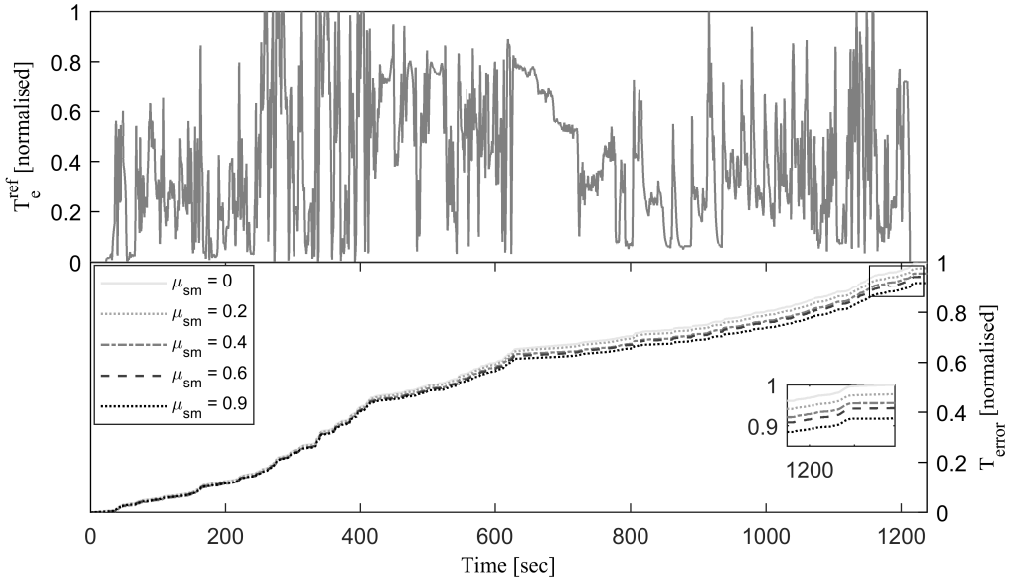

Figure 7.17: Reference torque profile (top) and cumulative error in torque reference tracking (bottom)

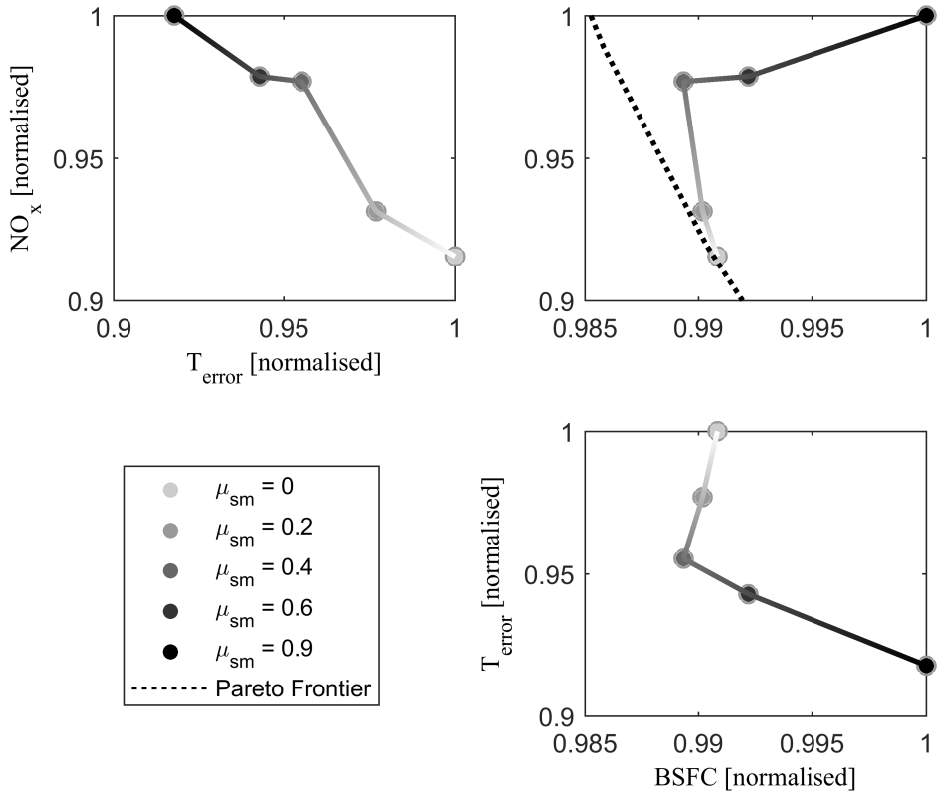

Figure 7.18: Trade-off between torque error and engine performance with different smoothing levels

strategy. To do this, μ_{sm} is adapted in a time window of 100 s. In each time window, μ_{sm} is selected from the already tested set of calibrations such that the cumulative $\mathrm{NO_x}$ emissions in the window are minimised while keeping fuel consumption and $\mathrm{T_e^{error}}$ less than or equal to the reference calibration, which is $\mu_{\mathrm{sm}} = 0.2$. This can be formulated as the following optimisation problem:

$$\begin{aligned} \min_{\mu_{sm}} \quad & \sum_{win} \mathrm{NO_x} \\ \text{subject to} \quad & \sum_{win} \dot{m}_f \leq \sum_{win} \dot{m}_f(\mu_{sm} = 0.2) \\ & \sum_{win} T_e^{\mathrm{error}} \leq \sum_{win} T_e^{\mathrm{error}}(\mu_{sm} = 0.2) \end{aligned} \tag{7.12}$$

where $win = 100$ s is the size of the time window, during which the performance parameters are cumulated and based on which the smoothing strategy

is chosen. The resulting time-varying calibration, i.e. sequence of μ_{sm}, is tested on the engine test-bench on the NRTC.

The strategy obtained from (Equation 7.12) is shown in the top plot in Figure 7.19. The normalised engine torque errors obtained from the fixed and time-varying strategies are shown in the bottom plot. The control actions and instantaneous engine performance are compared for the two strategies in Figure 7.20. The NO_x emissions are largely reduced from 300 to 500 s, with similar fuel consumption and improved drivability. From 600 to 900 s, with $\mu_{sm} = 0$, the calibration is optimal in terms of fuel consumption and NO_x emissions. The non-smooth maps have less impact on the drivability, as the driving cycle is largely non-transient during this time period.

For the purpose of analysis, the cycle can be divided into four distinct phases, based on engine speed, torque, and the amount of transient operation. The first phase ranges from 0 to 250 s and consists of medium load and medium transients, phase 2 is between 250 to 450 s consisting of high load and high transients, the third phase is between 450 to 900 s consisting of high load and low transients, and phase 4 is between 900 to 1238 s and has low load and medium transients.

Phase 1: With increased smoothness, x_{bg} is decreased and u_{soi} remains largely unaffected. Resulting in higher NO_x emissions with higher μ_{sm}. Therefore, the controller chose to operate at $\mu_{sm} = 0.2$.

Phase 2: With higher map smoothness, x_{bg} is reduced while u_{soi} is significantly retarded, resulting in less NO_x emissions. On the other hand, reducing x_{bg} has a positive impact on torque reference following capability of the engine. During high load transients, the fuel injection is temporarily reduced to avoid high soot emissions [Guzzella & Amstutz 1998]. This negatively influences the torque reference following capability. Therefore, a smooth actuation of x_{bg} and u_{soi} is desirable during this period. Another factor which positively influences torque reference following capability is the improved acceleration of the turbocharger with reduced x_{bg} during load jumps. The controller increases μ_{sm} to 0.9, resulting in reduced NO_x emissions and improved torque reference following capability of the engine.

Phase 3: With increasing smoothness, u_{soi} is retarded compared to the original maps. There is very little x_{bg} in both the smooth and non-smooth map. As a result, the NO_x emissions are reduced as shown in the bottom plot of Figure 9.5. Because the engine operation is less transient during this phase, the controller chooses $\mu_{sm} = 0$.

Phase 4: For medium loads at the end of the cycle, the x_{bg} and u_{soi} are more or less similar for all levels of smoothness. Therefore, the differences are minimal in the engine performance and thus $\mu_{sm} = 0.2$ is chosen.

Figure 7.21 shows the engine performance obtained with the time-varying

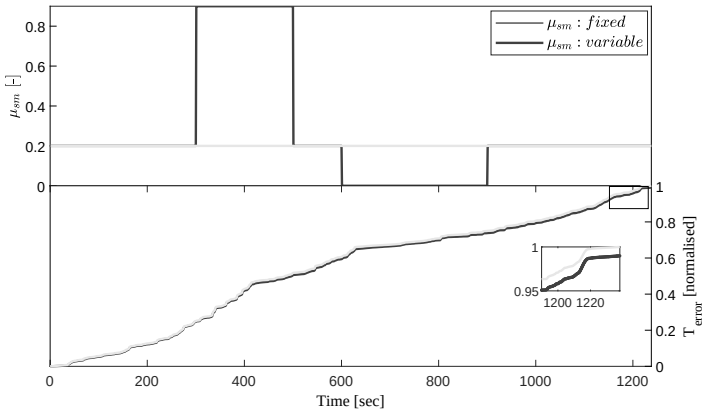

Figure 7.19: Top plot comparison of variable calibration smoothing and fixed calibration for NRTC cycle; bottom plot is the cumulative error in torque reference following

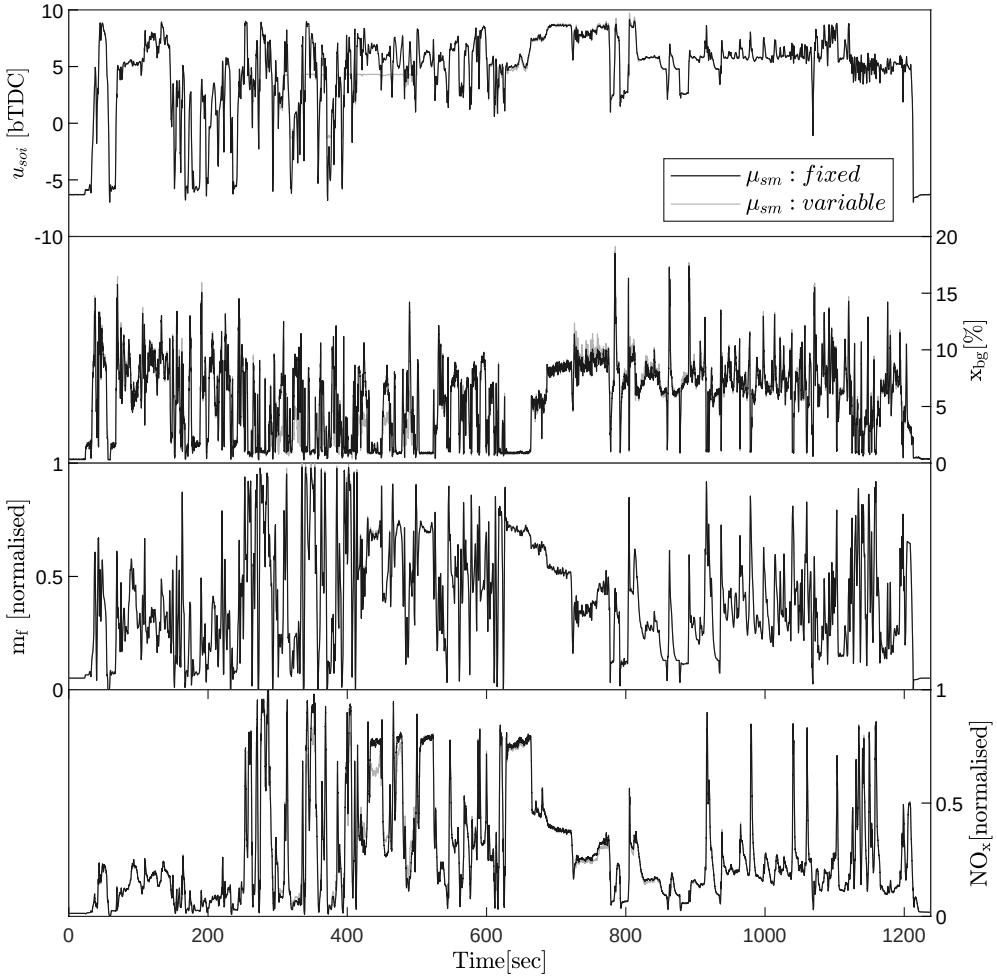

Figure 7.20: Performance trade-off comparison between fixed and variable smoothing method.

smoothness strategy, as compared to the fixed calibration strategy. With the time-varying smoothness, NO_x emissions can be reduced by 3-4% compared to the fixed calibration, while maintaining the same fuel consumption and torque reference following capability.

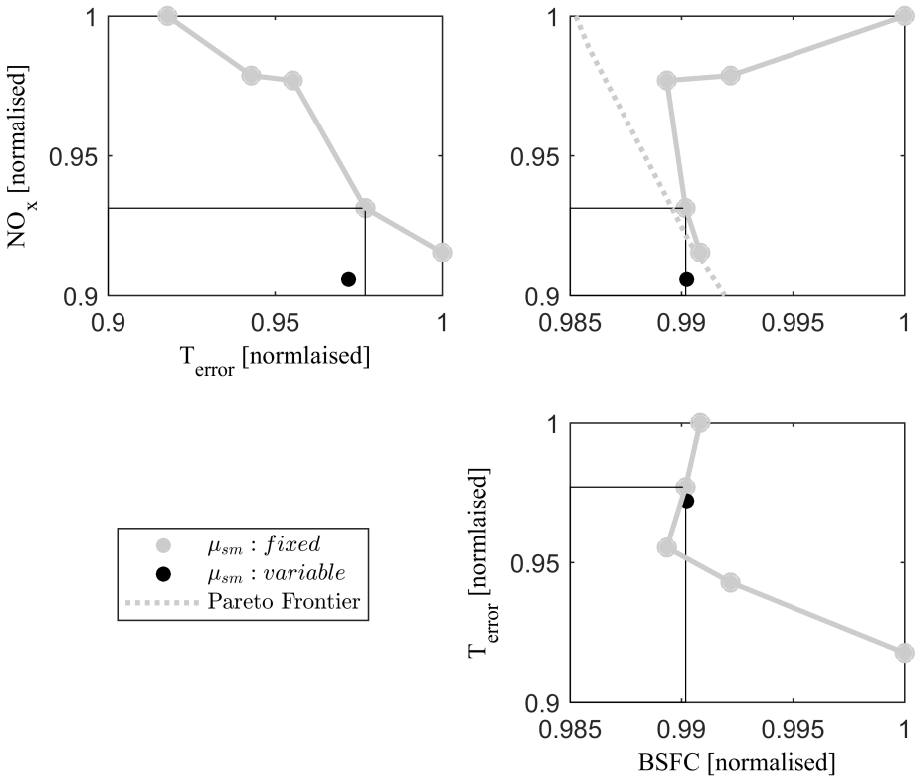

Figure 7.21: Comparison of engine performance for fixed and time-varying smoothness calibration.

The result highlights the potential of variable smoothing on a driving cycle. Although, this demonstration is made for the NRTC it can be extended to the real world scenario by online estimation of the error in torque,Brake Specific Fuel Consumption (BSFC) and NO_x emission. These estimations require a driving cycle prediction tool, an engine model and a supervisory controller to choose the optimal value of the proposed tuning parameter in real driving condition.

7.2.4 Summary and Conclusions

Drivability is improved by smoothing of optimal calibration maps obtained from model-based calibration. With smoothing of the calibration, the maps move away from the optimal settings. This results in a loss in optimality in terms of fuel consumption and NO_x emissions. This intervention is necessary especially during high transient engine operation, where a rough transition leads to poor drivability. A method is proposed to smoothen optimal calibration maps which are obtained from a model-based Diesel engine calibration approach. The non-smooth, x_{bg} and u_{soi} maps are optimal for a driving cycle to minimise fuel consumption with constraint on NO_x emissions. The smoothing method uses a tuning parameter μ_{sm} to reduce the total variation of the optimal maps to generate a set of smooth calibration maps. Drivability is addressed as the capability of the engine to follow the demanded torque profile and is shown to improve with the map smoothness. A trade-off between fuel consumption, NO_x emissions and torque error is obtained on the NRTC. Based on the results, an increase in μ_{sm} from 0 to 0.9 results in 9% increase in the NO_x emissions, 1% increase in fuel consumption and 9% decrease in T_e^{error}. A time varying smoothing method is proposed which adapts μ_{sm} in a moving time window based on the cumulative fuel consumption, the NO_x emissions and the torque error. In different phases of the cycle, the engine operates at different transient intensities. Having a degree of control freedom in map smoothness provide flexibility to adapt μ_{sm} based on the intensity of the transients. It has been demonstrated that same levels of torque reference tracking performance and fuel consumption can be achieved while reducing NO_x emissions by 3-4% with the application of time-varying smoothness strategy as compared to the state-of-the-art fixed calibration method.

- A variation-based methodology is proposed to change the smoothness of the calibration maps using a single tuning parameter. The additional degree of freedom can be used to trade off fuel consumption, NO_x emissions, and drivability. This flexibility can be of great help for the calibration engineer, while optimality is guaranteed at all times.

- A time-varying smoothness strategy is proposed to further improve engine performance and drivability. This is achieved by exploiting the fact that the driving cycle consists of various phases with the engine operation being more or less transient. By choosing an appropriate smoothing strategy for each phase, the NO_x emissions can be reduced, while having the same fuel consumption and drivability as in the case of a fixed smoothing strategy.

An additional degree-of-freedom has provided more flexibility to control the engine with the time-varying smoothness strategy. The proposed method can be extended to the real world scenario by including a driving cycle prediction model, an engine model and a controller that can optimally chose the proposed smoothness tuning parameter such that the fuel-efficiency is maximised while limiting the reference torque error and the NO_x emission.

7.3 Online optimal Energy Management strategy for Parallel HEV

7.3.1 Introduction and problem description

This chapter proposes an online Energy Management Strategy (EMS) for a plug-in Hybrid Electric Vehicle (pHEV) with the goal of minimising the fuel consumption while fulfilling the constraint on the terminal battery State-of-Charge (SoC) on a driving mission. In order to cope with limitations of both heuristic and Optimal Control (OC)approaches, several model based approaches have been proposed in past, most of them are based to some extent on OC, but sacrificing optimality for the sake of applicability. Amongst them, one can find Equivalent Consumption Minimization Strategy (ECMS) proposed by [Paganelli *et al.* 2000] and Deterministic or Stochastic Model Predictive Control as in [Johannesson *et al.* 2007]. The ECMS is probably the most widely explored approach with several versions, all of them showing near-optimal results with a challenge of properly determining the equivalent factor (EF) [Tulpule *et al.* 2011]. The values of EF are cycle-dependent and hence pose the issue of non-causality. The task of updating the co-state online as driving scenarios vary is referred to as co-state adaptation and the supervisory controller is referred to as adaptive optimal supervisory controller. Method falling in this category are referred in the literature as Adaptive-ECMS(A-ECMS) strategy [Onori *et al.* 2015, Lei *et al.* 2020]. The non-causality is addressed in the literature by taking advantage of the driving information [Payri *et al.* 2015, Yu *et al.* 2020] to estimate the suitable values of the weighting factor between fuel and battery energy sources. The adaptation techniques in the literature are classified in two categories: The first category is adaptation base on the driving cycle prediction. The equivalence factor is estimated online based on a look ahead horizon defined in terms of energy at the wheels, to determine at each instant the most likely behaviour. [Sciarretta *et al.* 2004, Ambuhl & Guzzella 2009]. In literature, the task of driving cycle prediction is usually performed using Neural-Network (NN) and Markov-Chain (MC) based methods. In the article by the authors in [Xie *et al.* 2018], a comparison of

the two approaches is shown in terms of prediction accuracy and computation speed. The MC based method is shown to outperform the NN based method. In the article [Sun *et al.* 2017], authors proposed a RBF-NN speed prediction method integrated to the A-ECMS. This method used open-loop speed prediction derived from the current vehicle state. The second category of the adaptation methods is by exploiting the fact that the equivalence factors are similar for cycles with similar statistical properties. To recognise the driving cycle characteristics, the authors in [Guardiola *et al.* 2013, Payri *et al.* 2012, Gu & Rizzoni 2006, il Jeon *et al.* 2000] use statistic and clustering techniques to classify the driving type. Most of the pattern recognition algorithms in the literature first identify the kind of driving conditions the vehicle is undergoing, and then select the most appropriate equivalence factors from a predefined set.

This application addresses the adaptation by using the first method mentioned above. In the original A-ECMS, introduced by the authors in [Musardo *et al.* 2005], the algorithm predicts mission that the vehicle is following and determines the optimal Equivalent Factor (EF) for the current mission by the direct optimization method. The cycle prediction is based on a fixed transition probability matrix for the entire route and it does not account for the deviation in the predicted and the actual vehicle velocity. To this end, a close-loop driving cycle prediction method based on the MC approach is introduced in the A-ECMS. The driving prediction uses the historical information to obtain space dependent transition probability matrices and then uses Markov principle to recursively predict the driving cycle and update the EF based on the online ECMS results. In this way, the predicted speed and the EF adapt themselves periodically during the Control Horizon Window (CHW) such that, at any instance the power split is optimal and the expected terminal SoC is close to the desired level.

The main objective of the study is to develop an online applicable EMS for a pHEV that exploits the information obtained when the vehicle recurrently covers a given route. For application purposes, a route of 21km including rural, highway and urban areas has been chosen. The route was covered by the same driver 50 times during consecutive working days.

Regarding the vehicle, a pHEV has been chosen to show the strategy potential while the method can be adapted to deal with other powertrain types (series, series-parallel, charge sustaining,...). In this architecture, i.e parallel arrangement ,the vehicle can be driven by the ICE, the EM, or both simultaneously. Thus, there are different solutions to provide the power required by the driver with different costs and impacts in future operation, which poses an interesting optimization problem. The battery is charged either by an external power source, by the ICE or by regenerative braking through the electric

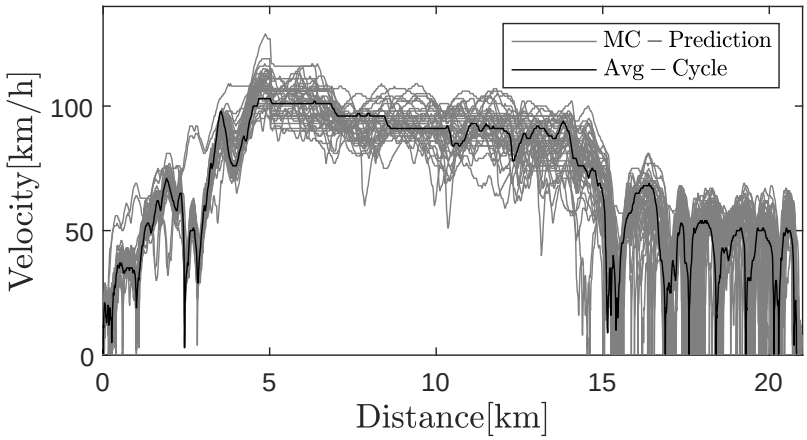

Figure 7.22: Real driving missions

motor. The main characteristics of the vehicle considered in the present work are shown in Table 3.1, while the layout and main energy flows in the powertrain are shown in Figure 3.9 The addressed problem will be to optimize the power-split of the pHEV in order to minimise the fuel consumption of the vehicle in the considered route avoiding SoC excursions over the battery limits.

7.3.2 Method Description

The problem previously described fits perfectly in the field of Optimal Control, as the extensive literature on EMS shows [Tang & Rizzoni 2016, Jiang *et al.* 2017, Du *et al.* 2016]. The associated Optimal Control Problem can be written as:

$$\begin{cases} \arg\min_u \int_0^T \dot{m}_f(u,v)dt \\ \dot{x} = g(x,u,v,\dot{v},\gamma) \\ h(x,u,v,\dot{v},\gamma) \leq 0 \end{cases} \tag{7.13}$$

where, for the sake of readability, the explicit dependence of the variables on time has been omitted, T is the driving cycle duration, g is the function describing the state dynamics (equation 3.18) and h represents the local constraints imposed on the state and control variables in order to guarantee the

physical operation limits (maximum and minimum limits on battery state of charge and power, speed and torque of powertrain elements).

Regarding the solution of system Equation 7.13 one can observe that provided the dependence on $T, v, \dot{v}$ and γ a proper estimation of such parameters is needed. In fact, the optimal solution of the problem can only be obtained if perfect knowledge of the driving cycle is available. Assuming a suitable approximation of those variables, there is a wide set of solutions in literature consolidated by the authors in [Zhang *et al.* 2020]. Amongst them, those derived from the Equivalent Consumption Minimization Strategy (ECMS) are widespread since provide a feasible on-board application. The ECMS is aimed to replace the integral problem presented in Equation 7.13 with a set of equivalent problems to be solved at every time step:

$$J = P_f + \mu P_b \tag{7.14}$$

where the parameter μ, is a weighting factor between fuel and battery energy sources. An analytical derivation of the ECMS can be obtained from the PMP [Serrao *et al.* 2009], in any case, intuition shows that a penalty on the battery use should be included in the cost function to avoid its depletion. The selection of the proper value of μ depending on the driving conditions is the key aspect of the ECMS. Provided a driving cycle ($T, v, \dot{v}$ and γ) the value of μ that fulfils with constraints in problem Equation 7.13, and particularly the limitations in the SoC.

According to the suitability of the ECMS method and requirement of an estimation of driving cycle, the proposed controller is presented in Figure 7.23.

The prediction block uses the current vehicle position (s_t) and speed (v_t) to estimate the driving cycle main parameters, consisting on the duration $\hat{T} - t$, vehicle speed and acceleration sequences ($\hat{v}_{t:\hat{T}}$ and $\hat{\dot{v}}_{t:\hat{T}}$) and estimated road slope evolution during the cycle ($\hat{\gamma}_{t:\hat{T}}$). The prediction block is based on the tool described in chapter 5.

Once the driving cycle is estimated, the power demand block calculates the desired torque and speed based on the vehicle model described in section 3.1 and using $\hat{T}$, $\hat{v}_{t:\hat{T}}$, $\hat{\dot{v}}_{t:\hat{T}}$ and $\hat{\gamma}_{t:\hat{T}}$.

The inputs to the μ calculation block are the estimated torque and speed vectors ($\hat{T}_{g_{t:\hat{T}}}$ and $\hat{\omega}_{g_{t:\hat{T}}}$) and the current SoC ($\mathrm{SoC_t}$). The optimal μ in the sense of that leading to minimum SoC at the end of the estimated driving cycle is calculated by an iterative method, in the case at hand the bisection method. Note that the condition of minimum SoC at the end of the cycle has been chosen due to the plug in nature of the powertrain and taking into account that the vehicle can be fully recharged at the end of the route. In any case, the target SoC can be modified adding a new calibration parameter to the control strategy. The calculated μ is applied during a predefined CHW,

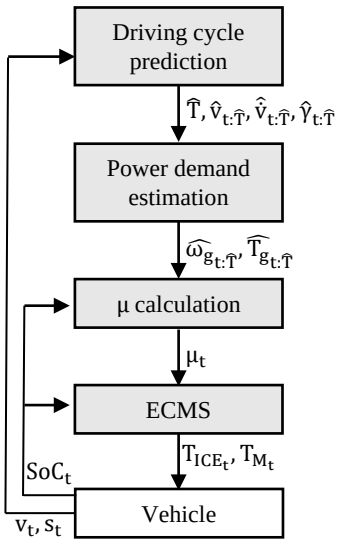

Figure 7.23: Proposed control architecture where s_t is the current vehicle position, $\hat{\cdot}$ represents an estimated variable and subindex $t : \hat{T}$ represent the evolution from current time (t) to the estimated end of the cycle ($\hat{T}$)

where the ECMS block calculates the optimal torque split between the ICE and the EM at every time-step. The CHW is a sliding distance window whose size decides the frequency at which the μ is updated during the trip in order to compensate the deviations in the SoC due to driving cycle estimation errors. In the present work a 1 km CHW is used to avoid excessive computation cost.

7.3.3 Design of case study for method verification and validation

There are four different energy management strategies tested in the simulations and Hardware-in-the-loop test environment for the purpose of comparison. The following is a list of the considered EMSs.

- CD-CS: The standard, Charge Depleting - Charge Sustaining strategy. For convenience, in CD-CS a low weighting factor μ is employed, from the beginning of the driving cycle until the battery SoC reaches the minimum value and then μ is increased or decreased online to keep the SoC as constant as possible.

- Average Cycle Prediction (ACP) + ECMS (ACP + ECMS): The driving cycle is not known in advance however, as the considered route has been previously covered 50 times, the average vehicle speed at every point

of the route (represented by black line in Figure 7.22) is used as an estimation of the driving cycle to feed the power demand estimation block in Figure 7.23, then calculate μ and apply the ECMS. The value of μ is updated after a given space window (1 km) to make up for deviations in the SoC.

- Markov Chain Process (MCP) + ECMS (MCP + ECMS): The driving cycle is not known in advance and the method proposed in section 5.2 is used following all the steps in Figure 5.1. Several predicted vehicle speed profiles are presented by the gray lines in Figure 7.22.

- Optimal (Equivalent Consumption Minimisation Strategy): The driving cycle is known in advance and an optimal weighting factor (μ) is applied during the complete driving cycle to minimise fuel consumption with a constraint in the minimum SoC.

In order to assess the performance of the proposed control strategy in a wide set of scenarios, a simulation campaign using forward versions of the powertrain model presented in section chapter 3 was done. Then, a verification of the method suitability is done experimentally on the test cell described in section section 6.1. A single driving cycle has been chosen to confirm the modelling results previously discussed. The simulation campaign consisted of running the vehicle model with 4 EMSs on 50 different driving cycles. On the other hand the experimental study comprised of running 4 EMSs on a single driving cycle.

7.3.4 Results

The scatter of the results with 4 EMSs (presented in the previous section) on several driving cycles is presented in Figure 7.24. Even though the objective of the control problem is to keep the SoC at 15% at the end of the mission, a tolerance is ± 5 was allowed during the study.

The dispersion of the fuel consumption for the similar value of the terminal SoC for each strategy is presented in Figure 7.25. It can be noticed that the MCP+ECMS strategy is nearest and CD-CS is farthest from the optimal; hence proving the potential of the current intervention. The performance of the CD-CS which does not take into account any prediction is inferior to the other two prediction based methods (MCP and ACP).

The implementation of the above four strategies in Hardware-In-Loop (HIL) setup was to further validate the results obtained from the simulation study. Figure 7.26 shows the driving cycle (vehicle speed) in the top plot, the evolution of μ and SoC with the tested strategies in the central

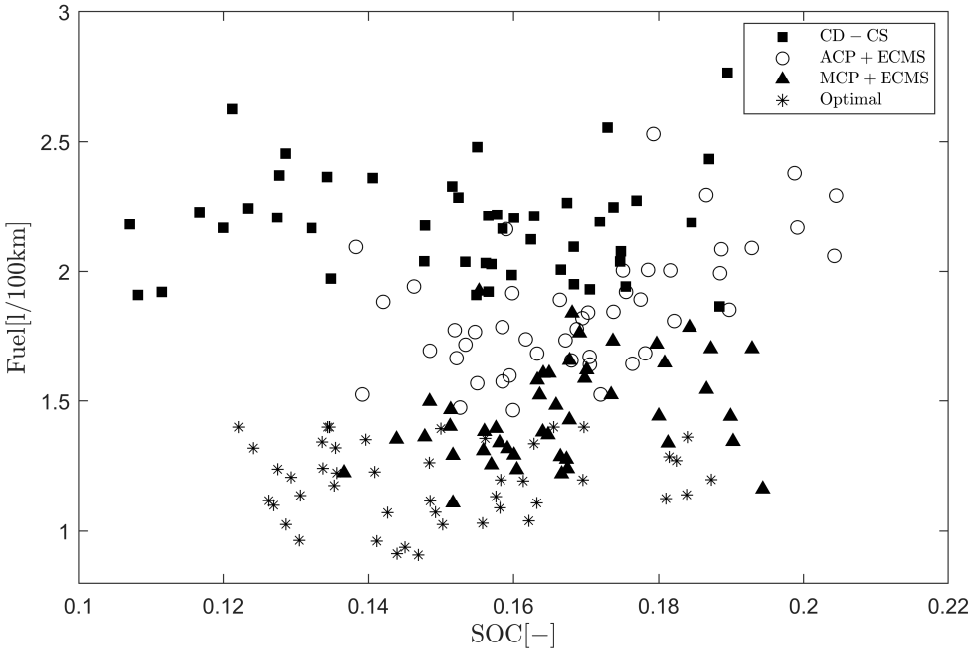

Figure 7.24: Simulation based verification of 50 different driving cycles, $*$ are the results with optimal EMS,$\bigcirc$ are the results with ACP + ECMS,$\triangle$ are the results with MCP + ECMS, $\square$ are the results with CD + CS

plots, and the accumulated fuel consumption in the bottom plot. One can observe, how knowing the driving cycle in advance (Optimal) allows to choose a constant weighting factor μ between fuel and battery energy that allows the ECMS to obtain the minimum fuel consumption fulfilling with the constraint in the minimum SoC of 0.15. Of course, the solution that minimises fuel consumption leads to the minimum SoC when the vehicle reaches the destiny and can be potentially recharged. On the opposite side, (CD − CS) leads to a substantial fuel increase despite fulfilling with the SoC constraint. It is clear that case-4 with the charge depleting - charge sustaining depletes the battery too early providing noticeable fuel savings in the first part of the cycle (until second 600) approximately but an excessive penalty in the last phase of the cycle. Regarding ACP − ECMS, it can be observed how the filtering due to driving cycle averaging leads to a smooth estimated driving cycle with too low dynamics, and this fact leads to a noticeable deviation from the optimal

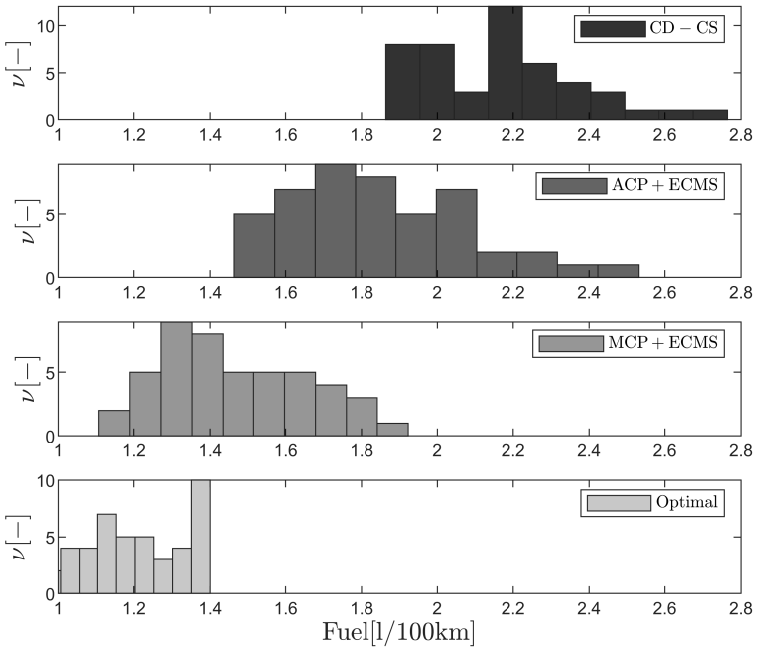

Figure 7.25: Spread in fuel consumption for similar level of terminal SoC for 50 driving cycles on the same route

(case 1) results despite it still improves the results with the CD-CS strategy, which at some point shows that despite, the average driving cycle provides some sort of description of the actual driving cycle. Finally, the proposed strategy (MCP + ECMS) leads to the nearest results to the optimal solution due to the better description of the driving cycle offered by the Markov based driving cycle estimator.

As a summary, Figure 7.27 shows the Pareto front obtained on a driving cycle applying constant μ with a priori knowledge of the cycle, and the rest of EMS considered. Provided the same SoC at the end of the driving cycle, the fuel consumption in $CD - CS$, $ACP + ECMS$ and $MCP + ECMS$ is 52%, 35% and 11% higher than the optimal as shown in Figure 7.28.

In Figure 7.29, the engine operating points are presented overlapping the efficiency map for the entire trip using four strategies. The black dots in figure represent the engine operating points in each scenario. The patches mark the boundary of operating points for each scenario. Clearly, in the case of optimal strategy the engine operates largely in the high efficiency zone. In $MCP + ECMS$ the patch area is smaller in comparison with $CD - CS$ and $ACP + ECMS$

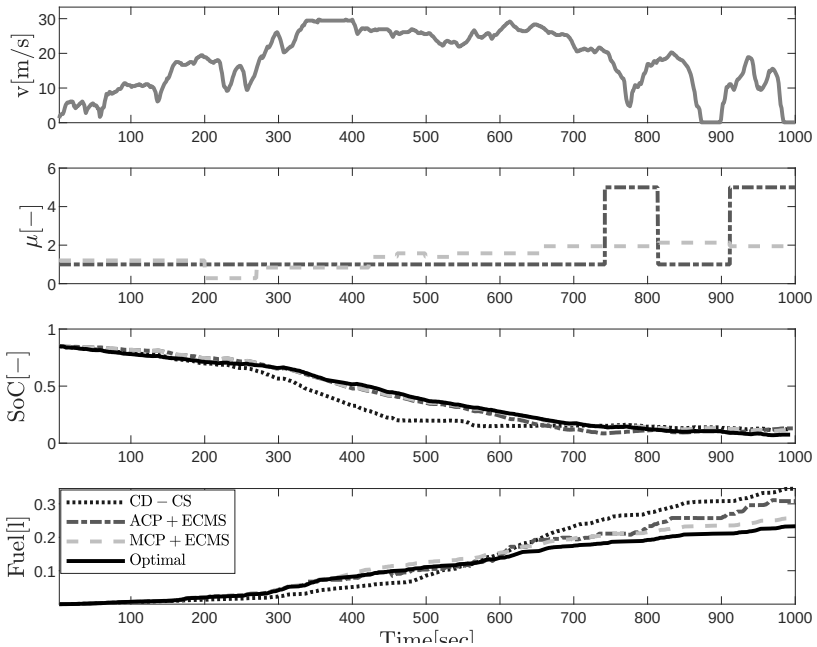

Figure 7.26: Evolution of experimental results in the considered driving cycle with strategies defined in cases 1 to 4.

7.3.5 Summary and conclusion

In a real driving mission the uncertainty in speed profiles lead to suboptimal energy management strategy in the pHEV. A new method based on the online speed prediction and adaptive ECMS is proposed to optimse the EMS while keeping the battery SoC close to the target. The developed method uses Markov based driving cycle prediction to adapt the μ based on the current SoC and the vehicle position. The method is validated using a simulation and an experiment based case study on a real-world driving mission. The experiments were conducted on an engine test bench with the help of vehicle model (Matlab/Simulink) in dSPACE environment. The developed method is compared with the three SOA methods: The CD-CS (Heuristic Approach), ACP+ ECMS (Online Approach) and ECMS (offline). The results from the developed online method show significant improvement in the fuel consumption as compared to the Adaptive ECMS and the Charge depleting strategy. As compared to the offline method, where the driving mission is known in advance the fuel consumption is 10% higher in the developed method. It is a step towards an optimal online control of the complex HEV energy management strategy. The proposed method can be extended to other HEV architectures and in future can be tested on the real vehicle which is commuting regularly between two destinations.

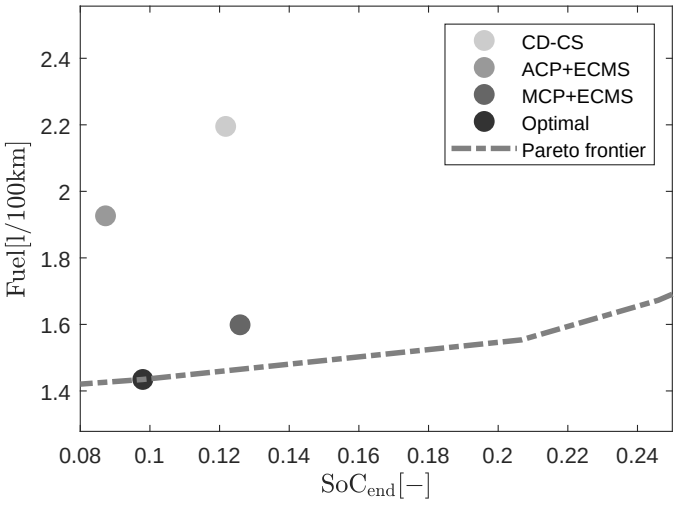

Figure 7.27: Experimental Validation of of four strategies. Trade-off between the SoC at the end of the cycle and fuel consumption, the dotted line is the experimental pareto frontier obtained by the optimal weighting factor.

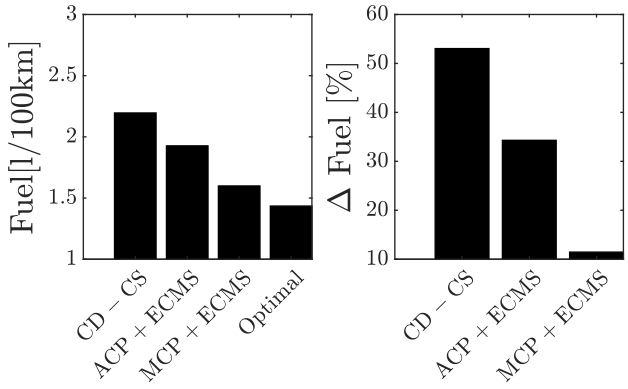

Figure 7.28: Relative difference between fuel consumption compared to the Case 1

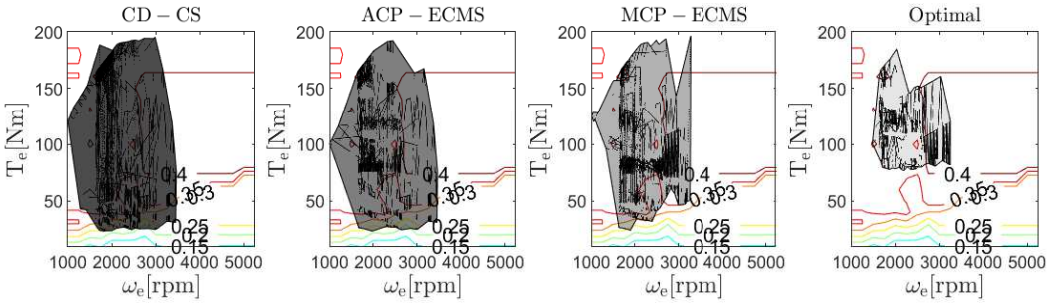

Figure 7.29: Engine Operating points overlapping the engine efficiency map

Chapter 8

Vehicle Speed Advisory Based Optimisation

Contents

8.1 Optimisation based on Traffic Light information

8.1.1 Introduction and problem description

The intrinsic complexity of optimising the speed profile of a vehicle driven on a route kept the researchers sceptical about the subject. Only until recently

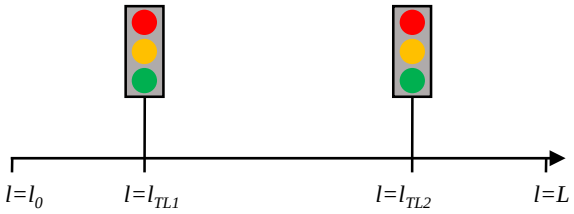

Figure 8.1: Scheme of the route analysed.

with the improvement in the computational capabilities, information availability through GPS, V2V and V2I have led to an increase in the research activities. The complexity arises due to several uncertainties in real driving conditions such as driver behaviour, traffic light, traffic situation, weather etc. The section addresses the impact of traffic light information availability in terms of fuel consumption and emissions by means of comparing 3 different scenarios that a driver of a diesel light duty vehicle may face when trying to cover a particular route of 1km with two traffic lights in between. The first scenario is that the driver does not know in advance the state of the traffic lights. The second scenario assumes that the driver knows the state of the traffic lights but has not modelling nor computation capabilities to solve the associated Optimal Control problem. In the third scenario, the driver knows in advance the state of the traffic lights and also is able to solve the corresponding Optimal Control problem that leads to fuel consumption or NO_x emissions minimisation. In the present study the vehicle speed trajectories associated to the previously described 3 scenarios have been computed and then tested in a Euro 5 Diesel vehicle installed in a chassis dynamometer presented in section 6.3.

The problem addressed in the application is to cover a particular route in less than a given time with minimum fuel consumption, or NO_x emissions, provided that several traffic lights are within the route. In particular, the route analysed is that of Figure 8.1, where l represents the route distance, l_0 and L are the starting and ending points respectively, while l_{TLi} represents the position of traffic light i. Any of the traffic lights has its own period (T_{TLi}) and a time at red ($t_{red,TLi}$). For the sake of simplicity, it is assumed that the traffic light goes directly from green to red (no orange lighting is considered). The particular values of the previous variables employed in this study are shown in Table 8.1

Table 8.1: Route description.

Variable	value
l_0	0 m
L	1000 m
l_{TL1}	250 m
l_{TL2}	750 m
T_{TL1}	90 s
T_{TL2}	90 s
$t_{red,TL1}$	30 s
$t_{red,TL2}$	30 s

8.1.2 Design of case study for method verification and validation

In particular, the paper addresses the impact of traffic light information availability in terms of fuel consumption and emissions by means of comparing 3 different scenarios when a driver faces a route with traffic lights. The first scenario is that the driver does not know in advance the state of the traffic lights, so he applies a sensible strategy, i.e. keeping constant velocity from the start to the end (if possible) to cover the distance in the required time. Of course, depending on the state of the traffic lights, the driver will need to correct his strategy due to stops. One may expect that if the driver needs to stop due to a traffic light, and spend some time stopped, then the increase in velocity needed to finish the route in the desired time may involve a noticeable penalty in terms of fuel consumption. The second scenario assumes that the driver knows the state of the traffic lights but has no modelling nor computation capabilities to solve the associated optimal control problem. In this case, a simple strategy is proposed and evaluated in the paper, which is based on keeping velocity as constant as possible without having to stop in a traffic light. In the third scenario, the driver knows in advance the state of traffic lights and also has modelling and computation capabilities to solve the corresponding Optimal Control problem that leads to fuel consumption or NO_x emissions minimisation. The study is carried out considering a particular driving route of 1km with two traffic lights in between. The comparison of the performance of the previous strategies under different scenarios will lead to conclusions on the potential of the traffic light information to improve the fuel consumption and emissions of the vehicle. The current model does not take into account the warm-up behaviour of the engine but could be done in future with ease by including coolant temperature models. In any case, the current optimization leads to a vehicle speed profile that consists in an aggressive ac-

celeration, then almost steady velocity and finally coasting, in this sense, the current optimized profile will contribute to the warm-up during the first phase of the cycle. If warm-up phase is included we expect that the optimization strategy will be to accelerate even faster in order to warm the engine as fast as possible.

8.1.3 Method description

Amongst the variables affecting the solution to a given optimisation problem, one may find three that are specially relevant:

- The optimisation objective. In the case at hand, two different objectives are to be considered. First, the minimisation of the fuel consumption. Then, the minimisation of the NO_x emissions since it is the most critical emission in Diesel powered vehicles and there is an increasing concern about Diesel vehicle NO_x emissions in urban areas. Note that a multi-objective optimisation can be carried out considering a cost function weighting both fuel and NO_x emissions like in works addressing the energy management of Diesel Hybrid Electric Vehicles [Simon *et al.* 2018, Huo *et al.* 2018].

- The information availability. In this case, two opposite situations are considered: the case where there is no information about the state of the traffic lights and the situation where the state of the traffic lights is a priori known.

- The computation burden. An online application of the strategy will require an estimator for fuel consumption and emissions (model) and a real time optimisation tool while generally, both have high computation. In this sense, two different situations are considered: the situation where there are no computation restrictions that allow the application of Optimal Control techniques, in the case at hand Dynamic Programming, and a sub-optimal solution with real time application. Note that if traffic disturbances are neglected, the vehicle speed trajectories can be precomputed and applied according to the traffic lights state.

Taking into account the previous aspects, 4 strategies are evaluated in the present paper:

(i) Driver without traffic light information ($woTLI$): In this situation, the driver does not have information on the current and future state of the traffic lights. Taking into account that his objective is to cover the

distance L within a time frame $[0, T]$, a sensible strategy is to try to set a target velocity (v_{sp}) such that:

$$v_{sp}(t) = \frac{L - l(t)}{T - t} \tag{8.1}$$

Of course, depending on the state of the traffic lights, the driver may have to stop. According to item 8.1, from this point the objective velocity $v_{sp}(t)$ will be increased to compensate for the stopped time.

(ii) Driver with traffic light information ($wTLI$): It is rather intuitive that keeping the velocity as constant as possible has a positive impact on engine efficiency, since the inertial term in the energy balance is minimised. It is also intuitive that stopping the vehicle in a traffic light should be avoided to minimise fuel consumption and emissions since on one hand it involves a kinetic energy dissipation during breaking followed by an energy expenditure to accelerate the vehicle again, and on the other hand it will force a higher velocity after the traffic light to compensate for the time stopped. According to the above arguments, a solution close to the optimum in the case without traffic lights would be to maintain a constant average speed that would take the vehicle to the end of the trip at the desired time. For sure, the existence of traffic lights will often make this solution infeasible, but knowing when the state of the traffic lights changes can be used to consider a limited number of cases in which the vehicle speed is as constant as possible. In this sense, the proposed strategy consists of considering a set of segments with constant velocity, and then choose the combination with lower velocity variations that does not incur in passing through a traffic light in red. The case at hand, with 2 traffic lights, leads to the 9 trajectories of constant velocity segments without crossing the traffic lights in red represented in Figure 8.2.

From an implementation point of view, the three following aspects should be considered:

- This strategy is not optimal in terms of fuel consumption, nor NO_x emissions since the quantity to minimise is how the velocity is deviated from the constant velocity, provided some restrictions on the vehicle position at different times (i.e. the vehicle should pass through the position of every traffic light when its state is green). The optimisation problem can be stated as:

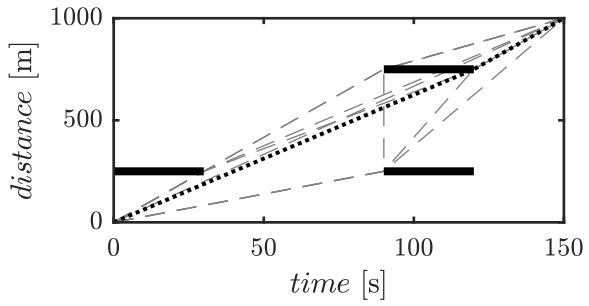

Figure 8.2: Scheme of the possible trajectories in the time-space plane that are considered in strategy $wTLI$ (in grey). The black thick lines represent traffic lights in red that can not be crossed, while the black dotted line shows the optimal trajectory in the sense of equation 8.2

$$\begin{aligned} & min \left\{ \sum_{j=1}^{j=n} \left(v_{sp,j} - \frac{L}{T} \right)^2 \right\} \\ & s.t. \\ & TL_i \left(l = l_{TL_i} \right) = green \end{aligned} \tag{8.2}$$

Where n is the number of segments in the route ($n-1$ is the number of traffic lights), $v_{sp,j}$ is the vehicle speed set point (the decision variable) in the segment j, and $TL_i \left(l = l_{TL_i} \right)$ is the state of the traffic light i when the vehicle passes through its position l_{TL_i}. According to the previous idea, this strategy does not require a model for fuel nor NO_x emissions since does not consider those variables.

- Strategies $woTLI$ and $wTLI$ provide exactly the same result if covering the distance at constant speed does not involve crossing a traffic light in red.
- Note that the calculation of the possible trajectories can be done offline, so the computation cost on board is strongly reduced.
- Note that the number of constant speed segments (see Figure 8.2) depends on the number of traffic lights since the timing when they change their state is used as a starting of ending point of the segment. Despite, in the case at hand, the number of cases to be tested is small, its number rapidly increases with the number of traffic lights in the route according to the following sequence:

  In order to consider many traffic lights within the route a more sophisticated optimization strategy than brute force, e.g. Dynamic Programming, should be applied.

Table 8.2: Number of cases (N_j) to consider in strategy $wLTI$ depending on the number of traffic lights (j).

j	1	2	3	4	n
N_j	3	9	23	53	$N_{n-1} + 2(1 + N_{n-1} - N_{n-2})$

(iii) Optimal speed profile to minimise fuel consumption with traffic light information (F^{opt}): This strategy considers the application of Dynamic Programming to the Optimal Control Problem of minimising fuel consumption while covering the distance L in a limited time T, provided that the vehicle cannot pass a Traffic Light in red.

(iv) Optimal speed profile to NO_x emissions with traffic light information (NO_x^{opt}): This strategy considers the application of Dynamic Programming to the Optimal Control Problem of minimising NO_x emissions while covering the distance$L$ in a limited time T, provided that the vehicle cannot pass a Traffic Light in red.

The Table 8.3, summarises main characteristics of the evaluated strategies:

Table 8.3: Description of the assessed strategies.

Strategy	Objective	TrafficLightInformation	RealTime
$woTLI$	NO	NO	Yes
$wTLI$	NO	Yes	Yes
F^{opt}	fuel	Yes	NO
NO_x^{opt}	NO_x	Yes	NO

Note that strategies (iii) and (iv) require a model for the estimation of fuel consumption and NO_x emissions. Details regarding the optimisation performed for those will be provided in following sections after describing the model used.

Fuel consumption and NO_x optimisation In the case of strategies (iii) and (iv), the model previously described has been used to calculate the vehicle speed sequence that minimises a given cost function (the fuel consumption or NO_x emissions respectively). In this sense, the associated Optimal Control

Problem (OCP) can be expressed as:

$$
\begin{aligned}
&min \left\{ \int_0^L \frac{h}{v} dl \right\} \\
&s.t. \\
&\frac{dv}{dl} = \frac{f}{v} \\
&\frac{dt}{dl} = \frac{1}{v} \\
&v(0) = 0 \\
&v(L) = 0 \\
&t(0) = 0 \\
&t(l_{TL1}) = t_{green,TL1} \\
&t(l_{TL2}) = t_{green,TL2} \\
&t(L) \leq T
\end{aligned}
\tag{8.3}
$$

Where the function h represents the fuel consumption (W_f) in the case of strategy (iii) or the NO_x emissions (W_{NO_x}) in case of strategy (iv). Function f represents equation of vehicle dynamics and $t_{green,TLj}$ represents the time range when the traffic light j is green. From the OCP presented in Equation 8.3 one can observe that:

- While the typical domain for OCPs is time, in this case, space (l) has been selected since it presents a more natural domain to include constraints related to traffic lights whose position is constant. The same approach is usually followed when constraints on the road gradient or vehicle speed limits are to be considered [Hellström *et al.* 2010a]
- The problem defined inEquation 8.3 has 2 states (v and t) and only one decision variable (u_{pedal}). In this sense, as the number of states and control variables is small, the problem is specially well suited for the application of Dynamic Programming (DP). In particular, the DP solver used in this work is a Matlab based code presented in [Sundstrom & Guzzella 2009].

8.1.4 Results

Independently on the availability of information concerning the state of the traffic lights, the starting time of the route with respect to the traffic light period, is a variable that is outside of control, at least this is the hypothesis followed in this work. In addition, it is obvious that the performance of any given strategy will strongly depend on the traffic light timing, and therefore on the instant of the traffic light period in which the travel starts. According to that, in the present work the timing of traffic lights when the trip starts is considered as a stochastic variable uniformly distributed between 0 and

T_{TL} (being T_{TL} the period of the traffic lights, in particular, 90 s according to Table 8.1). Then, any arbitrary performance index h (in practise fuel consumption or NO_x emissions) of a given strategy will be evaluated in terms of the expected value considering the average of the results obtained with different starting times (dT) distributed along the complete traffic light period.

To point out the impact of traffic light at the beginning of trip on the vehicle trajectory, Figure 8.3 shows the vehicle trajectories at 6 different timings (dT) of the 90 seconds period. In any of the trajectory plots (space as a function of time), the horizontal thick black lines represent the instants when traffic lights 1 and 2 remain red, the lines in grey scale represent the trajectories followed by vehicles with strategies $woTLI$ (in thick light grey line), $wTLI$ (black dotted line), F^{opt} (grey thick line) and NO_x^{opt} (in dark grey). It can be observed how the driver without Traffic Light information ($woTLI$) starts the trip with the same constant velocity independently on the starting time (dT). In particular, he follows a constant velocity profile (without considering the acceleration and breaking phases at the beginning and end of the trip) excepting cases $dT = 0$, $dT = 60$ and $dT = 75$ when the red state in any of the traffic lights forces the driver to stop. One may observe how in those cases, the driver needs to increase the velocity after the vehicle stop in the traffic light to make up for the time lost. In particular, in the case of $dT = 75$, despite increasing the vehicle velocity up to $50kmh$ (maximum allowed vehicle speed) after the stop in the second traffic light, the driver is not able to fulfil the time constraint and needs more then 150s to cover the travel length.

In spite of the fact that the fuel consumption in the cases without stop at the traffic lights may be low, cases $dT = 0$, $dT = 60$ and $dT = 75$ (and others around the same timing) where the vehicle needs to stop will harm the expected fuel consumption of the vehicle.

Strategy $wTLI$ coincides with $woTLI$ when no breaking due to traffic lights is required. In cases when the $woTLI$ strategy requires to stop the vehicle in a traffic light, the strategy $wTLI$ corrects the velocity profile to avoid hard breaking and subsequent acceleration.

Regarding the optimal strategies (F^{opt} and NO_x^{opt}) results show that a higher velocity at the first phases of the trip is preferable. The reason is that a faster acceleration and velocity during the first phases of the test allows the vehicle to coast at latter phases so there is not an associated fuel consumption nor NO_x emissions during those phases. Differences between F^{opt} and NO_x^{opt} trajectories are due to the fact that high efficiency areas in the engine do not correspond with low NO_x operating conditions. In fact, F^{opt} trajectories generally show more aggressive accelerations since the maximum efficiency area of the engine is placed at high loads, while the NO_x^{opt} strategy shows slower accelerations and velocities (see the slope of the trajectories plotted

in Figure 8.3) because the minimum NO_x emissions are obtained in the low engine speed and load area (see Figure 3.7) where EGR is implemented. It can also be observed how in some cases (e.g. dT=60) NO_x^{opt} and specially F^{opt} trajectories lead to cover the distance in a time substantially lower than the limit. In those cases, the particularities of the engine maps make more efficient (in fuel or in NO_x) to spend more mechanical energy than strictly necessary to make the engine work in a convenient operating condition.

The Figure 8.4 and Figure 8.5 show the experimental results obtained for the case of $dT = 0$. In this particular case, if the $woTLI$ results are observed it can be noticed how the vehicle is not able to cover the complete distance (L) with a constant speed (L/T) since it finds the second traffic light in red and needs to stop. Then, in after the second traffic light the vehicle needs to accelerate to a higher velocity to make up for the time lost. Note that this acceleration is responsible for a considerable percentage of the NO_x emitted and also leads to a substantial increase in the fuel consumption. The results with the $wTLI$ strategy show a slower vehicle speed until the second traffic light that allows the vehicle to reach this point just when the traffic light turns into green. Of course, some acceleration is needed after this point to recover the time lost due to a lower vehicle speed than necessary to cover the distance in time T =150s but this acceleration is smaller than in previous case, no substantial NO_x or fuel increase is observed. Both optimal strategies (F^{opt} and NO_x^{opt}) involve a high acceleration at the beginning up to a velocity level that allows to pass the first traffic light just after getting green. It can be noticed how the acceleration in the NO_x^{opt} case is slightly lower to avoid high loads where NO_x production is high. After this point, the velocity is again increased up to the maximum velocity in the cycle to allow the vehicle pass through the second traffic light before getting red, and then the vehicle speed is slowly reduced to the end of the route. Note that in both cases the vehicle needs less than 150s to cover the distance as this condition has been included as a constraint for the optimisation problem. In particular, the F^{opt} case requires only 132s since the maximum efficiency area of the engine is placed at a higher load than that required to cover the distance in 150s.

Similarly, Figure 8.6 and Figure 8.7 show the experimental results obtained for the case of $dT = 45$. In this particular situation, $woTLI$ and $wTLI$ solutions are exactly the same since keeping a constant velocity during the complete route of L/T does not involve crossing any traffic light in red. Optimal trajectories (F^{opt} and NO_x^{opt}) are again based in a maximum acceleration then cruising or coasting and finally breaking pattern. In any case, it can be observed how, as in this case the impact of the traffic lights on the $woTLI$ and $wTLI$ strategies is minimum, the differences in performance between those strategies and the optimal ones (particularly in terms of fuel

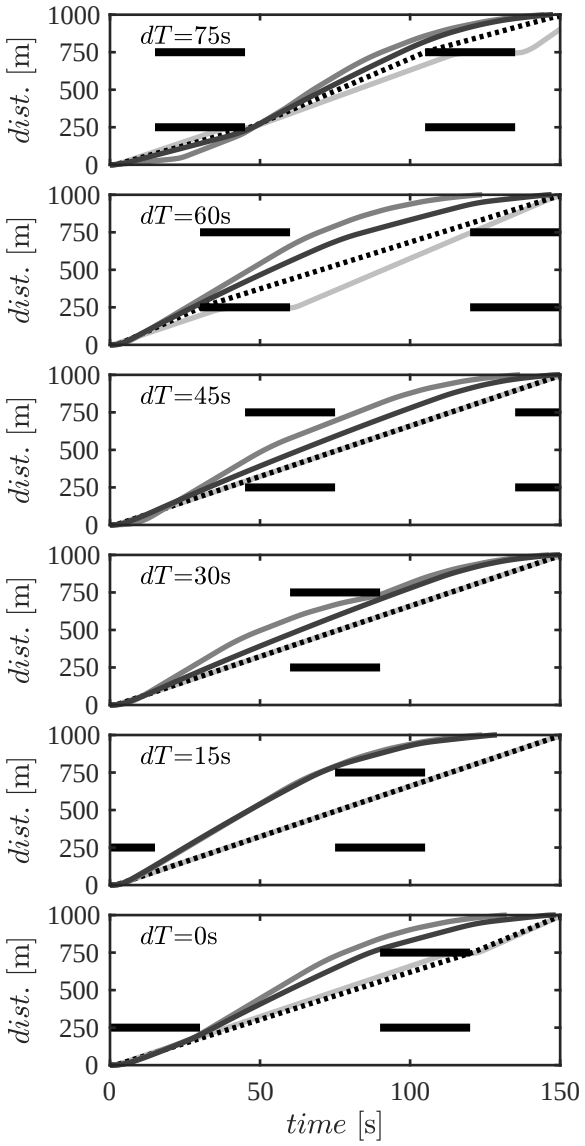

Figure 8.3: Vehicle trajectories at 6 different traffic light timings (dT). Light grey line: trajectory without traffic light information ($woTLI$). Black dotted line: trajectory with real time strategy and traffic light information ($wTLI$). Thick grey line: trajectory with Dynamic Programming optimisation for minimum fuel consumption (F^{opt}). Dark grey line: trajectory with Dynamic Programming optimisation for NO_x emissions (NO_x^{opt})

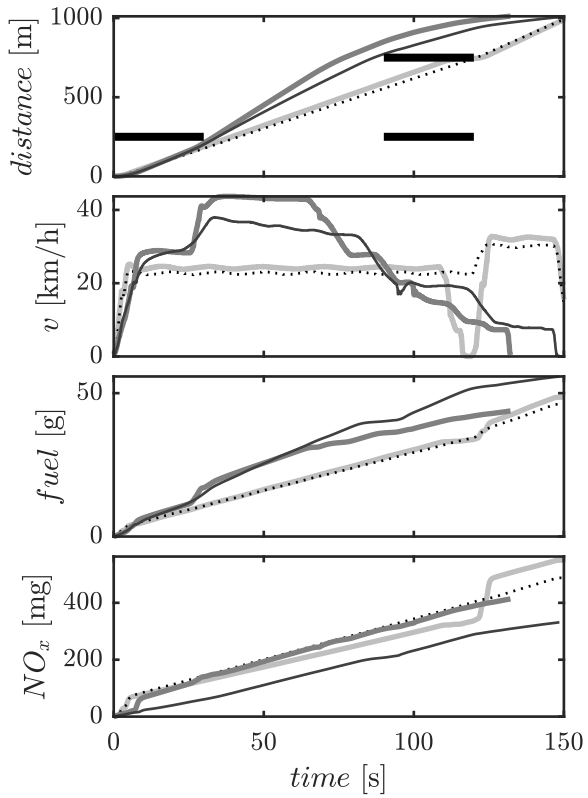

Figure 8.4: Experimental results (trajectories in upper plot, velocity profiles in second plot, fuel consumption in third plot and NO_x emissions in bottom plot) obtained for the case with dT =0s. Light grey line: trajectory without traffic light information ($woTLI$). Black dotted line: trajectory with real time strategy and traffic light information ($wTLI$). Thick grey line: trajectory with Dynamic Programming optimisation for minimum fuel consumption (F^{opt}). Dark grey line: trajectory with Dynamic Programming optimisation for NO_x emissions (NO_x^{opt}).

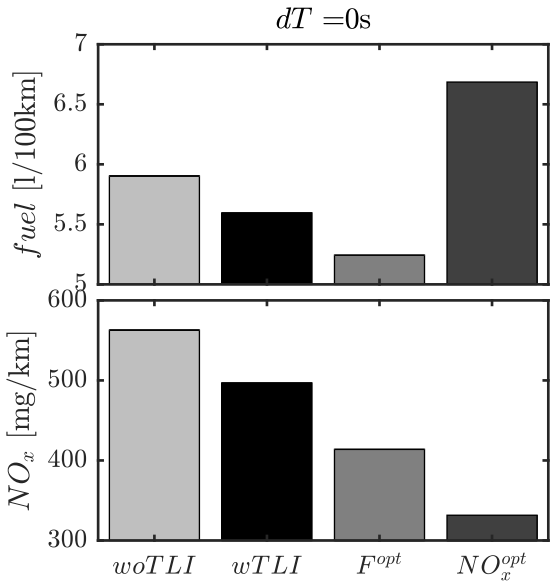

Figure 8.5: Accumulated fuel consumption (top plot) and NO_x emissions (bottom plot) obtained for the case with dT =0s.

consumption) is reduced.

The Figure 8.8 shows the average results obtained for the 6 different dT timings shown in Figure 8.3 as an estimation of the expected performance of the vehicle in the considered route. In average, a driver trying to keep a constant speed without traffic light information ($woTLI$) will have a fuel consumption of $5.9l/100km$ and produce $612g/km$ of NO_x emissions. Including information about the state of the traffic lights allows to reduce the fuel consumption to $5.45l/100km$ (-7.6%) and NO_x emissions to $533g/km$ (-12.9%) despite not using any vehicle model nor fuel consumption or NO_x optimisation that may require high computation efforts. As expected including computation capabilities aimed to model the actual vehicle performance and allowing its optimisation leads to an additional improvement in the considered performance index. In this sense, a fuel oriented optimisation will lead to a fuel consumption of $5.18l/100km$ (-12.2%) and NO_x emissions of $449g/km$ (-26.6%). If the objective is to minimise the NO_x emissions, they can be reduced up to $415g/km$ (-32.2%) at the expense of increasing fuel consumption to $6.4l/100km$ ($+8.5\%$).

8.1.5 Summary and conclusions

This section was aimed to assess the impact of traffic light information availability in terms of fuel consumption and NO_x emissions. In order to do that,

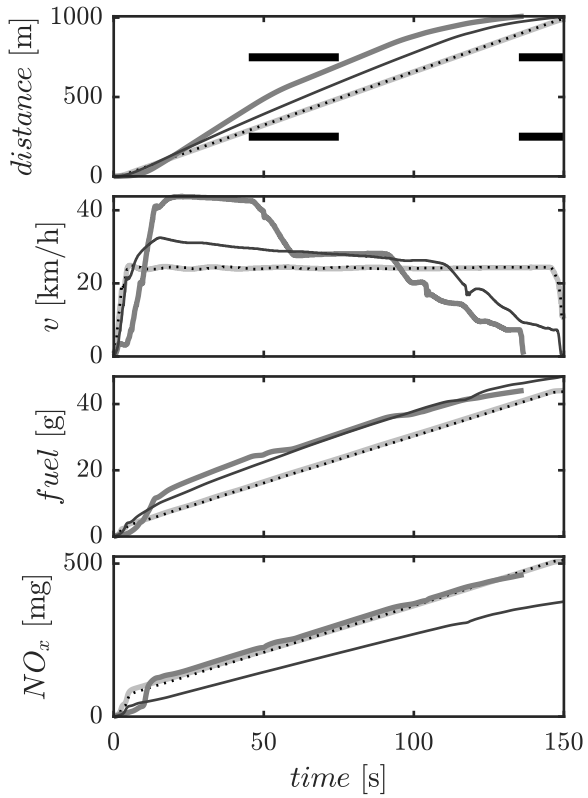

Figure 8.6: Experimental results (trajectories in upper plot, velocity profiles in second plot, fuel consumption in third plot and NO_x emissions in bottom plot) obtained for the case with dT =45s.Light grey line: trajectory without traffic light information ($woTLI$). Black dotted line: trajectory with real time strategy and traffic light information ($wTLI$). Thick grey line: trajectory with Dynamic Programming optimisation for minimum fuel consumption (F^{opt}). Dark grey line: trajectory with Dynamic Programming optimisation for NO_x emissions (NO_x^{opt}).

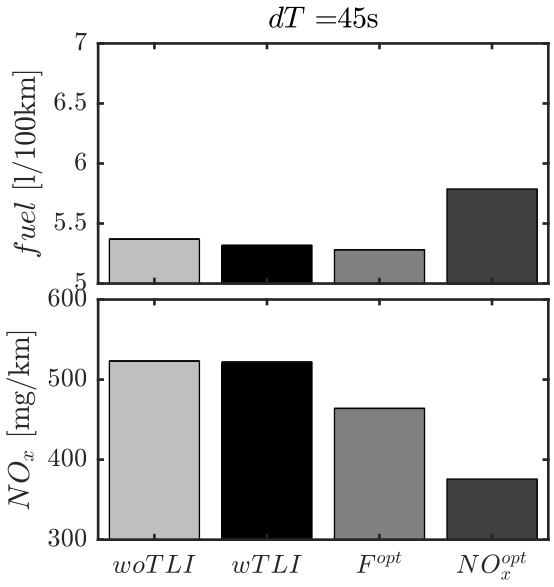

Figure 8.7: Accumulated fuel consumption (top plot) and NO_x emissions (bottom plot) obtained for the case with dT =45s.

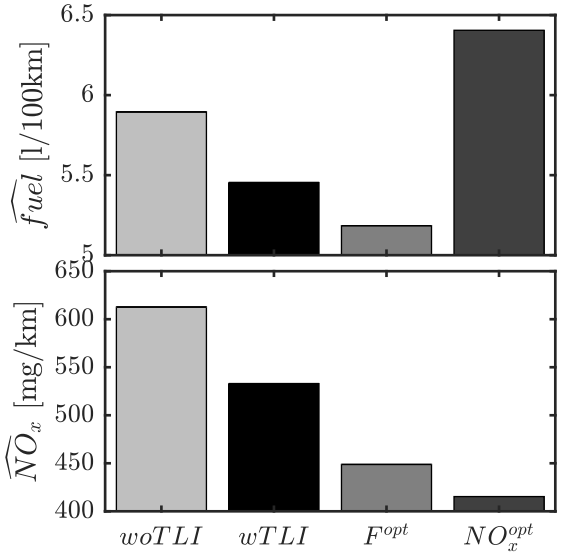

Figure 8.8: Average fuel consumption ($\widehat{fuel}$ in top plot) and NO_x emissions ($\widehat{NO}_x$ in bottom plot) for the six traffic light timings dT tested (see figure 8.3.

a non-linear dynamic vehicle model is developed to evaluate the performance of a vehicle in terms of fuel consumption and NO_x emissions in a route with different scenarios of information about the state of the traffic lights. In particular, three cases are studied: the case without information about the state of the traffic lights, a case where the state of the traffic lights is known but suboptimal strategies have to be used due to computation capabilities limitations and finally the case where the state of traffic lights is known and there are not computation limitations, so optimal control (DP) can be used. Previous strategies have been used with fuel consumption and with NO_x as optimisation objectives to check the impact of the solution on both parameters. The obtained trajectories have been evaluated experimentally in a chassis dynamometer with a Euro5 Diesel light duty vehicle.

8.2 Online vehicle speed advisor

8.2.1 Introduction and problem description

In the same line that the last work, the target of the present study is to explore the potential of speed profile optimisation in real driving conditions, by assessing the suitability of an application which recommends the driver the optimal vehicle speed sequence that minimises the fuel consumption for a particular route. To this aim, there are three main aspects to consider:

- The route: The optimal vehicle speed profile is route-dependent. In a final application, information about the route should be a priori available to allow the optimal trajectory computation.
- Model and optimisation tool: In order to provide any advice to the driver about the vehicle speed profile that minimises fuel consumption, a model able to estimate in advance the impact of driver decisions and particularly of the vehicle speed on fuel consumption is required. This model in combination with an optimisation tool allows to compute the optimal speed profile to be followed.
- Driver advisor: The computed optimal speed trajectory should be transmitted to the driver that will follow it in the best way possible. In the same way, the optimal speed trajectory should be continuously updated to make up for the deviations of the actual driving speed from the optimal profile.

This application deals with minimisation of fuel consumption under real driving conditions using a vehicle speed advisor. The aim is to explore the potential of speed profile optimisation in real driving conditions while assessing

the suitability of an application which recommends the driver the optimal vehicle speed sequence that minimises the fuel consumption on a particular route. The speed advisor is based on solving the Optimal Control problem of covering a particular route with minimum fuel consumption with a defined time constraint. The approach presented was applied to and implemented on a real passenger vehicle to obtain a trade-off between fuel consumption and travel time for several trips on the route. Experimental results are presented with and without advisory, demonstrating that with speed advisor the results approach the pareto front with lesser dispersion on the other hand without advisory the dispersion is higher and largely above the Pareto front. In the presented work, a particular route between two cities has been selected for the optimisation. The route consists mainly on highway driving with presence of speed limits and altitude variations but limited traffic and no vehicle stops. The route has been covered several times in order to identify an energy model of the vehicle and characterize the route. Then, the optimal control problem of covering the route with minimum fuel consumption in a given time has been solved by DP for different time constraints in order to assess the compromise between fuel consumption and trip time. The optimal vehicle speed is passed with a display to the driver as a reference to minimise fuel consumption. Despite the high computation cost and curse of dimensionality of DP, it allows storing not only the optimal control between initial and final states, but the optimal control sequence between any state contained in the feasible set and the final one. This property is used in the present work to correct any deviation from the optimal speed profile, due to non-considered disturbances or lack of accuracy of the driver.

8.2.2 Method description

The aim of this work is to explore the potential of speed profile optimisation in real driving conditions by means of a driving advisor application. In order to provide advice to the driver, a sensible possibility is to compute what is the velocity profile to minimize a given cost function and then provide this information to the driver. Regarding the speed profile computation, the fuel consumption is an intuitive cost function while the time spent during the trip seems a sensible constraint. Other restrictions that should be taken into account are the speed limits during the route or the limits of the vehicle and the powertrain. In any case, a generic control problem consisting in finding the control policy to drive a dynamic system from a given initial state to a defined final state with minimum cost and fulfilling a set of constraints fits in the field of Optimal Control. The formulation of an Optimal Control Problem (OCP) considers a cost index and constraints expressed in terms of system states

(x), system actuators (u), problem disturbances (w) and domain. Taking into account that, in the case at hand, the route is a priori known, the slope and speed limits (which are the problem disturbances) are space (s) dependent, it seems more convenient to consider s as the problem domain. In this case, the cost index can be defined as:

$$\mathcal{J} = \int_0^L \frac{\dot{m}_f}{v} ds \tag{8.4}$$

where L is the route length and for the sake of readability, the dependence of the fuel consumption on the actuator (u_p) has been omitted. The system, *i.e* the vehicle model described in chapter 3 can be condensed in the generic dynamic system:

$$\dot{x} = f(x, u, w, t) \tag{8.5}$$

Where the dependence of the state (velocity) evolution on the state itself, the control actions (in the case at hand u), disturbance (road slope) and time is described. Therefore, the state evolution with the problem domain (space) becomes:

$$\frac{dx}{ds} = \frac{f}{v} \tag{8.6}$$

Where the dependence of f on the system state, actions and disturbances has been omitted for the sake of clarity.

The vehicle should cover the defined distance (L) within a given time (T), which leads to the following integral constraint:

$$\int_0^L \frac{1}{v} ds \leq T \tag{8.7}$$

Road speed limits have to be respected which leads to the following path constraint:

$$v(s) \leq \hat{v}(s) \tag{8.8}$$

Limits on the engine (speed range and maximum power output) and brakes (maximum braking force) are also considered. Finally, the initial speed is also imposed. Despite the vehicle starts from rest a minimum vehicle speed is imposed to avoid divisions by 0 in the model (boundary constraint):

$$v(0) = \underline{v} \tag{8.9}$$

Regarding final speed, no restrictions are imposed beyond the maximum speed of the road.

In the present case, to analyse the performance of the speed advisor, a 60 km daily commute route between two cities in Spain (A7 route between Canals and Valencia) has been chosen. In this sense, Figure 8.9 shows the evolution of road slope and maximum vehicle speed along the route. Both variables have been considered in the optimisation problem as disturbance and path constraint respectively. The route was covered daily (during consecutive working days) with an instrumented vehicle to obtain a set of 45 tests. The experiments where carried out between 6:00 am and 7:00 am to avoid the rush hour and therefore traffic jams that complicate the optimisation. The occupancy in the road did not exceed 5% according to the measurements of the traffic agency (DGT). Despite traffic conditions can be included in the optimisation as vehicle speed constraints [Guardiola *et al.* 2019] if external information about their state is available, this is not considered in the present work.

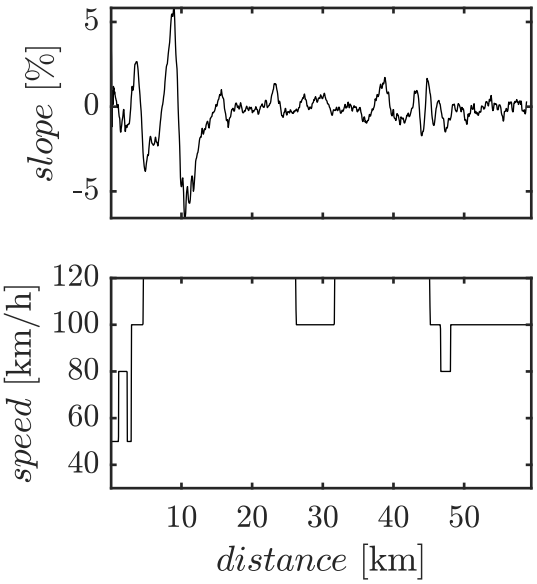

Figure 8.9: Maximum vehicle speed and slope along the considered route.

Therefore, the OCP leading to the speed reference for the driver consists in minimizing $\mathcal{J}$ (Equation 8.4) throughout a trajectory of length L and the speed constraints and slope shown in Figure 8.9, fulfilling the constraints Equation 8.7 to Equation 8.9.

Fuel consumption optimisation There are different families of OC methods that can be applied to solve a problem like the one described in the previous section, DP is among the most used, specially if the number of states (in

the case at hand 1) and actuators (also 1) remains low. The DP algorithm is the numerical implementation of the Hamilton-Jacobi-Bellman equation which is a sufficient condition for a global optimum in an OCP. The method is based on the discretization of the domain (S) in N steps, and also the state space (X) and control space (U) to build a set of possible trajectories between the defined boundary conditions. Then, a cost to go function J such that:

$$J(x_k, s_k) = min_u\{\mathcal{L}(X, U, s_k) + J(x_{k+1}, s_{k+1})\} \tag{8.10}$$

Where $k = 0, ..., N-1$ and L is the cost in a given step (term inside the integral in Equation 8.4), is calculated backwards in order to represent the minimal cost to reach a suitable terminal state from any feasible state at time-step k.

The model used in the present work has only one state (v) and one actuator (u), nevertheless, the time constraint represented by Equation 8.7 has to be handled. Since the problem does not explicitly depend on time, the time restriction can be addressed adding it to the cost function and using a weighting factor (α) that balances between fuel consumption and time:

$$\mathcal{L}' = \frac{\dot{m}_f}{v} + \alpha\Delta t \tag{8.11}$$

where Δt is the time needed to cover a step in the space discretization. Then, the DP can be applied with only one state, but a shooting method should be applied to find the proper value of α that allows to fulfil the integral constraint in Equation 8.7. The alternative used in this work is to consider time as a second state, in order to compute its evolution and assure that constraint in Equation 8.7 is hold. In this last case, the number of states of the problem increases to 2. Note that despite issues such as the curse of dimensionality, the recursive nature of DP allows it to compute not only the optimal trajectory but a set of optimal trajectories from any state in the feasible state space X at any instant k. This feature is specially interesting to implement a close loop advise on the driver that allows him to make up for any deviation from the optimal trajectory due to disturbances not considered in the optimization or due to the lack of accuracy in his driving when trying to follow the advised trajectory. Of course, this is only possible if constraint in Equation 8.7 is addressed by considering time as a state of the problem.

The Table 8.4 shows the settings used in the DP algorithm, and as an indicative number of the computation burden, the simulation of one route takes 1 hour in a standard laptop (Intel(R) Core(TM) i7-8550U CPU @ 1.8GHz and 8GB RAM).

Table 8.4: Discretisation employed in the optimisation algorithm DP

Variable	Range	Element size
Distance (s)	[0, 60]km	50m
Speed ($v = x_1$)	[30,120]km/h	1km/h
Time ($t = x_2$)	[0, T]	2s
Brake/Throttle (u)	[-10,100]%	2%

Vehicle speed advisor implementation The first result of the optimization described in the previous section is the optimal sequence in the states of the problem (particularly on the velocity) depending on the position of the vehicle ($v^*(s)$). This information would be enough to minimise the fuel consumption if the driver is able to perfectly follow it during the route. In this case, a direct interpolation in the $v^*(s)$ curve of the actual position of the vehicle (s_k) would be enough to display the actual and reference vehicle speeds. However, it is not possible for a standard driver to perfectly follow a prescribed speed profile due to both disturbances that may appear during the route (e.g. traffic) and the limited driver skills. Another important reason to not perfectly follow the advised vehicle speed may be drivability. As these criteria has not been taken into account in the optimization process the driver may feel uncomfortable following the advised speed profile in any part of the route. Note that any deviation from the optimal speed profile harms the optimality of the rest of the trip, if the driver continues following the advised speed trajectory after a deviation, in the best case the time constraint will not be fulfilled.

In this sense, some kind of feedback is necessary to keep optimality. To this aim, instead of using the optimal trajectory from the DP, the optimal control signal map (U^*) has been used, which specifies the optimal control u^* at each step k and at each state $x_k \in X$. In the case at hand:

$$U^* = u^*(s_k, v_k, t_k) \tag{8.12}$$

The optimal control signal map is combined with the vehicle model to obtain an optimal speed map, which provides the optimal velocity in the next step $k+1$ and depending on the current state $x_k \in X$ to be used as a set point for the driver:

$$v_{k+1}^{sp} = v_{k+1}^*(s_k, v_k, t_k) \tag{8.13}$$

The Figure 8.10 shows a set of optimal speed maps at different points of the route. Depending on the position of the vehicle (s) there is a map showing

what is the optimal velocity in the next step depending on the actual speed and time. A feasible region can be identified in any map, it is bounded by:

- Maximum speed depending on the speed constraint, which depends on the vehicle position
- Maximum time: if the vehicle passes through this point in the route latter than this maximum time, it will not be able to fulfil the time constraint, even driving from this moment at the maximum allowed speed.
- Minimum time: if the vehicle passes through this point in the route earlier than this minimum time, it will not be able to fulfil the time constraint, even driving from this moment at the minimum speed used in the optimization (30km/h). This limit does not have a practical purpose.

In the feasible area of v_{k+1}^{sp} maps, it can be observed how for a given position and velocity in the route, the advised velocity in the next time-step increases with the time consumed.

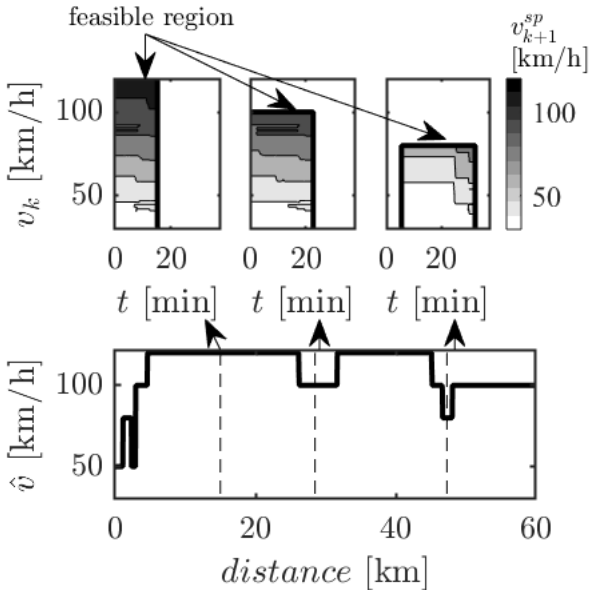

Figure 8.10: Optimal vehicle speed set point for a given vehicle position, time and current vehicle velocity.

As the current velocity, position and time consumed during the trip are available in the vehicle, the developed application use them to interpolate what is the optimal velocity during a moving window of 120 seconds and

displays it to the driver. In order to do that, the system should estimate the future positions of the vehicle by integrating the optimal velocity obtained in a given time step. Algorithm 1 shows a simple version of the process used. In the current work the algorithm is run every 5 seconds to update the optimal speed profile. N and δt are arbitrary numbers, in the case at hand 120 and 1 respectively to define a control horizon of 120 seconds.

8.2.3 Results

The Figure 8.11 shows a test carried out with the vehicle speed advisor. In the figure, one can observe how the optimal speed profile is strongly affected by the road slope. The stretch between 3 and 15 kilometres shows the steepest ups and downs, and the optimal speed profile consists on reducing speed uphill and increase it downhill in order to take advantage of road gradient and also to avoid exceeding the vehicle speed constraint. One can also observe how the speed limits play a key role in the optimization since optimal vehicle speed is limited by the maximum velocity in several parts of the cycle, namely during the first 3 kilometres, then between 26 and 32 and finally between 46 and 48. During most part of the route, where ramps are not stiff the recommended vehicle speed is almost constant.

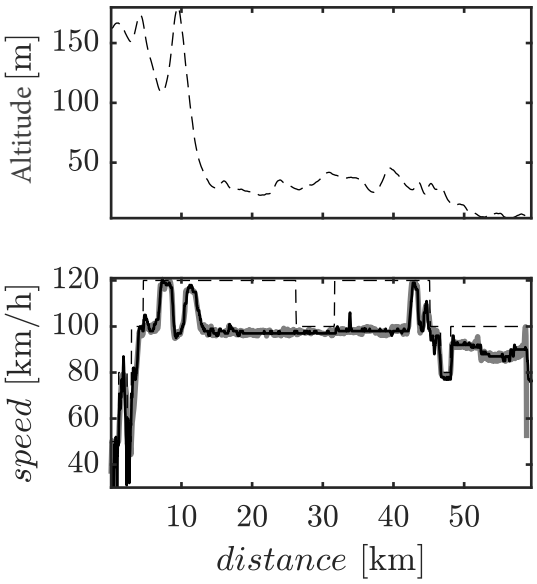

Figure 8.11: Upper plot: Road altitude during the route. Lower plot: Optimal vehicle speed profile for an average vehicle speed of 95 km/h from DP optimisation (grey) and driver ability to follow it (black line).

Regarding the improvement in fuel consumption with the driving advisor,

Figure 8.12 shows the trade-off between fuel consumption and travel time with (bullets) and without (circles) its use. The black line shows the theoretical pareto front computed by dynamic programming and the grey dashed lines the pareto front $\pm 0.1L/100km$. White circles show results obtained without speed advisor. Black dots represent results obtained with the speed advisor. Labels A and B point out two different tests with the same time but without and with the speed advisor respectively. The theoretical pareto front obtained from simulation with different time constraints is also shown (black line). It can be observed how results with the speed advisor approach the pareto front, on the contrary, results without any advisory have higher dispersion and are placed, in general clearly above the pareto front. In addition, Figure 8.12 points out that the higher the time to cover the route, the larger the potential of the speed advisor. The reason for that higher advisory potential, is that as the time increases, the impact of the maximum velocity constraint decreases so the space of feasible velocities is enlarged and accordingly the importance of optimisation increases. It is intuitive that if the time constraint is set to the minimum affordable value (in this particular route, 2000 seconds), the optimal speed profile matches the maximum speed constraint, so there is no room for optimisation.

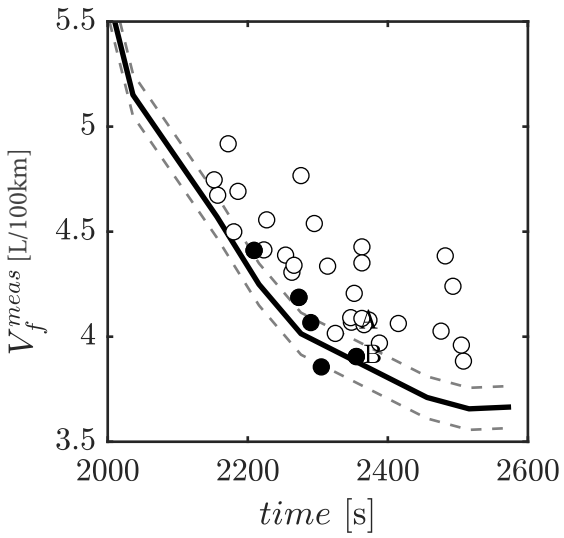

Figure 8.12: Trade-off between fuel consumption and time spent to cover the route.

The Figure 8.13 shows two routes taking the same time with (black) and without (grey) speed advisor (labelled as B and A in Figure 8.12). Amongst the set of driving cycles without speed advisor and same time than trip B,

A has been chosen because it is the one with minimum fuel consumption, so vehicle speed is kept almost constant during the trip and the positive effect of the ramps at the beginning of the cycle has been considered by the driver. Nevertheless, even in this case, there is a non-negligible improvement with the speed optimisation (a fuel saving of 4% at the end of the cycle). The main differences in the fuel consumption appear during the stretch with higher height differences, pointing out the importance of taking into account the road slope for the vehicle profile optimisation, and revealing that even small deviations from the optimal vehicle speed profile can involve a substantial penalty in fuel consumption.

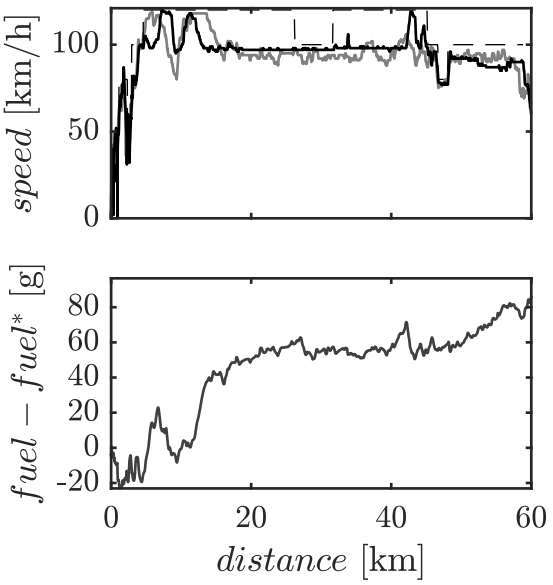

Figure 8.13: Comparison between two routes with the same time (average speed of 95km/h) with (black, B point in figure 8.12) and without (grey, A point in figure 8.12 speed advisor. Upper plot: vehicle speed. Lower plot: fuel consumption difference between the case without speed advisor and the case with speed advisor (*)

8.2.4 Summary and conclusions

The discrepancy observed in the declared and real world emissions has resulted in a strong trend of applications improving real driving emissions. One such application is presented in this section which is the speed advisor in real driving conditions. The application optimises the speed profile in real time and recommends the driver the optimal speed sequence that minimises the fuel consumption on a particular route. The real- time implementation of the

application shows the possibility to stay very close to the Pareto front. This is majorly possible because the developed application allows storing not only the optimal control between the initial and the final states, but also the optimal control sequence between any state contained in the feasible set and the final one. This property is used as a feedback to correct any deviation from the optimal speed profile, due to non-considered disturbances or lack of accuracy of the driver. The study also points out a strong dependence of optimal speed profile on road slope and vehicle speed constraint.

In particular, with the proposed application fuel consumption can be improved up to 4% without any penalty in travel time. Given the increasing use of information systems, which can lead to some degree of a priori knowledge of the vehicle speed trajectory, the results presented a step forward in understanding the potential of online optimization methods in advising the driver to save fuel in real driving conditions.

Chapter 9

Assessment of driving dynamics in RDE test on NO_X emission dispersion

Contents

9.1 Introduction and problem description

The EU6D emission regulation intends to bridge the gap between laboratory tests and the real driving conditions by the introduction of RDE testing. It requires the measurement of RDE as an additional type approval test in order to take into account the influence of the road profile, ambient conditions and traffic situations. An important amendment was included in Commission regulation (EU) 2016/646, limiting the driving dynamics and hence avoiding the biased testing of the vehicle. The emission measurement under real driving conditions pose a major challenge for OEMs since the situational environmental conditions such as temperature, traffic and the behaviour of the driver are not reproducible. As to investigate influences of hardware and software on the emission performance, constant or at least, reproducible conditions are necessary. The challenges in meeting RDE requirements are most pressing in early

development stages. This has created demand for alternative means of ensuring product compliance early in the development process without the need for costly on-vehicle testing, and the engine testing is an important solution to understand effect of such uncertainties. In this work, a driving cycle generator is developed to synthesize cycles meeting all the regulatory requirements of the RDE testing. The generator is based on the transition probability matrix obtained from each phase of the WLTP cycle. A single tuning parameter was introduced in the cycle generation method to control the driving dynamics of the output cycle. Using the tuning parameter several trips are generated with dynamics ranging from soft to aggressive within the regulatory limits. Finally, a Direct Injection Compression Ignition (DICI) 1.5L engine with a SOA after-treatment system was utilised to run the generated synthetic cycles to measure cumulative NOx emissions for different driving cycles.

EU6D Regulations To eliminate the difference between the declared and real emissions of a vehicle, EU6D regulations for light duty vehicles complement the dynamometer based type approval procedure with on road emission testing by means of portable emission measurement devices. To allow a progressive adaption of vehicle manufacturers to the new situation, the Conformity Factors (CF) leading to the maximum emission limits for RDE will be introduced in two phases. Temporarily CF_{NO_x} is 2.1 and from 2020, it will be decreased to 1.5. Accordingly, not to exceed limits (NTE) for real drive NO_x emission has been fixed to:

$$NTE_{NO_x} = CF_{NO_x} \times EU6_{NO_x} \tag{9.1}$$

where, $EU6_{\mathrm{NO}_x}$ represent the Euro 6 limit for NO_x emissions, which is 0.08g/km.

For a trip to be qualified for RDE type approval, it is required to have certain characteristics as listed in table 9.1 and it must also be within certain boundary conditions as summarized in table 9.1.

An RDE trip must cover three phases: urban u, rural r and motorway m. These phases are based on vehicle speed: a vehicle travelling up to 60km/h will be considered to be operating in urban conditions; at 60 to 90 km/h in rural and above 90km/h in motorway conditions. The trip is then binned (in phases) for assessment of the dynamics in each phase. The RDE regulation as in the document [201 2016], defines a lower and an upper boundary condition for the driving dynamics in each phase. This is in order to ensure that the vehicle is not driven in an excessively soft or aggressive style.

An excessively soft driving that would lead too low and non-realistic NO_x emissions is eliminated by lower boundary limits defined for Relative Positive

Altitude	0 to 700 m (Ext: 700 to 1300 m) cum. elevation 1200m/100km
Alt. difference	<100 m between start and end
Ambient temp.	Moderate: 0C to 30 C (Ext: -7C-0C and 30C-35C)
Dynamics	Max:$v.a_{pos}$ Min:RPA
Maximum speed	145 km/h(>100km/h for 5min)
Payload Maximum	90% of the max vehicle weight

Table 9.1: Regulatory requirements

Average Speeds	Urban	15 to 40 km/h
	Rural	< 60 km/h
	Motorway	> 90 km/h
Distance	Urban	> 16 km
	Rural	> 16 km
	Motorway	> 16 km
Trip Composition	Urban	29 % to 44%
	Rural	23 % to 43%
	Motorway	23 % to 43%
Total Trip Duration	-	90min to 120 min
Stop %	-	6-30% of urban

Table 9.2: Trip Characteristic Requirements

Acceleration (RPA) as in equation 9.2, which is defined as the integral of vehicle speed (v) multiplied with the time step and the positive acceleration(a_{pos}) for all accelerations $> 0.1\,m/s^2$, divided by the total distance of the cycle(d).

$$RPA_k = \frac{\sum_j [dt \cdot (v.a_{pos})_{j,k}]}{\sum_i d_{i,k}} \tag{9.2}$$

where i=1 to N_k; j=1 to M_k; $k = \{u,r,m\}$, RPA_k is the relative positive acceleration for u, r and m phases, dt is the time step equal to 1 second, M_k the sample number with positive acceleration in each phase and N_k is the total sample number in each phase.

An excessively aggressive driving will be eliminated by upper boundary limits defined for the 95^{th} percentile of the product between actual vehicle speed and positive acceleration($> 0.1\,m/s^2$) for each phase, denoted as $(v.a_{pos})_{k\_95}$.

The upper and lower boundary limits are defined as in equations 9.3, any of these condition makes a trip invalid. Where, $\bar{v}_k$ is the average velocity in a phase.

$$\begin{aligned}
&for\ \bar{v}_k < 74.6\ [\text{km/h}]; if\ (v \cdot a_{pos})_{k_95} > (0.136.\bar{v}_k + 14.44)\\
&\quad or\\
&for\ \bar{v}_k > 74.6\ [\text{km/h}]; if\ (v \cdot a_{pos})_{k_95} > (0.0742 \cdot \bar{v}_k + 18.966)\\
&\quad or\\
&for\ \bar{v}_k < 94.05\ [\text{km/h}]; if\ RPA_k < (-0.0016 \cdot \bar{v}_k + 0.1755)\\
&\quad or\\
&for\ \bar{v}_k > 94.05\ [\text{km/h}]; if\ RPA_k < 0.025
\end{aligned} \tag{9.3}$$

9.2 Method description

In the current study, the synthesis procedure uses Markov chain due to its relative simplicity in representing an unknown system. The basis of the Markov approach was described in chapter 5. The process of cycle synthesis in this application is different than the one described in chapter 5 in following ways:

- There are only three TPMs associated with each phase (urban, rural and motorway) of the WLTC and not for each kilometre of a real-world route.

- There is an additional filter to eliminate driving cycles which do not qualify according to the trip characterstics of the RDE regulated cycles.

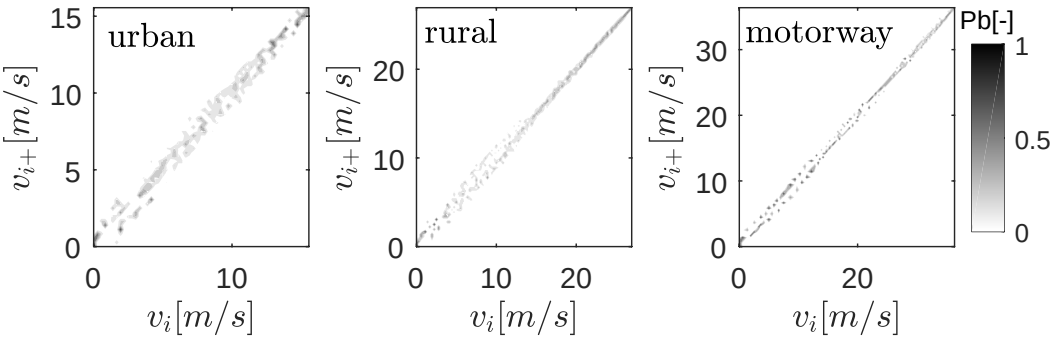

Figure 9.1: Speed transition probabilities from current speed v_i to v_{i+} in the urban, rural and motorway phase

- There is an additional tuning parameter for varying the driving aggressiveness.

In line with the driving cycle tool, the vehicle speed is the only system state ($x_n = v_n$) and its sequence in each phase of the WLTC is used to build the Transition Probability Matrices. For practical reasons, the data is discretised in steps of 1 km/h in velocity. The process of cycle synthesis is summarised as:

Step 1 : The transition probability matrices (TPM_k), where k represents the cycle phase, is extracted from the WLTC as shown in figure 9.1. In particular, the probabilities are assumed to be equal to the event frequency during a given WLTC phase. In this way, statistical properties of each phase of WLTC are retained, for example the low motorway driving dynamics and the speed range (0 to 120 km/h) are conserved during the synthesis itself.

It can be noted, that the distance between the zero probability entries and the main diagonal in figure 9.2 is an indicator of the cycle aggressiveness. In fact, this distance is a measure of the attainable acceleration since it provides a boundary on the difference between the current vehicle speed and the vehicle speed at next time step. This property is used to tune the cycle aggressiveness during the synthesis. The width of the non-zero values near the main diagonal of the TPM control the aggressiveness of the driving cycle as shown in figure 9.2 for the urban phase of the driving cycle.

Step 2 : The inputs to the generator are initial vehicle velocity (v_0), total time (T) and cumulative probability matrix (denoted by $CPF_{i,k}$) derived from phase-wise TPM_k extracted in **Step 1**. The generator randomly allots a time for each phase, such that $\sum_{k=u,r,m} t_k = T$ and fulfilling with composition requirements in table 2. Then the synthesis of each phase is dealt with

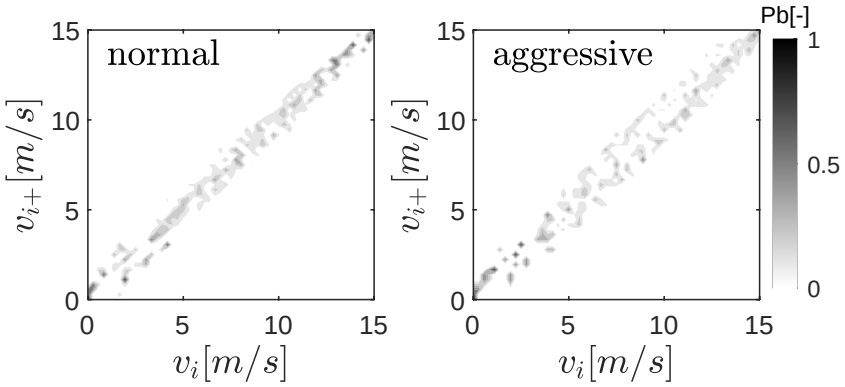

Figure 9.2: Speed transition probabilities from current speed v_i to v_{i+} in the urban phase, with normal and high aggressiveness

separately. The corresponding $CPF_{i,k}$ is used to randomly generate velocity for the next time step. Later the three phases are merged to form the entire cycle. It must be noted that in each phase the TPM are time independent.

Step 3 : Finally, the trip is validated for the statistical requirements of RDE regulations mentioned in table 9.1 in a for-loop and the qualified trips are retained for the analysis. The driving dynamics of each phase of the driving cycle must adhere to the boundaries in equation 9.5. The dynamics are graphically represented in figure 9.3 where the asterix represent the generated driving cycle and the line representing the upper limit in terms of the product of speed and positive acceleration the line representing the lower limit in terms of the relative positive acceleration (RPA).

The proposed method is able to synthesize driving cycles fast (0.26 s in a standard computer) and within the regulatory trip characteristics. A few driving cycles are shown in figure 9.4. The characteristics of a driving cycle can be classified according to several criteria, such as the speed trajectory, the operating modes (idling, cruising,...), the vehicle mass, the temperature, the altitude or the altitude gain. Most of them are covered by the RDE regulation in [201 2016], and amongst them, the driving dynamics (sequence of vehicle speed and acceleration) play a key role, also presented by author in [Ericsson 2001]. The sequence of vehicle speeds and acceleration is unique for a given driving cycle, but their dynamics can be captured by a set of parameters as shown by Ericsson in [Ericsson 2001], the regulation also considers two of them (RPA and $(v.a_{pos})$). The proposed method assures that the set of driving cycles generated keep the dynamic parameters so despite differences in the sequence of vehicle speed, the driving cycle dynamics will be comparable. Moreover, the method is able to include aggressiveness in the synthesis process,

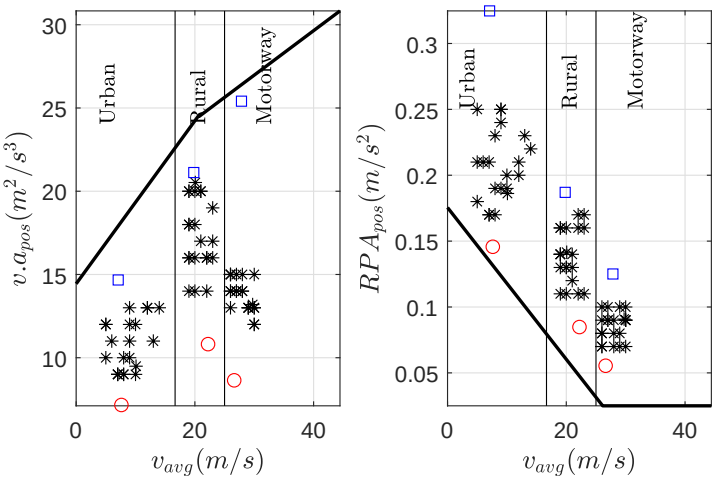

Figure 9.3: High and low dynamic boundaries; Synthetic trips within RDE protocol, ∘ is soft, ∗ are standard, □ is aggressive compared to WLTP dynamics

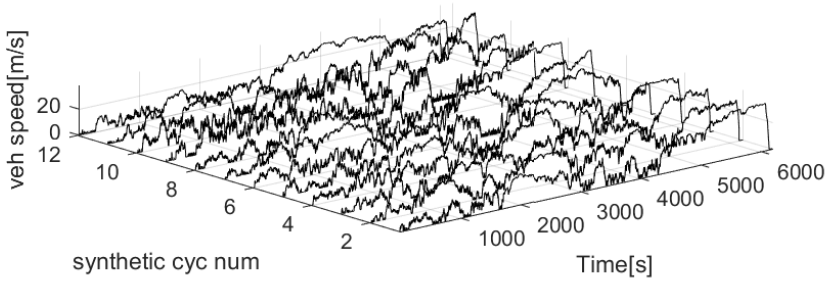

Figure 9.4: Set of synthesised cycles

and it is therefore widely applicable to study the impact of dynamics on emissions and fuel consumption. These cycles are run in an engine test bench facility, as explained in the following section, for assessing the impact of driving dynamics on NO_x emissions. To obtain realistic engine operating conditions from the vehicle speed profiles, a validated vehicle backward model based on longitudinal vehicle dynamics was used. The obtained trajectories of engine speed and torque are run on the following engine test setup.

9.3 Results

The objective of the experimental study is to measure the dispersion of NO_x emissions for a set of 20 driving cycles with aggressiveness ranging from low to high . A DICI engine was used to run the engine speed and torque profiles representative of the synthetic driving cycles. The instantaneous NO_x emission was measured for all the cycles. In figure 9.5, the evolution of accumulated NO_x emission is plotted for three driving cycles with aggressive intensities from low to high.

In figure 9.6, the engine perspective shows that the main difference in the frequency of engine operations is in the low and high engine speed and load conditions. The engine operation is spread over the bigger area in the aggressive cycle and the cumulative NO_x emissions are also high for this vehicle.

The dispersion of NO_x emission for the 20 driving cycles is presented in figure 9.7. The normal distribution curve is fitted for the sake of readability. This figure also shows the distribution of NO_x emissions for WLTC (run 10 times) in order to highlight the effect of measurement inconsistencies.

The dispersion in figure 9.7 can be used to infer the following:

- Before the catalyst, relative difference in the spread of the bell curve is 100%. In terms of the range, the spread is 0.3 g/km for the given vehicle. After the SCR, the relative difference is 60% and the range is 0.09g/km, which is in the range of Euro 6 NO_x limits, i.e. 0.08 g/km.

- For the synthetic cycles, minimum and maximum NO_x emissions are equal to 0.115 g/km and 0.06 g/km respectively. It must be noted that the minimum NO_x produced is for the least aggressive cycle and the maximum is for the most aggressive cycle. Indicating that, the tests closer to the lower dynamic limit in the RDE regulation could produce NO_x emissions even lower than the regulation limits.

- It can be inferred, that by using the after-treatment system, not only the absolute NO_x emission reduces but also the range of dispersion due to cycle dynamics is also curbed.

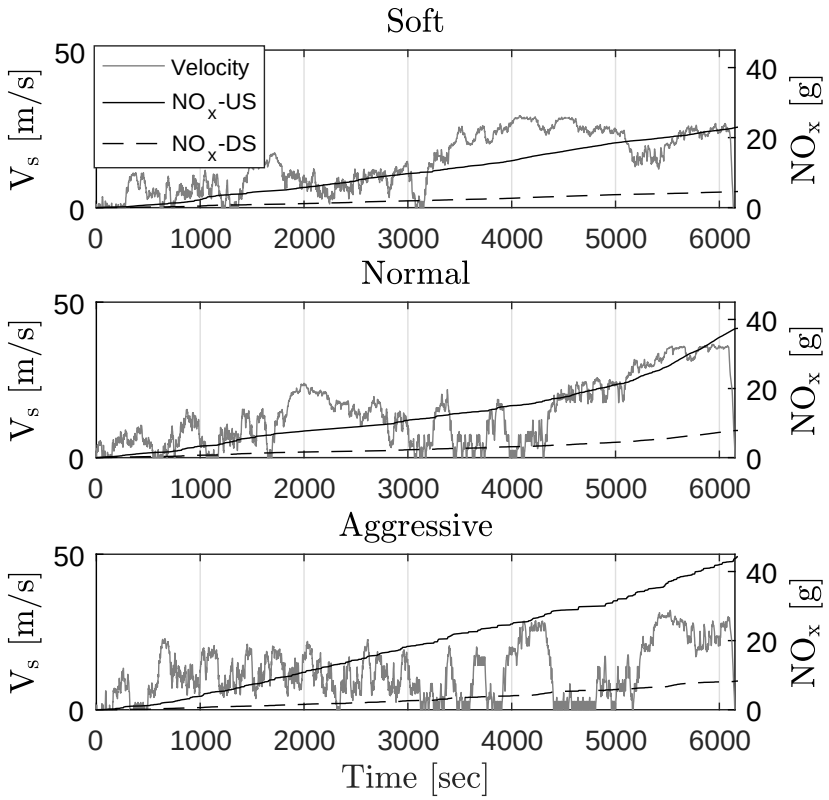

Figure 9.5: NO_x emissions for three RDE cycles soft, normal and aggressive

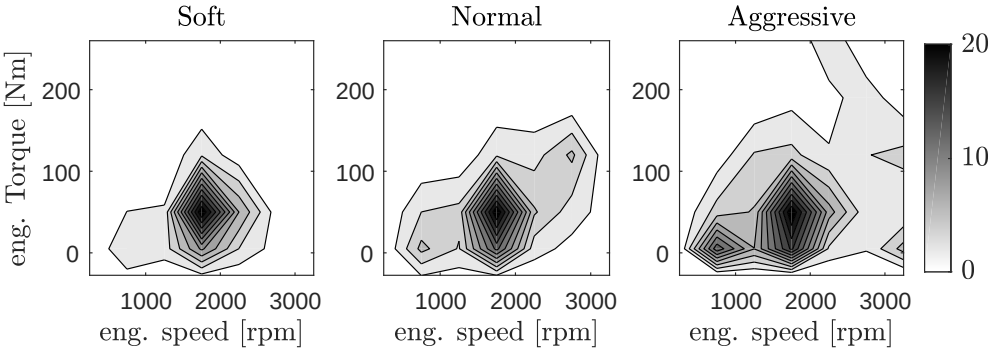

Figure 9.6: Frequency(%) of engine operation in Soft, Normal and aggressive driving

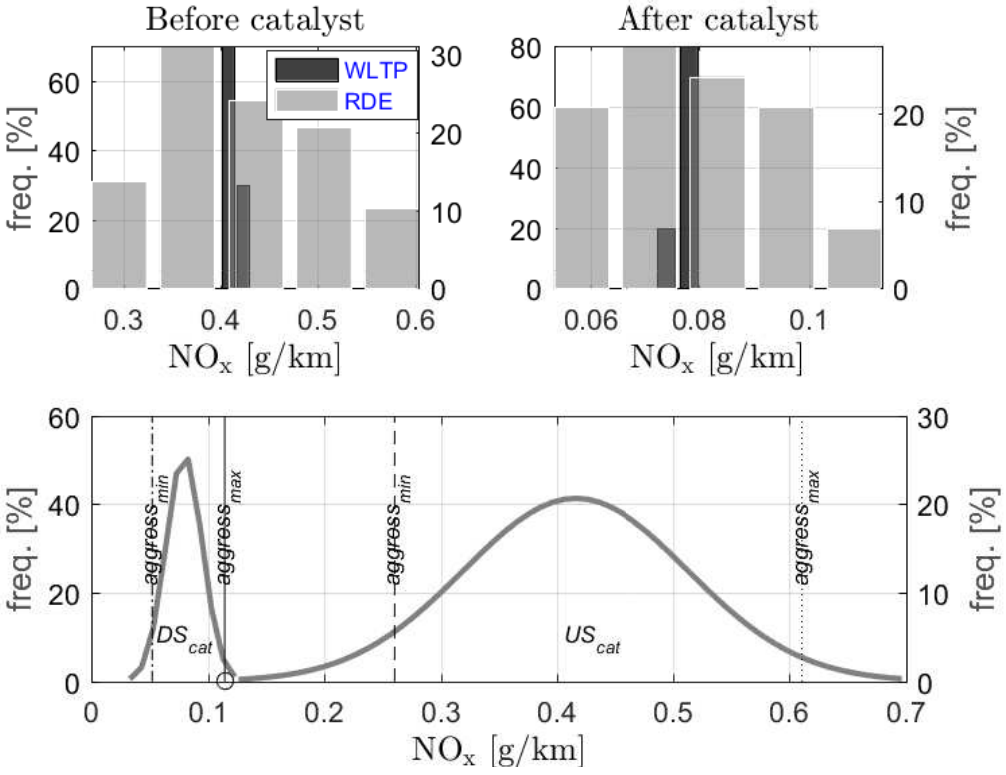

Figure 9.7: Dispersion in measured NO_x emissions for 20 synthetic cycles before and after catalyst

- For the WLTC, relative dispersion and the range in NO_x emission is less than 5% and 0.02g/km respectively before the catalyst and the relative dispersion and range is less than 2% and 0.002g/km after the catalyst. It can be inferred that the dispersion plotted in the figure are relatively less influenced by the measurement inconsistencies.

In present the trend of emissions due to dynamics, two variables- $(\mathrm{v} \cdot \mathrm{a}_{\mathrm{pos\_95}})_{\mathrm{avg}}$ and $(\mathrm{RPA_k})_{\mathrm{avg}}$ are defined as an average of trip dynamics in equations 9.4 and 9.5.

$$(v \cdot a_{pos\_95})_{avg} = \frac{\sum_{k=1}^{3}[(v \cdot a_{pos})_{k\_95}.t_k]}{\sum_{k=1}^{3}[t_k]} \tag{9.4}$$

$$(RPA_k)_{avg} = \frac{\sum_{k=1}^{3}[(RPA)_k.t_k]}{\sum_{k=1}^{3}[t_k]} \tag{9.5}$$

For all the drive cycles the average trip driving dynamics and NO_x emissions have been clustered in figure 9.8. The results show that the driving dynamics play a key role on NO_x emissions; the aggressive cycles tend to have higher NO_x emissions. However, there are other parameters that also affect NO_x and are outside the scope of the present study, i.e. one may think that two driving cycles, despite completely equal in the velocity sequence will go through different areas in the engine map if there are differences in the gear selected, so there will be differences on NO_x emissions.

Finally, the phase wise NO_x emissions are plotted in figure.9.9, the urban driving is seen to have maximum contribution in the overall NO_x emissions. In the urban phase, the relative difference obtained after catalyst is about 30% and the range is approximately 0.13 g/km, which is considerably high, considering exclusive limits on NO_x emissions in urban phase in EU6D norms. The regulation already demands 50% driving to be done by Type Approval Authority, which reduces the risk of biased driving style. this can be improved by demanding 50% driving by TAA in each phase of the trip especially in urban phase.

9.4 Summary and conclusion

A real driving cycle generator based on the velocity transition probability matrix obtained from the WLTC is developed. The method is found to be consistent and fast in producing the synthetic driving cycles. The driving dynamics are varied using a single tuning parameter within the regulatory limits. A vehicle model was used to obtain the engine speed and torque profile which were used to run on the engine test bench. The instantaneous

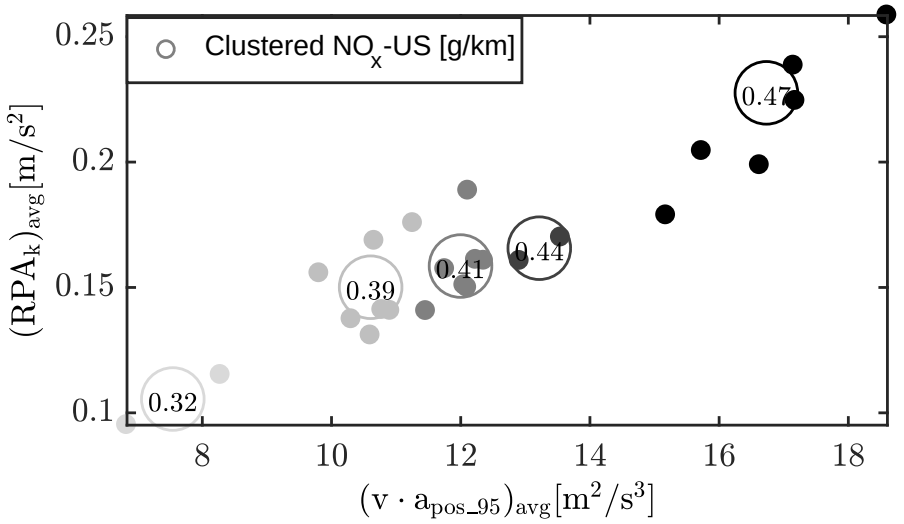

Figure 9.8: Clusters of NO_x emissions for varying driving dynamics

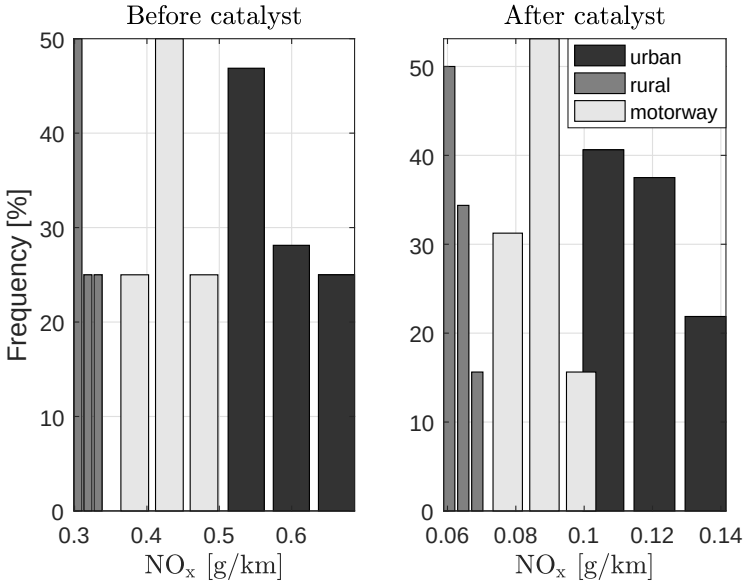

Figure 9.9: Phase wise distribution of NO_x emission for synthetic cycles

NO_x emission were measured and analysed. With the existing vehicle and within the RDE cycle characteristic protocols, a significant spread in the NO_x emissions was observed. The analysis of the results obtained in the tests (all of them complying with RDE restrictions in terms of driving dynamics) point out a noticeable 60% relative dispersion in the NO_x emissions downstream of the catalyst. Considering that this dispersion arises solely due to cycle dynamics, the dispersion is significantly high. Increase in the share of urban driving and driving aggressiveness is shown to increase the total NO_x emissions. Phase-wise distribution of NO_x emission shows that the driving in urban phase is the bottleneck in emission control because the dispersion during this phase is found to be the maximum. Therefore, the existing dynamic boundary limits may not be enough to estimate real driving emissions, especially during the urban phase. The NO_x emitted for the entire cycles is in the lower range and therefore the regulatory dynamic boundaries are appropriate for the NO_x estimation for the given vehicle. However, the dispersion indicates that even if the vehicle stays well within the boundaries, the NO_x emissions declared in an experiment may be a conjecture and fails to predict the real drive emissions for several trips within the protocol, especially during the urban phase.

The obtained dispersion is solely due to the variation in trip characteristics within the EU6D protocols, that is, even if the bell curve were to move leftwards, any method to account for the dispersion during engine calibration will remain a major challenge. But for real driving conditions, estimation of driving style and adaptive calibration, proposed in this thesis is a sought after solution to obtain close to optimal engine controls while staying within the regulatory limits. Moreover, it is necessary to address the dispersion in NO_x emissions due to trip dynamics in the future regulations. Wider spread compared to the well-defined drive cycles, like NEDC/WLTC seems unavoidable even with RDE regulations. Consideration of dispersion during the type approval will definitely reduce the difference between declared emissions and real drive emissions. Without which, the new RDE regulations may undermine its own objective which is to eliminate the gap between declared and real emissions.

The contribution of the proposed method lies not only in the fact that it synthesises driving cycles as stochastic process and is capable of tuning the driving dynamics based on RDE regulations, but it also presents the range of dispersion possible in NO_x emissions solely due to the driving dynamics. The methodology followed in the present work could be an essential step in future engine developments, where testing the engine prototypes on the entire range of driving dynamics in the engine test bench facility could provide interesting insights about the expected NO_x emissions in RDE testing. Consideration of the dispersion during the vehicle development is indispensable. To achieve

the RDE objective, on one hand, the manufacturer must develop their vehicle calibration for the worse case scenario while on the other hand the regulators must include it during type approval testing. Therefore, during the development phase of any vehicle the presented cycle synthesis tool accompanied by an engine test bench facility would be very useful tool to have a sense of required engine calibration in order to reduce the risk of failure during the Type approval.

The EU6D regulation which mandates the vehicle to pass emission norms individually in urban phase is an appropriate control and an additional control over urban driving style will definitely improve the confidence in the estimation of real driving emissions. The regulation already demands 50% driving to be done by TAA to reduce the risk of biased driving style, can be improved by demanding 50% driving by TAA in each phase of the trip.

Part V

Conclusion and Outlook

Chapter 10

Conclusions and Outlook

Contents

In this chapter, there are two sections: the first section summarises important conclusion that can be drawn from the thesis. In the second section, potential future directions in this line of research are outlined, along with the potential challenges that would need to be tackled in each of them.

10.1 Summary of the presented results

In this thesis, the automotive control methods are investigated for reducing the vehicle emissions in real driving condition. In general, the automotive control problem was tackled using the optimal control theory by defining an objective function (to be minimised) and a set of constraints related to the system and the environment. The three tools that were often used to perform the specific task of larger applications are developed using state-of the art techniques. In chapter 3, the backward vehicle modelling technique based on the quasi steady approach was described. This chapter introduced the modelling of vehicle longitudinal dynamics and then the most relevant powertrain components of a conventional vehicle and a hybrid electric vehicle. The engine and the motor models were data driven and therefore their utility was limited to the specific goal or application. In chapter 4, the state-of the-art optimal control methods which were used in the thesis were presented. The dynamic programming was derived from the Bellmans principle and an example was presented to calculate the optimal vehicle speed profile in real

driving condition. The limitation of the dynamic programming in real time due its exponential complexity to the number of states lead to the utilisation of the PMP in the control applications. As an implication of the Pontryagin's principle, the optimal solution to the problem of minimizing the total fuel consumption over a driving cycle must also minimize the instantaneous equivalent fuel consumption, was defined using the opportune equivalence factors in ECMS. The chapter 5, presented a driving cycle prediction tool using the Markov chain principle. Design of driving cycle generator was illustrated with the help of an example. Later in chapter 6, all the experimental setups which were used during the thesis were presented. The rapid prototyping using the dSpace microautobox or the PXI allowed to test the control strategies on test benches and on a vehicle. Using the tools described in chapter 3, chapter 4 and chapter 5, few applications were developed and presented in the following chapters.

In general two approaches were investigated in this thesis. The first approach was to optimise the powertrain control in real driving condition. For which, chapter 7present a novel adaptive control of diesel engine to minimise fuel consumption with constrained NO_x emissions on a real driving mission. MC based driving cycle prediction method is able to capture important driving characteristics in real-time. The experimental campaign shows that, if the driving aggressiveness of the predicted cycle is greater than or equal to the actual cycle the controller is able to meet the target NO_x emissions. However, underestimating the aggressiveness leads to excessive emissions. In another application in chapter 7, a calibration method was presented, which included a single tuning parameter to trade-off between, fuel consumption, NO_x emissions and drivability of the engine. The additional degree of freedom give flexibility to the calibration engineer, while optimality is guaranteed at all times. This tuning parameter was used to obtain a time-varying calibration of the diesel engine for NRTC to improve the engine performance and drivability. The comparison of the fixed and variable calibration strategies showed that, with variable strategy the NO_x emissions can be reduced upto 3% while maintaining similar levels of fuel consumption and drivability. The last section in chapter 7 was regarding the optimal control of the HEV powertrain. It presented a new method based on the online speed prediction and adaptive ECMS to optimse the EMS while tracking the battery SoC close to the target. The method was validated using a simulation and an experiment based case study on a real driving mission. The developed method was compared with three SOA methods: The ECMS (optimal and offline approach), ACP+ECMS (online approach) and the CD-CS (online approach). The results from the developed online method show significant improvement in the fuel consumption compared to the other online methods. in comparison to the offline method,

where the driving mission is known in advance the fuel consumption is 10% higher in the developed method.

The second approach was to optimise the speed profiles of the vehicle based on the available data from the infrastructure. The controllability (either passive or active control) is limited in real-time for such an application. The limitation is due to the amount of information (I2V or V2V) that is required to be processed in real time. For this in chapter 8, an application was aimed to assess the impact of traffic light information availability in terms of fuel consumption and NO_x emissions. An efficient management of vehicle speed is a key factor for fuel and NO_x minimisation. Traffic light information is essential for vehicle speed management, even if suboptimal strategies are used, substantial reductions in terms of both fuel consumption (7%) and emissions (12%) may be obtained. One may note that this level of reduction is, by far, higher to what can be attained with online optimisation of the engine control itself. Another application in chapter 8 was regarding optimal speed advisory in real driving mission. The application optimises the speed profile in real-time and recommends the driver optimal speed sequence that minimises the fuel consumption on a particular route. The real-time implementation of the application shows the possibility to stay very close to the Pareto front obtained by trading off travel time and fuel consumption. In particular 4% reduction in fuel consumption was recorded for the same travel time using the developed application.

Finally, in chapter 9, a real driving cycle generator based on the velocity TPM obtained from the WLTC was presented. A single tuning parameter was used to vary the cycle dynamics within the EU6D regulatory limits. A vehicle model was used to obtain the engine speed and torque profile which were then run on the engine installed in a SOA engine test bench. The instantaneous NO_x emission were measured and analysed. With the existing vehicle and within the RDE cycle characteristic protocols, a noticeable 60% relative dispersion in the NO_x emissions downstream of the catalyst was recorded. The assessments highlight the importance of considering this dispersion during the engine calibration to succeed in TA process.

10.2 Future directions

Include more states to the quasi-steady engine model The powertrain control performance rely heavily upon the engine model. In the work, quasi steady engine model was used as described in chapter 3. These models were based on interpolated maps depending on only a few states. With complexity of these models increasing linearly with the number of states, this

thesis limited them to two for focusing on the controller development. However, more states can be easily integrated in the current engine models at the cost of implementation complexity in the rapid prototyping controller (due to limited memory). A straightforward research direction would be to explore new methods for engine modelling such as neural network.

Include more states in the driving cycle predictor for improved accuracy The global objective of this investigation was to minimise the driving uncertainties in real driving conditions for calculating the optimal actuations. The driving cycle prediction tool developed in this thesis was based on the MC principle. The states included in the TPM were vehicle velocity and position. Even though the cycle predictions were able to capture the main characteristics of driving such as aggressiveness, the model can be enhanced with 'time' as an additional state in the TPM. This would further improve the capability of the model to capture the traffic intensities in urban driving conditions. This can be realised by modelling the traffic flow on an urban street using experimental data and tools such as SUMO. Such a model is capable of providing velocity speed profiles as a function of time and position and with this information three dimensional (current velocity, time, position) TPMs can be easily formulated. Finally, the speed prediction process can also include the current information of other vehicles in the route.

Include ATS temperature as an additional state in the control problem to capture cold state problems in HEV During the development of online EMS of HEV, the only state considered was battery SoC however, there are other parameters that influence the performance of the HEV controller in real driving conditions. For instance, by including the thermal model of the after-treatment system, the temperature of the ATS can be included as an additional state. The new cost function will also include another co-state related to the vehicle emissions addressing the cold start problem of diesel engine based HEV.

Explore combined powertrain and ADAS optimisation In this thesis, online optimal control methods for powertrain and ADAS were explored separately. Applications and case studies were used to demonstrate the capabilities of both the approaches. In future, application can be developed with combined optimisation of powertrain and ADAS with the same objective. For example, the driver is advised of speed based on traffic situation to minimise the fuel consumption and maintain the terminal SoC while the EMS adaptively controls the torque-split torwards the same objective. As the basis for

online control of HEV was speed prediction, a speed advisory would further reduce the uncertainty arising due to the driver.

Appendices

Appendix A

Appendix Example

A.1 Algorithm for Bisection method

Algorithm 2 Calculate Optimal μ_s^*

$j \leftarrow 1$ $TOL \leftarrow tolerance$ $MaxItr \leftarrow Maximum\ number\ of\ iterations$
$sa_j \leftarrow a$ $sb_j \leftarrow b$ $\mu_{s,j}^* \leftarrow b$ $SoC_a \leftarrow f(\overrightarrow{T_{est}}, \overrightarrow{\omega_{est}}, a)$ $SoC_b \leftarrow f(\overrightarrow{T_{est}}, \overrightarrow{\omega_{est}}, b)$
while $abs(SoC_c - SoC_{target}^{dyn}) > TOL \mid\mid j > MaxItr$ **do**
  $sc \leftarrow \frac{(sa_j + sb_j)}{2}$
  $SoC_c \leftarrow f(\overrightarrow{T_{est}}, \overrightarrow{\omega_{est}}, sc)$
  if $SoC_{a,j} < SoC_{target}^{dyn}$ & $SoC_c < SoC_{target}^{dyn}$ **then**
    $sa_{j+1} \leftarrow sc$
    $sb_{j+1} \leftarrow sb_j$
  else $\{SoC_{a,j} < SoC_{target}^{dyn}$ & $SoC_c > SoC_{target}^{dyn}\}$
    $sa_{j+1} \leftarrow sa_j$
    $sb_{j+1} \leftarrow sc$
  $\mu_{s,j}^* \leftarrow sc$
  $j \leftarrow j + 1$
$\mu_s^* \leftarrow \mu_s^*(end)$

Bibliography

[201 2016] *Commission regulation EU 2016/646 of 20th april 2016 amending Regulation EC No 692/2008 as regards emissions from light passenger and commercial vehicles (Euro6)*, 2016. (Cited on pages 158 and 162.)

[Alonso *et al.* 2007] Jos M. Alonso, Fernando Alvarruiz, Jos M. Desantes, Leonor Hernndez, Vicente Hernndez and Germn Molt. *Combining Neural Networks and Genetic Algorithms to Predict and Reduce Diesel Engine Emissions*. IEEE Transactions on Evolutionary Computation, vol. 11, no. 1, pages 46–55, feb 2007. (Cited on page 17.)

[Ambuhl & Guzzella 2009] D. Ambuhl and L. Guzzella. *Predictive Reference Signal Generator for Hybrid Electric Vehicles*. IEEE Transactions on Vehicular Technology, vol. 58, no. 9, pages 4730–4740, nov 2009. (Cited on page 119.)

[Andreas *et al.* 2010] A. Malikopoulos Andreas, Y.Papalambros Panos and N. Assanis Dennis. *Online Identification and Stochastic Control for Autonomous Internal Combusiton Engines*. Journal of Dynamic Systems, Measurement, and Control, 2010. (Cited on page 22.)

[AQR 2019] *Air quality in Europe — 2019 report*, 2019. (Cited on page 3.)

[Asprion *et al.* 2014] Jonas Asprion, Oscar Chinellato and Lino Guzzella. *Optimal control of diesel engines: Numerical methods, applications, and experimental validation*. Mathematical Problems in Engineering, vol. 2014, 2014. (Cited on pages 17 and 22.)

[Assis *et al.* 2003] Edgard Marcelo De Assis, Ricardo Kurauchi, Marcelo Conti Carloti, J. Celso Ribeiro, Liao Dai Lon and Adriano Cardon Castro. *Drivability Improvements on Electronic Diesel Engines*. In SAE Technical Paper Series. SAE International, nov 2003. (Cited on page 17.)

[Atkinson *et al.* 2008] Chris Atkinson, Marc Allain and Houshun Zhang. *Using Model-Based Rapid Transient Calibration to Reduce Fuel Consumption and Emissions in Diesel Engines.* In SAE Technical Paper Series. SAE International, apr 2008. (Cited on page 20.)

[Aubert & Kornprobst 2006] Gilles Aubert and Pierre Kornprobst. Mathematical problems in image processing. Springer New York, 2006. (Cited on page 104.)

[Authors 2006] V Authors. *Reciprocating internal combustion engines. Exhaust emission measurement. Test-bed measurement of gaseous and particulate exhaust emissions.* BS ISO 8178-1: 2006, 2006. (Not cited.)

[Bachler *et al.* 2003] Johann Bachler, Peter Mathis and Martin Rzehorska. *Calibration Methodologies for Online Optimisation of Diesel Engines with Regard to Emissions, NVH and Performance.* In SAE Technical Paper Series. SAE International, jan 2003. (Cited on page 17.)

[Bageshwar *et al.* 2004] V.L. Bageshwar, W.L. Garrard and R. Rajamani. *Model Predictive Control of Transitional Maneuvers for Adaptive Cruise Control Vehicles.* IEEE Transactions on Vehicular Technology, vol. 53, no. 5, pages 1573–1585, sep 2004. (Cited on page 32.)

[Bakibillah *et al.* 2018] A.S.M. Bakibillah, M.A.S. Kamal, C.P. Tan, T. Hayakawa and J. Imura. *Eco-driving on Hilly Roads Using Model Predictive Control.* In 2018 Joint 7th International Conference on Informatics, Electronics & Vision (ICIEV) and 2018 2nd International Conference on Imaging, Vision & Pattern Recognition (icIVPR). IEEE, jun 2018. (Cited on page 30.)

[Baldi *et al.* 2015] Francesco Baldi, Gerasimos Theotokatos and Karin Andersson. *Development of a combined mean value–zero dimensional model and application for a large marine four-stroke Diesel engine simulation.* Applied Energy, vol. 154, pages 402–415, sep 2015. (Cited on page 20.)

[Barth & Boriboonsomsin 2009] Matthew Barth and Kanok Boriboonsomsin. *Energy and emissions impacts of a freeway-based dynamic eco-driving system.* Transportation Research Part D: Transport and Environment, vol. 14, no. 6, pages 400–410, aug 2009. (Cited on page 30.)

[Bellman 1970] Richard Bellman. *Dynamic programming and inverse optimal problems in mathematical economics.* Journal of Mathematical Anal-

ysis and Applications, vol. 29, no. 2, pages 424–428, feb 1970. (Cited on page 53.)

[Berger *et al.* 2011] Benjamin Berger, Florian Rauscher and Boris Lohmann. *Analysing Gaussian Processes for Stationary Black-Box Combustion Engine Modelling.* IFAC Proceedings Volumes, vol. 44, no. 1, pages 10633–10640, jan 2011. (Cited on page 20.)

[Berger 2012] Benjamin Berger. *Modeling and Optimization for Stationary Base Engine Calibration.* PhD thesis, TECHNISCHE UNIVERSITAT MUNCHEN, 2012. (Cited on page 105.)

[BLOCKEY & HARTLEY 1995] P. N. BLOCKEY and L. R. HARTLEY. *Aberrant driving behaviour: errors and violations.* Ergonomics, vol. 38, no. 9, pages 1759–1771, sep 1995. (Cited on page 29.)

[Bradley & Frank 2009] Thomas H. Bradley and Andrew A. Frank. *Design, demonstrations and sustainability impact assessments for plug-in hybrid electric vehicles.* Renewable and Sustainable Energy Reviews, vol. 13, no. 1, pages 115–128, jan 2009. (Cited on page 23.)

[Bryson & Ho 2018] Arthur E. Bryson and Yu-Chi Ho. Applied optimal control. Routledge, may 2018. (Cited on page 26.)

[Bu *et al.* 2010] Fanping Bu, Han-Shue Tan and Jihua Huang. *Design and field testing of a Cooperative Adaptive Cruise Control system.* In Proceedings of the 2010 American Control Conference. IEEE, jun 2010. (Cited on page 31.)

[Buie *et al.* 2004] Lawrence Buie, Malcolm Fry, Peter Fussey and Chad Mitts. *An Application of Cost Based Power Management Control Strategies to Hybrid Fuel Cell Vehicles.* In SAE Technical Paper Series. SAE International, mar 2004. (Cited on page 27.)

[Canale & Malan 2002] M. Canale and S. Malan. *Analysis and Classification of Human Driving Behaviour in an Urban Environment.* Cognition, Technology Work, vol. 4, no. 3, pages 197–206, sep 2002. (Cited on page 29.)

[Cao *et al.* 2017] Jianfei Cao, Jiankun Peng and Hongwen He. *Research on Model Prediction Energy Management Strategy with Variable Horizon.* Energy Procedia, vol. 105, pages 3565–3570, may 2017. (Cited on page 28.)

[Guardiola *et al.* 2016] Guardiola Carlos, Pla Benjamin, Bares Pau and Waschl Harald. *Adaptive calibration for reduced fuel consumption and emissions.* Journal of Automotive Engineering, 2016. (Cited on page 23.)

[Castagné *et al.* 2008] M. Castagné, Y. Bentolila, F. Chaudoye, A. Hallé, F. Nicolas and D. Sinoquet. *Comparison of Engine Calibration Methods Based on Design of Experiments (DoE).* Oil & Gas Science and Technology - Revue de IFP, vol. 63, no. 4, pages 563–582, jul 2008. (Cited on page 15.)

[Cavazzuti 2013] Marco Cavazzuti. Optimization methods. Springer Berlin Heidelberg, 2013. (Cited on page 20.)

[Chen & Borken-Kleefeld 2014] Yuche Chen and Jens Borken-Kleefeld. *Real-driving emissions from cars and light commercial vehicles–Results from 13 years remote sensing at Zurich/CH.* Atmospheric Environment, vol. 88, pages 157–164, 2014. (Cited on page 88.)

[con 2019] *Worldwide Emission Standards and Related Regulations*, 2019. (Cited on page 19.)

[Corti *et al.* 2013] Enrico Corti, Giorgio Mancini, Claudio Forte and Davide Moro. *Automatic Combustion Phase Calibration With Extremum Seeking Approach.* In Volume 1: Large Bore Engines; Advanced Combustion; Emissions Control Systems ; Instrumentation, Controls, and Hybrids. American Society of Mechanical Engineers, oct 2013. (Cited on page 22.)

[Cramton 1969] Roger C. Cramton. *Driver Behavior and Legal Sanctions: A Study of Deterrence.* Michigan Law Review, vol. 67, no. 3, pages 421–454, 1969. (Cited on page 29.)

[Debert *et al.* 2012] Maxime Debert, Thomas Miro Padovani, Guillaume Colin, Yann Chamaillard and Lino Guzzella. *Implementation of comfort constraints in dynamic programming for hybrid vehicle energy management.* International Journal of Vehicle Design, vol. 58, no. 2/3/4, page 367, 2012. (Cited on page 26.)

[Demuynck *et al.* 2012] Joachim Demuynck, Dirk Bosteels, Michel De Paepe, Cécile Favre, John May and Sebastian Verhelst. *Recommendations for the new WLTP cycle based on an analysis of vehicle emission measurements on NEDC and CADC.* Energy Policy, vol. 49, pages 234–242, 2012. (Cited on page 4.)

[Die 2019] *Brochure: EU actions since Dieselgate - An overview from 2015 until today*, 2019. (Cited on page 4.)

[Du *et al.* 2016] Yongchang Du, Yue Zhao, Qinpu Wang, Yuanbo Zhang and Huaicheng Xia. *Trip-oriented stochastic optimal energy management strategy for plug-in hybrid electric bus.* Energy, vol. 115, pages 1259–1271, nov 2016. (Cited on page 121.)

[EEA 2019] *Monitoring of CO2 emissions from passenger cars – Regulation (EU) 2019/631*, 2019. (Cited on page 3.)

[EGD 2019] *COMMUNICATION FROM THE COMMISSION TO THE EUROPEAN PARLIAMENT, THE EUROPEAN COUNCIL, THE COUNCIL, THE EUROPEAN ECONOMIC AND SOCIAL COMMITTEE AND THE COMMITTEE OF THE REGIONS The European Green Deal COM/2019/640 final*, 2019. (Cited on page 3.)

[Elbert *et al.* 2017] Philipp Elbert, Alois Amstutz and Christopher Onder. *Adaptive Control for the Real Driving Emissions of Diesel Engines.* MTZ worldwide, vol. 78, no. 12, pages 68–74, nov 2017. (Cited on page 105.)

[Englund *et al.* 2016] Cristofer Englund, Lei Chen, Jeroen Ploeg, Elham Semsar-Kazerooni, Alexey Voronov, Hoai Hoang Bengtsson and Jonas Didoff. *The Grand Cooperative Driving Challenge 2016: boosting the introduction of cooperative automated vehicles.* IEEE Wireless Communications, vol. 23, no. 4, pages 146–152, aug 2016. (Cited on page 31.)

[Ericsson 2001] Eva Ericsson. *Independent driving pattern factors and their influence on fuel-use and exhaust emission factors.* TRANSPORT RESEARCH PART D, 2001. (Cited on page 162.)

[Fazal *et al.* 2010] Syed Fazal, Allen Dobryden S.N., Grand Carrie, McGee Ryan and Filev Dimitar. *Design and Analysis of an Adaptive RealTime Advisory System for Improving Real World Fuel Economy in a Hybrid Electric Vehicle.* SAE Journal, 2010. (Cited on page 22.)

[Feneley *et al.* 2017] Adam J. Feneley, Apostolos Pesiridis and Amin Mahmoudzadeh Andwari. *Variable Geometry Turbocharger Technologies for Exhaust Energy Recovery and Boosting-A Review.* Renewable and Sustainable Energy Reviews, vol. 71, pages 959–975, may 2017. (Cited on page 6.)

[Fernandes & Nunes 2012] Pedro Fernandes and Urbano Nunes. *Platooning With IVC-Enabled Autonomous Vehicles: Strategies to Mitigate Communication Delays, Improve Safety and Traffic Flow.* IEEE Transactions on Intelligent Transportation Systems, vol. 13, no. 1, pages 91–106, mar 2012. (Cited on page 31.)

[François 2017] Cuenot François. *Real world fuel economy measurements.* Technical report, groupe PSA, transport and environment, France nature environnement (FnE) and Bureau Veritas, 2017. (Cited on page 22.)

[Frieske *et al.* 2013] Benjamin Frieske, Matthias Kloetzke and Florian Mauser. *Trends in vehicle concept and key technology development for hybrid and battery electric vehicles.* In 2013 World Electric Vehicle Symposium and Exhibition (EVS27). IEEE, nov 2013. (Cited on page 6.)

[Fröberg *et al.* 2006] Anders Fröberg, Erik Hellström and Lars Nielsen. *Explicit Fuel Optimal Speed Profiles for Heavy Trucks on a Set of Topographic Road Profiles.* In SAE Technical Paper, 2006. (Cited on page 32.)

[Galindo *et al.* 2020] Jose Galindo, Hector Climent, Benjamin Pla and Chaitanya Patil. *EGR Transient Operations in Highly Dynamic Driving Cycles.* International Journal of Automotive Technology, vol. 21, no. 4, pages 865–879, jul 2020. (Cited on page 6.)

[George F Wolfe 1938] John I Spencer George F Wolfe. *Automatic speed control for vehicles*, 1938. (Cited on page 31.)

[Günter Reichart *et al.* 1998] S.F Günter Reichart, Dorrer Claus, Rieker Heinrich, Drechsel Eberhard and Wermuth Gisbert. *Potentials of BMW Driver Assistance to Improve Fuel Economy.* FISITA 1998 World Automotive Congress, 1998. (Cited on page 22.)

[Gokul *et al.* 2019] S. Sankar Gokul, C. Shekhar Rohan, Manzie Chris, Sano Takeshi and Nakada Hayato. *Model Predictive Controller with Average Emissions Constraints for Diesel Airpath.* Control Engineering Practice, 2019. (Cited on page 23.)

[Gong *et al.* 2007] Qiuming Gong, Yaoyu Li and Zhong-Ren Peng. *Trip Based Power Management of Plug-in Hybrid Electric Vehicle with Two-Scale Dynamic Programming.* In 2007 IEEE Vehicle Power and Propulsion Conference. IEEE, sep 2007. (Cited on page 25.)

[Gong *et al.* 2008] Qiuming Gong, Yaoyu Li and Zhong-Ren Peng. *Trip-Based Optimal Power Management of Plug-in Hybrid Electric Vehicles*. IEEE Transactions on Vehicular Technology, vol. 57, no. 6, pages 3393–3401, nov 2008. (Cited on page 24.)

[Gong *et al.* 2011] Q. Gong, Mohler S. Midlam, V. Marano and Rizzoni G. *An iterative markov chain approach for generating vehicle driving cycles*. SAE International Journal of Engines, 2011. (Cited on page 21.)

[Grahn *et al.* 2012] Markus Grahn, Krister Johansson, Christian Vartia and Tomas McKelvey. *A Structure and Calibration Method for Data-Driven Modeling of NOX and Soot Emissions from a Diesel Engine*. In SAE Technical Paper Series. SAE International, apr 2012. (Cited on page 20.)

[Gschweitl *et al.* 2001] Kurt Gschweitl, Horst Pfluegl, Tiziana Fortuna and Rainer Leithgoeb. *Increasing the efficiency of model-based engine applications through the use of CAMEO online DoE toolbox*. ATZ worldwide, vol. 103, no. 7-8, pages 17–20, jul 2001. (Cited on pages 105 and 106.)

[Gu & Rizzoni 2006] Bo Gu and Giorgio Rizzoni. *An Adaptive Algorithm for Hybrid Electric Vehicle Energy Management Based on Driving Pattern Recognition*. In Dynamic Systems and Control, Parts A and B. ASMEDC, jan 2006. (Cited on page 120.)

[Guardiola *et al.* 2012] Carlos Guardiola, Antonio Gil, Benjamín Pla and Pedro Piqueras. *Representation Limits of Mean Value Engine Models*. In Identification for Automotive Systems, pages 185–206. Springer London, 2012. (Cited on page 20.)

[Guardiola *et al.* 2013] C. Guardiola, B. Pla, D. Blanco-Rodríguez and A. Reig. *Modelling driving behaviour and its impact on the energy management problem in hybrid electric vehicles*. International Journal of Computer Mathematics, vol. 91, no. 1, pages 147–156, sep 2013. (Cited on pages 28 and 120.)

[Guardiola *et al.* 2014] Carlos Guardiola, Benjamin Pla, David Blanco-Rodriguez and Pierre Olivier Calendini. *ECU-oriented models for NOx prediction. Part 1: a mean value engine model for NOx prediction*. Proceedings of the Institution of Mechanical Engineers, Part D: Journal of Automobile Engineering, vol. 229, no. 8, pages 992–1015, nov 2014. (Cited on page 20.)

[Guardiola *et al.* 2016] Carlos Guardiola, Benjamín Pla, Pau Bares and Harald Waschl. *Adaptive calibration for reduced fuel consumption and emissions.* Proceedings of the Institution of Mechanical Engineers, Part D: Journal of Automobile Engineering, vol. 230, no. 14, pages 2002–2014, aug 2016. (Cited on page 105.)

[Guardiola *et al.* 2018] C. Guardiola, B. Pla, P. Bares and A. Barbier. *A combustion phasing control-oriented model applied to an RCCI engine.* IFAC-PapersOnLine, vol. 51, no. 31, pages 119–124, 2018. (Cited on page 6.)

[Guardiola *et al.* 2019] Carlos Guardiola, Benjamín Pla, Varun Pandey and Richard Burke. *On the potential of traffic light information availability for reducing fuel consumption and NOx emissions of a diesel light-duty vehicle.* Proceedings of the Institution of Mechanical Engineers, Part D: Journal of Automobile Engineering, page 0954407019867167, 2019. (Cited on page 149.)

[Gutjahr *et al.* 2017] Tobias Gutjahr, Thomas Kruse and Thorsten Huber. *ADVANCED MODELING AND OPTIMIZATION FOR VIRTUAL CALIBRATION OF INTERNAL COMBUSTION ENGINES.* 2017. (Cited on pages 105 and 106.)

[Guzzella & Amstutz 1998] L. Guzzella and A. Amstutz. *Control of diesel engines.* IEEE Control Systems, vol. 18, no. 5, pages 53–71, oct 1998. (Cited on page 114.)

[Guzzella & Onder 2010] Lino Guzzella and Christopher H. Onder. Introduction to modeling and control of internal combustion engine systems. Springer Berlin Heidelberg, 2010. (Cited on page 18.)

[Guzzella & Sciarretta 005] L. Guzzella and A. Sciarretta. Vehicle propulsion systems. introduction to modeling and optimization,. Berlin:Springer-Verlag, pp. 190, 2005. (Not cited.)

[Guzzella & Sciarretta 2005] L Guzzella and A Sciarretta. Vehicle propulsion systems. Introduction to modeling and optimization. Springer-Verlag, 2005. (Cited on pages 24, 44 and 54.)

[Hafner & Isermann 2003] Michael Hafner and Rolf Isermann. *Multiobjective optimization of feedforward control maps in engine management systems towards low consumption and low emissions.* Transactions of the Institute of Measurement and Control, vol. 25, no. 1, pages 57–74, mar 2003. (Cited on pages 20 and 105.)

[Han *et al.* 2019] Jihun Han, Ardalan Vahidi and Antonio Sciarretta. *Fundamentals of energy efficient driving for combustion engine and electric vehicles: An optimal control perspective.* Automatica, vol. 103, pages 558–572, may 2019. (Cited on page 7.)

[Hellström *et al.* 2009] Erik Hellström, Maria Ivarsson, Jan Åslund and Lars Nielsen. *Look-ahead control for heavy trucks to minimize trip time and fuel consumption.* Control Engineering Practice, vol. 17, no. 2, pages 245–254, 2009. (Cited on page 32.)

[Hellström *et al.* 2010a] Erik Hellström, Jan Åslund and Lars Nielsen. *Design of an efficient algorithm for fuel-optimal look-ahead control.* Control Engineering Practice, vol. 18, no. 11, pages 1318–1327, 2010. (Cited on page 138.)

[Hellström *et al.* 2010b] Erik Hellström, Jan Åslund and Lars Nielsen. *Design of an efficient algorithm for fuel-optimal look-ahead control.* Control Engineering Practice, vol. 18, no. 11, pages 1318–1327, 2010. (Cited on page 32.)

[Hellström *et al.* 2013] E. Hellström, D. Lee, L. Jiang, A. G. Stefanopoulou and H. Yilmaz. *On-Board Calibration of Spark Timing by Extremum Seeking for Flex-Fuel Engines.* IEEE Transactions on Control Systems Technology, vol. 21, no. 6, pages 2273–2279, 2013. (Cited on pages 7 and 22.)

[Hiroyasu *et al.* 2002] T. Hiroyasu, M. Miki, J. Kamiura, S. Watanabe and H. Hiroyasu. *Multi-Objective Optimization of Diesel Engine Emissions and Fuel Economy using Genetic Algorithms and Phenomenological Model.* In SAE Technical Paper Series. SAE International, oct 2002. (Cited on page 17.)

[Hochschwarzer *et al.* 1992] Helmuth Hochschwarzer, Wolfgang Kriegler and Manfred Schon. *Fully Automatic Determination and Optimization of Engine Control Characteristics.* SAE Transactions, vol. 101, pages 380–391, 1992. (Cited on page 20.)

[Hofman *et al.* 2006] T. Hofman, M. Steinbuch, R.M. van Druten and A.F.A. Serrarens. *RULE-BASED ENERGY MANAGEMENT STRATEGIES FOR HYBRID VEHICLE DRIVETRAINS: A FUNDAMENTAL APPROACH IN REDUCING COMPUTATION TIME.* IFAC Proceedings Volumes, vol. 39, no. 16, pages 740–745, 2006. (Cited on page 24.)

[Hooker 1988] J N Hooker. *Optimal driving for single-vehicle fuel economy.* Transportation Research Part A: General, vol. 22, no. 3, pages 183–201, 1988. (Cited on page 32.)

[Hou *et al.* 2014] Cong Hou, Minggao Ouyang, Liangfei Xu and Hewu Wang. *Approximate Pontryagin's minimum principle applied to the energy management of plug-in hybrid electric vehicles.* Applied Energy, vol. 115, pages 174–189, feb 2014. (Cited on page 27.)

[Huo *et al.* 2018] Yi Huo, Fengjun Yan and Daiwei Feng. *A hybrid electric vehicle energy optimization strategy by using fueling control in diesel engines.* Proceedings of the Institution of Mechanical Engineers, Part D: Journal of Automobile Engineering, page 0954407017747372, 2018. (Cited on page 134.)

[il Jeon *et al.* 2000] Soon il Jeon, Sung tae Jo, Yeong il Park and Jang moo Lee. *Multi-Mode Driving Control of a Parallel Hybrid Electric Vehicle Using Driving Pattern Recognition.* Journal of Dynamic Systems, Measurement, and Control, vol. 124, no. 1, pages 141–149, aug 2000. (Cited on page 120.)

[Isermann 2014] Rolf Isermann. Engine modeling and control: Modeling and electronic management of internal combustion engines. Berlin, Germnay: Springer, 2014. (Cited on page 15.)

[Jiang *et al.* 2009] Li Jiang, Julien Vanier, Hakan Yilmaz and Anna Stefanopoulou. *Parameterization and Simulation for a Turbocharged Spark Ignition Direct Injection Engine with Variable Valve Timing.* In SAE Technical Paper Series. SAE International, apr 2009. (Cited on page 20.)

[Jiang *et al.* 2012] Shugang Jiang, Donald Nutter and Anthony Gullitti. *Implementation of Model-Based Calibration for a Gasoline Engine.* In SAE Technical Paper, 2012. (Cited on page 7.)

[Jiang *et al.* 2017] Qi Jiang, Florence Ossart and Claude Marchand. *Comparative Study of Real-Time HEV Energy Management Strategies.* IEEE Transactions on Vehicular Technology, vol. 66, no. 12, pages 10875–10888, dec 2017. (Cited on page 121.)

[Jie & Debbie N 2002] Lin Jie and Niemer Debbie N. *An exploratory analysis comparing a stochastic driving cycle to California's regulatory cycle.* Atmospheric Environment, 2002. (Cited on page 21.)

[Johannesson *et al.* 2007] Lars Johannesson, Mattias Asbogard and Bo Egardt. *Assessing the Potential of Predictive Control for Hybrid Vehicle Powertrains Using Stochastic Dynamic Programming.* IEEE Transactions on Intelligent Transportation Systems, vol. 8, no. 1, pages 71–83, mar 2007. (Cited on pages 25, 32 and 119.)

[Jonas *et al.* 2014] Aspiron Jonas, Chinellato Oscar and Guzzella Lino. *Optimal Contorl of Diesel Engines: Numerical methods, Application, and Experimental Validation.* Hindawi Publishing corporation, Mathematical Problems in Engineering, 2014. (Cited on page 22.)

[Josevski & Abel 2016] Martina Josevski and Dirk Abel. *Distributed predictive control approach for fuel efficient gear shifting in hybrid electric vehicles.* In 2016 European Control Conference (ECC). IEEE, jun 2016. (Cited on page 28.)

[Josh & Vicente 2016] Miller Josh and Franco Vicente. *IMPACT OF IMPROVED REGULATION OF REAL-WORLD NOx EMISSIONS FROM DIESEL PASSENGER CARS IN THE EU 2015 2030.* Technical report, International Council on Clean Transportation, 2016. (Cited on page 22.)

[Jung 2003] Merten Jung. *Mean-value modelling and robust control of the airpath of a turbocharged diesel engine.* 2003. (Cited on page 20.)

[Kampelmühler *et al.* 1993] F. T. Kampelmühler, R. Paulitsch and K. Gschweitl. *Automatic ECU-Calibration - An Alternative to Conventional Methods.* In SAE Technical Paper Series. SAE International, mar 1993. (Cited on page 16.)

[Kianfar *et al.* 2012] Roozbeh Kianfar, Bruno Augusto, Alireza Ebadighajari, Usman Hakeem, Josef Nilsson, Ali Raza, Reza S. Tabar, Naga VishnuKanth Irukulapati, Cristofer Englund, Paolo Falcone, Stylianos Papanastasiou, Lennart Svensson and Henk Wymeersch. *Design and Experimental Validation of a Cooperative Driving System in the Grand Cooperative Driving Challenge.* IEEE Transactions on Intelligent Transportation Systems, vol. 13, no. 3, pages 994–1007, sep 2012. (Cited on page 31.)

[Kim *et al.* 2014] N. W. Kim, D. H. Lee, C. Zheng, C. Shin, H. Seo and S. W. Cha. *Realization of pmp-based control for hybrid electric vehicles in a backward-looking simulation.* International Journal of Automotive Technology, vol. 15, no. 4, pages 625–635, may 2014. (Cited on page 25.)

[Kum *et al.* 2013] Dongsuk Kum, Huei Peng and Norman K. Bucknor. *Optimal Energy and Catalyst Temperature Management of Plug-in Hybrid Electric Vehicles for Minimum Fuel Consumption and Tail-Pipe Emissions*. IEEE Transactions on Control Systems Technology, vol. 21, no. 1, pages 14–26, jan 2013. (Cited on page 25.)

[Langouët *et al.* 2011] Hoël Langouët, Ludovic Métivier, Delphine Sinoquet and Quang-Huy Tran. *Engine calibration: multi-objective constrained optimization of engine maps*. Optimization and Engineering, vol. 12, no. 3, pages 407–424, Sep 2011. (Cited on page 17.)

[Larsson & Ericsson 2009] Hanna Larsson and Eva Ericsson. *The effects of an acceleration advisory tool in vehicles for reduced fuel consumption and emissions*. Transportation Research Part D: Transport and Environment, vol. 14, no. 2, pages 141–146, 2009. (Cited on page 29.)

[Lee *et al.* 2020] Heeyun Lee, Changhee Song, Namwook Kim and Suk Won Cha. *Comparative Analysis of Energy Management Strategies for HEV: Dynamic Programming and Reinforcement Learning*. IEEE Access, vol. 8, pages 67112–67123, 2020. (Cited on page 26.)

[Lei *et al.* 2020] Zhenzhen Lei, Datong Qin, Liliang Hou, Jingyu Peng, Yonggang Liu and Zheng Chen. *An adaptive equivalent consumption minimization strategy for plug-in hybrid electric vehicles based on traffic information*. Energy, vol. 190, page 116409, jan 2020. (Cited on page 119.)

[Li & Goerges 2017] Guoqiang Li and Daniel Goerges. *Hybrid Modeling and Predictive Control of the Power Split and Gear Shift in Hybrid Electric Vehicles*. In 2017 IEEE Vehicle Power and Propulsion Conference (VPPC). IEEE, dec 2017. (Cited on page 28.)

[Li & Gorges 2019] Guoqiang Li and Daniel Gorges. *Fuel-Efficient Gear Shift and Power Split Strategy for Parallel HEVs Based on Heuristic Dynamic Programming and Neural Networks*. IEEE Transactions on Vehicular Technology, vol. 68, no. 10, pages 9519–9528, oct 2019. (Cited on page 26.)

[Li *et al.* 2011] Shengbo Li, Keqiang Li, Rajesh Rajamani and Jianqiang Wang. *Model Predictive Multi-Objective Vehicular Adaptive Cruise Control*. IEEE Transactions on Control Systems Technology, vol. 19, no. 3, pages 556–566, may 2011. (Cited on pages 30, 31 and 32.)

[Li *et al.* 2016] Liang Li, Sixiong You, Chao Yang, Bingjie Yan, Jian Song and Zheng Chen. *Driving-behavior-aware stochastic model predictive control for plug-in hybrid electric buses.* Applied Energy, vol. 162, pages 868–879, jan 2016. (Cited on page 28.)

[Luján *et al.* 2018] Jose Manuel Luján, Carlos Guardiola, Benjamín Pla and Alberto Reig. *Optimal control of a turbocharged direct injection diesel engine by direct method optimization.* International Journal of Engine Research, vol. 20, no. 6, pages 640–652, may 2018. (Cited on pages 17 and 22.)

[Luján *et al.* 2019] José Manuel Luján, Carlos Guardiola, Benjamín Pla and Varun Pandey. *Impact of driving dynamics in RDE test on NOx emissions dispersion.* Proceedings of the Institution of Mechanical Engineers, Part D: Journal of Automobile Engineering, page 095440701988158, nov 2019. (Cited on page 102.)

[Ma *et al.* 2015] He Ma, Hongming Xu, Jihong Wang, Thorsten Schnier, Ben Neaves, Cheng Tan and Zhi Wang. *Model-Based Multiobjective Evolutionary Algorithm Optimization for HCCI Engines.* IEEE Transactions on Vehicular Technology, vol. 64, no. 9, pages 4326–4331, sep 2015. (Cited on page 20.)

[Markel 2006] Tony Markel. *Plug-in Hybrid Electric VehiclesCurrent Status, Long-Term Prospects and Key Challenges.* Technical report, National Renewable Energy Laboratory, 8 May 2006. (Cited on page 23.)

[Maroteaux & Saad 2015] Fadila Maroteaux and Charbel Saad. *Combined mean value engine model and crank angle resolved in-cylinder modeling with NOx emissions model for real-time Diesel engine simulations at high engine speed.* Energy, vol. 88, pages 515–527, aug 2015. (Cited on page 22.)

[Martin *et al.* 2018] Jaime Martin, Francisco Arnau, Pedro Piqueras and Angel Auñon. *Development of an Integrated Virtual Engine Model to Simulate New Standard Testing Cycles.* In SAE Technical Paper Series. SAE International, apr 2018. (Cited on page 20.)

[Marx & Soffker 2012] Matthias Marx and Dirk Soffker. *Optimization of the powerflow control of a hybrid electric powertrain including load profile prediction.* In 2012 IEEE Vehicle Power and Propulsion Conference. IEEE, oct 2012. (Cited on page 28.)

[Mat 2017] The MathWorks, Inc. *MathWorks Model-Based Calibration Toolbox - CAGE User's Guide. ., 2017*, September 2017. (Cited on pages 105 and 106.)

[Michel 1996] Andre Michel. *Driving Cycles Development: Characterization of the Methods*. SAE Technical Papers, 1996. (Cited on page 21.)

[Milanes *et al.* 2014] Vicente Milanes, Steven E. Shladover, John Spring, Christopher Nowakowski, Hiroshi Kawazoe and Masahide Nakamura. *Cooperative Adaptive Cruise Control in Real Traffic Situations*. IEEE Transactions on Intelligent Transportation Systems, vol. 15, no. 1, pages 296–305, feb 2014. (Cited on page 31.)

[Millo *et al.* 2018] Federico Millo, Pranav Arya and Fabio Mallamo. *Optimization of automotive diesel engine calibration using genetic algorithm techniques*. Energy, vol. 158, pages 807–819, sep 2018. (Cited on page 20.)

[Minett *et al.* 2011] Claire F. Minett, A. Maria Salomons, Winnie Daamen, Bart van Arem and Sjon Kuijpers. *Eco-routing: Comparing the fuel consumption of different routes between an origin and destination using field test speed profiles and synthetic speed profiles*. In 2011 IEEE Forum on Integrated and Sustainable Transportation Systems. IEEE, jun 2011. (Cited on page 30.)

[Mock *et al.* 2012] Peter Mock, John German, Anup Bandivadekar and Iddo Riemersma. *Discrepancies between type-approval and "real-world" fuel-consumption and CO*. Technical report, International Council on Clean Transportation, 2012. (Cited on page 4.)

[Mock *et al.* 2013] Peter Mock, Uwe Tietge, Vicente Franco, John German, Anup Bandivadekar, Udo Lambrecht, Jörg Kühlwein and Iddo Riemersma. *From laboratory to road*. Technical report 30, International Council on Clean Transportation, 2013. (Cited on page 4.)

[Moro & Helmers 2015] Alberto Moro and Eckard Helmers. *A new hybrid method for reducing the gap between WTW and LCA in the carbon footprint assessment of electric vehicles*. The International Journal of Life Cycle Assessment, vol. 22, no. 1, pages 4–14, sep 2015. (Cited on page 6.)

[Moura *et al.* 2011] Scott Jason Moura, Hosam K. Fathy, Duncan S. Callaway and Jeffrey L. Stein. *A Stochastic Optimal Control Approach for Power Management in Plug-In Hybrid Electric Vehicles*. IEEE Transactions

on Control Systems Technology, vol. 19, no. 3, pages 545–555, may 2011. (Cited on page 24.)

[Musardo *et al.* 2005] Cristian Musardo, Giorgio Rizzoni, Yann Guezennec and Benedetto Staccia. *A-ECMS: An Adaptive Algorithm for Hybrid Electric Vehicle Energy Management*. European Journal of Control, vol. 11, no. 4-5, pages 509–524, jan 2005. (Cited on page 120.)

[Naranjo *et al.* 2003] J. E. Naranjo, C. González, J. Reviejo, R. García and T. de Pedro. *Adaptive fuzzy control for inter-vehicle gap keeping*. IEEE Transactions on Intelligent Transportation Systems, vol. 4, no. 3, pages 132–142, 2003. (Cited on page 30.)

[Nessler *et al.* 2006] Adrian Nessler, Carsten Haukap and Karsten Roepke. *Global evaluation of the drivability of calibrated diesel engine maps*. In 2006 IEEE Conference on Computer Aided Control System Design, 2006 IEEE International Conference on Control Applications, 2006 IEEE International Symposium on Intelligent Control. IEEE, oct 2006. (Cited on page 18.)

[Niedernolte *et al.* 2006] H. Niedernolte, F. Klopper, A. Mitterer and F. Schwarzer. *Workflow for data evaluation during basic calibration of combustion engines*. In 2006 IEEE Conference on Computer Aided Control System Design, 2006 IEEE International Conference on Control Applications, 2006 IEEE International Symposium on Intelligent Control. IEEE, oct 2006. (Cited on page 18.)

[Nishio & Shen 2019] Yui Nishio and Tielong Shen. *Model predictive control with traffic information-based driver's torque demand prediction for diesel engines*. International Journal of Engine Research, page 146808741985167, may 2019. (Cited on page 23.)

[Nishio *et al.* 2018] Yui Nishio, Yutaka Murata, Yukihisa Yamaya and Masato Kikuchi. *Optimal calibration scheme for map-based control of diesel engines*. Science China Information Sciences, vol. 61, no. 7, page 70205, Jun 2018. (Cited on page 18.)

[Onori *et al.* 2015] Simona Onori, Lorenzo Serrao and Giorgio Rizzoni. *Adaptive Optimal Supervisory Control Methods*. In SpringerBriefs in Electrical and Computer Engineering, pages 79–87. Springer London, dec 2015. (Cited on page 119.)

[Ortiz-Soto *et al.* 2012] Elliot Ortiz-Soto, Dennis Assanis and Aristotelis Babajimopoulos. *A comprehensive engine to drive-cycle modelling*

framework for the fuel economy assessment of advanced engine and combustion technologies. International Journal of Engine Research, vol. 13, no. 3, pages 287–304, 2012. (Cited on page 28.)

[Ozatay *et al.* 2014a] E. Ozatay, S. Onori, J. Wollaeger, U. Ozguner, G. Rizzoni, D. Filev, J. Michelini and S. Di Cairano. *Cloud-Based Velocity Profile Optimization for Everyday Driving: A Dynamic-Programming-Based Solution.* IEEE Transactions on Intelligent Transportation Systems, vol. 15, no. 6, pages 2491–2505, 2014. (Cited on page 32.)

[Ozatay *et al.* 2014b] Engin Ozatay, Simona Onori, James Wollaeger, Umit Ozguner, Giorgio Rizzoni, Dimitar Filev, John Michelini and Stefano Di Cairano. *Cloud-based velocity profile optimization for everyday driving: A dynamic-programming-based solution.* IEEE Transactions on Intelligent Transportation Systems, vol. 15, no. 6, pages 2491–2505, 2014. (Cited on pages 22 and 30.)

[Ozatay *et al.* 2014c] Engin Ozatay, Umit Ozguner, John Michelini and Dimitar Filev. *Analytical solution to the minimum energy consumption based velocity profile optimization problem with variable road grade.* IFAC Proceedings Volumes, vol. 47, no. 3, pages 7541–7546, 2014. (Cited on pages 22 and 30.)

[Paganelli *et al.* 2000] G Paganelli, T. M. Guerra, S Delprat, J-J Santin, M Delhom and E Combes. *Simulation and assessment of power control strategies for a parallel hybrid car.* Proceedings of the Institution of Mechanical Engineers, Part D: Journal of Automobile Engineering, vol. 214, no. 7, pages 705–717, jul 2000. (Cited on pages 25 and 119.)

[Park *et al.* 2017] Sangki Park, Youngkun Kim, Seungchul Woo and Kihyung Lee. *Optimization and calibration strategy using design of experiment for a diesel engine.* Applied Thermal Engineering, vol. 123, pages 917–928, aug 2017. (Cited on page 17.)

[Passenberg *et al.* 2009] B. Passenberg, P. Kock and O. Stursberg. *Combined time and fuel optimal driving of trucks based on a hybrid model.* In European Control Conference, pages 4955–4960, 2009. (Cited on page 32.)

[Payri *et al.* 2005] F. Payri, X. Margot, A. Gil and J. Martin. *Computational Study of Heat Transfer to the Walls of a DI Diesel Engine.* In SAE Technical Paper Series. SAE International, apr 2005. (Cited on page 20.)

[Payri *et al.* 2012] F. Payri, C. Guardiola, B. Pla and D. Blanco-Rodriguez. *On a Stochastic Approach of the (ECMS) Method for Energy Management in Hybrid Electric Vehicles.* IFAC Proceedings Volumes, vol. 45, no. 30, pages 341–348, 2012. (Cited on pages 28 and 120.)

[Payri *et al.* 2014] F. Payri, C. Guardiola, B. Pla and D. Blanco-Rodriguez. *A stochastic method for the energy management in hybrid electric vehicles.* Control Engineering Practice, vol. 29, pages 257–265, aug 2014. (Cited on page 27.)

[Payri *et al.* 2015] F Payri, José M Luján, Carlos Guardiola and B Pla. *A challenging future for the ic engine: new technologies and the control role.* Oil & Gas Science and Technology–Revue IFP Energies nouvelles, vol. 70, no. 1, pages 15–30, 2015. (Cited on pages 6, 21 and 119.)

[Pelkmans & Debal 2006] Luc Pelkmans and Patrick Debal. *Comparison of on-road emissions with emissions measured on chassis dynamometer test cycles.* Transportation Research Part D: Transport and Environment, vol. 11, no. 4, pages 233–241, 2006. (Cited on pages 21 and 28.)

[Peng *et al.* 2015] Jiankun Peng, Hao Fan, Hongwen He and Deng Pan. *A Rule-Based Energy Management Strategy for a Plug-in Hybrid School Bus Based on a Controller Area Network Bus.* Energies, vol. 8, no. 6, pages 5122–5142, jun 2015. (Cited on page 24.)

[Peng *et al.* 2017] Jiankun Peng, Hongwen He and Rui Xiong. *Rule based energy management strategy for a series–parallel plug-in hybrid electric bus optimized by dynamic programming.* Applied Energy, vol. 185, pages 1633–1643, jan 2017. (Cited on page 24.)

[Petit *et al.* 2011] Nicolas Petit, Antonio Sciarretta*et al.* *Optimal drive of electric vehicles using an inversion-based trajectory generation approach.* In Proceedings of the 18th IFAC World Congress, pages 14519–14526, 2011. (Cited on page 32.)

[Petri *et al.* 2018] Sebastian Petri, Giovanni Vagnoni, Ferenc Aubeck, Johan Lindberg, Esteban R. Gelso, Nikolce Murgovski, Mohammed R. Karim, Joschka Schaub and Andrea Pantaleo. *Predictive engine and aftertreatment control concepts for a heavy-duty long-haul truck.* In 27th Aachen Colloquium Automobile and Engine Technology 2018, 2018. (Cited on page 23.)

[Pinamonti *et al.* 2017] Silvio A. Pinamonti, Domenico Brancale, Gerhard Meister and Pablo Mendoza. *A Correlation Methodology between AVL*

Mean Value Engine Model and Measurements with Concept Analysis of Mean Value Representation for Engine Transient Tests. In SAE Technical Paper Series. SAE International, sep 2017. (Cited on page 20.)

[Ping *et al.* 2019] Peng Ping, Wenhu Qin, Yang Xu, Chiyomi Miyajima and Kazuya Takeda. *Impact of Driver Behavior on Fuel Consumption: Classification, Evaluation and Prediction Using Machine Learning*. IEEE Access, vol. 7, pages 78515–78532, 2019. (Cited on page 29.)

[Pla *et al.* 2020] Benjamin Pla, Pau Bares, Enrique Sanchis and André Aronis. *Ammonia injection optimization for selective catalytic reduction aftertreatment systems*. International Journal of Engine Research, page 146808742093312, jul 2020. (Cited on page 6.)

[Ploeg *et al.* 2011] Jeroen Ploeg, Bart T. M. Scheepers, Ellen van Nunen, Nathan van de Wouw and Henk Nijmeijer. *Design and experimental evaluation of cooperative adaptive cruise control*. In 2011 14th International IEEE Conference on Intelligent Transportation Systems (ITSC). IEEE, oct 2011. (Cited on page 31.)

[Ploeg *et al.* 2014] Jeroen Ploeg, Dipan P. Shukla, Nathan van de Wouw and Henk Nijmeijer. *Controller Synthesis for String Stability of Vehicle Platoons*. IEEE Transactions on Intelligent Transportation Systems, vol. 15, no. 2, pages 854–865, apr 2014. (Cited on page 31.)

[Popovic *et al.* 2006] D. Popovic, M. Jankovic, S. Magner and A.R. Teel. *Extremum seeking methods for optimization of variable cam timing engine operation*. IEEE Transactions on Control Systems Technology, vol. 14, no. 3, pages 398–407, may 2006. (Cited on page 22.)

[Rajan *et al.* 2012] Brahmadevan V Padma Rajan, Andrew McGordon and Paul A Jennings. *An investigation on the effect of driver style and driving events on energy demand of a PHEV*. World Electric Vehicle Journal Vol. 5, 2012. (Cited on page 22.)

[Rakha & Kamalanathsharma 2011] Hesham Rakha and Raj Kishore Kamalanathsharma. *Eco-driving at signalized intersections using V2I communication*. In 2011 14th International IEEE Conference on Intelligent Transportation Systems (ITSC). IEEE, oct 2011. (Cited on page 30.)

[Rao *et al.* 1979] Harish S Rao, A I Cohen, J A Tennant and K L Van Voorhies. *Engine Control Optimization Via Nonlinear Programming*.

SAE Transactions, vol. 88, 1979, pp. 667–676., 1979. (Cited on pages 16 and 20.)

[Reig 2017] Alberto Reig. *Optimal Control for Automotive Powertrain Applications*. PhD thesis, 2017. (Cited on page 32.)

[Ritter & Tillotson 1924] George F Ritter and Harry C Tillotson. *Carburetor*, 1924. (Cited on page 14.)

[Ross 1994] M Ross. *Automobile Fuel Consumption and Emissions: Effects of Vehicle and Driving Characteristics*. Annual Review of Energy and the Environment, vol. 19, no. 1, pages 75–112, nov 1994. (Cited on page 29.)

[Rudin *et al.* 1992] Leonid I. Rudin, Stanley Osher and Emad Fatemi. *Nonlinear total variation based noise removal algorithms*. Physica D: Nonlinear Phenomena, vol. 60, no. 1-4, pages 259–268, nov 1992. (Cited on pages 104 and 106.)

[Saboohi & Farzaneh 2009] Y. Saboohi and H. Farzaneh. *Model for developing an eco-driving strategy of a passenger vehicle based on the least fuel consumption*. Applied Energy, vol. 86, no. 10, pages 1925–1932, 2009. (Cited on page 32.)

[Sampson 2009] D Sampson. *Use of Model-Based Calibration in the Test Cell*. In In Proceedings of the 5th conference Design of Experiments (DOE) in Engine DEvelopment, 2009. (Cited on page 17.)

[Samuel *et al.* 2005] S Samuel, D Morrey, M Fowkes, C D H Taylor, L Austin, T Felstead and S Latham. *Real-world fuel economy and emission levels of a typical EURO-IV passenger vehicle. Proceedings of the Institution of Mechanical Engineers*. Part D: Journal of Automobile Engineering, 2005. (Cited on page 4.)

[Schöggl *et al.* 2002] P. Schöggl, H. M. Koegeler, K. Gschweitl, H. Kokal, P. Williams and K. Hulak. *Automated EMS Calibration using Objective Driveability Assessment and Computer Aided Optimization Methods*. In SAE Technical Paper Series. SAE International, mar 2002. (Cited on page 16.)

[Schüler 2001] M. Schüler. *Stationäre Optimierung der Motorsteuerung von PKW-Dieselmotoren mit Abgasturbolader durch Einsatz schneller neuronaler Netze*. PhD thesis, TU Darmstadt, 2001. (Cited on page 105.)

[Schmied 2004] A Schmied. *Stochastic optimisation methods for engine calibration; Methodes stochastiques d'optimisation appliquees a la mise au point moteur*, 2004. (Cited on page 20.)

[Schwarzkopf & Leipnik 1977] A. B. Schwarzkopf and R. B. Leipnik. *Control of highway vehicles for minimum fuel consumption over varying terrain.* Transportation Research, vol. 11, no. 4, pages 279–286, 1977. (Cited on page 31.)

[Sciarretta & Vahidi 2020a] Antonio Sciarretta and Ardalan Vahidi. Energy-efficient driving of road vehicles. Springer International Publishing, 2020. (Cited on page 7.)

[Sciarretta & Vahidi 2020b] Antonio Sciarretta and Ardalan Vahidi. Energy-efficient driving of road vehicles. Springer, 2020. (Cited on page 32.)

[Sciarretta *et al.* 2004] A. Sciarretta, M. Back and L. Guzzella. *Optimal Control of Parallel Hybrid Electric Vehicles.* IEEE Transactions on Control Systems Technology, vol. 12, no. 3, pages 352–363, may 2004. (Cited on page 119.)

[Sciarretta *et al.* 2015a] Antonio Sciarretta, Giovanni De Nunzio and Luis Leon Ojeda. *Optimal ecodriving control: Energy-efficient driving of road vehicles as an optimal control problem.* IEEE Control Systems, vol. 35, no. 5, pages 71–90, 2015. (Cited on pages 22 and 30.)

[Sciarretta *et al.* 2015b] Antonio Sciarretta, Giovanni De Nunzio and Luis Leon Ojeda. *Optimal Ecodriving Control: Energy-Efficient Driving of Road Vehicles as an Optimal Control Problem.* IEEE Control Systems, vol. 35, no. 5, pages 71–90, 2015. (Cited on page 32.)

[Scordia *et al.* 2005] J. Scordia, M. Desbois Renaudin, R. Trigui, B. Jeanneret, F. Badin and C. Plasse. *Global optimisation of energy management laws in hybrid vehicles using dynamic programming.* International Journal of Vehicle Design, vol. 39, no. 4, page 349, 2005. (Cited on page 26.)

[Sequenz 2013] H. Sequenz. *Emission Modelling and Model-Based Optimisation of the Engine Control.* PhD thesis, Technischen Universitat Darmstadt, 2013. (Cited on page 105.)

[Serrao *et al.* 2009] Lorenzo Serrao, Simona Onori and Giorgio Rizzoni. *ECMS as a realization of Pontryagins minimum principle for HEV control.* In 2009 American Control Conference. IEEE, 2009. (Cited on page 122.)

[Simon *et al.* 2018] A Simon, D Nelson-Gruel, A Charlet, T Jaine, C Nouillant and Y Chamaillard. *Optimal supervisory control of a Diesel HEV taking into account both DOC and SCR efficiencies.* IFAC-PapersOnLine, vol. 51, no. 9, pages 323–328, 2018. (Cited on page 134.)

[Sims *et al.* 2014] R Sims, Schaeffer R, Creutzig F, Cruz-Núñez X, D'Agosto M, Dimitriu D, Figueroa Meza M.J, Fulton L, Kobayashi S, Lah O, McKinnona A, Newman P, Ouyang M, Schauer J.J, Sperling D and Tiwari G. *Transport. In: Climate Change 2014: Mitigation of Climate Change. Contribution of Working Group III to the Fifth Assessment Report of the Intergovernmental Panel on Climate Change [Edenhofer, O., R. Pichs-Madruga, Y. Sokona, E. Farahani, S. Kadner, K. Seyboth, A. Adler, I. Baum, S. Brunner, P. Eickemeier, B. Kriemann, J. Savolainen, S. Schlömer, C. von Stechow, T. Zwickel and J.C. Minx (eds.)].* Technical report, Cambridge University Press, Cambridge, United Kingdom and New York, NY, USA, 2014. (Cited on page 3.)

[Singh *et al.* 2019] Krishna Veer Singh, Hari Om Bansal and Dheerendra Singh. *A comprehensive review on hybrid electric vehicles: architectures and components.* Journal of Modern Transportation, vol. 27, no. 2, pages 77–107, mar 2019. (Cited on page 6.)

[Stanger & del Re 2013] T. Stanger and L. del Re. *A model predictive Cooperative Adaptive Cruise Control approach.* In American Control Conference, pages 1374–1379, 2013. (Cited on pages 30 and 32.)

[Stanglmaier *et al.* 2002] Rudolf H. Stanglmaier, Ryan C. Roecker, Charles E. Roberts and Jr.Daniel W. Stewart. *NOx aftertreatment system and method for internal combustion engines*, 2002. (Cited on page 14.)

[Stephan *et al.* 2014] Zentner Stephan, Asprion Jonas, Onder Christopher and Guzzella Lin. *An Equivalent Emission Minimization Strategy for Causal Optimal Control of Diesel Engines.* Energies, 2014. (Cited on page 23.)

[Stuhler *et al.* 2002] Harald Stuhler, Thomas Kruse, Axel Stuber, Kurt Gschweitl, Walter Piock, Horst Pfluegl and Peter Lick. *Automated Model-Based GDI Engine Calibration Adaptive Online DoE Approach.* In SAE Technical Paper, 2002. (Cited on page 7.)

[Sugaya 1978] Kazuyoshi Sugaya. *Fuel pressure regulator*, 1978. (Cited on page 14.)

[Sun *et al.* 2017] Chao Sun, Fengchun Sun and Hongwen He. *Investigating adaptive-ECMS with velocity forecast ability for hybrid electric vehicles.* Applied Energy, vol. 185, pages 1644–1653, jan 2017. (Cited on page 120.)

[Sundstrom & Guzzella 2009] O. Sundstrom and L. Guzzella. *A generic dynamic programming Matlab function.* In 2009 IEEE Control Applications, (CCA) Intelligent Control, (ISIC), pages 1625–1630, July 2009. (Cited on page 138.)

[Sung *et al.* 2007] Alexander Sung, Florian Klöpper, Alexander Mitterer, Georg Wachtmeister and Andreas Zell. *Modellbasierte Online-Optimierung in der Simulation und am Motorenprüfstand.* MTZ - Motortechnische Zeitschrift, vol. 68, no. 1, pages 42–48, jan 2007. (Cited on page 17.)

[Tagliaferri *et al.* 2016] Carla Tagliaferri, Sara Evangelisti, Federica Acconcia, Teresa Domenech, Paul Ekins, Diego Barletta and Paola Lettieri. *Life cycle assessment of future electric and hybrid vehicles: A cradle-to-grave systems engineering approach.* Chemical Engineering Research and Design, vol. 112, pages 298–309, aug 2016. (Cited on page 6.)

[Tan *et al.* 2017] Qingyuan Tan, Prasad Divekar, Ying Tan, Xiang Chen and Ming Zheng. *Online calibration of combustion phase in a diesel engine.* Control Theory and Technology, vol. 15, no. 2, pages 129–137, may 2017. (Cited on page 17.)

[Tang & Rizzoni 2016] Li Tang and Giorgio Rizzoni. *Energy management strategy including battery life optimization for a HEV with a CVT.* In 2016 IEEE Transportation Electrification Conference and Expo, Asia-Pacific (ITEC Asia-Pacific). IEEE, jun 2016. (Cited on page 121.)

[Teetor 1950] Ralph R Teetor. *Speed control device for resisting operation of the accelerator*, 1950. (Cited on page 31.)

[Thangaraja & Kannan 2016] J. Thangaraja and C. Kannan. *Effect of exhaust gas recirculation on advanced diesel combustion and alternate fuels - A review.* Applied Energy, vol. 180, pages 169–184, oct 2016. (Cited on page 6.)

[TK & ZS 2011] Lee TK and Filipi ZS. *Synthesis of real-world driving cycles using stochastic process and statistical methodology.* International Journal of Vehicle Design, 2011. (Cited on page 21.)

[Tong *et al.* 2000] H.Y. Tong, W.T. Hung and C.S. Cheung. *On-Road Motor Vehicle Emissions and Fuel Consumption in Urban Driving Conditions.* Journal of the Air & Waste Management Association, vol. 50, no. 4, pages 543–554, apr 2000. (Cited on page 29.)

[Torregrosa *et al.* 2011] Antonio J. Torregrosa, Pablo Olmeda, Jaime Martín and Carlos Romero. *A Tool for Predicting the Thermal Performance of a Diesel Engine.* Heat Transfer Engineering, vol. 32, no. 10, pages 891–904, sep 2011. (Cited on page 20.)

[Tran *et al.* 2020] Dai-Duong Tran, Majid Vafaeipour, Mohamed El Baghdadi, Ricardo Barrero, Joeri Van Mierlo and Omar Hegazy. *Thorough state-of-the-art analysis of electric and hybrid vehicle powertrains: Topologies and integrated energy management strategies.* Renewable and Sustainable Energy Reviews, vol. 119, page 109596, mar 2020. (Cited on pages 23 and 24.)

[Tschanz *et al.* 2013] Frédéric Tschanz, Alois Amstutz, Christopher H Onder and Lino Guzzella. *Control of diesel engines using NOx-emission feedback.* International Journal of Engine Research, vol. 14, no. 1, pages 45–56, 2013. (Cited on page 28.)

[Tsugawa *et al.* 2011] S. Tsugawa, S. Kato and K. Aoki. *An automated truck platoon for energy saving.* In 2011 IEEE/RSJ International Conference on Intelligent Robots and Systems. IEEE, sep 2011. (Cited on page 31.)

[Tulpule *et al.* 2011] Pinak Tulpule, Vincenzo Marano and Giorgio Rizzoni. *Effect of Traffic, Road and Weather Information on PHEV Energy Management.* In SAE Technical Paper Series. SAE International, sep 2011. (Cited on pages 27 and 119.)

[Tutuianu *et al.* 2013] Monica Tutuianu, Alessandro Marotta, Heinz Steven, Eva Ericsson, Takahiro Haniu, Noriyuki Ichikawa and Hajime Ishii. *Development of a World-wide Worldwide harmonized Light duty driving Test Cycle (WLTC).* Technical report, WLTP DHC Chair, 2013. (Cited on page 6.)

[Ulleberg & Rundmo 2003] Pål Ulleberg and Torbjørn Rundmo. *Personality, attitudes and risk perception as predictors of risky driving behaviour among young drivers.* Safety Science, vol. 41, no. 5, pages 427–443, jun 2003. (Cited on page 29.)

[Vagg *et al.* 2013] Chris Vagg, Chris Brace, Deepak Hari, Sam Akehurst and Lloyd Ash. *A driver advisory tool to reduce fuel consumption.* Technical report, SAE Technical Paper, 2013. (Cited on page 29.)

[van Arem *et al.* 2006] Bart van Arem, Cornelie J. G. van Driel and Ruben Visser. *The Impact of Cooperative Adaptive Cruise Control on Traffic-Flow Characteristics.* IEEE Transactions on Intelligent Transportation Systems, vol. 7, no. 4, pages 429–436, dec 2006. (Cited on page 31.)

[van Dooren *et al.* 2019] Stijn van Dooren, Camillo Balerna, Mauro Salazar, Alois Amstutz and Christopher H. Onder. *Optimal Diesel Engine Calibration using Convex Modelling of Pareto Frontiers.* Control Engineering Practice, 2019. ,Revision submitted in October 2019. (Cited on page 105.)

[Veerle *et al.* 2016] Heijne Veerle, Kadijk Gerrit, Ligterink Norbert, derMark Petervan, Spreen Jordy and Stelwagen Uilke. *NOx emissions of fifteen Euro 6 diesel cars: Results of the Dutch LD road vehicle emission testing programme 2016.* Technical report, TNO, 2016. (Cited on page 4.)

[Verma *et al.* 2013] Rajeev Verma, Nikhil Nahar, Zhijun Tang and Benjamin Saltsman. *A Driver Assistance System for Improving Commercial Vehicle Fuel Economy.* In SAE Technical Paper Series. SAE International, jan 2013. (Cited on page 29.)

[Vinot *et al.* 2007] Emmanuel Vinot, Rochdi Trigui, Bruno Jeanneret, Julien Scordia and Frangois Badin. *HEVs Comparison and Components Sizing Using Dynamic Programming.* In 2007 IEEE Vehicle Power and Propulsion Conference. IEEE, sep 2007. (Cited on page 26.)

[Weiss *et al.* 2011] Martin Weiss, Pierre Bonnel, Rudolf Hummel, Urbano Manfredi, Rinaldo Colombo, Gaston Lanappe, Philippe Le Lijour, Mirco Sculati*et al. Analyzing on-road emissions of light-duty vehicles with Portable Emission Measurement Systems (PEMS).* JRC Scientific and Technical Reports, EUR, vol. 24697, 2011. (Cited on pages 21 and 28.)

[Weiss *et al.* 2012] Martin Weiss, Pierre Bonnel, Jörg Kühlwein, Alessio Provenza, Udo Lambrecht, Stefano Alessandrini, Massimo Carriero, Rinaldo Colombo, Fausto Forni, Gaston Lanappe*et al. Will Euro 6 reduce the NOx emissions of new diesel cars?–Insights from on-road tests with Portable Emissions Measurement Systems (PEMS).* Atmospheric Environment, vol. 62, pages 657–665, 2012. (Cited on page 6.)

[Weißmann *et al.* 2018] Andreas Weißmann, Daniel Görges and Xiaohai Lin. *Energy-optimal adaptive cruise control combining model predictive control and dynamic programming.* Control Engineering Practice, vol. 72, pages 125–137, mar 2018. (Cited on page 32.)

[Xie *et al.* 2018] Shaobo Xie, Xiaosong Hu, Zongke Xin and Liang Li. *Time-Efficient Stochastic Model Predictive Energy Management for a Plug-In Hybrid Electric Bus With an Adaptive Reference State-of-Charge Advisory.* IEEE Transactions on Vehicular Technology, vol. 67, no. 7, pages 5671–5682, jul 2018. (Cited on pages 28 and 119.)

[Yang *et al.* 2019] Yalian Yang, Huanxin Pei, Xiaosong Hu, Yonggang Liu, Cong Hou and Dongpu Cao. *Fuel economy optimization of power split hybrid vehicles: A rapid dynamic programming approach.* Energy, vol. 166, pages 929–938, jan 2019. (Cited on page 26.)

[Yang *et al.* 2020] Hao Yang, Fawaz Almutairi and Hesham Rakha. *Eco-Driving at Signalized Intersections: A Multiple Signal Optimization Approach.* IEEE Transactions on Intelligent Transportation Systems, pages 1–13, 2020. (Cited on page 30.)

[Yu *et al.* 2020] Yuanbin Yu, , Junyu Jiang, Pengyu Wang and Jinke Li. *A-EMCS for PHEV based on real-time driving cycle prediction and personalized travel characteristics.* Mathematical Biosciences and Engineering, vol. 17, no. 6, pages 6310–6341, 2020. (Cited on page 119.)

[Yuche & Jens 2014] Chen Yuche and Broken-Kleefeld Jens. *Real-driving emissions from cars and light commercial vehicles – Results from 13 years remote sensing at Zurich/CH.* Atmospheric Environment, 2014. (Cited on page 4.)

[Zacharof *et al.* 2016] N Zacharof, U Tietge, V Franco and P Mock. *Type approval and real-world CO2 and NOx emissions from EU light commercial vehicles.* International Council on Clean Transportation, Germany, 2016. (Cited on page 4.)

[Zakaria *et al.* 2019] HAJI Zakaria, MOUNIR Hamid, EL MARJANI Abdellatif and AMARIR Imane. *Recent Advancements and Developments for Electric Vehicle Technology.* In 2019 International Conference of Computer Science and Renewable Energies (ICCSRE). IEEE, jul 2019. (Cited on page 6.)

[Zentner *et al.* 2013] Stephan Zentner, Erika Schäfer, Christopher Onder and Lino Guzzella. *Model-Based Injection and EGR Adaptation and its*

Impact on Transient Emissions and Drivability of a Diesel Engine. IFAC Proceedings Volumes, vol. 46, no. 21, pages 89–94, 2013. (Cited on page 18.)

[Zhang *et al.* 2018] Yunfan Zhang, Quan Zhou, Ziyang Li, Ji Li and Hongming Xu. *Intelligent transient calibration of a dual-loop EGR diesel engine using chaos-enhanced accelerated particle swarm optimization algorithm*. Proceedings of the Institution of Mechanical Engineers, Part D: Journal of Automobile Engineering, vol. 233, no. 7, pages 1698–1711, may 2018. (Cited on page 20.)

[Zhang *et al.* 2020] Fengqi Zhang, Lihua Wang, Serdar Coskun, Hui Pang, Yahui Cui and Junqiang Xi. *Energy Management Strategies for Hybrid Electric Vehicles: Review, Classification, Comparison, and Outlook*. Energies, vol. 13, no. 13, page 3352, jun 2020. (Cited on pages 27 and 122.)

[Zhi *et al.* 2016] Zhanjiang Zhi, Baoli Shi and Yi Sun. *Primal-dual method to smoothing TV-based model for image denoising*. Journal of Algorithms & Computational Technology, vol. 10, no. 4, pages 235–243, jul 2016. (Cited on pages 104 and 106.)

[Zhijia *et al.* 2013] Yang Zhijia, Stobart Richard and Winward Edward. *Online adjustment of start of injection and fuel rail pressure based on combustion process parameters of diesel engine*. SAE International, 2013. (Cited on page 22.)

Online Control of Automotive Systems for Improved Real-World Performance

Abstract: The need of improving the real-world fuel consumption and emission of automotive applications is the basis of this thesis. To this end, two verticals are explored: First is the online control of the powertrain systems. In state-of-the-art Optimal Control techniques (such as Dyanmic Programming, Pontryagins Minimum Principle, etc...) are extensively used to formulate the optimal control laws. These laws are stored in the production ECUs in the form of feedforward calibration maps. The unaccounted uncertainities related to the real-world during the powertrain calibration result in suboptimal operations of the powertrain in actual driving. Therefore, adaptive control methods are proposed in this work which, optimise the energy management of the conventional and the HEV powertrain control on real driving mission. The second vertical is regarding the vehicle speed control (popularly known as Eco-Driving in the literature) methods in real driving condition. In particular, speed advisory systems are proposed for real time application on a vehicle. The control methods developed for each application are described in details with their verification and validation on the designed case studies. Apart from the developed control methods, there are three tools that were developed and used at various stages of this thesis: A vehicle model, A driving cycle prediction tool and optimal control methods (dynamic programming, PMP and ECMS). Depending on the application, the developed methods were implemented on the Hardware-In-Loop Internal Combustion Engine testing setup or on a real vehicle. The results show significant improvements in the performance of the powertrain in terms of fuel economy and emissions in comparison to the state-of-the-art methods.

Keywords: Optimal Control, Model based control, Hybrid Electric Vehicle, Energy Management Strategy, Adaptive control, Calibration Smoothing, Real Driving Emissions, Eco-Driving, Vehicle speed Optimisation

Control de sistemas propulsivos de automoción para la mejorara del rendimiento en condiciones reales de conducción

Resumen: La necesidad de mejorar el consumo de combustible y las emisiones de los sistemas propulsivos de automoción en condiciones reales de conducción es la base de esta tesis. Para ello, se exploran dos ejes: En primer lugar, el control de los sistemas de propulsión. El estado del arte de control en los sistemas propulsivos de automoción se basa en gran medida en el uso de técnicas de optimización que buscan las leyes de control que minimizan una función de coste en un conjunto de condiciones de operación definidas a priori. Estas leyes se almacenan en las ECUs de producción en forma de mapas de calibración de los diferentes actuadores del motor. Las incertidumbres asociadas al conjunto limitado de condiciones en el proceso de calibración dan lugar a un funcionamiento subóptimo del sistema de propulsión en condiciones de conducción real. Por lo tanto, en este trabajo se proponen métodos de control adaptativo que optimicen la gestión de la planta propulsiva a las condiciones esperadas de funcionamiento para un usuario y un caso determinado en lugar de a un conjunto genérico de condiciones. El segundo eje se refiere a optimizar, en lugar de los parámetros de control del sistema propulsivo, la demanda de potencia de este, introduciendo al propio conductor en el bucle de control, sugiriéndole las acciones a tomar. En particular, este segundo eje se refiere al control de la velocidad del vehículo (conocido popularmente como Eco-Driving en la literatura) en condiciones reales de conducción. Se proponen sistemas de aviso en tiempo real al conductor acerca de la velocidad óptima para minimizar el consumo del vehículo. Los métodos de control desarrollados para cada aplicación se describen en detalle en la tesis y se muestran ensayos experimentales de validación en los casos de estudio diseñados. Ambos ejes representan un problema de control óptimo, definido por un sistema dinámico, unas restricciones a cumplir y un coste a minimizar, en este sentido las herramientas desarrolladas en la tesis son comunes a los dos ejes: Un modelo de vehículo, una herramienta de predicción del ciclo de conducción y métodos de control óptimo (Programación Dinámica, Principio Mínimo de Pontryagin y Estrategia de Consumo Equivalente Mínimo). Dependiendo de la aplicación, los métodos desarrollados se implementaron en varios entornos experimentales: un motor térmico en sala de ensayos simulando el resto del vehículo, incluyendo el resto del sistema de propulsión híbrido y en un vehículo real. Los resultados muestran mejoras significativas en el rendimiento del sistema de propulsión en términos de ahorro de combustible y emisiones en comparación con los métodos empleados en el estado del arte actual.

Control de sistemes propulsius d'automoció per a la millorara del rendiment en condicions reals de conducció

Resum: La necessitat de millorar el consum de combustible i les emissions dels sistemes propulsius d'automoció en condicions reals de conducció és la base d'aquesta tesi. Per a això, s'exploren dos eixos: En primer lloc, el control dels sistemes de propulsió. L'estat de l'art de control en els sistemes propulsius d'automoció es basa en gran manera en l'ús de tècniques d'optimització que busquen les lleis de control que minimitzen una funció de cost en un conjunt de condicions d'operació definides a priori. Aquestes lleis s'emmagatzemen en les Ecus de producció en forma de mapes de calibratge dels diferents actuadors del motor. Les incerteses associades al conjunt limitat de condicions en el procés de calibratge donen lloc a un funcionament subòptim del sistema de propulsió en condicions de conducció real. Per tant, en aquest treball es proposen mètodes de control adaptatiu que optimitzen la gestió de la planta propulsiva a les condicions esperades de funcionament per a un usuari i un cas determinat en lloc d'un conjunt genèric de condicions. El segon eix es refereix a optimitzar, en lloc dels paràmetres de control del sistema propulsiu, la demanda de potència d'aquest, introduint al propi conductor en el bucle de control, suggerint-li les accions a prendre. En particular, aquest segon eix es refereix al control de la velocitat del vehicle (conegut popularment com Eco-*Driving en la literatura) en condicions reals de conducció. Es proposen sistemes d'avís en temps real al conductor sobre la velocitat òptima per a minimitzar el consum del vehicle. Els mètodes de control desenvolupats per a cada aplicació es descriuen detalladament en la tesi i es mostren assajos experimentals de validació en els casos d'estudi dissenyats. Tots dos eixos representen un problema de control òptim, definit per un sistema dinàmic, unes restriccions a complir i un cost a minimitzar, en aquest sentit les eines desenvolupades en la tesi són comunes als dos eixos: Un model de vehicle, una eina de predicció del cicle de conducció i mètodes de control òptim (Programació Dinàmica, Principi Mínim de *Pontryagin i Estratègia de Consum Equivalent Mínim). Depenent de l'aplicació, els mètodes desenvolupats es van implementar en diversos entorns experimentals: un motor tèrmic en sala d'assajos simulant la resta del vehicle, incloent la resta del sistema de propulsió híbrid i en un vehicle real. Els resultats mostren millores significatives en el rendiment del sistema de propulsió en termes d'estalvi de combustible i emissions en comparació amb els mètodes emprats en l'estat de l'art actual.